THREE DIMENSIONAL FORMULATION FOR THE STRESS-STRAIN-DILATANCY ELASTO-PLASTIC CONSTITUTIVE MODEL FOR SAND UNDER CYCLIC BEHAVIOUR

Thesis by
Saumyasuchi Das

Submitted in
June 2014

In partial fulfilment of the requirements
For the degree of
Master of Engineering (Civil)

Supervised by
Dr. Brendon Bradley and Prof. Misko Cubrinovski

Department of Civil and Natural Resources Engineering
College of Engineering
University of Canterbury
Christchurch, New Zealand

Acknowledgement

The author appreciates continuous encouragement and support from Dr. Brendon Bradley throughout the postgraduate research, without which the research would not have taken the present shape. The author wishes to thank Professor M. Cubrinovski for his insightful advices. The author also acknowledges constructive comments from Professor Yannis F. Dafalias.

The author takes this opportunity to acknowledge that the course on the Theory of Plasticity conducted by Bengal Engineering and Science University Shibpur (Indian Institute of Engineering, Science and Technology) has immensely helped him during the research, which is almost entirely founded on the Theory of Plasticity.

The author expresses his deep gratitude to his wife for her patience, understanding and help during the postgraduate research.

The author acknowledges the financial support from the University of Canterbury and Education New Zealand.

Last, but not the least, the author conveys his gratitude for the support provided by the Department of Civil Engineering, and his postgraduate peers.

Abstract

Recent experiences from the Darfield and Canterbury, New Zealand earthquakes have shown that the soft soil condition of saturated liquefiable sand has a profound effect on seismic response of buildings, bridges and other lifeline infrastructure. For detailed evaluation of seismic response three dimensional integrated analysis comprising structure, foundation and soil is required; such an integrated analysis is referred to as Soil Foundation Structure Interaction (SFSI) in literatures. SFSI is a three-dimensional problem because of three primary reasons: first, foundation systems are three-dimensional in form and geometry; second, ground motions are three-dimensional, producing complex multiaxial stresses in soils, foundations and structure; and third, soils in particular are sensitive to complex stress because of heterogeneity of soils leading to a highly anisotropic constitutive behaviour. In literatures the majority of seismic response analyses are limited to plane strain configuration because of lack of adequate constitutive models both for soils and structures, and computational limitation. Such two-dimensional analyses do not represent a complete view of the problem for the three reasons noted above. In this context, the present research aims to develop a three-dimensional mathematical formulation of an existing plane-strain elasto-plastic constitutive model of sand developed by Cubrinovski and Ishihara (1998b). This model has been specially formulated to simulate liquefaction behaviour of sand under ground motion induced earthquake loading, and has been well-validated and widely implemented in verifcation of shake table and centrifuge tests, as well as conventional ground response analysis and evaluation of case histories.

The approach adopted herein is based entirely on the mathematical theory of plasticity and utilises some unique features of the bounding surface plasticity formalised by Dafalias (1986). The principal constitutive parameters, equations, assumptions and empiricism of the existing plane-strain model are adopted in their exact form in the three-dimensional version. Therefore, the original two-dimensional model can be considered as a true subset of the three-dimensional form; the original model can be retrieved when the tensorial quantities of the three dimensional version are reduced to that of the plane-strain configuration. Anisotropic Drucker-Prager type failure surface has been adopted for the three-dimensional version to accommodate triaxial stress path. Accordingly, a new mixed hardening rule based on Mroz's approach of homogeneous surfaces (Mroz, 1967) has been introduced for the

virgin loading surface. The three-dimensional version is validated against experimental data for cyclic torsional and triaxial stress paths.

Table of Contents

List of Tables

List of Figures

1.0 Introduction and Scope

1.1 Background

1.1.1 Seismic performance of New Zealand buildings and bridges during the Canterbury earthquakes

Soil Foundation Structure Interaction (SFSI) studies are necessary for holistic and accurate assessment of seismic performance of structures including geotechnical structures which are founded on soft and potentially liquefiable sandy soils. New Zealand is tectonically very active as the converging movements of the Australian and the Pacific plate boundaries along the Hikurangi trough in the North Island and along the Puysehur trench in the South Island are accommodated by a labyrinth of faults traversing the entire country. There are not only some well-known faults like the Wellington Fault in the North Island, the 650km long Alpine Fault and the Marlborough Fault Zone in the South Island, but there are also numerous buried faults distributed throughout the Southern Alps and the Canterbury plains in the South Island. The Australian and Pacific plates converge at an approximate rate of 40mm every year across the plate boundary on which New Zealand resides. The recent M_w7.1, 4 September 2010 Darfield and M_w6.3, 22 February Christchurch 2011 earthquakes (henceforth will be collectively referred to as Canterbury earthquakes), and the February earthquake in particular, had caused considerable damage to the infrastructure of the city of Christchurch and disruption to business owing to closure of its Central Business District for approximately one year imposing economic losses as high as 10% of the country's Gross Domestic Product (New Zealand Parliament, 2011).

Amongst other reasons, a significant amount of damage was primarily due to liquefaction induced ground subsidence and lateral spreading resulting in foundation failures from excessive settlements and lateral stretch. Amplification of ground motion was observed in the Central Business District because of very deep soil deposit of approximately 400m in depth beneath the city of Christchurch (Cubrinovski et al., 2010; Cubrinovski et al., 2011a,b; Eleni et al., 2011). The epicentre of the February earthquake was within the city precincts and such close proximity to the source was the prime reason for the severity of damages observed (Bradley, 2012b; Bradley and Cubrinovski, 2011). After the February earthquake, almost 50% of building stock in the city was declared unsafe and had to be demolished (Kam et al., 2011). The landmark and iconic buildings in the urban landscape of the city, such as the Christchurch Cathedral, the Pyne Gould Corp Building, the Canterbury Television Building,

and the modern high rise buildings such as the Grand Chancellor Hotel and the Forsyth Barr Building were destroyed beyond the scope of economic repair during the February earthquake. At least ten bridges suffered moderate to severe damage, primarily due to lateral spreading (Wotherspoon et al., 2011; Cubrinovski et al., 2014).

1.1.2 Significance of Soil Foundation Structure Interaction (SFSI) in soft soil condition

The response spectra during both the Darfield and the Christchurch earthquakes had exceeded 475 year mean recurrence interval design spectrum of the New Zealand seismic code (NZS 1170.5 2004) for periods longer than 1.4 sec (Kam et al., 2010; Kam et al., 2011) which coupled with liquefaction of foundation soil imposed high seismic demands on buildings and bridges. The lateral period [only considering the horizontal displacements as the primary degrees of freedom (DOF)] of 1.4 sec corresponds to a building height of 150 feet (45 m) with reinforced concrete moment resistance frame with fixed base (Goel and Chopra, 1997), which is a typical configuration of many multi-storied buildings in the Christchurch. However the assumption of fixed base is only valid when the horizontal deformability of foundation is negligible, which is not the case in the Canterbury region as, evidenced by foundation movements in many cases. Many buildings of lower heights were affected despite having lower fixed base periods because flexibility of foundation had lengthened the fundamental period of building-foundation-soil system to well within the range of amplified response; besides, progressive softening of structures and soils due to cyclic inelastic excursion are also likely to lengthen the periods of initially stiffer systems to fall within the amplified range; liquefaction caused excessive settlement of foundations exceeding the serviceability limits. A large body of literatures cited herein on extensive post-earthquake reconnaissance and damage surveys stands as a testimony to the severity of February earthquake resulting from soft soil conditions.

The 2012 New Zealand Society for Earthquake Engineering Annual Conference held in the opportune time with the theme of “implementing lessons learned” attracted about 61 contributions from national and international researchers. Though it is generally recognized that SFSI) significantly affects seismic performance but only one paper out of 61 (Butt and Omenzetter, 2012) was dedicated to SFSI. There were only two effective stress based SFSI studies conducted prior to the Darfield and the Christchurch earthquakes based on local soil conditions (Bowen and Cubrinovski, 2008; Bradley et al., 2010). Both were conducted on

seismic performance of the Fitzgerald Avenue Bridge; liquefaction predicted by these studies was consistent with the observed damage at the bridge site.

1.1.3 Limitations in conventional SFSI analysis

An elegant yet elementary treatment of SFSI is available in the text by Clough and Penzien (1993). Consideration of SFSI increases degrees of freedom (DOF) of structure; the additional DOF are assigned to foundations, and foundations are then supported by deformable or compliance soil mass. For the sake of simplicity, often the deformability of soils is represented through lumped springs and dashpots, often referred to as Beams on Nonlinear Winkler Foundation approach (Boulanger et al., 2003). However, such a simple representation does not provide accurate picture about the inelastic behaviour of soils under complex three-dimensional ground motion and is incapable of simulating liquefaction behaviour of sandy soils. At a phenomenological level, soil is a continuum, and therefore its plastic behaviour, unlike discrete beam-column assemblages in structures, depends on the complex multiaxial state of stress rather than on approximately uniaxial stress.

The analytical modelling of the plastic behaviour of continua is generally based on the Theory of Plasticity, which basically aims to derive a coupled relation among all six components of stresses and strains in an incremental form (such relations are often non-integrable). The theory was originally postulated by observing the mechanical behaviour of metals at low temperatures (Drucker and Seereeram, 1987; Chakrabarty, 2006) under multiaxial stresses. The advantage of the plasticity theory is that it provides a rigorous mathematical framework based on which several constitutive relations can be developed. However, the constitutive behaviour of soils and metals being significantly different, some strongly held postulations of the conventional theory of metal plasticity are found to be inapplicable to soils; one such example is the postulation of associated flow. Therefore, the application of the Theory of Plasticity to soils is not straightforward.

1.2 Objective: statement of the problem

During earthquake vertical upward propagation of shear waves impose bidirectional shear stress on soil. It has been experimentally observed that bidirectional shear stress increases liquefaction potential of saturated sand. Figure 1.1, taken from Ishihara and Yamazaki (1980), illustrates that cyclic stress ratio triggering liquefaction under different modes of bidirectional shear such as elliptical, circular and alternate loading, is considerably

lower than that of the unidirectional shear; a maximum reduction to 60 percent of the unidirectional cyclic stress ratio can be observed. The cyclic stress ratio reduces with the corresponding increase in bidirectional effect as the ratio of the smaller to the larger cyclic stress is increased.

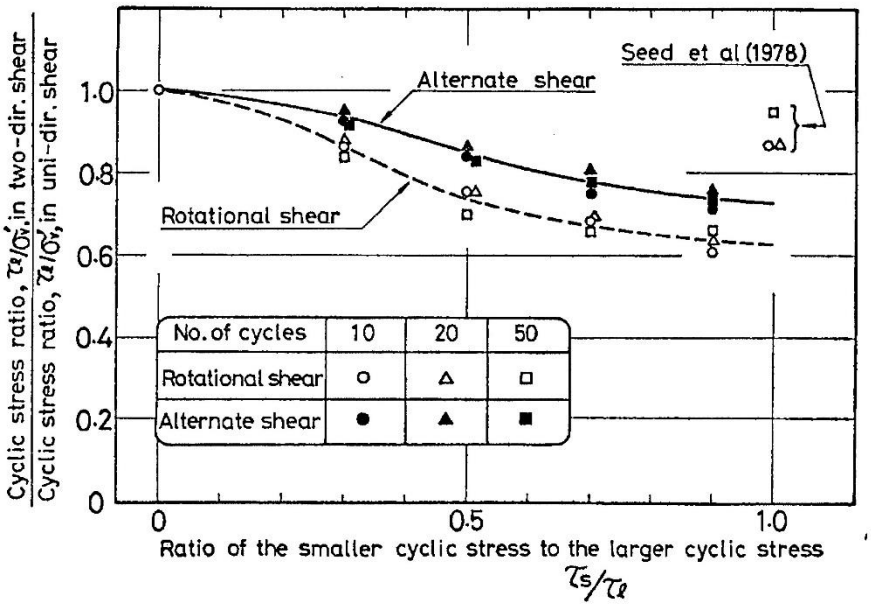

Figure 1.1 Cyclic strength under bidirectional shear loading normalised to the unidirectional shear loading (Ishihara and Yamazaki, 1980)

Hence, in order to facilitate accurate assessment of seismic performance of structures including geotechnical structures situated on liquefiable sandy soils under bidirectional horizontal components of ground motion, a computationally efficient three dimensional constitutive model is required. Although some three dimensional models are available in literatures, their application is limited to plane-strain. The constitutive modelling of sand in three dimensions is not only highly complex and challenging, but also the behaviour is not fully understood yet. In order to realise the degree of complexity involved in constitutive modelling, a succinct discussion on principal constitutive behaviour of sands is provided herein.

Liquefaction is observed in undrained saturated sand due to progressive loss of effective stress with cyclical stress loading involving rotation of principal stresses, which is induced during earthquakes principally by vertically propagating horizontally polarised shear waves. The reduction of principal stresses also leads to accumulation of large plastic shear strain and consequently plastic volumetric strain that is large enough to cause almost

complete loss of isotropic stress (Ishihara and Towhata, 1983). This complex link between the plastic shear strain and the plastic volumetric strain which is known as the dilatancy, particularly under cyclic loading, is perhaps the most complex and least understood constitutive behaviour of sandy soils. The majority of constitutive models available in literatures vary significantly both in concept and in their detailed mathematical formulation of the dilatancy behaviour. It is noteworthy that the dilatancy behaviour is the most critical aspect of the plastic behaviour of saturated sand. An elementary treatment on dilatancy behaviour under cyclic loads is available in Pradhan and Tatsuoka (1989); Pradhan et al. (1989) and Shahnazari and Towhata (2002).

Another interesting feature of the constitutive behaviour of sandy soils under cyclic stress is that the direction of the principal plastic strain increment is different from that of the principal stress. Wong and Arthur (1986) exhibited using a directional shear cell apparatus that the direction of principal plastic strain increment differs from that of the principal stress by as much as 30 degrees even when the specimen is sheared along its isotropic bedding plane. Furthermore, the stress-dilatancy relation was also effected by continuous rotation of principal stresses leading to non-coincidence of principal plastic strain increment and principal stresses; the specimen subjected to rotating principal stress exhibited higher dilatancy than the one with fixed principal stress direction. The authors conjectured that the specimens developed anistropy as a result of the variation in the direction of principal stresses; such anisotropy which is produced by loading is often referred to as induced anisotropy. Similar observations were also recorded in the experimental work by Miura et al. (1986) and Gutierrez et al. (1991).

In addition to the induced anisotropy, soils, in general, also exhibit inherent anisotropy which develops as a result of the deposition process which renders them a sedimentary structure. The plane of deposition is known as the bedding plane, and the normal of the bedding plane is typically assumed parallel to the direction of gravity. It is generally assumed that inherent anisotropy exists in planes that are perpendicular to the bedding plane. The response of soils depends on the direction of the major principal stress relative to the bedding plane. It is well-known that Mohr-Coulomb hexagonal yield locus does not exactly fit the observed failure surface of the soils; strength in triaxial extension is always significantly less than that of the Mohr-Coulomb yield criterion. The difference in the direction between the bedding plane and the major principal stress governs the failure surface

of the soils. Mohr-Coulomb criterion is still isotropic and only reflects the effect of the intermediate principal stress, or, the b value; $b = (\sigma_2 - \sigma_3)/(\sigma_1 - \sigma_3)$ where $\sigma_1 \geq \sigma_2 \geq \sigma_3$ are the principal stresses. In triaxial compression, the major principal stress coincides with bedding plane (a plane is referenced by its outward normal), thus yielding the maximum strength; in triaxial extension, the major principal stress is perpendicular to the bedding plane, thus yielding the minimum strength. Yoshimine et al. (1996) in their landmark experimental work have conclusively shown that even for a constant b value, sand becomes softer and more dilative as the direction of the major principal stress is rotated from zero to 90 degrees with respect to the bedding plane. A similar observation was also made by Miura et al. (1986). During vertical propagation of shear waves, sandy soils are continuously subjected to rotation of major principal stress relative to the bedding plane which governs the response. There are only few models (described elsewhere in the thesis) which consider, albeit empirically, such inherent anisotropy effect on sand behaviour.

Plastic behaviour of sands occurs mostly from the action of shear stress. Plastic volumetric strain due to change in normal stresses are controlled by two mechanisms: consolidation mechanism and particle breakage. It is normally assumed that the former component is elastic because the majority of such strain is recoverable as it involves arrangement and re-arrangement of particles, whereas the latter component is plastic, as the physical change in the microstructure due to particle breakage is irreversible. The principal mechanism of the plastic volumetric strain for sand is due to the particle breakage. Such plastic volumetric strain in sands occurs when the isotropic stress reaches the order of magnitude of 10MPa (Pestana and Whittle, 1995). In the post particle breakage region, the behaviour of sand becomes less complex and gradually approaches to that of the clays with effect of initial density gradually fading out (Lade and Bopp, 2005). Hence, cap models like the Cam Clay model (Schofield and Wroth, 1968) or its derivate usually fits experimental behaviour; one such example is the model of Miura et al. (1984), where the plastic modulus is expressed in terms of bulk modulus, instead of shear modulus, considering the plastic volumetric strain as the prime component. Coupled with this, the fact that the physical mechanism of the seismic site response to the vertically propagating horizontally polarised shear wave is better understood than even the simple case of vertically propagating compressive-extensional body waves (Beresnev et al., 2002; Elgamal and He, 2004) did not

promote investigation of sand behaviour under isotropic or anisotropic compression as extensive as those under simple or torsional shear.

The foregoing discussion has been based on externally applied shear stress dependent behaviour. Sand also has some unique intrinsic features that influence its constitutive behaviour. Sand behaviour greatly depends on its coexisting void ratio and isotropic stress. These two parameters are used to describe the instantaneous state of sand with respect to the critical state. The monotonic stress-strain relationship of soils is often represented by hyperbolic function where the ultimate stress is reached asymptotically. Ultimate stress is reached at large strains and when such a stress is reached, the tangent modulus becomes zero. Then soil flows like a viscid fluid with a constant shear stress and exhibits no dilatancy induced volumetric strain. This state is defined as the steady state of deformation by Poulos (1981). This state is also the critical state in the plasticity based constitutive modelling of soils, and is often used to describe the bounding or failure surfaces. It has been observed that the constitutive behaviour of sand depends on its state, defined by the combination of void ratio and isotropic stress, relative to the critical state. An excellent experimental demonstration of this behaviour is available in Verdugo and Ishihara (1996). This concept was introduced by Roscoe and Poorooshasb (1963); Been and Jeffries (1985) and later on adopted in different mathematical form by Cubrinovski and Ishihara (1998a); Wang et al. (2002); amongst others. The state-dependence enables characterisation of sand depending on the degree of compaction within a given fabric. The critical state depends on the shape and size of grains (Poulos, 1985), while the instantaneous state depends on how dense the particles are packed within the same fabric. In the present state-of-the-art in sand modelling, critical state is often considered as a reference state. However, the critical state line is not invariant as it also depends on the stress path or more correctly, the deformation history leading to the critical state through continuous evolution of new fabric (Wan and Guo, 2001). Despite such complexities, principal constitutive parameters are expressed as functions of state parameter for sake of simplicity and limited understanding of the role of micro-structure on macroscopic expressions of stresses and strains.

There are several sand models in literatures with different levels of emphasis on different aspects of sand behaviour; no single model is currently considered either perfect or adequate for all problems. At present there is no benchmarking study on different plasticity based constitutive models of sand available. The selection of an appropriate model depends

upon the purpose of analysis and there will be always a compromise between accuracy or mathematical rigour and pragmatism. In seismic response analysis, it is generally assumed that vertically propagating shear wave causes bidirectional horizontal ground motions. In this backdrop, the objective of the thesis is to develop a computationally efficient and simple three dimensional constitutive model for SFSI analysis in liquefiable sand with bidirectional ground motions. The seismic stress path is orthogonal to triaxial stress path. Hence, complications arising from consideration of different b values can be avoided for computational ease. The features of sand behaviour such as continuous accumulation of plastic strain during rotation of principal stress; non-coincidence of principal plastic strain increment with the principal stress and its effect on stress-dilatancy relation; state-dependence; effect of inherent anisotropy, play more vital role than the b value which can be considered as a constant at 0.5 for bidirectional seismic stress paths. The model should require a minimum numbers of parameters for definition all of which can be obtained from experiments in a straight-forward manner; the model parameters should have clear physical interpretation and must not be mere curve-fitting parameters. It is desirable that various postulations of the plasticity theory should be framed empirically by observing experimental sand behaviour in order to reinforce the theory with physical understanding.

1.3 Scope

The sand model formulated by Cubrinovski and Ishihara (1998b) has many desirable features discussed in the preceding section. The model is based on the earlier contributions by Kabilamany and Ishihara (1990); Gutierrez et al. (1991, 1993); Cubrinovski and Ishihara (1998a). The unique features of this model are as follows.

1. Hypoplastic flow rule. The hypoplastic flow rule was postulated by Gutierrez et al. (1991) by observing how the direction of plastic strain increment changed along the deviatoric neutral stress path as well as with the magnitude of the deviatoric principal stress in a series of experiments on hollow cylindrical air-pluviated Toyoura sand specimens in a torsional shear apparatus. The hypoplastic flow rule enables to predict accumulation of plastic strain strain, and hence dilatancy induced volumetric strain, even along neutral stress paths (i.e. rotation of principal stresses).
2. Strain-dependent stress-dilatancy relation. Strain dependent stress-dilatancy relationship was formulated by Kablimany and Ishihara (1990). The underlying

concept was the same as the Granta-gravel model (Schofield and Wroth, 1968) that sand is rigidly plastic with no recoverable strain, and the energy dissipated in deforming a sand mass is proportional to the isotropic stress or simply, the confining pressure. However, in contrast to the Granta-gravel model, the dissipated energy normalised by the confining pressure is assumed to vary with the plastic shear strain and is well-supported by experimental findings. In fact such correlation between the dissipated energy and the plastic shear strain has been found to be independent of stress paths as well as the state parameters. At large strains, the relationship converges to the concept of critical state soil mechanics, such as the Granta-gravel model, as the rate of dissipation of energy with the plastic shear strain becomes constant.

3. Non-coaxial stress-dilatancy relation. Gutirrez et al. (1993) modified the stress-dilatancy relationship to incorporate the effect of non-coincidence of principal plastic deviatoric strain increment and the principal deviatoric stress. This resulted in more dilative response than the case where there is coincidence. This phenomenon was experimentally observed earlier by Wong and Arthur (1986).

4. State dependence. Cubrinovski and Ishihara (1998a,b) formulated the failure surface and the strain hardening relationship as functions of the state parameter. The state parameters continuously change during a deformation process thereby affecting the overall constitutive behaviour. This can be viewed as a macrosopic expression of the deformation induced change in the micro-structure.

This model has been successfully implemented in many case studies involving seismic response analysis and also in verification of shake table and centrifuge tests. However, the entire model formulation is based on plane-strain and cannot be applied for three dimensional situations, such as in SFSI analysis with bidirectional ground motions.

The scope of thesis is to enhance the mathematical capability of the model to three-dimensions. The principal constitutive relations of the two-dimensional model will be adopted in their exact form. The two-dimensional model should be a true subset of the proposed three dimensional model. However, the cyclic hardening rule for anisotropic failure surface needs to be simplified for computational reasons and this is proposed to be achieved by adopting Mroz's approach (Mroz, 1967). The focus of the thesis is on the plasticity based constitutive modelling of sandy soils.

1.4 Organisation of the thesis

The thesis is divided in seven chapters and one appendix. Chapter 1 discusses the regional seismic vulnerability arising from liquefiable soil conditions, in addition to the geological consideration. This chapter echoes the need of conducting three-dimensional SFSI analysis for proper seismic performance assessment of buildings, bridges and other lifeline structures constructed on liquefiable sand. Widespread liquefaction and consequent foundation failures had been observed during the recent Canterbury earthquakes. In order to carry out three-dimensional SFSI analysis in liquefiable sandy soils, there is a need for a computationally simple yet conceptually rigorous three-dimensional constitutive model. This provides the background for the chosen area of research. The principal constitutive behaviour of sand under cyclic loading is discussed to highlight the complexity of the problem. The plane-strain model formulated by Cubrinovski and Ishihara (1998b) has been chosen to develop the three-dimensional model. The model of Cubrinovski and Ishihara is specifically formulated for liquefaction behaviour. Therefore the model has the advantage that it elegantly captures the governing constitutive relations for liquefaction phenomenon in a relatively simple mathematical framework. It is thus most attractive amongst the contemporary models for its computational pragmatism.

Chapter 2 reviews the basic concepts and postulations of the rate independent incremental plastic flow theory to provide a background for the subsequent chapters of the thesis. This chapter also reviews the earliest application of the theory of plasticity to soils in the form of Mohr-Coulomb and Drucker-Prager yield criteria. Subsequent development of the 'cap' models is also discussed in the light of Granta-gravel and Cam-clay models. A major development in the theory of plasticity for soils is the bounding surface plasticity (Dafalias and Popov, 1977; Dafalias, 1986). Salient features of the bounding surface plasticity are also discussed in this chapter.

Chapter 3 provides a comprehensive review of the state-of-the-art 14 plasticity based constitutive models for shear deformation of sand under cyclic loading, out of which 11 are based on the concept of isotropic fabric and 3 on anisotropic fabric. These models can be considered as new generation models which are based on non-associated flow, eliminating the requirement of having a closed-form expression of the 'cap' yield surface. In all of such models, the flow is 'contained' (Chen and Baladi, 1985) by the stress-dilatancy relation.

These models being without active 'cap' surface are applicable for low to moderate effective pressure range without significant particle crushing.

Chapter 4 contains the derivation of the mathematical formulation of the three dimensional model along with detailed discussion. To facilitate an understanding of the existing plane strain model in a three dimensional context, the salient constitutive relations are recast in the framework of the bounding surface plasticity, with a degenerate yield criterion as a point, both at conceptual and computational levels. An anisotropic Drucker-Prager yield criterion is used as the definition of the bounding surface. The anisotropic definition is adopted merely to fit triaxial compression and extensional stress paths, while for seismic stress paths, the bounding surface becomes isotropic. The hypoplastic flow rule, where the direction of the plastic strain increment depends on the magnitude of the deviatoric stresses as well as the deviatoric stress increment, is interpreted as a classic case of radial projection rule with specific projection centre and image point. The hydrostatic component of the flow rule is obtained from the stress-dilatancy relation. The backbone curve for monotonic loading is also viewed upon as a special kind of distance mapping rule of the bounding surface plasticity. The hardening rule is interpreted as a deviant of approach of Mroz (1967) of homogeneous nested surface. The entire mathematical formulation is presented in tensorial notation for general stress state; the plane strain version can be obtained by suitably reducing the tensors in a straightforward manner to the order of two in two-dimensional stress space.

Chapter 5 is dedicated to the validation and verification of the model. The model is validated using a single set of parameters for undrained simple shear and triaxial stress paths; drained p-constant torsional and triaxial stress paths; and, undrained cyclic triaxial stress path. The high quality experimental data required for validation is collected from different literatures for dry-deposited Toyoura sand. As the model specialises on simulating bidirectional shear stress, it is necessary to verify the algorithm for cyclic bidirectional stress paths of realistic complexity. In order to achieve the level of complexity in bidirectional stress paths as observed in actual ground motions, bidirectional shear stresses are generated from the horizontal components of two contrasting ground motions which are used for verification by drained p-constant simulations. This chapter also contains the results of undrained simulations under bidirectional shear stress, which highlight the importance of

considering bidirectional shear stress in seismic response analysis as the liquefaction resistance could be significantly lower than that of the unidirectional shear stress.

Chapter 6 identifies the scope for future research. Both the three dimensional model developed in Chapter 4 and the plane-strain model of Cubrinovski and Ishihara (1998b) are based on the assumption that the soil is in isotropic state prior to the shear deformation. In reality, soil is always under anisotropic stress in in-situ state due to lateral confinement, which needs to be incorporated within the existing framework. Moreover, as the bounding surface is of Drucker-Prager type, independent of Lode angle, it is complicated and difficult to simulate triaxial stress path. In order to overcome the aforementioned two limitations of the model, a novel expression for the dilatancy coefficient is proposed; and Lode angle dependent expressions for the bounding and the loading surfaces are developed along with the solution for the anisotropic hardening rule. Furthermore, it has been observed during model simulation that strain saturation occurs during cyclic mobility, which can be improved by suitably modifying the stress-dilatancy relation following the methods adopted by the other sand models. The validation of the two new plasticity based modelling features already developed herein and the improvement of the stress-dilatancy relation is identified as scope for future research.

Chapter 7 summarises the thesis and draws conclusion thereof. The thesis not only develops a three dimensional model on rigorous mathematical foundation, but also leads the direction for further improvement of the model by developing novel mathematical expressions. Another contribution of the thesis is it provides a holistic view of the state-of-the-art in constitutive modelling of sand behaviour.

Finally, the appendix contains the listing of the FORTRAN program developed for stress integration of the three dimensional model and its C++ interface for implementation in OPENSEES (Open System for Earthquake Simulation, downloadable from http://opensees.berkeley.edu/).

2.0 Review of the Theory of Plasticity

2.1 Introduction

The theory of plasticity provides a mathematical framework for plastic analysis of continua. More precisely, it is a method to derive an incremental stress-strain relationship during inelastic behaviour. Such stress-strain relationships are generally highly non-linear and thus, non-integrable, evolving continuously with plastic deformation and other physical states of a material. The variables pertaining to those physical states which govern the constitutive behaviour are collectively termed as state or internal variables. Identification of internal variables and their effects on constitutive behaviour are obtained experimentally and phenomenologically. Hence, plasticity theory may appear to be attractive for its elegant mathematical foundation, but its application still requires considerable empiricism and a phenomenological approach. The theory of plasticity plays a significant role in seismic response analysis which often requires non-linear dynamic analysis. In the finite element method, the incremental restoring, or hypo-elastic, forces are determined as: $\oint [B]^T \{d\sigma\}\, dV$; where the integral is over the volume V of a finite element; $[B]$ is the strain displacement matrix; and $\{d\sigma\}$ is the multiaxial incremental stress vector, which is a function of the incremental multiaxial strain vector $\{d\varepsilon\}$ and the internal variables. The relationship between $\{d\sigma\}$ and $\{d\varepsilon\}$, the so-called constitutive relationship, is obtained by the application of the theory of plasticity. The category of the theory of plasticity discussed herein is the rate-independent theory. A distinctive feature of this class of plasticity theory is that the incremental stress-strain relation is independent of strain or stress rate; or in other words, the deformation process is infinitely slow and rate-independent plasticity evolves as 'the limit of classical viscoplasticity for infinite slow processes' (Lubliner, 1990). Hence rate of straining has no influence, at least on theoretical considerations, on plastic behaviour.

The Theory of Plasticity was originally postulated to explain the behaviour of metals under multiaxial stresses at low temperature. However, the constitutive behaviour of metals and soils are significantly different. The Theory of Plasticity only provides a basis for the mathematical description of macroscopic physical behaviour of a continuum by assuming uniform physical properties across a finite volume under consideration. However, idealising soils as a continuum introduces more approximation than for the metals because soils are not only discontinuous, but are also highly heterogeneous. In order to alleviate such complexity

for engineering applications, it is usually considered that the scale of observation is sufficiently large to enable application of the theory by idealisation of soils as a continuum, relative to the actual physical complexity. In order to predict soil behaviour as closely as possible within the scope of computational feasibility, the classical form of the Theory of Plasticity has been greatly modified to bounding surface plasticity. Nevertheless, the central postulations remain the same as in the classical approach.

In this backdrop, the intent of this chapter is to provide an introduction to the Theory of Plasticity and its applicability to soil mechanics without delving into mathematical details which can be found elsewhere, yet maintaining the essential concepts; and wherever possible, providing a physical interpretation. A treatise on soil plasticity by Chen and Baladi (1985) is an excellent source on the evolution of the theory in soil mechanics.

2.2 Definitions of stress and strain

2.2.1 Stress

Generally there will be six components of stress acting on all six faces of an elemental volume represented as a rectangular parallelepiped as shown in Figure 2.1.

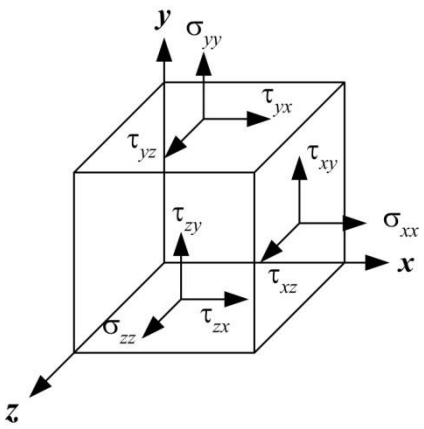

Figure 2.1 The complex stress state notation

Such a state of multidirectional stresses is known as the complex stress state. The first subscript represents the direction of the stress and the second subscript represents the plane of action (a plane is denoted by the direction of its outward normal); the reverse interpretation is also admissible. The stresses can be written as a single entity in matrix format:

$$\sigma_{ij} = \begin{bmatrix} \sigma_{xx} & \tau_{xy} & \tau_{xz} \\ \tau_{yx} & \sigma_{yy} & \tau_{yz} \\ \tau_{zx} & \tau_{zy} & \sigma_{zz} \end{bmatrix} \quad \textbf{(2.1)}$$

However, stresses are mathematically tensors because their transformation is given by the following relationship as shown in Equation 2.2 using the standard indicial notation (i.e. summation over repeated indices).

$$\sigma_{ij}{}' = t_{ik} t_{jl} \sigma_{kl} \tag{2.2}$$

where σ_{ij} and $\sigma_{ij}{}'$ are the stress tensors with respect to two different coordinate systems, with and without prime, respectively; t_{ij} is the direction cosine of the unit vector i of the primed coordinate system with respect to the unit vector j of the coordinate system without the prime; therefore, t_{ij} is an element of the transformation matrix. In the state of principal stress, the matrix representation will only comprise diagonal elements. Therefore, any given stress matrix can be diagonalised using the eigen solution method, where the eigenvector matrix represents the direction cosines of the three principal planes, or the transformation matrix t_{ij} between the general and principal stress planes. When the eigen solution is sought by the determinant method, then the parameters of the characteristic equation are known as the invariants, because they do not depend upon the choice of axis or the eigenvectors. Therefore, these parameters do not change by the transformation of the stress tensors, and are considered as the most important parameters in the theory of plasticity. Since there will be three eigenvalues, the characteristic equation will be cubic with three independent parameters. The expressions of these three parameters are given in Equation 2.3, where $|\sigma_{ij}|$ is the determinant of the stress tensor matrix.

$$\left.\begin{array}{c} I_1 = \sigma_{ii} \\ I_2 = \left(\sigma_{ij}\sigma_{ij} - \sigma_{ii}\sigma_{jj}\right)/2 \\ I_3 = |\sigma_{ij}| \end{array}\right\} \tag{2.3}$$

The stress tensor can be resolved in two components: the hydrostatic stress and the deviatoric stress, as shown in Equation 2.4.

$$\sigma_{ij} = \sigma_{kk}/3\,\delta_{ij} + s_{ij} \tag{2.4}$$

where δ_{ij} is the Kronecker delta function ($\delta_{ij} = 1$ for $i = j$; $\delta_{ij} = 0$ for $i \neq j$); $\sigma_{kk}/3\,\delta_{ij}$ is the hydrostatic stress tensor; s_{ij} is the deviatoric stress tensor (note that $s_{ii} = 0$). The inverse relationship between s_{ij} and σ_{ij} is represented as $s_{ij} = \mathrm{Dev}(\sigma_{ij}) = \sigma_{ij} - \sigma_{kk}/3$, where $\mathrm{Dev}(\sigma_{ij})$ is known as the deviatoric transform of the total stress tensor, σ_{ij}. The hydrostatic

stress produces only volumetric strain and the shape of the element is thus preserved; while the deviatoric stress produces only distortional strain and thus the volume of the element remains unchanged. In metal plasticity, the failure criterion in complex stress state depends only upon the deviatoric stress, sometimes also referred to as generalized shear stress. The method of determining principal deviatoric stresses and the formulae of the invariants are exactly the same as that of the total stress invariant. The deviatoric stress invariants are denoted by the symbols $J_1 = 0, J_2 = s_{ij}s_{ij}/2\,, J_3 = s_{ij}s_{jk}s_{ki}/3$, respectively.

2.2.2 Strain

The classical definition of strain rate is that it is a measure of relative velocity between two particles on an elemental volume. During a rigid-body movement, the relative velocity is zero, and hence, there is no material straining. In Figure 2.2, the instantaneous velocities of two particles situated at points P and Q are shown as v_i and $v_i + dv_i$ respectively, where dv_i is the relative velocity at Q with respect to P; the respective position vectors are denoted as x_i and $x_i + dx_i$. The relative velocity can be expressed as $dv_i = \left(\partial v_i/\partial x_j\right)dx_j$, following tensorial notation. The relative velocity is resolved in a pair of symmetric and anti-symmetric components as shown in Equation 2.5

$$dv_i = \dot{\varepsilon_{ij}}dx_j + \omega_{ij}dx_j \tag{2.5}$$

where

$$\dot{\varepsilon_{ij}} = \frac{1}{2}\left(\frac{\partial v_i}{\partial x_j} + \frac{\partial v_j}{\partial x_i}\right) \tag{2.5a}$$

$$\omega_{ij} = \frac{1}{2}\left(\frac{\partial v_i}{\partial x_j} - \frac{\partial v_j}{\partial x_i}\right) \tag{2.5b}$$

Thus, $\dot{\varepsilon_{ij}} = \dot{\varepsilon_{ji}}$ and $\omega_{ij} = -\omega_{ji}$; the component $\omega_{ij}dx_j$ is the component of the relative velocity due to rigid body rotation about the point P. The classical linear formulas of strain can be obtained by integrating Equation 2.5a with respect to time.

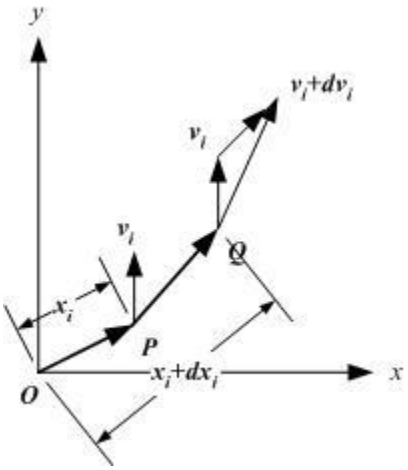

Figure 2.2 Instantaneous velocity of a deforming body, adopted from Chakrabarty (2006)

2.2.3 Objective stress rate

The stress rate $\dot{\sigma}_{ij}$ should vanish in the event of rigid body rotation. Such a definition of stress rate is known as the objective stress rate. When stresses are expressed with respect to a coordinate system attached to a deforming body, then the stress rate is known as the objective stress rate. The theory of plasticity deals only with the objective stress rate because during rigid body rotation strain does not occur and hence stress does not change, implying that the objective stress rate is zero. If stress is expressed with respect to a fixed coordinate system, mathematically stress changes even during rigid body rotation as the transformation matrix t_{ij} between the global and local coordinate system also changes; needless to say, such a change in stress is purely mathematical due to the spin tensor ω_{ij} and is not related to the constitutive behaviour.

2.3 General postulations in the rate-independent plastic flow theory

The central postulation of the plasticity theory is existence of a yield criterion. The yield criterion is the condition of yielding of a continuum in complex stress state, mathematically expressed as:

$$f(J_2, J_3, K) = 0 \tag{2.6}$$

where J_2, J_3 are the second and third deviatoric stress invariants; and K is a material parameter. A simplest example of yield criteria is Von-Mises yield criteria, shown in Equation 2.7, where σ_0 is the yield stress of a prismatic bar under uniaxial tension.

$$\sqrt{J_2} - \sigma_0/\sqrt{3} = 0 \qquad \textbf{(2.7)}$$

In view of Equation 2.6, material behaviour is governed by the theory of elasticity as long as $f < 0$. Equation 2.6 also represents a surface in stress space which envelopes all possible complex stress states (i.e. combinations of all six independent stress quantities of Equation 2.1) for elastic behaviour. Plastic behaviour only occurs when a stress state reaches the yield surface or satisfies Equation 2.6. Von-Mises criterion, given by Equation 2.7, is a cylindrical surface with the radius equals to $\sqrt{J_2}$ and the longitudinal axis inclined along the hydrostatic stress axis.

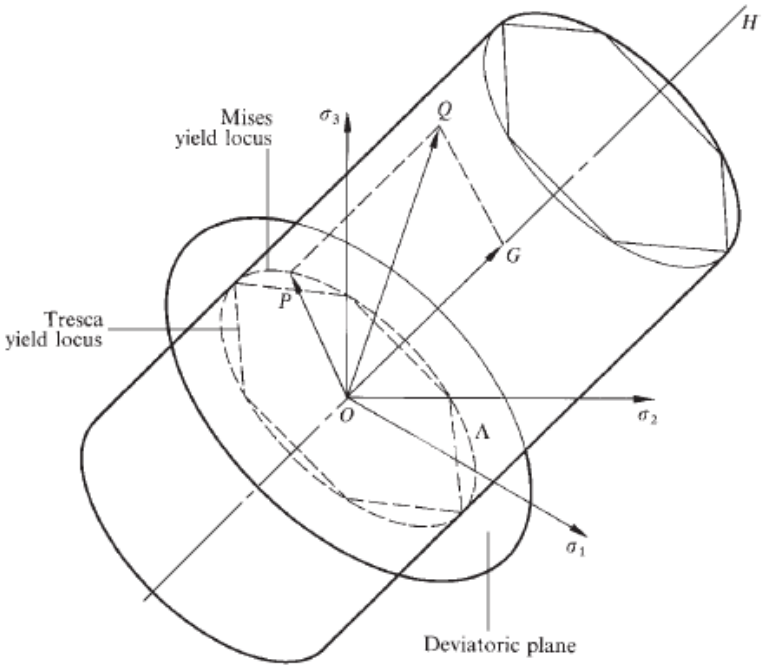

Figure 2.3 Geometrical representation of Von-Mises yield criterion in principal stress space, extracted from Chakrabarty (2006)

A physical interpretation of Von-Mises yield criterion is available in the text by Timoshenko (1940) where Von-Mises yield criterion has been derived by equating the distortional strain energy in a complex stress state to that of a prismatic bar of the same material under uniaxial tension at incipient yielding. Therefore, yield criterion can be also interpreted as a correlation of the physical state under complex stress with that of the simple stress. The distortional strain energy is a convenient measurable physical state which is invariant of the components of stresses involved.

It can be seen from Equation 2.7 as well as from Figure 2.3, elimination of J_3 results in a circular yield surface on the deviatoric plane (the cross-section of the cylinder).

Incorporation of J_3 in Equation 2.6 results in a more complicated shape of the yield surface with radius varying along the circumference. Dependence of yield criterion only on stress invariants implies that yielding depends only upon the magnitude of the principal deviatoric stresses rather than their directions, and thus tacitly assumes that material is isotropic. The isotropic yield criterion comprises six segments which can be folded upon each other. For non-circular yield criterion, it is easier to understand the role of J_3 by expressing the principal deviatoric stresses in terms of J_2 and J_3 using Equations 2.8 and 2.9, where $s_1 \geq s_2 \geq s_3$ are the principal deviatoric stresses. As shown in Figure 2.4, Equation 2.8 is actually a polar equation of an isotropic yield criterion. The condition of isotropy is implemented via the restriction on the range of θ from 0 to $\pm\pi/3$, which generates six foldable segments. One such example is the representation of Mohr-Coulomb failure criterion for geo-materials by the theory of plasticity for complex stress state.

$$s_1 = 2\sqrt{\frac{J_2}{3}}\cos\theta \qquad\qquad s_{2,3} = -2\sqrt{\frac{J_2}{3}}\cos\left(\frac{\pi}{3} \pm \theta\right) \tag{2.8}$$

where

$$\cos 3\theta = \frac{J_3}{2}\left(\frac{3}{J_2}\right)^{3/2} \qquad\qquad 0 \leq \theta \leq \frac{\pi}{3} \tag{2.9}$$

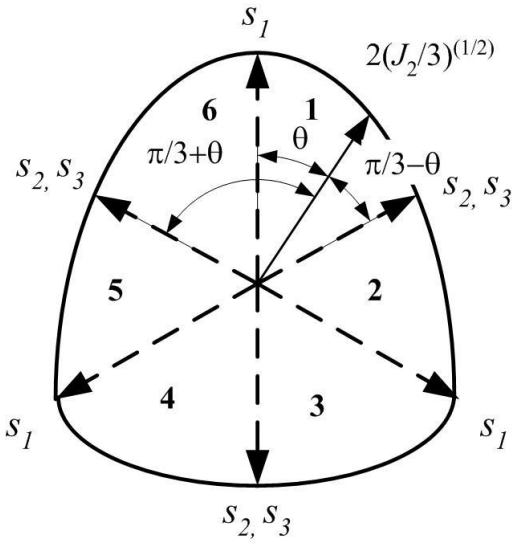

Figure 2.4 A generalised isotropic yield criterion expressed as a function of J_2 and J_3 comprising six foldable segments

During plastic behaviour, it is generally observed materials become soft resulting in a larger deformation than the elastic for a given stress increment. The deformation in excess of

the elastic deformation is considered as the plastic deformation. Hence, the second postulation is that the total strain increment $(d\varepsilon_{ij})$ is composed of elastic strain increment $(d{\varepsilon_{ij}}^{e})$ and plastic strain increment $(d{\varepsilon_{ij}}^{p})$ as shown by Equation 2.10.

$$d\varepsilon_{ij} = d{\varepsilon_{ij}}^{e} + d{\varepsilon_{ij}}^{p} \tag{2.10}$$

For hypo-elastic materials, stress increment is given as in Equation 2.11, which is the same as for the elastic behaviour. Hence, there is no direct relationship between the stress increment and the plastic deformation.

$$d\sigma_{ij} = E_{ijkl} d{\varepsilon_{kl}}^{e} \tag{2.11}$$

where $d\sigma_{ij}$ is the stress increment; and E_{ijkl} is the rank 4 constitutive tensor.

The plastic strain increment is given by Equation 2.12, which is also known as the so-called flow rule.

$$d{\varepsilon_{ij}}^{p} = d\lambda \frac{\partial g(J_2, J_3)}{\partial \sigma_{ij}} \tag{2.12}$$

where the function g is known as the plastic potential function with the same parametric form as the yield criterion. The gradient of the surface is the direction of the plastic strain increment, also known as the plastic flow. If the gradient is normalised, i.e. $\partial g/\partial \sigma_{ij} : \partial g/\partial \sigma_{ij} = 1$, then $d\lambda$ is the magnitude of the plastic strain. The directions of principal components of the plastic strain increment are the same as that of the principal stress components producing a unique direction of plastic flow. However, sand behaviour deviates from this uniqueness condition; the plastic flow is non-unique and depends additionally on the stress increment (Gutierrez, 1991).

The magnitude of the plastic strain increment is given as:

$$d\lambda = \frac{1}{H_p} \frac{\partial f(J_2, J_3)}{\partial \sigma_{ij}} d\sigma_{ij} \tag{2.13}$$

where H_p is the plastic modulus; and the function f is the yield criterion. The component of the stress increment along the gradient of the yield surface at a current stress point is the effective stress increment. H_p is determined from experimental monotonic stress-strain curve obtained from uniaxial stress state. If complex stress state such as triaxial test is used then the backbone curve is expressed in terms of second stress and strain invariants, respectively.

Since a single curve is used to describe the physical state under complex stress state, this postulation is also known as the single curve hypothesis (Kachanov, 1971). It appears that a physically better approach to relate uniaxial behaviour with that of the complex stress state is to express H_p as a function of the dissipated energy, rather than accepting the single curve hypothesis based on invariants which lacks a physical basis. It is frequently assumed plastic potential function is the same as the yield criterion $(g = f)$ on deviatoric plane. Such a case of plastic flow is known as the associated flow. However, non-associated flow i.e. $g \neq f$ is also assumed in some sand models, which are discussed in Chapter 3.

It is assumed in the rate-independent plastic flow theory that no stress point can lie outside the yield surface. Hence, the evolution rule of the yield criterion is given as Equation 2.14, which is also known as the so-called consistency condition.

$$df = 0 \tag{2.14}$$

In order to satisfy the consistency condition, the yield surface can undergo two types of evolution with the stress state: isotropic hardening and kinematic hardening. In the case of isotropic hardening, the yield surface expands uniformly in all directions while maintaining its shape, hence the terminology; in case of kinematic hardening, the yield surface translates rigidly in stress space. The isotropic hardening rule accounts for strain hardening while the kinematic hardening accounts for stress-induced anisotropy, such as Bauschinger effect in metals. In practice, a combination of the both types of hardening is often followed, which is known as the anisotropic hardening. The individual hardening rules are shown in Figure 2.5.

(a) **(b)**

Figure 2.5 Two types of hardening or evolution of yield surface: (a) isotropic hardening and (b) kinematic hardening, after Kachanov (1971)

The plastic flow theory is only applicable for work-hardening or stable materials. Figure 2.6 shows conceptually two possible kinds of real materials (Kachanov, 1971): case

(a) work-hardening or stable material as additional stresses do positive work ($\Delta\sigma\Delta\varepsilon > 0$); and case (b) work softening or unstable material ($\Delta\sigma\Delta\varepsilon < 0$).

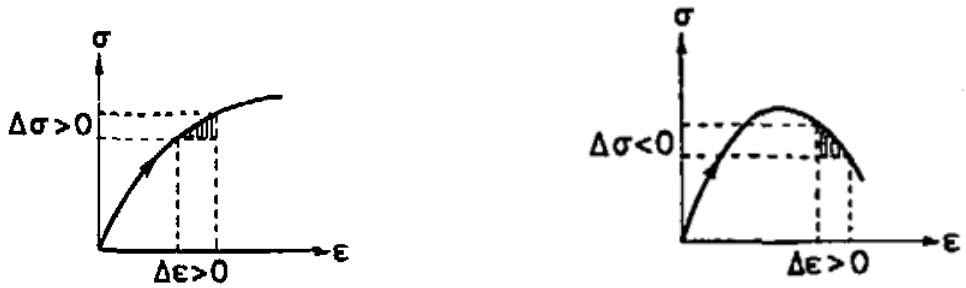

(a) **(b)**

Figure 2.6 Two kinds of material behaviour; (a) work-hardening or stable material; and (b) work-softening or unstable material after Kachanov (1971)

Drucker postulated that in a complete cycle of loading and unloading, during plastic deformation additional stresses cause dissipation of energy or perform positive work which is path-dependent, and during elastic deformation no work is performed. The corollary of this postulation is that the yield surfaces should be convex and the flow should be associated, as illustrated in Figure 2.7. The expression for the work done along the cyclical path A-B-C-A in Figure 2.7a is $\oint(\sigma_{ij} - {\sigma_{ij}}^0)d\varepsilon_{ij}$ which should be positive as the point C lies outside the yield surface Σ. Based on Equation 2.10, as the work done corresponding to the elastic deformation ${d\varepsilon_{ij}}^e$ should be zero, it simply follows that $\oint(\sigma_{ij} - {\sigma_{ij}}^0){d\varepsilon_{ij}}^p > 0$ which implies that $(\sigma_{ij} - {\sigma_{ij}}^0){d\varepsilon_{ij}}^p > 0$ along the path B-C because the paths A-B and C-A are elastic and hence the work done along these two paths will be zero. The geometrical interpretation of the inequality $(\sigma_{ij} - {\sigma_{ij}}^0){d\varepsilon_{ij}}^p > 0$ is that the yield surface should be convex and the flow should be associated, as illustrated in Figure 2.7b; Figure 2.7c shows a concave surface which violates the aforementioned inequality. The plastic flow theory is strictly applicable for stable or work-hardening materials.

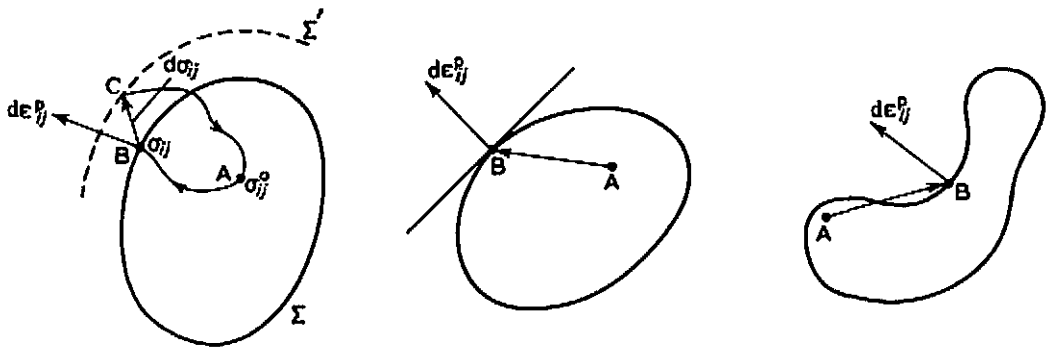

(a) **(b)** **(c)**

Figure 2.7 Geometrical interpretation of Drucker's postulation for work-hardening materials, after Kachanov (1971)

2.4 Soil plasticity: Mohr-Coulomb yield criterion

One of the earliest and most successful applications of the plasticity theory in soil mechanics is the representation of the Mohr-Coulomb failure criterion for complex stress state. The classical form of Mohr-Coulomb failure criterion is $s = c + \sigma \tan \phi$, where s is the shear stress; c is the cohesion; and ϕ is the angle of internal friction. In terms of principal stresses the Mohr-Coulomb failure criterion can be written as in Equation 2.15.

$$\sigma_1 - \sigma_3 = (\sigma_1 + \sigma_3) \sin \phi + 2c \cos \phi \tag{2.15}$$

where $\sigma_1 \geq \sigma_2 \geq \sigma_3$ are the principal stresses. Equation 2.15 is obtained from the Mohr circle along the plane of major and minor principal stresses (i.e. the $\sigma_1 - \sigma_3$ plane). It is to be noted that the Mohr circle is largest in this plane, providing an upper bound envelope of the Mohr-Coulomb failure criterion. The generalisation to complex stress is easily achieved by expressing Equation 2.15 in terms of stress invariants. By applying Equation 2.3 and 2.8, the following expressions can be derived: $\sigma_1 = I_1/3 + 2\sqrt{J_2/3} \cos \theta$ and $\sigma_3 = I_1/3 - 2\sqrt{J_2/3} \cos(\pi/3 - \theta)$. Substituting these expressions in Equation 2.15 renders the complex stress generalisation of the Mohr-Coulomb failure criterion, as shown in Equation 2.16.

$$\sqrt{3J_2} \left\{ \sqrt{3} \sin\left(\frac{\pi}{3} + \theta\right) - \sin \phi \cos\left(\frac{\pi}{3} + \theta\right) \right\} = I_1 \sin \phi + 3c \cos \phi \tag{2.16}$$

A geometrical interpretation of Equation 2.16 is illustrated in Figure 2.8. The yield criterion varies with the angle θ, or, the stress invariant J_3. In soil mechanics, such dependence is often attributed to the so-called b-value, where $b = (\sigma_2 - \sigma_3)/(\sigma_1 - \sigma_3)$, and $2b - 1 = \sqrt{3} \tan(\theta - \pi/6)$. Figure 2.8 shows that the Mohr-Coulomb failure criterion is isotropic,

consisting of six foldable segments, each subtending an angle of $\pi/3$ at the centre. In the figure, the reference planes of an elemental volume are denoted as 1, 2 and 3 respectively. It is to be observed that each major apex of the yield function simply represents the major principal deviatoric stress acting on the respective reference planes. Similarly, each minor apex represents the minor principal deviatoric stress acting on the same reference planes.

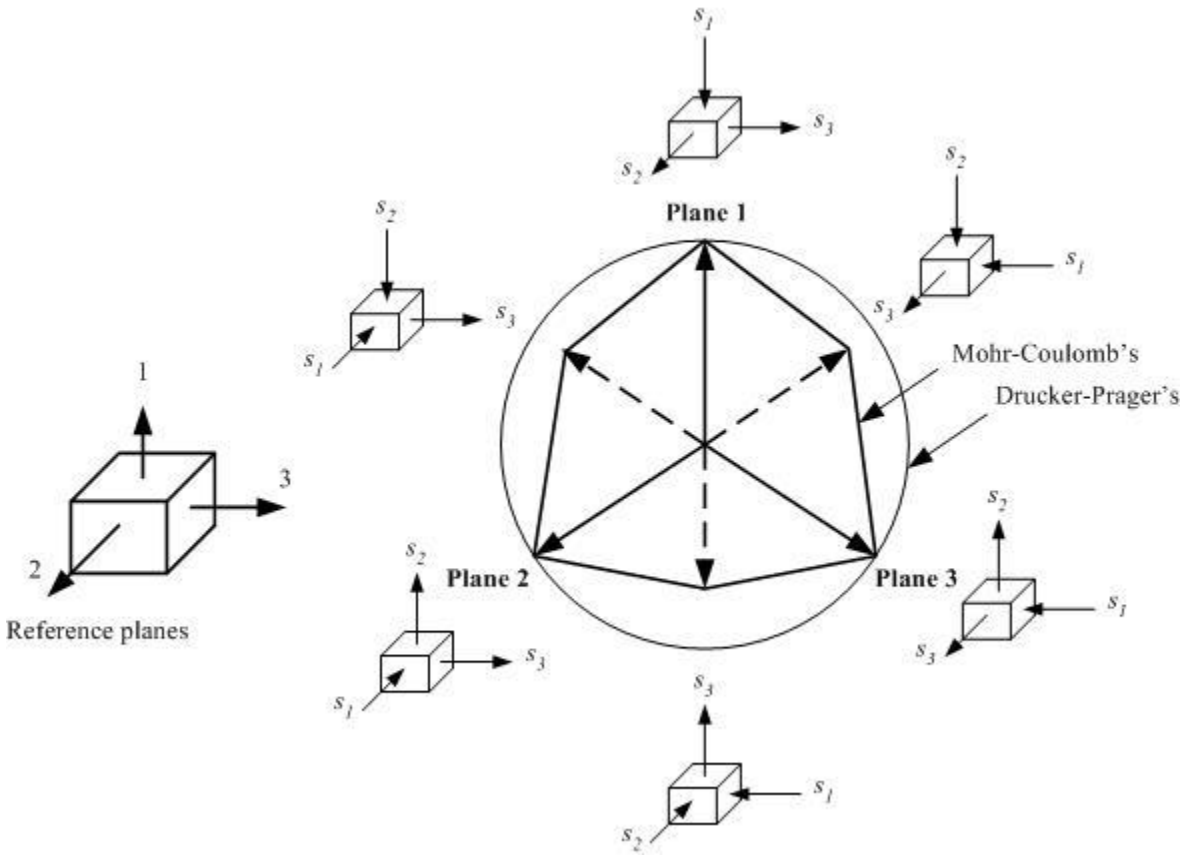

Figure 2.8 Representation of Mohr-Coulomb failure criterion for complex stress state; Drucker-Prager yield criterion; and interpretation of triaxial stress state by Mohr-Coulomb failure criterion

2.4.1 Interpretation of triaxial test

Triaxial compression simulates a principal stress condition with $\sigma_2 = \sigma_3$. Therefore, the principal deviatoric stresses are: $s_1 = 2/3\,(\sigma_1 - \sigma_3)$; $s_2 = s_3 = -1/3\,(\sigma_1 - \sigma_3)$. The negative sign indicates that stresses are extensional in nature. In triaxial extension, the principal stress condition is $\sigma_1 = \sigma_2$; thus, the corresponding principal deviatoric stresses are $s_1 = s_2 = 1/3\,(\sigma_1 - \sigma_3)$; $s_3 = -2/3\,(\sigma_1 - \sigma_3)$. The complex stress states in triaxial compression and extension are shown in Figure 2.8, with the corresponding major and minor deviatoric principal planes coinciding with each of the reference planes in turn. Therefore, the triaxial compression and extension are represented by the three major and three minor apices,

respectively. For granular materials, $c = 0$; therefore, the Mohr-Coulomb's failure criterion can be represented as: $\sqrt{J_2} - \eta p = 0$ for a given θ where $p = I_1/3$ is the effective confining stress and η is the so-called friction angle. The values of η in triaxial compression (η_{TC}), the major apex, and triaxial extension (η_{TE}), the minor apex, can be obtained by putting $\theta = 0$ and $\theta = \pi/3$, respectively, in Equation 2.15; the corresponding expressions are given in Equation 2.16.

$$\eta_{TC} = \frac{2\sqrt{3}\sin\phi}{3 - \sin\phi} \qquad \eta_{TE} = \frac{2\sqrt{3}\sin\phi}{3 + \sin\phi} \tag{2.17}$$

2.4.2 Drucker-Prager yield criterion

Although the Mohr-Coulomb failure criterion provides an elegant mathematical representation of the triaxial test, its discontinuous nature becomes a mathematical hindrance. A considerable simplification can be achieved by if a yield criterion can be formulated by eliminating J_3, i.e. of Von-Mises type, which will be matched with Mohr-Coulomb criterion for any given value of θ. In Figure 2.8, the Drucker-Prager yield criterion is shown matched with the Mohr-Coulomb at $\theta = 0$. However, such simplification fails to account for the b value. There are some examples of smooth rendition of the Mohr-Coulomb's criterion, such as that of Lade and Duncan (1975): $pJ_2 - J_3 - (pa)^3 = 0$, where $p = I_1/3$ and a is the parameter related to the friction angle η as: $a^3 = \eta^2 - 2(\eta/\sqrt{3})^3 \cos 3\theta$. Again, it is to be noted that matching between the Lade-Duncan and the Mohr-Coulomb is only possible for a single value of θ. Some more such examples are cited in Chapter 3, where several sand models are reviewed.

2.5 Critical state soil mechanics and the plasticity theory

The Mohr-Coulomb yield criterion represents a pyramidal surface in stress space which is an envelope outside which no stress point could lie; in other words, the surface delineates the possible from the impossible physical states. As per the foregoing discussion on the various postulations of the plasticity theory, it would be proper to consider the plastic potential function same as the yield function. The yield surface can be represented by a straight line in $q - p$ space, where q is some measure of $\sqrt{J_2}$ and $p = I_1/3$, along a given meridian or θ, as shown in Figure 2.9a. If the flow is assumed to be associated as per Drucker's postulation, then the normal of this line will be the direction of the plastic strain

increment. It can be seen that such an approach predicts very large negative dilatancy, where dilatancy is defined as the ratio of the plastic volumetric strain increment to the plastic shear strain, where the volumetric strain is $\dot{v}^p/v$ (v is the specific volume) and the plastic shear strain is $\dot{\epsilon}$. This contradicts actual soil behaviour. If the ultimate state of soil is considered as the critical state (Poulos, 1981), then the Mohr-Coulomb failure criterion is simply a mathematical representation of such an ultimate state, and is not a yield surface because yielding does not necessarily mean reaching the ultimate state.

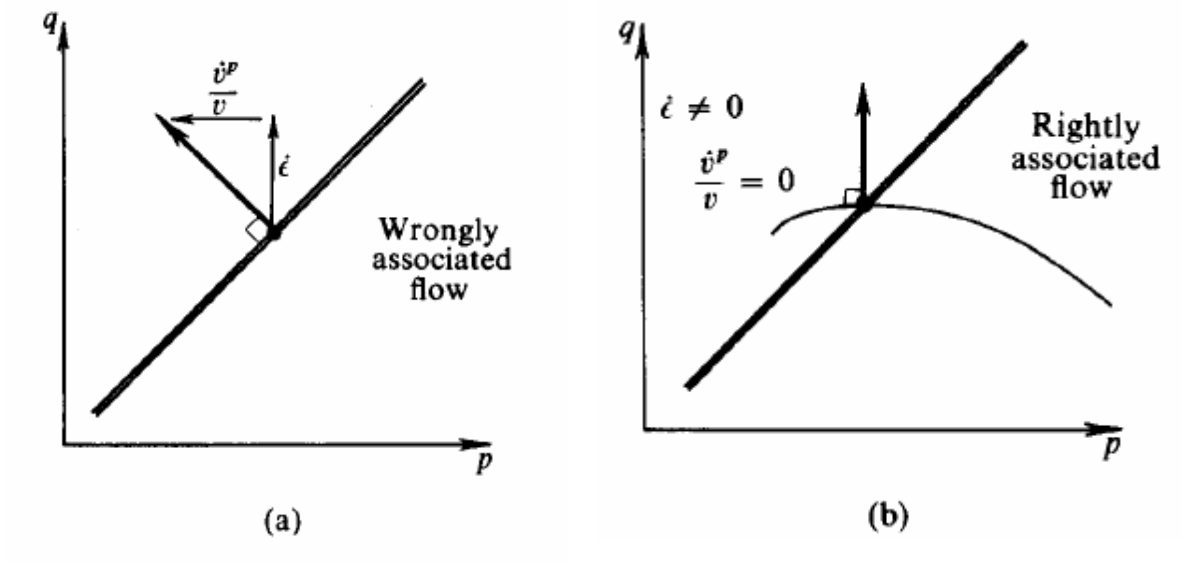

Figure 2.9 Application of the associated flow for the Granta-gravel and the Cam-clay models; taken from Schofield and Wroth (1968)

Therefore, the presence of another yield surface is conceived which strictly satisfies the criterion that at the critical state the dilatancy should be zero, as shown in Figure 2.9b. Since the curvilinear yield surface becomes a 'cap' closing the open end of the pyramidal or conical surface represented by the Mohr-Coulomb or the Drucker-Prager yield criteria, respectively, such models are often known as 'cap' models. The earliest models based on this concept are the Granta-gravel and the Cam-clay models (Schofield and Wroth, 1968). Furthermore, the stable physical states lie within the 'cap' surfaces, thereby satisfying Drucker's postulation for the work-hardening materials as shown in Figure 2.10.

The success of the Granta-gravel and the Cam-clay models lies in bridging the gap between critical state soil mechanics and plasticity theory. However, the applicability of such 'cap' models is very limited for sandy soils because the compressibility of sand is negligible as compared to that of the clays. In the majority of sand models, 'cap' surfaces are not

explicitly used. By assuming a suitable stress-dilatancy relationship, a 'cap' surface is implicitly implemented via stress integration as the primary purpose of the 'cap' is to predict realistic dilatancy values at various deviatoric stress levels.

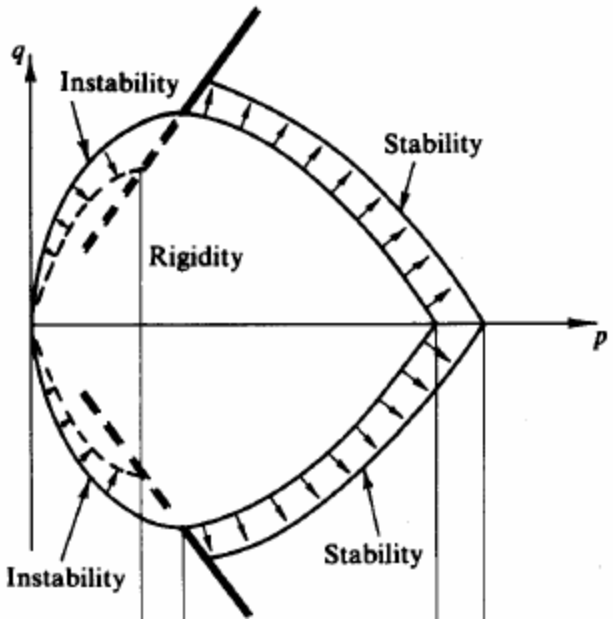

Figure 2.10 Yield surface of the Granta-gravel model, taken from Schofield and Wroth (1968)

2.6 Bounding surface plasticity

Soils behave inelastically even at low stress levels, which in view of conventional plasticity theory means a small yield surface degenerating to a point in the sense of limit. Bounding surface plasticity is a specialisation of the plasticity theory for materials with vanishingly small yield surface. This type of materials does not have any prominent yield point and reaches ultimate state asymptotically, with the plastic modulus degrading with increase in stress levels. A conceptual representation of such work-hardening function is shown in Figure 2.11 for a simple uniaxial stress state. As shown in the figure, the plastic modulus degrades as a smooth and continuous function of stress, finally reaching the minimum value at some limiting stress levels. These limiting stress levels are annotated as 'bound' in the figure; such a 'bound' is an isotropically expanding surface, similar to yield surface, in a complex stress state, and hence the terminology bounding surface plasticity. As shown in the figure, plastic behaviour begins when the stress is at a distance of δ_{in} from the 'bound' and then the plastic modulus continuously decreases with the distance δ; when the 'bound' is reached i.e. $\delta = 0$, the plastic modulus becomes constant given by the slope of the 'bound'. This concept is the cornerstone of the bounding surface plasticity. In soil mechanics,

the critical state is often conceptualised as a stationary bounding surface with zero plastic modulus.

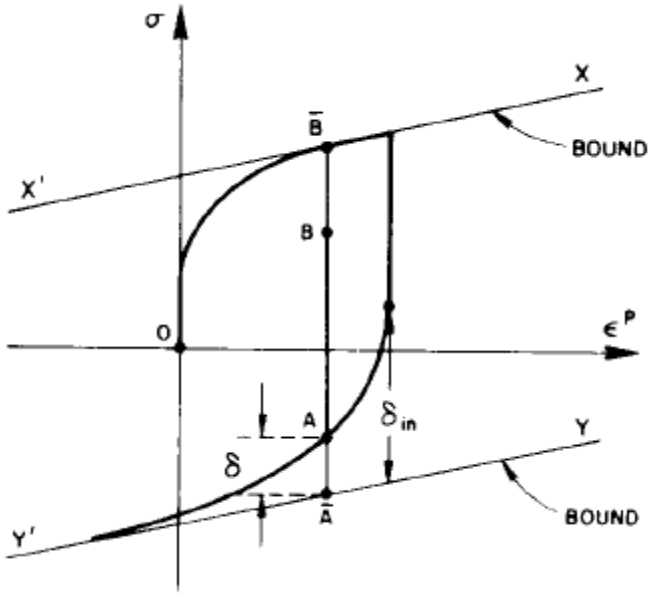

Figure 2.11 A schematic representation of a work-hardening material under uniaxial stress with plastic modulus degrading with increase in stress and attaining the minimum value at some bounding stress level, taken from Dafalias and Popov (1977)

The formal framework of bounding surface plasticity is shown in Figure 2.12, where α_{ij} and β_{ij} are the origin (the so-called deviatoric back-stress tensor) of the yield and the bounding surfaces, respectively. The stress point is shown as $a = \sigma_{ij}$ and its conjugate point on the bounding surface as $\bar{a} = \bar{\sigma}_{ij}$, which is known as the image point. It may be noted that points A and $\bar{A}$ shown in Figure 2.11 for the uniaxial case are the same as points a and $\bar{a}$ for the complex stress state. The hardening rule for the yield and bounding surfaces should be such that the yield surface approaches the bounding surface tangentially. This is similar to Mroz's kinematic hardening rule (Mroz, 1967) where a smaller yield surface reaches a stationary larger yield surface tangentially along the direction μ_{ij}. The kinematic hardening of the yield surface with respect to the bounding surface, drawing an analogy with the stationary larger yield surface of Mroz's kinematic hardening rule, is given as $\dot{\alpha}_{ij} - \dot{\beta}_{ij}$. Therefore, the condition of tangency becomes: $\dot{\alpha}_{ij} - \dot{\beta}_{ij} = M\mu_{ij}$ where M is a scalar multiple. In the special case of a vanishingly small yield surface, $\alpha_{ij} = \sigma_{ij}$, the bounding surface plays the role of yield surface for determining the loading direction ($\partial f/\partial \sigma_{ij}$ in Equation 2.13) as well as the direction of the plastic strain increment ($\partial g/\partial \sigma_{ij}$ in Equation 2.12) in view of Drucker's postulation of convex yield surface and existence of associated

flow. The gradient $\partial f/\partial \sigma_{ij}$ is evaluated at the image point, $\bar{a}$, and the plastic modulus depends on the distance δ between a and $\bar{a}$.

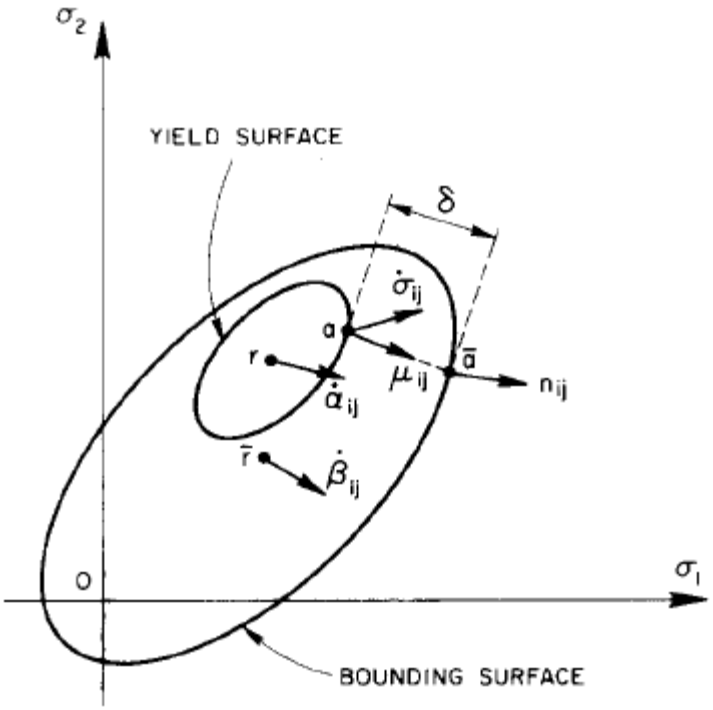

Figure 2.12 The formal framework of the bounding surface plasticity showing yield surface and the bounding surface for complex stress state taken from Dafalias and Popov (1977)

It is evident from the foregoing discussion that the success of bounding surface plasticity depends on how the image point is located. There should be a one-to-one geometrical relation between the stress point and the image point, termed the mapping rule, which can be defined in numerous ways. The most widely followed mapping rule is known as the radial mapping rule, postulated by Dafalias (1986). The rule can be simply stated as $\bar{\sigma}_{ij} = b(\sigma_{ij} - \alpha_{ij}) + \alpha_{ij}$, where b is a scalar multiple and α_{ij} is known as the projection centre which is conceptually the same as the deviatoric back-stress tensor of an yield surface. During the first cycle of loading, $\alpha_{ij} = 0$, and during the load reversal, α_{ij} is the stress reversal point which is constant during a current loading cycle until the subsequent load reversal occurs updating α_{ij}. Several examples of such constitutive models of sandy soils are cited in Chapter 3. In models with vanishingly small yield surface degenerating to stress point, $\alpha_{ij} = \sigma_{ij}$, as previously discussed, the radial projection rule is applied along the direction of stress rate, l_{ij}, which is a special case of hypoplasticity. Thus, for hypoplastic materials, the strain rate depends additionally on the stress rate. The mapping rule for such

materials can be easily modelled as $\bar{\sigma}_{ij} = \sigma_{ij} + bl_{ij}$ where l_{ij} is the direction of $\dot{\sigma}_{ij}$; now the plastic strain rate depends on $\dot{\sigma}_{ij}$, via the image point. This rule was postulated by Dafalias (1986) and is followed in the proposed three-dimensional formulation of the stress-dilatancy model presented in Chapter 4. Finally, the expression of the plastic modulus is modified by Dafalias (1986) as shown in Equation 2.18 (Equation 28 of Dafalias, 1986).

$$K_p = \bar{K}_p + h(\|\boldsymbol{\delta_{in}}\|)\frac{\boldsymbol{\delta}:\boldsymbol{n}}{\langle(\boldsymbol{\delta_{in}} - \boldsymbol{\delta}):\boldsymbol{n}\rangle} \tag{2.18}$$

where K_p is the plastic modulus at the current stress point; $\bar{K}_p$ is the plastic modulus related with the rate of isotropic hardening of the bounding surface with plastic strain; $\boldsymbol{\delta_{in}} = \bar{\sigma}_{ij} - \alpha_{ij}$ (bold-faced notations are tensor quantities shown without the subscripts); $\boldsymbol{\delta} = \bar{\sigma}_{ij} - \sigma_{ij}$; $\boldsymbol{n}$ is the gradient of the bounding surface at $\bar{\sigma}_{ij}$; h is a scalar shape hardening parameter; $\|.\|$ is the double contraction tensor operation on a single tensor quantity; $\langle . \rangle$ is the Macaulay's bracket. As the stress-strain relationship either in uniaxial stress state, or in principal stress state, such as in triaxial test, is always observed along the direction of the plastic strain increment, the distance between the stress and its corresponding image point in Equation 2.18 is also considered along the direction of the plastic strain increment given as $\boldsymbol{n}$ in view of the associated flow rule. Moreover, as the yield surface is always considered as a point in the bounding surface approach, the consistency condition is trivially satisfied at every point within the bounding surface. Therefore, the distance mapping rule of Equation 2.18 offers an alternative way to determine the plastic modulus. Bounding surface plasticity has achieved significant success in modelling of sand behaviour under complex cyclical loading conditions.

2.7 Summary

This chapter presented a formal introduction to rate-independent plasticity theory in a succinct manner with a focus on the physical interpretation of the theory. While the purpose of this chapter was to establish a conceptual link between the plasticity theory and its applicability to the soil mechanics, some discussions on the basic mathematical concepts, such as definition of stress tensors, physical interpretation of material straining during motion, stress invariants, objective stress rates, Drucker's postulations of convex surfaces and associated flow, are felt necessary because these concepts are building blocks of the theory.

It is emphasised that the plasticity theory does not provide any independent failure criterion for geo-materials; it rather provides a mathematical expression for applying the Mohr-Coulomb failure criterion for complex stress state. The Mohr-Coulomb failure criterion is strictly isotropic but recognises the effect of the intermediate principal stress, which is equivalent to the Bauschinger effect in steel. To elucidate this concept, the principal deviatoric stress conditions during triaxial test are interpreted with respect to the Mohr-Coulomb failure criterion. The Drucker-Prager yield criterion as the simplest possible yield criterion for granular materials is discussed. Lade-Duncan yield criterion is also presented as an example of smooth rendition of the Mohr-Coulomb yield criterion.

The real success of plasticity theory in soil mechanics was the introduction of 'cap' surfaces as a result of the understanding that Mohr-Coulomb, or any equivalent yield criteria are failure surfaces that depict only the ultimate stage which culminated from a multitude of successive yielding. This idea necessitated consideration of a separate 'cap' surface, not only to define yielding from the viewpoint of the theory, but also to distinguish yielding from failure. The examples of the Granta-gravel and the Cam-clay models are cited in this context.

The chapter concludes with a discussion on bounding surface plasticity, which not only provides a solution for materials with vanishingly small yield surfaces, but also lays down an elegant framework for defining plastic modulus during complex cyclic loading dispensing with the need of any elaborate multiple yield surface approach of the classical theory. In fact, the majority of plasticity-based sand models, with and without cap, are founded on the bounding surface plasticity approach.

3.0 Review of plasticity- based constitutive models for shear deformation of sands under cyclic loading

3.1 Introduction

The theory of plasticity assumes a material to be homogeneous continuum and represents average stresses and strains at an element level. However, soil being granular and discontinuous medium, its constitutive behaviour is largely influenced by the disposition of grains (the so-called fabric) and their mutual kinematic and dynamic interaction. The plasticity theory does not have any framework to explicitly consider the effects of micro-mechanical features, such as the influence of fabric, on constitutive behaviour. Hence, the general approach is to frame empirical constitutive relations at a macroscopic level, which supposedly consider the micro-mechanical effects, and at the same time can be conveniently handled by the plasticity theory. Due to such empiricism, which also reflects the limited understanding of the constitutive behaviour under complex stress state, there is a lack of unified approach in constitutive modelling of soils leading to several plasticity-based models varying widely in concept and formulation.

In this context, the present chapter reviews the chronological development of the plasticity theory based constitutive models for shear deformation of sands for complex cyclic loading conditions, which are encountered during earthquake induced ground motions, by scrutinising 11 models based on isotropic fabric and 3 models based on anisotropic fabric. The review is primarily focussed on the mathematical representation of the physical constitutive mechanisms for complex stress state under general loading condition. This has been a major challenge in the area of plasticity-based modelling because the principal constitutive relations have been established under proportional loading condition for simple stress states which are not often encountered in real situations. The review also elaborated upon relatively new theoretical considerations that have been postulated to address the complex behaviour of sand under different physical conditions.

The other perspective of the review could be to examine the comparative performance of the models for practical requirement, such as in terms of matching with liquefaction resistance curve; monotonic and cyclic stress-strain response; and verification of case histories. The author is not aware of any benchmarking studies on the aforementioned aspects of the models; scrutinising the models to such a depth on a common set of criteria is an

onerous task and is beyond the present scope of research. However, an attempt has been made to emphasise the key postulations for certain behaviour of sand which are partially understood, and are yet to be experimentally verified. Table 3.1 provides a comparative summary of the examined models elaborated upon herein.

3.2 New generation versus classical 'cap' based models

The early plasticity-based models, such as the Cam clay model of Schofield and Worth (1968), were based on the concept of 'cap' surface that permitted to apply the associated flow rule while restricting the predicted dilatancy to that of the observed behaviour. While these models were elegant in concept, they only addressed monotonic behaviour along triaxial stress path. However, during earthquakes the vertically propagating horizontally polarised shear waves impose complex cyclic stress paths which are orthogonal to the triaxial stress path and cause significant rotation of principal stresses. The classical soil plasticity being primarily based on monotonic stress path in principal stress space is inapplicable for seismic response analysis.

The new generation of constitutive models used successfully in seismic response analysis involving liquefaction behaviour of sand are: Prevost (1985); Bardet (1986); Wang et al. (1990); Cubrinovski and Ishihara (1998b) (the model was originally formulated by Cubrinovski, 1993); Manzari and Dafalias (1997); Li and Dafalias (2000); Li and Dafalias (2002); Li and Dafalias (2004); Li (2002); Yang et al. (2003); Dafalias and Manzari (2004); Dafalias et al. (2004); Yang and Elgamal (2008); Zhang and Wang (2012); amongst others. A close review of these new generation models reveals that unlike classical soil plasticity, two independent plastic mechanisms of shear and volumetric deformation are assumed. Each of these mechanisms separately produces plastic shear and volumetric strains. The respective hardening parameters of the two independent mechanisms are the plastic shear strain and the plastic volumetric strain, and therefore, the corresponding plastic moduli are the shear modulus and the bulk modulus. Because these models specialise on predicting liquefaction behaviour, the plastic volumetric mechanism is dormant, and in some models implicitly ignored as could be understood from the review of the aforementioned new generation models reviewed herein, for reasons elaborated upon below.

In contrast to the aforementioned approach of the new generation models, the models based on the classical soil plasticity approach comprising 'cap' surfaces, (e.g. Miura et al.,

1984; Yao et al., 2004) consider only the volumetric mechanism. Applicability of such classical 'cap' based models is restricted to high effective pressure region where particle crushing is imminent, such as in the stability analysis of high embankments and dams, calculation of point resistance of piles etc. Studies on the compression behaviour of sand are limited. In one of such pioneering work by Pestana and Whittle (1995), the authors have conclusively shown that there is a threshold pressure, equivalent to pre-consolidation pressure of clays, at which particles begin to crush; thereafter, the void ratio (e) and effective pressure (p) response becomes unique and independent of the initial state, similar to that of the normally consolidated clays. The authors coined the term 'Limiting Compression Curve' (LCC) to describe the $e - p$ response in the particle crushing region. The threshold pressure in case of sand is typically in the order of magnitude of mega-pascal (e.g. 5.5MPa at e = 1 for Toyoura sand) as shown in Figure 3.1.

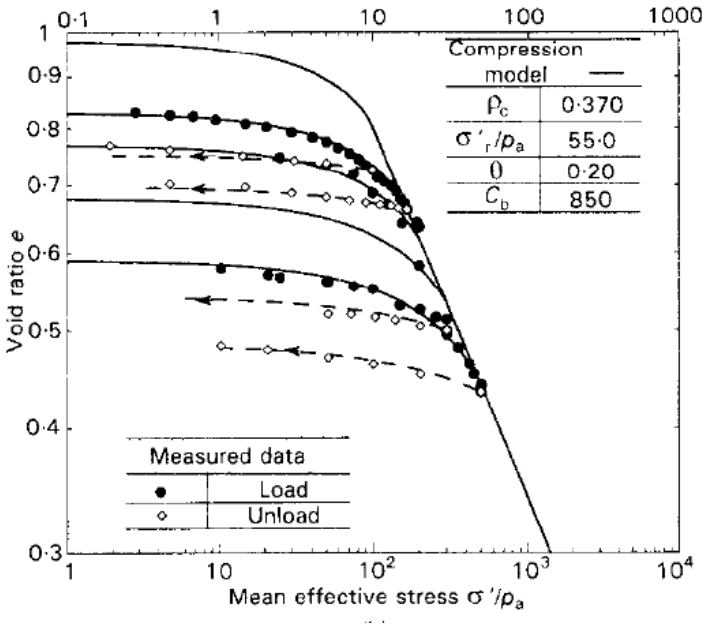

Figure 3.1 Isotropic compression of Toyoura sand showing existence of Limiting Compression Curve (LCC) in particle crushing region with the threshold pressure of 5.5MPa at void ratio of 1.0 and merging of compression lines with LCC at effective pressures exceeding 10MPa, after Pestana and Whittle (1995) and Miura et al. (1984);

The LCC defines the failure surface of the volumetric mechanism. A recent study by Lade and Bopp (2005) on high pressure isotropic compression of sands have also shown specimens with different initial void ratios converge to a unique relation like clays, thereby supporting the concept of LCC. In 'cap' models, LCC is the hardening parameter and is generally approximated as a straight line in $e - \log p$ space. Pestana and Whittle (1995) have

used the distance mapping rule of bounding surface plasticity (Dafalias, 1986) to derive the plastic bulk modulus at lower effective pressures based on the distance from the LCC at a given void ratio.

The effective pressure at shallow depth, where soil is susceptible to liquefaction (generally at depths not exceeding 30m where the effective confining pressure in saturated condition is in the range of 0-300kPa), is so insignificant as compared to the LCC that the volumetric mechanism can be reasonably assumed to be elastic. Moreover, as the effective pressure diminishes during undrained response, and unless the maximum pressure which a soil has previously experienced is exceeded, the volumetric mechanism remains elastic. On the other end, at very high effective pressure conducive for particle crushing, the shear failure envelope such as Mohr-Coulomb criterion becomes sufficiently large in comparison to the actual shear stress justifying elastic shear deformation mechanism. Thus, in the most of the practical applications, it may be inferred that the shear and volumetric plastic mechanisms are disjointed; and hence the volumetric mechanism in the new generation models is invariably considered as elastic during liquefaction phenomenon, which can be considered as low effective stress problem.

Another distinguishing feature of the new generation models is the assumption of non-associated flow, eliminating the requirement of having a closed-form expression of a curved yield surface like that of a 'cap'. Chen and Baladi (1985) remarked that non-associated flow is admissible if the flow could be 'contained' for all possible stress paths. They referred to the stress-dilatancy relation as a means for containment of the flow. Thus, the flow is 'contained' by positive dilatation below the phase-transformation line (Ishihara et al. 1975); zero dilation on the phase-transformation line; and negative dilation above the phase transformation line. The new generation models contain the flow by adopting such stress-dilatancy relationships.

The key features of constitutive behaviour of sand in shear deformation mode that the aforementioned new generation plasticity based models collectively strive to address are:

1. The effect of inherent anisotropy. It is invariably assumed that the sand is transversely isotropic material. The isotropy is preserved along the bedding or the depositional plane. The models of Li and Dafalias 2002; Dafalias et al. 2004; Li and Dafalias 2004,

explicitly account for effects of such unidirectional fabric anisotropy on overall constitutive behaviour.

2. Exclusion of neutral stress path (neutral stress path in expeimental soil mechanics is often referred to as rotation of principal stresses at a constant magnitude which traces a circular stress path on deviatoric plane). Sands exhibit accumulation of plastic strain during neutral stress paths (Ishihara and Towhata, 1983; Wong and Arthur, 1985). The experiments conducted by Ishihara and Towhata using torsional apparatus, and Wong and Arthur by directional shear cell apparatus, involved rotation of principal stresses across the bedding plane. Hence, initially it was understood that such phenomenon was due to the inherent anisotropy. However, Wong and Arthur in their later work (Wong and Arthur, 1986) showed the same phenomenon by rotating the principal stresses along the bedding plane, which is considered to be isotropic; a large difference in the angle, up to 30°, was observed between the principal deviatoric stress and the plastic shear strain increment.

3. Critical state. The critical state characterises a state in which sands experience continuous accumulation of shear strain without strain hardening and dilatancy. At critical state sand flows like a viscid fluid. The physical state corresponding to the critical state is known as the steady state of deformation (Poulos, 1981). The existence of critical state implies existence of a bounding surface (Dafalias, 1986).

4. State concept. The constitutive parameters, particularly those related to the definitions of various plasticity-based modelling components, such as failure and dilatancy surfaces, and the elastic and plastic moduli depend on the instantaneous state of sand relative to the critical state. The state of sand is defined by the combination of the void ratio and the co-existing confining effective pressure. Critical state can be considered as the signature of a unique fabric that evolved as a result of plastic deformation mechanism leading to the critical state. The dependence of constitutive properties on the relative state is a macroscopic expression of the effect of continuously evolving microstructure or fabric during a plastic deformation process. This concept was popularised by Been and Jefferies (1985), and later on adopted in various models in different mathematical forms.

3.3 Models based on isotropic fabric

A detailed review of the following plasticity based models of sands is presented herein to understand the chronological development in this relatively new area of plasticity-based constitutive modelling for sands. The nomenclature adopted herein is to depict the key feature of the models and is not necessarily that of the respective authors. The following models assume an isotropic fabric.

- Multiple surface based model by Prevost (1985);
- Critical state and bounding surface based model by Bardet (1986);
- Hypoplastic and bounding surface based model by Wang et al. (1990);
- Hypoplastic and strain dependent stress-dilatancy model by Cubrinovski (1993); Cubrinovski and Ishihara (1998b);
- Bounding surface based model with state concept by Manzari and Dafalias (1997);
- Bounding surface with state dependent based dilatancy model by Li and Dafalias (2000) and Li (2002);
- Multiple surface based model without Lode angle effect by Yang et al. (2003) and with Lode angle effect by Yang and Elgamal (2008);
- Bounding surface based model with fabric effect on dilatancy by Dafalias and Manzari (2004);
- Bounding surface plasticity based on large deformation mechanism by Zhang and Wang (2012);

3.3.1 Multiple surface based model by Prevost (1985)

The model is based on multiple, homogeneous and nested yield surface approach of Mroz (1967). Therefore, each yield surface is also a locus of constant plastic modulus. The yield surfaces are circular and hence, the model only considers a fixed b value of 0.5 as the third stress invariant is zero. However, Prevost (1985) included an initial deviatoric back-stress tensor to simulate triaxial compression and extension behaviour. Associated flow rule is assumed for the deviatoric and non-associated for the hydrostatic components. The flow

rule for the deviatoric component is taken as the gradient of the active yield surface, as per the classical plasticity theory. A purely kinematic hardening rule is adopted. The radii of the family of yield surfaces can be determined from drained stress-strain curve (the backbone curve), where the stresses and strains are expressed as octahedral components. The model is conceptually simple. The practical advantage of this model is that one does not require any cyclic test for calibration, but at the same time accuracy of the model under cyclic condition could not be verified or improved; simple, conventional monotonic triaxial compression and extension test is sufficient. However, model validation was not presented. To demonstrate the computational strength of the model, a case study on seismic-induced liquefaction of a backfill behind a retaining wall was presented.

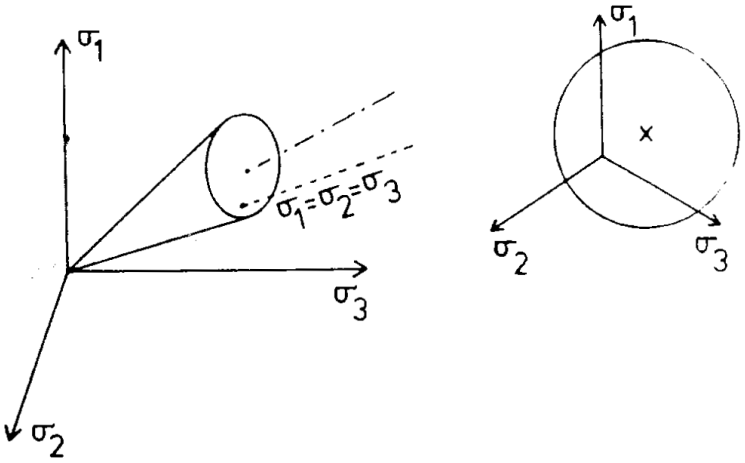

Figure 3.2 Yield surface in principal stress space, after Prevost (1985)

3.3.2 Critical state and bounding surface based model by Bardet (1986)

This model has several similarities to the Cam-clay model of Schofield and Wroth (1968). A bounding surface replaces the yield surface of the Cam-clay model in the recognition that there is no elastic nucleus. The analytical formulation of the bounding surface is elliptical in shear stress-effective pressure space, the same as the Cam-clay model, as shown in Figure 3.3. The gradient of the bounding surface at an image point gives the direction of the plastic strain increment. Hence, it can be inferred that an associated flow rule has been followed both for the deviatoric and the hydrostatic components. Therefore, dilatancy is given as normal to the bounding surface at the image point in shear stress-effective pressure space. The radial projection rule is adopted with the projection centre at the origin, as shown in Figure 3.3. The plastic modulus is obtained as sum of the plastic moduli at current stress point and at the corresponding image point. The plastic modulus at the stress

point is based on the distance mapping rule while that of the image point is obtained by applying consistency condition on the bounding surface. The bounding surface enlarges by translating its point of intersection with the hydrostatic axis along the isotropic compression line in void ratio-effective pressure space. Hence, the plastic modulus is expressed in terms of volumetric strain. The model was validated against both monotonic and cyclic triaxial compression and extension test on Sacramento and Fuji river sands. A good match can be observed in the high confining pressure range of 1MPa to 5MPa, which is typical of all 'cap' models. The model implicitly incorporates the particle crushing effect in this high pressure zone because plastic modulus is expressed in terms of bulk modulus instead of shear modulus.

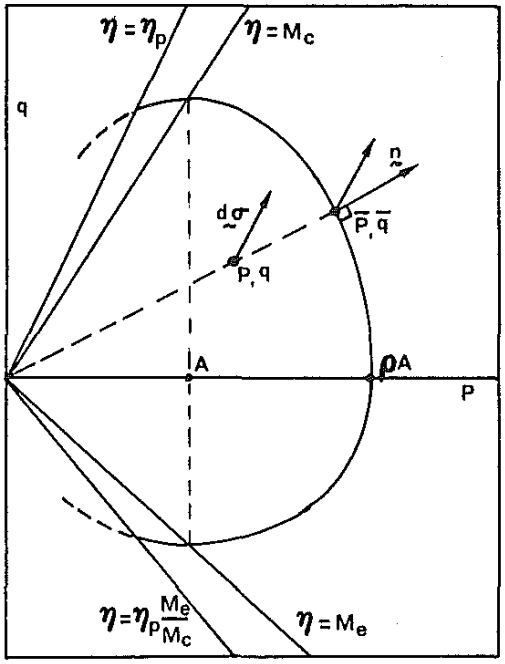

Figure 3.3 Bounding surface and projection rule, after Bardet (1986)

3.3.3 Hypoplastic and bounding surface based model by Wang et al. (1990)

This model is distinctive from the other models of its class and deserves more detailed discussion than the others. The motivation for the development of this model was to simulate behaviour of sands under the neutral or 'rotational' stress paths. Therefore, the prime requirement is that the model should be hypoplastic (Dafalias, 1986) so that the directions of principal stresses and those of the plastic strain increment become non-coaxial. In hypoplastic models, the direction of plastic strain increment depends on the stress rate. Another novelty of this model is that the stress dilatancy relation is not explicitly used.

The model considers both the deviatoric and hydrostatic mechanisms. The stress increment is therefore resolved in two components as shown by Equation 3.1 (Equation 3 of Wang et al, 1990).

$$\dot{\boldsymbol{\sigma}} = p\dot{\boldsymbol{r}} + \frac{\boldsymbol{\sigma}}{p}\dot{p} \tag{3.1}$$

where $\boldsymbol{\sigma}$ is the stress tensor (boldfaced symbols denote tensor quantities); p is the effective pressure; $\boldsymbol{r}$ is the deviatoric stress ratio; the corresponding symbols with dots represent the rate. The first term on the right hand side of the equation is the deviatoric mechanism and the second term, the volumetric mechanism. In the majority of the models for shear deformation of sands, only the deviatoric mechanism is considered plastic. The corresponding plastic strain increment is given by Equation 3.2 (Equation 5 of Wang et al, 1990).

$$\begin{aligned}\dot{\boldsymbol{\epsilon}}^{\boldsymbol{p}} = &\left(\frac{1}{H_r}\boldsymbol{n_D} + \frac{1}{3K_r}\boldsymbol{I}\right)(p\dot{\boldsymbol{r}}:\boldsymbol{n_N}) \\ &+ \left(\frac{1}{H_p}\boldsymbol{r} + \frac{1}{3K_p}\boldsymbol{I}\right)H(p - p_m)\langle\dot{p}\rangle\end{aligned} \tag{3.2}$$

where $\dot{\boldsymbol{\epsilon}}^{\boldsymbol{p}}$ is the total plastic strain increment; $\boldsymbol{n_D}$ is the direction of the deviatoric component of the plastic increment due to the deviatoric mechanism; $\boldsymbol{n_N}$ is the loading direction of the stress increment $\dot{\boldsymbol{r}}$; H_r and H_p are the plastic shear moduli (the suffixes denote the corresponding deviatoric and volumetric mechanisms); K_r and K_p are the plastic bulk moduli; $\boldsymbol{I}$ is the Kronecker delta; p_m is the maximum effective pressure which specimen has experienced in previous loading history; tensor operation $\boldsymbol{a}:\boldsymbol{b} = a_{ij}b_{ij}$; $H(.)$ is the Heaviside step function; and $\langle . \rangle$ is Macaulay's bracket. Therefore, p_m can be considered as the effective pressure at the end of a consolidation process prior to any undrained deviatoric action on the material. During undrained behaviour, the second term vanishes as $\dot{p} < 0$. From the deviatoric mechanism depicted by the first term of the equation, it can be seen that dilatancy is given as the ratio H_r/K_r; furthermore, the flow rule is non-associated as $\boldsymbol{n_D} \neq \boldsymbol{n_N}$.

The key model components are depicted in Figure 3.4. In this figure, $\hat{f} = 0$ is the bounding surface, and $\bar{f} = 0$ the virgin loading surface which forms during a consolidation process. The load reversal point is shown as $\boldsymbol{\alpha}$. The radial projection rule is followed with $\boldsymbol{\alpha}$ as the centre of projection to derive the direction $\bar{\boldsymbol{n}}$ at $\bar{\boldsymbol{r}}$ on $\bar{f}$. The direction $\hat{\boldsymbol{n}}$ at $\hat{\boldsymbol{r}}$ is obtained by considering $\boldsymbol{r}$ as the centre of projection along the direction of $\dot{\boldsymbol{r}}$. Now, the effective

loading direction $\boldsymbol{n_N}$ and the direction of plastic strain increment $\boldsymbol{n_D}$ are obtained by linear combination of $\bar{\boldsymbol{n}}$ and $\hat{\boldsymbol{n}}$ as shown in Equation 3.3 (Equations 14 and 15 of Wang eta al., 1990), where z_n and z_D are scalar multiples. Here lies the hypoplastic feature of the model. The plastic shear modulus is determined by the distance mapping rule between the projection centre $\boldsymbol{\alpha}$ and $\bar{\boldsymbol{r}}$.

$$\left.\begin{aligned} \boldsymbol{n_N} &= \boldsymbol{N_n}|\boldsymbol{N_n}|^{-1}; \quad \boldsymbol{N_n} = z_n\bar{\mathbf{n}} + (1-z_n)\bar{\mathbf{n}} \\ \boldsymbol{n_D} &= \boldsymbol{N_D}|\boldsymbol{N_D}|^{-1}; \quad \boldsymbol{N_D} = z_D\bar{\mathbf{n}} + (1-z_D)\bar{\mathbf{n}} \end{aligned}\right\} \tag{3.3}$$

The general polar form of the homogeneous surfaces of $\hat{f} = 0$ and $\bar{f} = 0$ is $Q = Q_c g(\theta, c)$ where Q_c is the stress ratio at critical state in triaxial compression and can be expressed in terms of $\sqrt{J_2}$ (J_2 is the second deviatoric stress invariant); c is the ratio of the stress ratios in triaxial extension to triaxial compression; θ is Lode angle; and $g(\theta, c)$ is an interpolating function to interpolate the radius for different values of θ between triaxial compression and triaxial extension; for triaxial compression, $g(\theta, c) = 1$ and for triaxial extension, $g(\theta, c) = c$. The parametric equation of the bounding surface: $Q = Q_c g(\theta, c)$ has been used in all subsequent bounding surface plasticity based models discussed herein.

It can be understood from the foregoing discussion that the model is immensely complex entailing 15 constants, out of which, only 6 constants have physical interpretation; the remaining 9 constants are highly empirical and data-fitting ones. The calibration method is also complicated. The calibration methods of the important parameters of z_n and z_D are not described, instead the respective values of 0.5 and 0.85 are adopted for model validation. The model shows good match with the experimental results for the various stress paths shown in Figure 3.5. In view of the complexity, it was remarked by the authors that the model is especially useful for complicated multidirectional stress paths 'involving pronounced feature of rotational shear'. The problem of rotational shear is mainly applicable for bidirectional cases on which there is a scarcity of experimental data and analytical studies (Kammerer, 2002). Therefore, the model performance is undetermined at the present. However, it is well understood that plasticity modelling for rotational stress paths is more challenging than that of the unidirectional stress path; this model can be considered as one of the early achievements in the application of the theory of plasticity for three dimensional simulation of constitutive behaviour of sand.

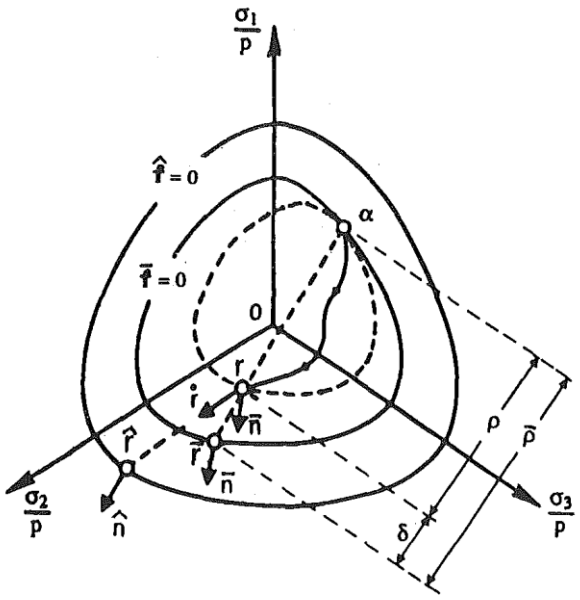

Figure 3.4 Illustration of the deviatoric mechanism in deviatoric stress space ratio, after Wang et al. (1990)

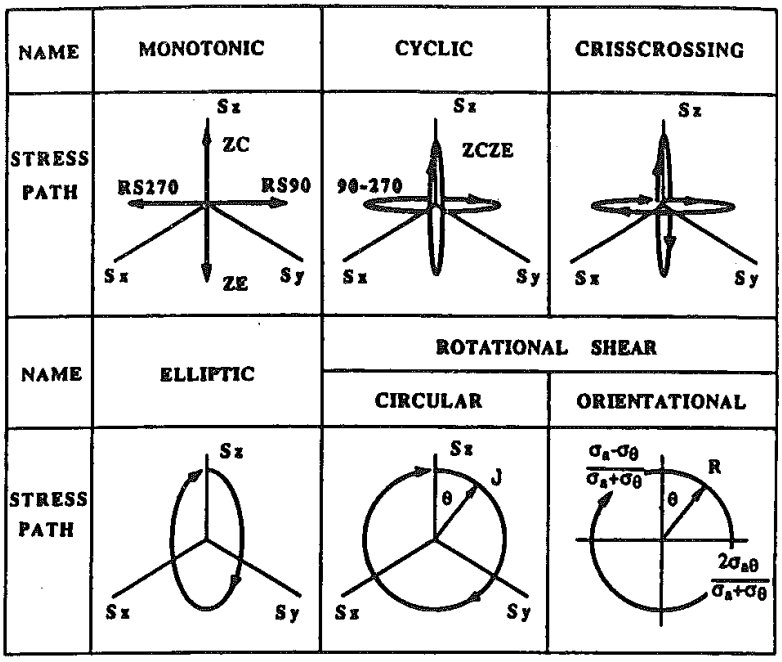

Figure 3.5 Various stress paths in deviatoric space used for model validation, after Wang et al. (1990)

3.3.4 Hypoplastic and strain dependent stress-dilatancy model by Cubrinovski (1993); Cubrinovski and Ishihara (1989b)

This model is the culmination of the previous works by Kabilamany and Ishihara (1990); Gutierrez et al. (1991); Gutierrez et al. (1993); Cubrinovski (1993). The main features of this model are: strain dependent and non-coaxial stress-dilatancy relation; hypoplastic flow

rule; and state concept. The state concept was introduced by Cubrinovski (1993); Cubrinovski and Ishihara (1998a). The model is formulated for plane strain configuration. The failure surface, which is analytically a bounding surface, is circular and isotropic. The flow rule shown in Figure 3.6 was postulated by Gutierrez et al. (1991) based on experimental findings. The gradient of the bounding surface at an image point gives the direction of the deviatoric plastic strain increment, $\boldsymbol{n}$ (boldfaced notations are vectors). The image point is located by a special projection rule with the centre of the projection at the current deviatoric stress ratio $\boldsymbol{r}$ and the direction along $\dot{\boldsymbol{r}}$. It is interesting to note that such hypoplastic flow rule was formalised earlier by Dafalias (1986) and was also implemented by Wang et al. (1990) in a variant form.

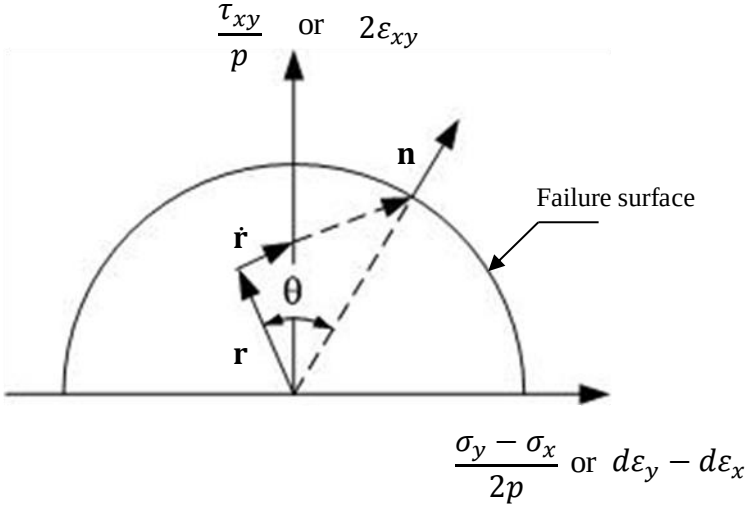

Figure 3.6 The hypoplastic flow rule postulated by Gutierrez et al., 1991

The stress-dilatancy relation is defined by Equation 3.4 and 3.5 respectively, which was originally derived by Kabilamany and Ishihara (1990) (Equation 3.4 and 3.5 are Equation 11 and 33 of Kablimany and Ishihara, 1990, respectively).

$$D = \frac{\mathrm{d}\varepsilon_v^p}{|\mathrm{d}\gamma|} = \mu - c\frac{q}{p} \tag{3.4}$$

where

$$\mu = \mu_0 + \frac{2}{\pi}(M - \mu_0)\tan^{-1}\left(\frac{\gamma}{S_c}\right) \tag{3.5}$$

$d\varepsilon_v^p$ is the plastic volumetric strain increment; $d\gamma$ is the plastic shear strain increment given as $\sqrt{\left(d\varepsilon_x - d\varepsilon_y\right)^2 + \left(2d\varepsilon_{xy}\right)^2}$ neglecting the contribution of elastic shear strain; q is the shear stress given as $\sqrt{\left\{\left(\sigma_y - \sigma_y\right)/2\right\}^2 + {\tau_{xy}}^2}$; p is the effective pressure given as $\left(\sigma_y + \sigma_y\right)/2$; and $c = \cos\theta$ is known as the non-coaxiality factor. The dilatancy coefficient μ is the slope of the normalised dissipated energy versus plastic shear strain plot. The parameters μ_0 and M are the slopes of the same plot at zero or small plastic strain and at infinite or large plastic strain at critical state, respectively; in view of Equation 3.4, M can be also set equal to the stress ratio $\eta = q/p$ at critical state, which is defined as the quasi steady state of Alarcon-Guzman et al. (1988). The parameter S_c is a reference plastic strain at which the slope is $(\mu_0 + M)/2$. The stress dilatancy relation is based on the approach similar to the Cam-clay model (Schofield and Wroth, 1968) with the underlying assumption that sand is rigidly plastic with no recoverable strain, and the dissipated energy is proportional to the effective pressure. When the dissipated energy normalised by effective pressure is plotted as a function of plastic shear strain, then a unique relation is observed which is invariant of the stress path as well as the current state. The derivatives or the slopes of this plot at small and large strain levels are μ_0 and M, respectively.

The state index is defined by Cubrinovski and Ishihara (1998a) as $I_s = (e_U - e)/\left(e_U - e_Q\right)$, where e_U is the void ratio of an upper reference line; e_Q is the void ratio of the quasi steady state line; and e is the current void ratio. The upper reference line is either the isotropic consolidation line at the loosest state or the horizontal line through the intercept of the quasi steady-state line with the void ratio axis. From the definition of the state index, it is apparent that when $I_s = 1$, the state is at critical or quasi steady-state; when $I_s > 1$, the state is denser than the critical and sand will undergo dilation; and when $I_s < 1$, the state is looser than the critical and will reproduce contractive behaviour. The reason for considering quasi-steady state as a reference state is to incorporate the effect of initial fabric on the constitutive behaviour of sandy soils via the state index. It was demonstrated by Zlatovic and Ishihara (1997) that the quasi-steady state line of medium to loose sand depends on sample preparation method, as different methods produce different initial fabrics. For example, it was shown in Zlatovic and Ishihara (1997) that the quasi steady state lines in the void ratio-effective pressure space of the samples prepared by dry-deposition method lies

above those prepared by moist-placement and water sedimentation method. The steady state lines, on the contrary, are achievable at such large strains [e.g. approximately 25 to 30% axial strain using a triaxial apparatus for Toyoura sand prepared by moist placement method (Verdugo and Ishihara, 1996)] where the signature of the initial fabric is lost. However, for medium to dense sand, which shows a dilative behaviour, quasi-steady state line may not exist as there is no drop in the deviatoric stress; in such cases the quasi-steady state and the steady state lines can be considered as the same. Although μ is considered as a material constant independent of I_s, the state dependent dilatancy behaviour is implemented through dependence of μ on strain γ, and γ depends on I_s via the plastic modulus.

The plastic modulus is obtained from a hyperbolic backbone curve, asymptotic to the radius of the failure surface (η_{max}) with an initial tangent (G_N). Both the parameters η_{max} and G_N depend linearly on I_s. Although the backbone curve is hyperbolic, which is strictly strain-hardening, the model is able to partially reproduce strain softening behaviour for sands denser than the critical through dependence of η_{max}on I_s, because η_{max} reduces as I_s approaches unity. A similar approach is followed in Dafalias and Manzari (1997), where strain softening or hardening behaviour depends on the size of the bounding surface relative to the critical state surface, which in turn depends on the relative state of sand.

The model adopts a mixed hardening rule for cyclic behaviour based on the concept of nested surfaces homogeneous to the failure surface. Each of such nested surfaces, termed as loading surface, is a locus of equal plastic modulus. The hardening rule is a specialisation of Mroz's approach with infinite surfaces. It is suggested in the literature that during load reversal, the value of c in Equation 3.5 also reverses sign, which can, therefore, simulate relatively large contractive behaviour during load reversals. However, this is not always the case because loading and unloading criterion is based on the geometry of loading surfaces, which has no connection with c, and there could be several instances of unloading under complex loading conditions when c does not change its sign. Therefore, applicability of Equation 3.5 is limited to more restrictive stress path along τ_{xy} which is always the case during plane-strain simulations of ground motions.

The practical viability and the veracity of the plane strain formulation of the model have been established by several numerical and experimental studies. Cubrinovski et al. (2008) cites further references where the stress-dilatancy model has been rigorously verified

by shake table and centrifuge tests. The model constants, in contrast to the general bounding surface models, have clear physical interpretation with least empiricism which renders the calibration process relatively simple.

3.3.5 Bounding surface based model with state concept by Manzari and Dafalias (1997)

This model is historically important because it is the first of its kind based on bounding surface plasticity comprising bounding, critical and dilatancy surfaces, respectively. These surfaces are Lode angle or J_3 (the third deviatoric stress invariant) dependent and are homogeneous. The critical surface, which represents critical state, is the reference surface. The other two surfaces evolve depending upon the state parameter defined by Been and Jefferies (1985) as $\psi = e - e_c$ where ψ is the state index; e is the current void ratio; and e_c is the void ratio at critical state. The relationships between these surfaces are given by Equation 3.6 (Equations 3a and 4a of Manzari and Dafalias, 1997, respectively).

$$\begin{aligned} M_c^b &= M_c + k_c^b\langle -\psi \rangle \\ M_c^d &= M_c + k_c^d \psi \end{aligned} \tag{3.6}$$

where M_c is the stress ratio at critical state in triaxial compression; M_c^b and M_c^d are the stress ratios at the bounding and dilatancy surfaces, respectively, in triaxial compression; k_c^b and k_c^d are positive material constants. Thus, for states denser than the critical, $M_c^b > M_c > M_c^d$; and vice-versa for states looser than the critical; at critical state, $M_c^b = M_c = M_c^d$. The model components are shown in Figure 3.7. The model assumes a very small but finite yield surface which can only undergo kinematic hardening. An associated flow rule is assumed in the deviatoric space. The purpose of introducing a small radius for the yield surface is simply to evaluate the direction of plastic strain increment. One important feature of this model is that the bounding surface is not considered as a failure surface and is primarily used to simulate strain hardening and softening behaviour, depending upon the state index, just before critical state is reached. The strain softening response is shown by sand denser than the critical and strain hardening response by sand looser than the critical (Verdugo and Ishihara, 1996), and hence the relation between the bounding and critical surfaces, as shown in Equation 3.6. The stress point $\boldsymbol{r}$ (boldfaced notations are tensors) can lie outside the bounding surface, thereby enabling a strain softening response prior to the attainment of critical state. The plastic modulus and dilatancy are dependent on the projected distances of $\boldsymbol{\alpha^b} - \boldsymbol{\alpha}$ and $\boldsymbol{\alpha^d} - \boldsymbol{\alpha}$ along

n, respectively. The model requires 11 constants, out of which, 5 constants are merely numerical parameters which are relatively difficult to calibrate. Model validation was shown for drained and undrained monotonic triaxial compression, and undrained triaxial cyclic tests. However, cyclic mobility is not well captured by the model.

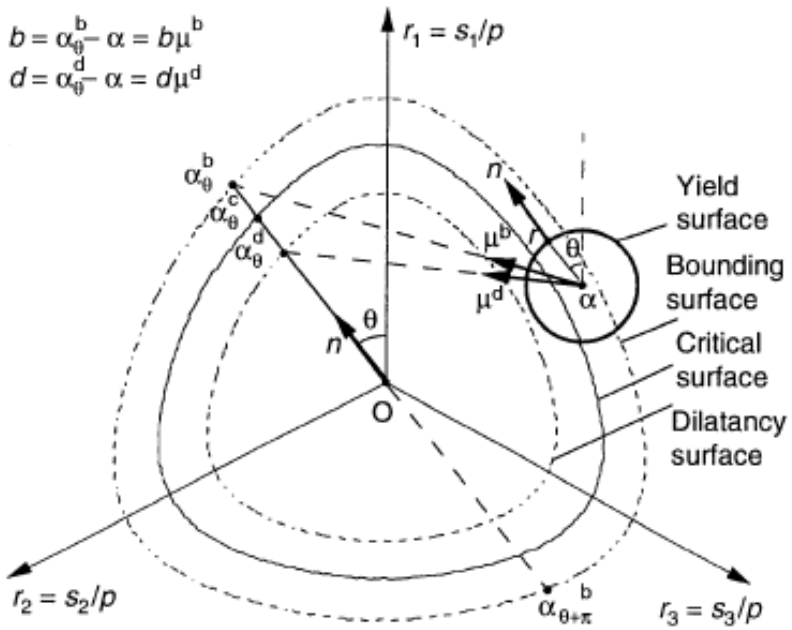

Figure 3.7 Illustration of the bounding, critical, dilatancy and yield surfaces, after Manzari and Dafalias (1997)

3.3.6 Bounding surface with state dependent based dilatancy model by Li and Dafalias (2000) and Li (2002)

The speciality of the model by Li (2002) is the use of state dependent stress-dilatancy relation developed by Li and Dafalias (2000). The state dependent stress-dilatancy relation is given by Equation 3.7 (Equation 15 of Li and Dafalias, 2000).

$$d = \frac{d_0}{M_c}\{M_c \exp(m\psi) - \eta\} \quad \textbf{(3.7)}$$

where d is the dilatancy; M_c is the stress ratio at critical state in triaxial compression; η is the stress ratio in triaxial compression; m is a positive material constant; ψ is the state parameter defined by Been and Jefferies (1985); d_0 is a calibration constant and equals to M at critical state when $\psi = 0$. Therefore, depending upon ψ, the phase transformation stress ratio, $M_c \exp(m\psi)$ can be either less than M_c (when $\psi < 0$ for states denser than the critical); or greater than M_c (when $\psi > 0$ for states looser than the critical); or equal to M_c (for $\psi = 0$ at

critical state). Thus, even if stress ratio becomes M_c, sand can still undergo either dilation or contraction depending upon the state parameter ψ. Li and Dafalias (2000) further proposed a rudimentary model for monotonic triaxial compression stress path where stress ratio at the bounding surface is defined as $M_c^b = M_c \exp(-n\psi)$, n being another positive material constant. This approach is analytically different from Manzari and Dafalias (1997) where an additive term had been used ($M_c^b = M_c + k_c^b\langle -\psi \rangle$). These concepts were extended by Li (2002) to formulate a model in generalised stress space.

The bounding surface comprises a conical Lode angle dependent surface with a flat cap. The cap represents the volumetric mechanism; while the plasticity formulation of the cap surface is similar to that of Wang et al. (1990) in some aspects, but unlike it, the volumetric mechanism remains active even during undrained deviatoric stress path. Thus, the plastic volumetric strain is accumulated from both the deviatoric and the volumetric mechanisms. Because the volumetric mechanism is often rudimentary unless the effective pressure is large enough to produce particle crushing, review of this part is not pursued further.

The bounding surface and the projection rule for the deviatoric mechanism are shown in Figure 3.8. As shown in the figure, a radial projection rule is proposed with $\boldsymbol{\alpha}$, the stress reversal point (boldfaced symbols indicating tensors), as the projection centre. The plastic modulus is defined in Equation 3.8 (Equation 20 of Li, 2002).

$$K_P = \frac{Gh}{\bar{R}}\left\{M_c \exp(-n\psi) g(\bar{\theta}) \left(\frac{\bar{\rho}_1}{\rho_1}\right) - \bar{R}\right\} \qquad \textbf{(3.8)}$$

where G is the elastic shear modulus; $g(\bar{\theta})$ is an interpolating function for various Lode angle $\bar{\theta}$ ($\bar{\theta} = -30°$ for triaxial compression and $\bar{\theta} = 30°$ for triaxial extension); $\bar{R}$ is the stress ratio associated with $\bar{\boldsymbol{r}}$; $\bar{\rho}_1$ and ρ_1 are illustrated in Figure 3.8; h is a calibration constant; and M_c is as previously defined. At the start of loading, the bounding surface is defined as $\bar{R} = M_c \exp(-n\psi) g(\bar{\theta})$. Then the bounding surface hardens isotropically with accumulation of plastic deviatoric strain. The plastic strain increment associated with the stress point $\boldsymbol{r}$ is $\mathrm{d}L = p\,\bar{\boldsymbol{n}}\mathrm{d}\boldsymbol{r}/K_{\boldsymbol{p}}$. Now applying consistency condition on $F_1 = 0$ at $\bar{\boldsymbol{r}}$, one has $dF_1 = 0$, or, $p\bar{\boldsymbol{n}}\mathrm{d}\bar{\boldsymbol{r}} = \overline{K_{\boldsymbol{p}}}\mathrm{d}L$ where $\overline{K_{\boldsymbol{p}}}$ is the plastic modulus of the bounding surface at $\bar{\boldsymbol{r}}$. $\overline{K_{\boldsymbol{p}}}$ can be obtained by substituting $\bar{\rho}_1 = \rho_1$ in Equation 3.8. However, the direction for $\mathrm{d}\bar{\boldsymbol{r}}$ should be additionally specified. It can be assumed along $\bar{\boldsymbol{n}}$ for simplicity. The above procedure enables simulation of strain softening behaviour in a more elegant way than that of Manzari and

Dafalias (1997) because the bounding surface not only depends on ψ, but also evolves with the plastic strain. The stress dilatancy relation is expressed by Equation 3.9 (Equation 23 of Li, 2002), which is a multiaxial generation of Equation 3.7; d_1 is a calibration constant and R is the stress ratio associated with $\boldsymbol{r}$.

$$D = \frac{d_1}{M_c g(\bar{\theta})}\left\{M_c \exp(m\psi) g(\bar{\theta}) \sqrt{\frac{\bar{\rho}_1}{\rho_1}} - R\right\} \tag{3.9}$$

The model requires 19 parameters, out of which, 4 parameters are regarded as 'default' without any requirement for calibration. The remaining 15 parameters can be easily calibrated using conventional drained and undrained triaxial monotonic tests. The model is nicely capturing the effect of state on the dilatancy behaviour during both monotonic drained and cyclic undrained simulations. A rudimentary version of this model was presented in Li and Dafalias (2000) where validation against drained and undrained monotonic triaxial compression was shown.

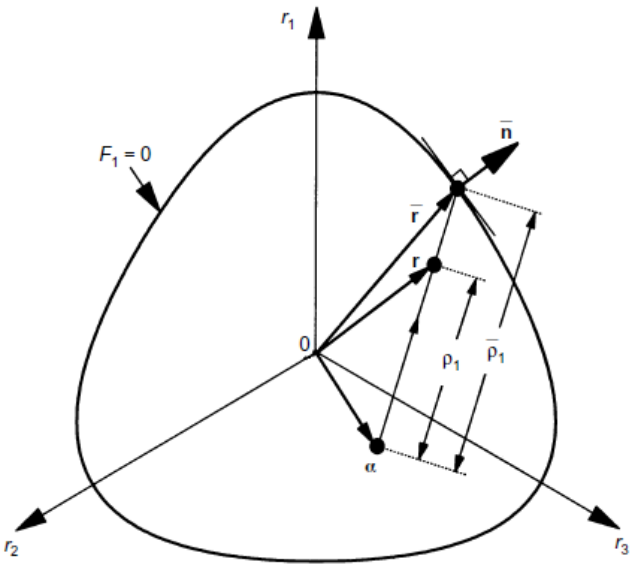

Figure 3.8 Bounding surface and projection rule in deviatoric stress ratio space, after Li (2002)

3.3.7 Multiple surface based model without Lode angle effect by Yang et al. (2003) and with Lode angle effect by Yang and Elgamal (2008)

The formulation of both these models is based on the approach of Prevost (1985). These models consist of multiple nested homogeneous surfaces, defining the backbone curve,

subjected to a kinematic hardening rule of Mroz (1967). The largest yield surface (failure surface) is circular in Yang et al. (2003); while in the model of Yang and Elgamal (2008), Lade and Duncan (1975) failure surface is adopted, as shown in Figure 3.9 and 3.10, respectively. The nested yield surfaces are homogeneous to the respective failure surfaces. Hence, the Lode angle dependent surfaces do not strictly follow Lade and Duncan yield criterion. The primary purpose of these models is to capture the spread of plastic deviatoric strain during cyclic mobility, and therefore, compromises with the other essential features of sand behaviour, such as exclusion of neutral stress paths, dependence on state parameter and critical state framework. To meet this purpose, following stress-dilatancy relations are phenomenologically framed (Equation 3.10 and 3.11 are Equation 6 and 8 of Yang et al., 2003, respectively).

$$D = \left(1 - \text{sign}(\dot{\eta})\frac{\eta}{\eta_{PT}}\right)(c_1 + c_2\varepsilon_c) \quad \textbf{(3.10)}$$

$$D = \left(1 - \frac{\eta}{\eta_{PT}}\right) d_1(\gamma_d)^d \quad \textbf{(3.11)}$$

where D is the dilatancy; η is the shear stress ratio; η_{PT} is η at the phase transformation; γ_d is the accumulated deviatoric strain during a dilation phase; c_1, c_2 , ε_c , d_1, d are positive calibration constants. Equation 3.11 is applicable for dilation phase when $\eta > \eta_{PT}$ and $\dot{\eta} > 0$; and Equation 3.10 is applicable for contraction phase. If the term $c_2\varepsilon_c$ is omitted from Equation 3.10, then the model will not be able to reproduce progressive cyclic loss of effective pressure associated with the onset of cyclic mobility. To numerically achieve this, it is assumed that dilatancy should increase during an unloading phase depending upon the negative plastic volumetric strain which accumulated during the previous dilation phase. Therefore, the positive parameter ε_c evolves during a dilation phase as $\dot{\varepsilon_c} = -\dot{\varepsilon_v}$ (ε_v is the plastic volumetric strain); and during unloading phase, ε_c reduces via the same expression until ε_c becomes zero.

During cyclic mobility when effective pressure becomes very low, almost approaching zero, large shear strain develops prior to the subsequent dilation phase. This phase of shear strain accumulation is termed as the 'neutral' phase and D is set to zero until some predefined limit of shear strain is reached. This limit has been denoted as γ_s; when γ_s is exceeded, Equation 3.11 becomes active implementing the dilation phase. Development of shear strain during cyclic mobility is easily realised by increasing γ_s, and thereby deferring

the application of Equation 3.11 and hence the dilation phase. When γ_d exceeds its previous value during a dilation phase, γ_s also increases by the same amount as γ_d. If any initial static shear is present, then γ_s in the direction of static shear is increased, and in the opposite direction decreased by the same amount, thereby mimicking kinematic hardening of shear strain space along the direction of static shear stress. This algorithm is illustrated in Figure 3.11. However, this algorithm is not completely supported by any experimental observations and is entirely phenomenologically driven. The model requires 15 parameters. The dilatancy parameters are calibrated by simulating centrifuge tests. This method of calibration suggests a relatively weak conceptual foundation because the rate-independent incremental plastic flow theory assumes the deformation process is infinitely slow. Therefore, the calibration should be ideally based on tests with very low strain rate, typically 0.01 per minute for undrained and 0.005 per minute for drained tests, (Verdugo and Ishihara, 1996) rather than simulating dynamic tests such as centrifuge, which involve several mathematical idealisations other than the constitutive model.

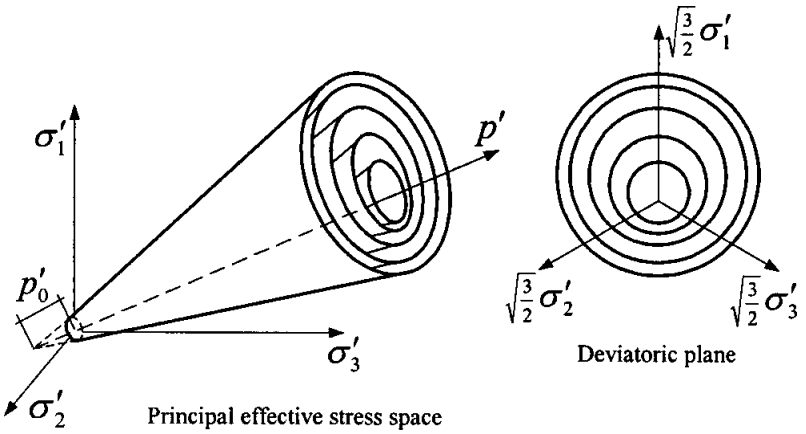

Figure 3.9 Yield surfaces in principal stress space and on deviatoric plane, after Yang et al. (2003)

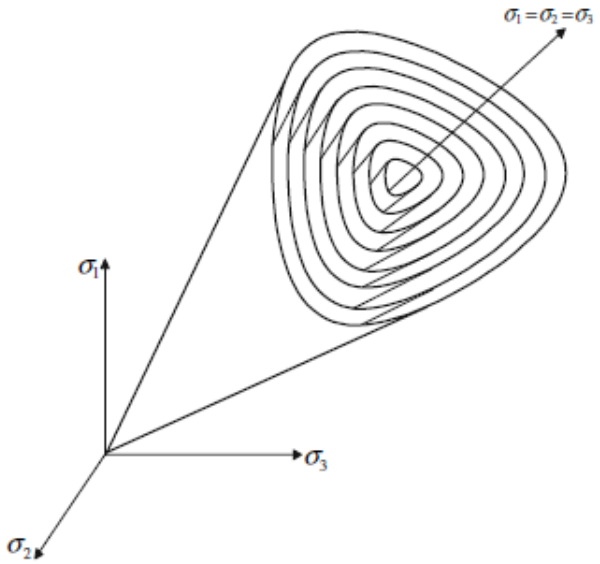

Figure 3.10 Yield surfaces in principal stress space with Lode angle effect; only the failure surface follows Lade-Duncan yield criterion while the others are homogeneous to the failure surface, after Yang and Elgamal (2008)

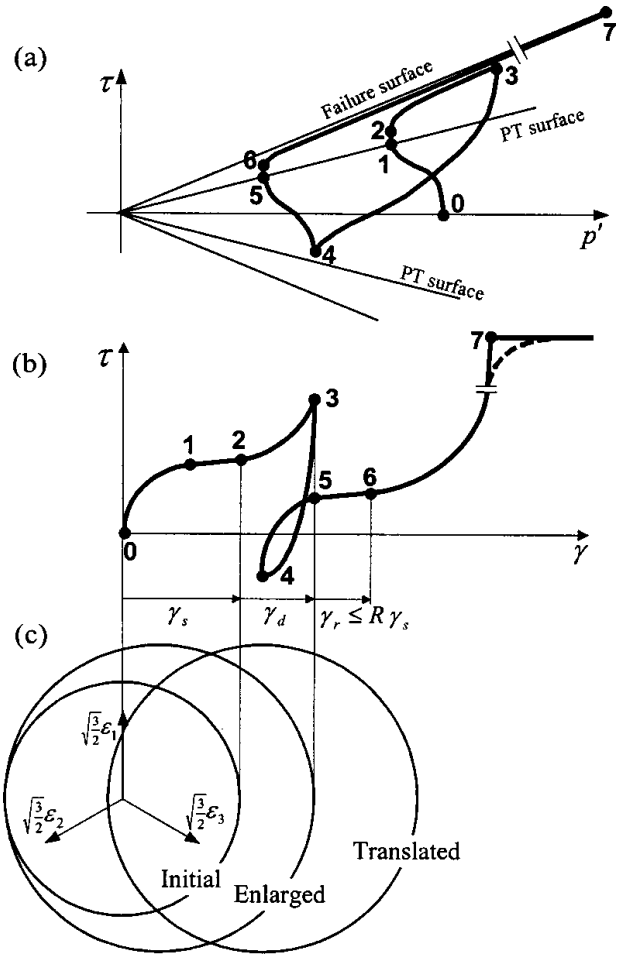

Figure 3.11 Illustration of the algorithm to achieve development of shear strain during cyclic mobility, after Yang et al. (2003)

3.3.8 Bounding surface based model with fabric effect on dilatancy by Dafalias and Manzari (2004)

This model is an improved version of the two-surface model developed earlier by the same authors (Manzari and Dafalias, 1997). The model comprises a rudimentary yield surface and three homogeneous Lode-angle dependent surfaces, namely, the bounding, critical and dilatancy surfaces. The purpose of the yield surface, which is circular in shape, is to provide a direction of the effective stress increment, or the loading direction. In the previous model of Manzari and Dafalias (1997), associated flow was assumed for the deviatoric component. Thus, the gradient of the yield surface also provided the direction of plastic deviatoric strain increment. However, in the present model non-associated flow rule is assumed, where the critical surface has been used as the plastic potential surface. The model framework illustrating the surfaces and primary state variables are shown in Figure 3.12.

The model is state dependent. The critical surface is defined using triaxial compression stress ratio and is the reference surface based on which the bounding and dilatancy surfaces are defined using Equation 3.12 (Equations 9 and 10 of Dafalias and Manzari, 2004).

$$\begin{aligned} M_c^b &= M_c \exp(-n_b \psi) \\ M_c^d &= M_c \exp(n_d \psi) \end{aligned} \tag{3.12}$$

where M_c is the stress ratio in triaxial compression at the steady state (assumed as critical state); M_c^b and M_c^d are the corresponding stress ratios on the bounding and dilatancy surfaces respectively; ψ is the state parameter defined by Been and Jefferies (1985); n_b and $n_d$are positive material constants. Therefore, for states denser than the critical, one always has $\psi < 0$; $M_c^b > M_c > M_c^d$; for critical state, $\psi = 0$; $M_c^b = M_c = M_c^d$; and for state looser than the critical, $\psi > 0$; $M_c^b < M_c < M_c^d$. It is worthwhile to review the expression for the plastic modulus. The plastic modulus is defined in Equation 3.13 (obtained by combining Equations 23 and 24 of Dafalias and Manzari, 2004).

$$K_p = \frac{2}{3} p b_0 \frac{(\boldsymbol{\alpha_\theta^b} - \boldsymbol{\alpha}) : \boldsymbol{n}}{(\boldsymbol{\alpha} - \boldsymbol{\alpha_{in}}) : \boldsymbol{n}} \tag{3.13}$$

where K_p is the plastic modulus; p is the effective pressure; b_0 is a positive material constant; $\boldsymbol{\alpha_\theta^b}, \boldsymbol{n}$ (boldfaced symbols indicate tensors) are defined in Figure 3.12; $\boldsymbol{\alpha_{in}} = \boldsymbol{\alpha}$ at stress reversal. It can be seen that K_p can be negative when $\boldsymbol{\alpha}$ is outside the bounding surface,

which is generally observed for dense sands. However, as the yield surface kinematically hardens in the direction of $\boldsymbol{\alpha}_{\boldsymbol{\theta}}^{\boldsymbol{b}} - \boldsymbol{\alpha}$, it will finally move inwards, approaching the bounding surface. As the bounding surface depends on ψ, it can be assumed that soon after the peak stress is attained ($K_p = 0$), $\psi \to 0$ and hence, $M_c^b \to M$. Therefore, eventually, $\boldsymbol{\alpha}$ will collapse on the critical surface indicating that actual critical state has reached.

The most interesting feature of this model is the introduction of a parameter that supposedly accounts for fabric change effect on dilatancy behaviour of sands. The stress-dilatancy relation is expressed as Equation 3.14 (Equations 25 and 27 Dafalias and Manzari, 2004).

$$\left.\begin{aligned} D &= A_d\left(\boldsymbol{\alpha}_{\boldsymbol{\theta}}^{\boldsymbol{d}} - \boldsymbol{\alpha}\right):\boldsymbol{n} \\ A_d &= A_0(1 + \langle \boldsymbol{z}:\boldsymbol{n}\rangle)\left(\boldsymbol{\alpha}_{\boldsymbol{\theta}}^{\boldsymbol{d}} - \boldsymbol{\alpha}\right) \end{aligned}\right\} \quad \textbf{(3.14)}$$

where D is the dilatancy; A_d and A_0 are positive material constants; $\boldsymbol{z}$ is the fabric tensor; $\langle . \rangle$ is Macaulay's bracket. The term $\langle \boldsymbol{z}:\boldsymbol{n}\rangle$ accounts for fabric change effect on the dilatancy behaviour. It has been seen that when this term is ignored, the model fails to simulate cyclic mobility. Therefore, there was a need to augment the coefficient A_0 during an unloading phase immediately following a dilatancy phase. This is achieved through the quantity $\boldsymbol{z}$ which evolves according to $d\boldsymbol{z} = -c_z\langle -d\varepsilon_v^p\rangle(z_{max}\boldsymbol{n} + \boldsymbol{z})$, where c_z and z_{max} are positive material constants; $d\varepsilon_v^p$ is the plastic volumetric strain rate. Whenever dilation is encountered, $\boldsymbol{z}$ evolves as $d\varepsilon_v^p < 0$ and continues until $d\varepsilon_v^p > 0$, which occurs during the subsequent unloading phase, thereby augmenting A_0 to A_d. For numerical stability, peak value of $\boldsymbol{z}$ is restricted to z_{max}. The exact evolution of $\boldsymbol{z}$ is made dependent on $\boldsymbol{n}$ to capture the events of loading and unloading during arbitrary change of direction in generalised stress state. When a very simple unidirectional case is considered, such as triaxial compression and extension, $\boldsymbol{z}$ can be treated as a scalar quantity (denoted henceforth as z) and $\boldsymbol{n} = \pm 1$ for the respective directions. It can be seen that z accumulates to the maximum value of z_{max} during dilatation phase in triaxial compression, and then reduces to the minimum of zero during the dilation phase but in the direction of triaxial extension; and A_0 is incremented to A_d only during the unloading phases.

The model requires 15 parameters, out of which, 4 are empirical, which are difficult to calibrate and require considerable trial and error. The value of z_{max} is arbitrary because its

sole purpose is to reduce the effective pressure to a very low value by increasing the dilatancy during cyclic unloading phases. It is felt that lack of any calibration procedure for z_{max} is primarily due to lack of any quantitative definition for cyclic mobility. There is an excellent match for the monotonic behaviour along triaxial compression for various densities and confining pressures of Toyoura sand specimens. Improvement of the model over its previous format (Manzari and Dafalias, 1997) by adopting non-associated flow has been also demonstrated. However, the cyclic behaviour is not well-validated. Recently, Boulanger and Ziotopoulou (2012) have modified the original model of Dafalias and Manzari (2004) at 'equation level' in an effort to achieve better calibration against experimental data and case history based correlations. The model is degenerated to the plane-strain version, and thus the generality of the model of Dafalias and Manzari (2004) is compromised with accuracy, which is achieved only along the torsional stress path.

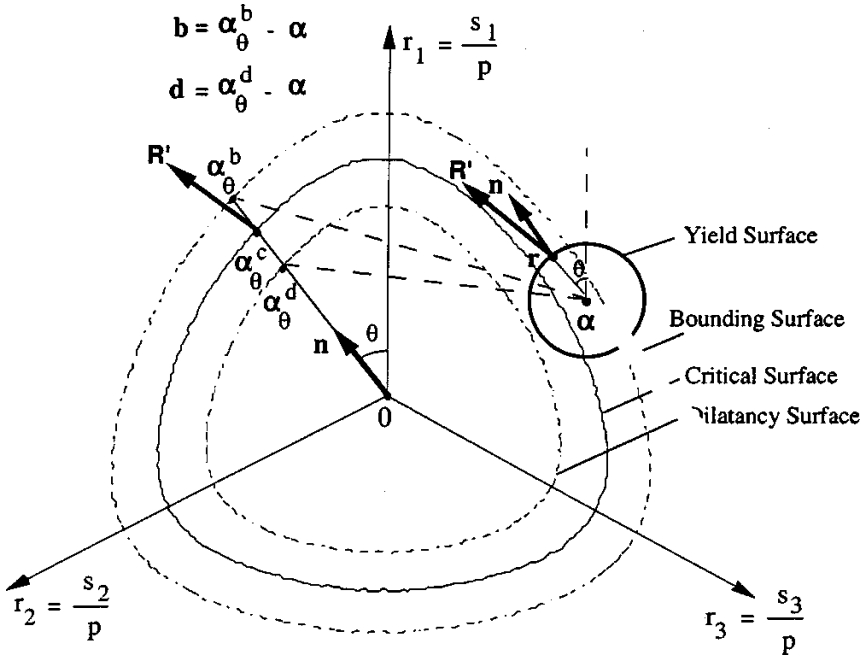

Figure 3.12 Illustration of the yield, bounding, critical and dilatancy surfaces in principal deviatoric space, after Dafalias and Manzari (2004)

3.3.9 Bounding surface plasticity based on large deformation mechanism by Zhang and Wang (2012)

This work is important because the authors have strived to provide a physical understanding of the post-liquefaction deformation mechanism of sand which other models reviewed herein did not attempt. The previous models are based on the concepts of critical

state and state index, and do not have any specific formulation to predict development of plastic shear strain for loose sands during cyclic mobility once a state of zero confining effective stress is achieved. In this respect the model of Zhang and Wang (2012) has been able to achieve significant improvement as compared to other more theoretically accomplished models.

The authors conjectured that shear induced volumetric strain (ε_{vd}) has two components: an irreversible component ($\varepsilon_{vd,ir}$) and a reversible component ($\varepsilon_{vd,r}$). The irreversible component increases monotonically with shear strain and number of cycles in a cyclic stress path, and is always positive (contraction). However, the rate of accumulation of $\varepsilon_{vd,ir}$ gradually decreases as the number of cycles increases. The reversible component, on the other end, can assume both positive and negative (dilation) values. During undrained behaviour volumetric strain must be zero. So, the elastic volumetric strain (ε_{vc}) must be equal and opposite to the total shear induced volumetric strain both from the irreversible and reversible components, i.e. $\varepsilon_{vc} = -(\varepsilon_{vd,ir} + \varepsilon_{vd,r})$. The elastic volumetric strain is the result of inter-granular contact stresses, which in macroscopic sense, is the effective pressure. There exists a 'threshold' limit of ε_{vc} denoted as $\varepsilon_{vc,0}$ such that liquefaction occurs when $\varepsilon_{vc} \leq \varepsilon_{vc,0}$. Depending upon whether $\varepsilon_{vc} > \varepsilon_{vc,0}$, or, $\varepsilon_{vc} < \varepsilon_{vc,0}$, or, $\varepsilon_{vc} = \varepsilon_{vc,0}$, three mechanisms have been postulated. In the first case, the particles are in contact with each other and can carry shear stress by internal friction like any regular granular material; in the second case, the particles have lost contact and are in suspension state, producing large deformation by behaving essentially as a fluid with negligible shear strength; in the third case, the particles are just in contact with negligible contact pressure, and the contact pressure may either increase through dilative behaviour or the contact may be lost reverting the physical state to the second case, depending upon the direction of shear strain. The particle arrangement and rearrangement during these three physical states are illustrated in Figure 3.13a. The transition from the suspension state to the solid state via the third state is the physical interpretation of the phase transformation; this lucid interpretation is applicable for loose sands for which quasi steady state exists as the phase transformation takes place at low confining stresses. It is during the temporary solid phase, γ_d is produced as shown in Figure 3.13a,b; while the third phase requires a strain of γ_0 to enter into the temporary solid phase.

The reversible component $\varepsilon_{vd,r}$ can be expressed as: $\varepsilon_{vd,r} = -(\varepsilon_{vd,ir} + \varepsilon_{vc,0})$ at liquefaction stage. As both $\varepsilon_{vd,ir}$ and $\varepsilon_{vc,0}$ are positive quantities, $\varepsilon_{vd,r}$ is a negative quantity (dilation) that increases in magnitude with γ_0. For phase transformation to take place twice during each cycle, $\varepsilon_{vd,r}$ must assume such a peak value so that $\varepsilon_{vc} = -(\varepsilon_{vd,r} + \varepsilon_{vd,ir})$ becomes greater than or equal to $\varepsilon_{vc,0}$. This is illustrated in Figure 3.14a. However, negative $\varepsilon_{vd,r}$ cannot increase infinitely and it has a peak value of $-\varepsilon_{vd,r,min}$. If the peak value is attained and the resulting elastic volumetric strain is still less than or equal to $\varepsilon_{vc,0}$, then flow liquefaction can occur even after few initial cycles of mobility (Figure 3.14b) as there are no subsequent dilation phases. It is natural that when a static initial stress exists, $\varepsilon_{vd,ir}$ increases thereby increasing the possibility of flow slide.

Zhang and Wang (2012) adopted the framework of the bounding surface plasticity in its simplest form developed by Dafalias and his co-workers discussed previously. The bounding surface incorporates Lode angle, and a radial projection rule is used to determine the direction of the deviatoric plastic strain and the plastic modulus. There is no yield surface; during monotonic loading, the origin, and during cyclic loading, the stress reversal point, become the centre of projection, respectively. The model ingredients are shown in Figure 3.15. The novelty of this model is three stress-dilatancy relations discussed as follows. The expression for the irreversible component is shown in Equation 3.15 (Equation 57 of Zhang and Wang, 2012).

$$D_{ir} = \frac{d_{ir}\exp(-\alpha\varepsilon_{vd,ir}^{p})}{(1+\gamma_{mono}/\gamma_{d,r})^{2}} \tag{3.15}$$

where D_{ir} is the irreversible dilatancy component; $d_{ir}, \alpha, \gamma_{d,r}$ are positive material constants; $\varepsilon_{vd,ir}^{p}$ is the accumulated irreversible plastic volumetric strain; γ_{mono} is the accumulated shear strain from the recent load reversal point. Therefore, it can be seen that D_{ir} is always positive, $\varepsilon_{vd,ir}^{p}$ accounts for the entire loading history, and γ_{mono}, the current cycle. The negative reversible component is expressed by Equation 3.16 (Equation 51 of Zhang and Wang, 2012).

$$D_{re,gen} = d_{re,1}(M_{d,c}g(\theta_\sigma) - \eta) \tag{3.16}$$

where $D_{re,gen}$ is the negative part of the reversible dilatancy that generates negative plastic volumetric strain; $d_{re,1}$ is a positive material constant; $M_{d,c}$ is the stress ratio in triaxial

compression which can be approximated to the stress ratio at phase transformation; $g(\theta_\sigma)$ is the interpolating function for various Lode angle (θ_σ) values; η is the stress ratio. This equation is only applicable for $\eta \geq M_{d,c}g(\theta_\sigma)$ during a loading phase i.e. when $\dot{\eta} > 0$; during an unloading phase i.e. when $\dot{\eta} < 0$ or $\eta < M_{d,c}g(\theta_\sigma)$, Equation 3.17 (Equation 54 of Zhang and Wang, 2012) is applicable.

$$D_{re,rel} = \left(d_{re,2}\varepsilon^p_{vd,re}\right)^2 \quad \textbf{(3.17)}$$

where $D_{re,rel}$ is the positive part of the reversible dilatancy that releases the negative volume accumulated during previous dilation phases; $d_{re,2}$ is a material constant; $\varepsilon^p_{vd,re}$ is the negative plastic volume accumulated via Equation 3.16 during dilation phases. Therefore, Equation 3.17 is not activated until Equation 3.16.

The most difficult and crucial part of the implementation is the calibration of the three parameters $d_{ir}, \alpha, \gamma_{d,r}$ of Equation 3.15. Zhang and Wang (2012) recommended that these parameters can be calibrated by fitting with the number of cycles to initial liquefaction or single amplitude shear strain of 6% after initial liquefaction. The parameters $d_{re,1}$ and $M_{d,c}$ can be obtained by fitting a straight line to a stress-dilatancy plot, typically obtained in drained tests. However, initial cycles should be neglected in order to eliminate the effect of irreversible dilatancy. The parameter $d_{re,2}$ can be arbitrarily set to large values such as 1000-1500, so that ε^p_{vd}becomes almost zero during unloading following a dilation phase during cyclic mobility. The model is validated by cyclic element simulation of Toyoura and Nevada sands. Verification studies have been also conducted by simulating centrifuge modelling for one dimensional ground response for both level and sloping grounds. The authors also demonstrated the capability of the model to capture post-liquefaction response by performing a seismic response analysis of Daikai subway station during the 1995 Kobe earthquake in Japan. The model simulations almost matched exactly with the experimental results during post liquefaction response in terms of the maximum shear strain attained. It appears from the element simulation that the model is nicely capturing the cyclical development of shear strain during cyclic mobility, which is due to the specific aforementioned three stress-dilatancy relations postulated by Zhang and Wang (2012). As the parameters like plastic strain cannot be determined from a current state, initialisation of strain-dependent stress-dilatancy relation

is difficult for initial anisotropic samples. This also applies for the model of Cubrinovski (1993); Cubrinovski and Ishihara (1998b).

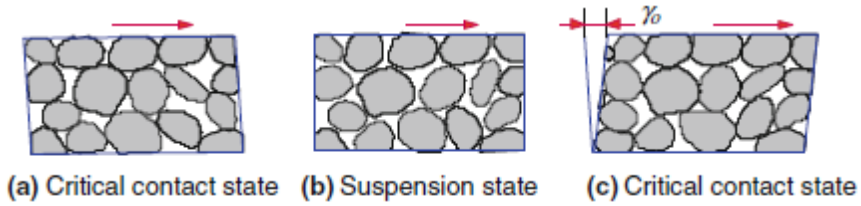

(a)

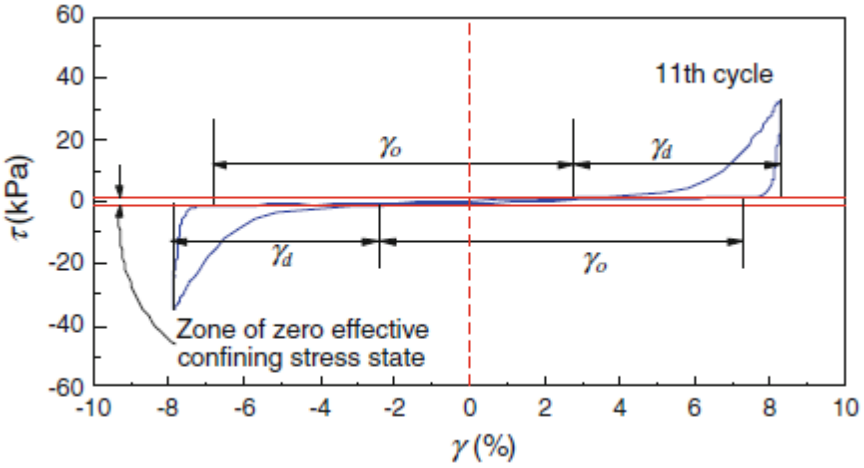

(b)

Figure 3.13 (a) Three physical states during post-liquefaction behaviour; (b) the post liquefaction shear strain in the suspension state, after Zhang and Wang (2012)

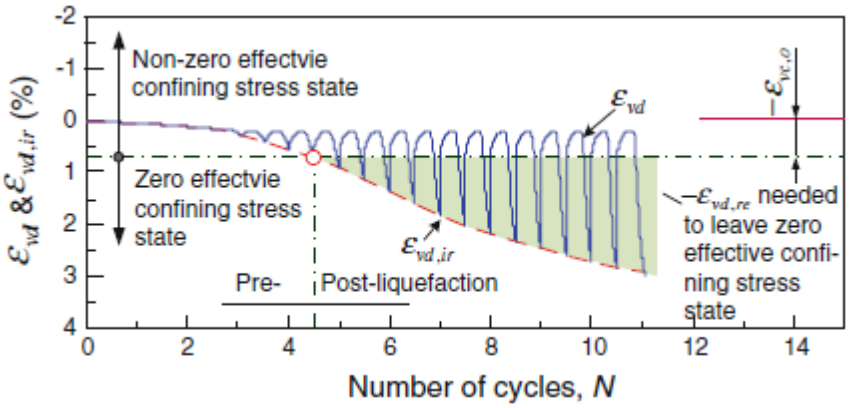

(a)

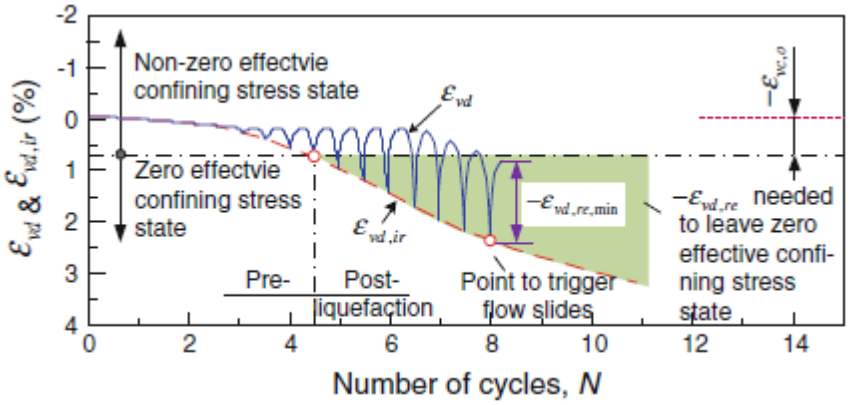

(b)

Figure 3.14 Interpretation of the role of irreversible and reversible components of dilatancy (a) during cyclic mobility; and (b) during flow type deformation, after Zhang and Wang (2012)

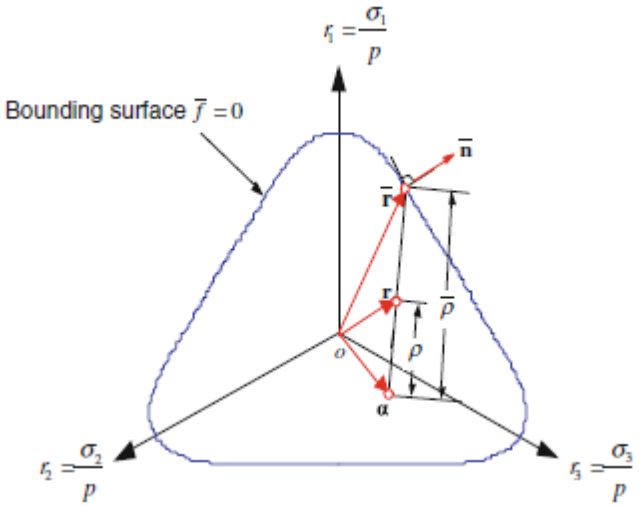

Figure 3.15 The bounding surface and the projection rules, after Zhang and Wang (2012)

3.4 Models based on anisotropic fabric

Anisotropy in constitutive behaviour of sand develops due to some specific orientation of non-spherical particles. The orientation is largely influenced by the deposition process; for example, Arthur and Menzies (1972) had shown how different deposition directions affected the constitutive behaviour. For the sake of simplicity, if it is assumed that the deposition of sand occurs under gravity, then elongated particles usually orient themselves with their major axis along the plane of deposition, thereby rendering a sedimentary or a stratified structure. The reason for such a preferred orientation can be intuitively connected to the requirement of the lowest potential energy for stability. Such anisotropy is known as the so-called inherent or fabric anisotropy. It is important to recognise that dependence on Lode angle is not a mathematical representation of the inherent or fabric anisotropy because the material strength in triaxial compression, or extension, or for even torsional stress path, is considered identical in three mutually perpendicular directions. The bedding or the depositional plane is generally considered isotropic, thereby limiting the fabric anisotropy to the direction perpendicular to the bedding plane. Hence, the fabric anisotropy is unidirectional. This simplified view of the fabric anisotropy is applicable for level ground, because on sloping ground the bedding plane is also anisotropic. There is a second component of anisotropy, the so-called induced anisotropy (Wong and Arthur, 1985, 1986), which develops as a result of particle rearrangement in response to applied stress paths. The

models discussed herein are based on the fabric anisotropy and do not consider induced anisotropy.

The non-uniqueness of critical state for various stress paths is already well established. For example, the mobilised friction angle or the stress ratio at the steady state of deformation is nearly identical in triaxial compression and extension, but the critical state line is not so in void ratio – effective pressure space (Vaid et al., 1990). It is postulated by the models based on the concept of fabric anisotropy that such non-uniqueness of the critical state line of the same sand (i.e. of the same initial fabric) for different stress paths is due to the anisotropy of the initial fabric as the final fabric also carries significant characteristics of the initial one (Wan and Guo, 2001). The direction of the fabric anisotropy is referenced to the direction of major principal deviatoric stress.

In the models based on isotropic fabric, critical state is invariably considered as a reference state, independent of the stress path. The various constitutive parameters and plasticity-based modelling features like the bounding and dilatancy surfaces being dependent upon critical state parameters and state index, are also invariant of stress path or deformation history. Therefore, the common technique adopted to include the effect of fabric anisotropy is to modify the critical state parameters for stress paths relative to the bedding plane. The underlying assumption is that if a fabric is isotropic, then critical state will be path independent. Furthermore, the initial fabric is so endurable that it can sustain large strains to reach critical state. These fabric-dependent models do not consider continuous evolution of new fabrics or the induced anisotropy. Therefore, the effect of induced anisotropy is virtually absent. The effect of fabric anisotropy on the constitutive behaviour is included in the following bounding surface plasticity based constitutive models.

- Li and Dafalias (2002) based on the platform model of Li (2002);
- Dafalias et al. (2004) based on the platform model Dafalias and Manzari (2004);
- Model for rotational shear loading with fabric anisotropy by Li and Dafalias (2004);

The platform models are the fabric-independent models which are subsequently modified by introducing additional fabric-dependent internal variables to consider the effect

of anisotropy; in other words, the platform models are the fabric-independent counterparts of the fabric-dependent models. The fabric-dependent model of Dafalias et al. (2004) is relatively simple and will be discussed first in order to understand the general approach for considering fabric anisotropy in platform models.

3.4.1 Dafalias et al. (2004) based on the platform model of Dafalias and Manzari (2004)

In the fabric-dependent model by Dafalias et al. (2004), an additional fabric tensor term (F_{ij}) is introduced to represent the so-called fabric of the sand. The expression of F_{ij} is given by Equation 3.18 (Equation 1 of Dafalias et al, 2004).

$$F_{ij} = \frac{1}{2N}\sum_{k=1}^{2N} u_i^k \, u_j^k \tag{3.18}$$

where N is the number of particles in a representative volume; u_i^k is the i^{th} component of a unit vector along the major axis of k^{th} particle. Since both the directions of u^k and $-u^k$ are considered, the summation is over $2N$ terms. The two important properties of this tensor are that $F_{ii} = 1$ and $F_{ij} = F_{ji}$. It is assumed that the bedding plane is transversely isotropic as shown in Figure 3.16. The z plane is the plane of isotropy; if the subscript 1 represents the z-plane, and 2 and 3 the r and θ planes respectively, then F_{ij} can be expressed by Equation 3.19 (Equation 2 of Dafalias et al, 2004).

$$\boldsymbol{F} = \begin{pmatrix} a & 0 & 0 \\ 0 & \dfrac{1-a}{2} & 0 \\ 0 & 0 & \dfrac{1-a}{2} \end{pmatrix} \tag{3.19}$$

where a varies from 0 to 1. If none of the particles have any projection along z axis, then from Equation 3.18, $a = 0$; similarly if all the particles are parallel to z axis, then $a = 1$; if the particles have equal direction cosines along all the three directions, then one has an isotropic fabric with $a = 1/3$. From the consideration of the lowest potential energy configuration, $0 \leq a \leq 1/3$. The anisotropic parameter a is the additional internal variable.

The main objective to introduce $\boldsymbol{F}$ is to define a scalar-valued internal variable, termed as anisotropic state variable (A) that will combine the effect of non-coincidence of the major principal deviatoric stress and the z plane, as well as the Lode angle effect via the b-

value, defined as $b = (s_2 - s_3)/(s_1 - s_3)$, where $s_1 \geq s_2 \geq s_3$ are the principal deviatoric stresses. The parameter A is then used to modify the critical state line in the void ratio-effective pressure space, thereby controlling the rest of the constitutive parameters via the state index. The critical state line in the platform model is defined as $e_c = e_0 - \lambda_c(p_C/p_{at})^{\xi}$, where e_0 is the void ratio at effective pressure $p_c = 0$; p_{at} is the atmospheric pressure; λ_c and ξ are curve fitting parameters. The critical state line is modified by $e_0 = e_A \exp(-A)$ (Equation 14 of Dafalias et al, 2004) in view of anisotropy, where e_A is the void ratio of the critical state line at zero effective pressure for a given value of A; the definition of A is such that for an isotropic fabric, $A = 0$ and $e_0 = e_A$. The modification of the critical state line for triaxial compression and triaxial extension stress paths is shown in Figure 3.17. Had the fabric been isotropic, i.e. $A = 0$, there would have been no effect of stress path on the constitutive behaviour producing a unique critical state line. However, during determination of A for various stress paths, the fabric tensor $\boldsymbol{F}$ is considered constant. Therefore, the model does not account for induced anisotropy.

The anisotropic state variable A is defined in Equation 3.20 (Equation 5 of Dafalias et al, 2004).

$$A = g(\theta, c)\boldsymbol{F}:\boldsymbol{n} \tag{3.20}$$

where $g(\theta, c)$ is an interpolating function used in the equation of the critical state surface of the platform model Dafalias and Manzari (2004) to interpolate the stress ratios for different Lode angle θ, and depends upon the ratio of the stress ratios in triaxial extension to triaxial compression, denoted as c. However, in this equation c is expressed in terms of the absolute values of A in triaxial extension and compression; $\boldsymbol{n}$ is the gradient of the yield surface (boldfaced symbols indicate tensor quantities). For radial load path (with fixed θ), the direction $\boldsymbol{n}$ is the same as that of the principal deviatoric stress tensor. In principal space, the deviatoric stresses s_1, s_2, s_3 can be easily expressed in terms of the b-value by using the relation $s_1 + s_2 + s_3 = 0$, where $s_1 \geq s_2 \geq s_3$. In order to determine A, $\boldsymbol{F}$ which is expressed in Equation 3.19 with respect to $z - r - \theta$ coordinate system (Figure 3.16), is transformed to the principal space, only for mathematical convenience, prior to substitution in Equation 3.20. By knowing the angle α, this transformation can be carried out as shown in Equation 3.21.

$$\overline{F_{ij}} = a_{ik}a_{jk}F_{kl}$$
$$\boldsymbol{a} = \begin{bmatrix} \cos\alpha & 0 & -\sin\alpha \\ 0 & 1 & 0 \\ \sin\alpha & 0 & \cos\alpha\ 0 \end{bmatrix} \quad \textbf{(3.21)}$$

The variation of A with α for various b-values is shown in Figure 3.18. It can be shown that $A = 0$ for $a = 1/3$, an isotropic fabric. Therefore, A combines the Lode angle effect and the non-coincidence between the bedding plane and the major principal plane measured by the angle α, which are inseparable in any physical measurements of stresses and strains. Tests have shown that for a given b-value, response becomes softer with increase in α (Yoshimine et al., 1998). This particular behaviour is captured by lowering the critical state line depending upon the value of A, and thereby lowering the value of the state index resulting in a more contractive behaviour. The model is well validated under monotonic loading for various combinations of b-value and α.

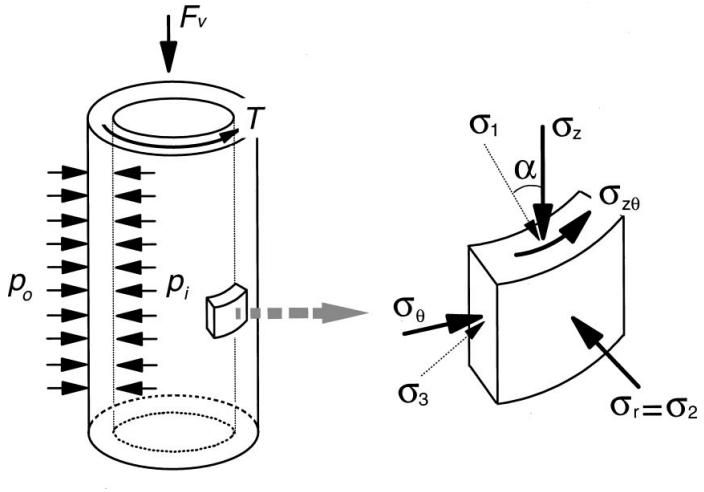

Figure 3.16 Illustration of the bedding plane (z-plane) in a hollow cylindrical sample of torsional apparatus, after Yoshimine et al. (1998) and Dafalias et al. (2004)

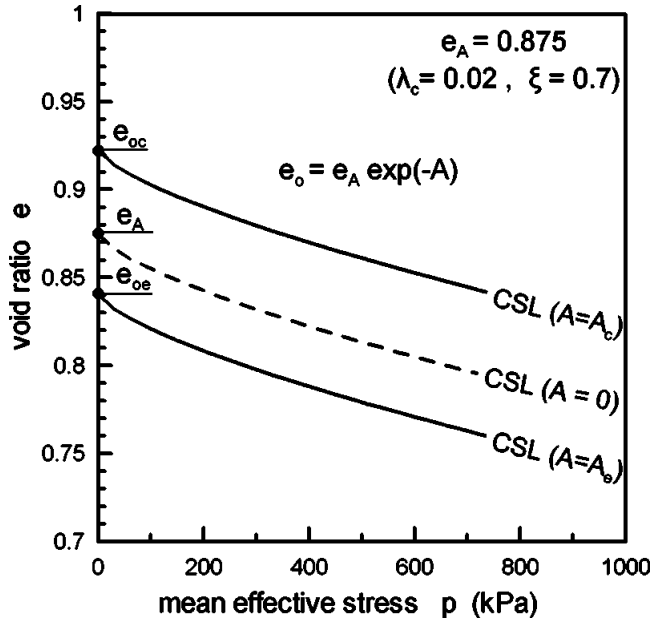

Figure 3.17 Modifications in the theoretical critical state lines for various *A* values, after Dafalias et al. (2004)

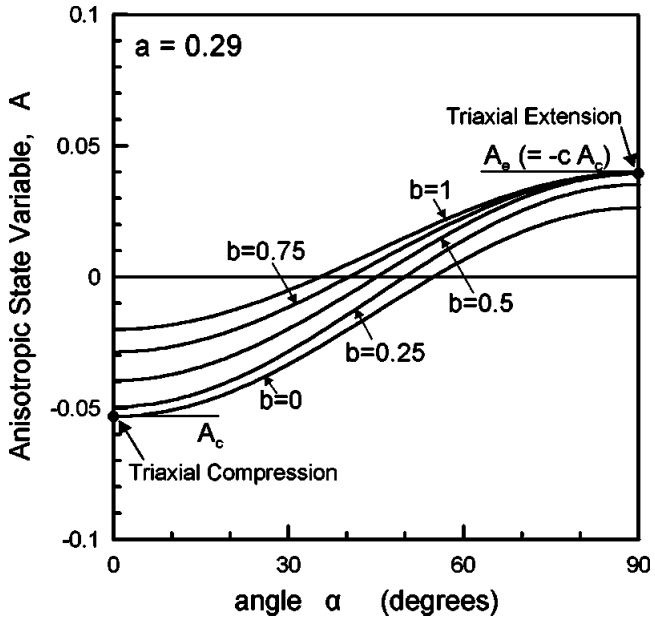

Figure 3.18 Variation of the anisotropic state parameter *A* with α for various *b*-values (Dafalias et al. 2004)

3.4.2 Li and Dafalias (2002) based on the platform model of Li (2002)

The philosophy of the fabric-dependent model of Li and Dafalias (2002) is the same as Dafalias et al. (2004), only differing in the mathematical details of the anisotropic state variable *A*, and the dependence of the critical state line (in void ratio-effective pressure space) on *A*.

The critical state line, in view of anisotropy, is modified as $e_A = e_0 + k_\Gamma A|A|$ (Equation 24 of Li and Dafalias, 2002), where e_A is the void ratio of the critical state line at zero effective confining pressure, denoted as e_Γ in the literature; e_0 is the same as e_A for $A = 0$, an isotropic fabric, denoted as $e_{\Gamma 0}$ in the literature; k_Γ is a postive model constant. Thus it can be seen that for positive values of A, the critical state line is raised, thereby simulating a more dilative behaviour than the platform model; and vice-versa for negative values of A.

The anisotropic state variable (A) is defined as in Equation 3.22 (Equation 22 of Li and Dafalias, 2002).

$$A = \frac{\tilde{R}}{M_c g(\tilde{\theta})} - 1 \qquad \textbf{(3.22)}$$

where $\tilde{R} = \sqrt{3/2 \tilde{r_{ij}} \tilde{r_{ij}}}$; M_c is the stress ratio in triaxial compression at the critical state without the fabric anisotropic effect. Since the fabric anisotropic effect will be inherently present in all naturally occurring specimens, it seems that M_c corresponds to $\alpha = 0$. It is to be noted that in the platform model the equation of the critical state surface is $R - M_c g(\theta) = 0$ where $R = \sqrt{3/2 r_{ij} r_{ij}}$; r_{ij} is the deviatoric stress ratio; and $g(\theta)$ is an interpolating function to interpolate the radius of the surface for various Lode angle (θ) values in between triaxial compression and extension stress paths, such that $g(\theta) = 1$ for triaxial compression. Therefore, it is difficult to consider a physically viable definition of M_c without the fabric anisotropic effect, as suggested by Li and Dafalias (2002). $\tilde{\theta}$ corresponds to the deviatoric tensor $\tilde{r_{ij}}$ instead of the actual deviatoric stress ratio r_{ij}. $\tilde{r_{ij}}$ is the deviatoric component of the stress ratio tensor ($\widetilde{T_{ij}}$) modified to take into account the fabric effect; $\widetilde{T_{ij}}$ is defined by Equation 3.23 (Equation 15 Li and Dafalias, 2002).

$$\widetilde{T_{ij}} = \frac{1}{6}\left(\widehat{\sigma_{ik}} {F_{kj}}^{-1} + {F_{ik}}^{-1} \widehat{\sigma_{kj}}\right) \qquad \textbf{(3.22)}$$

where $\widehat{\sigma_{ik}} = \widehat{r_{ij}} + \delta_{ij}$; δ_{ij} is the Kronecker delta; $\widehat{r_{ij}} = \sqrt{2/3}\, M_c g(\theta) r_{ij} / \sqrt{r_{mn} r_{mn}}$. Thus, $\widehat{r_{ij}}$ is the image point on the critical surface located by radial projection from the origin through r_{ij}. F_{kj} is the fabric tensor as defined in Equation 3.19 and ${F_{ik}F_{kj}}^{-1} = \delta_{ij}$. The fabric tensor is expressed in terms of the vector magnitude Δ where $a = (1 - \Delta)/(3 + \Delta)$.

For an isotropic fabric, $\Delta = 0$; $\widetilde{r_{ij}} = \widehat{r_{ij}}$; $A = 0$. The value of A depends upon the b-value and α. Figure 3.19 shows the variation of A with α for different b-values.

The model requires 3 parameters to incorporate the effect of inherent anisotropy in addition to the 12 parameters required by the platform model of Li (2002). Calibration of Δ is difficult in absence of any micromechanical statistical data. The 3 additional parameters can be determined by solving 3 nonlinear equations which can framed if the critical state line is known for 3 different stress paths such as triaxial compression, triaxial extension and torsional. However, Li and Dafalias (2002) have assumed a value of $\Delta = 0.2$, which corresponds to $a = 0.25$ for dry deposited Toyoura sand, and determined the other 2 parameters from the critical state lines for triaxial compression and extension. It can be noted that the value of a assumed by Dafalias et al. (2004) is 0.29 for the same sand. The model validation is shown for various combinations of b-value and α under monotonic load path.

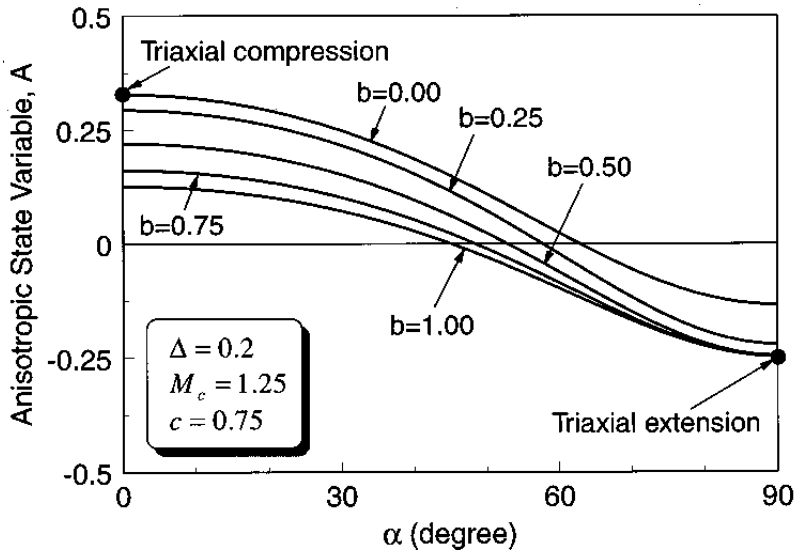

Figure 3.19 Variation of the anisotropic state variable (A) with α and b-values, after Li and Dafalias (2002)

3.4.3 Model for rotational shear loading with fabric anisotropy by Li and Dafalias (2004)

This model is a further improvement of the fabric-dependent model developed by the same authors (Li and Dafalias, 2002) by including a plastic mechanism for neutral or rotational stress path. The platform model (Li, 2002) has two plastic mechanisms: deviatoric and hydrostatic. The deviatoric mechanism cannot predict plastic strain for rotational stress

path because the model is not hypoplastic. Hence, there is a requirement of a third mechanism which should be hypoplastic. Li and Dafalias (2004) assumed that plastic mechanism under rotational stress path is due to the fabric or inherent anisotropy. If an isotropic fabric is assumed, then the third mechanism becomes inactive as per the model formulation.

As shown in Figure 3.20, the direction of the plastic strain increment associated with the first deviatoric non-rotational mechanism is given by the gradient of the bounding surface at the image point $\bar{\boldsymbol{r}}$ (boldfaced notations indicate tensor quantities). For the third deviatoric rotational mechanism, the reference direction is shown as $\boldsymbol{n}$, which is evaluated at another image point located by radial projection rule with origin as the centre of projection. It is assumed that the directions of $\boldsymbol{r}$ and $\boldsymbol{n}$ are parallel; however, owing to the Lode angle dependent definition of the bounding surface, $\boldsymbol{n}$ will generally deviate from the direction of $\boldsymbol{r}$. Since such deviations are usually small, one can assume that $\boldsymbol{n}$ is parallel or coaxial with $\boldsymbol{r}$. It is to be noted that $\boldsymbol{n}$ is not the direction of plastic deviatoric strain increment associated with rotational stress path. The stress increment, $\mathrm{d}\boldsymbol{r}$ is resolved in two components: one along $\boldsymbol{n}$ and the other perpendicular to $\boldsymbol{n}$. The second component is the increment along rotational stress path, and is denoted as $\mathrm{d}\boldsymbol{r}'$ where $\mathrm{d}\boldsymbol{r}' = \mathrm{d}\boldsymbol{r} - (\boldsymbol{n}:\mathrm{d}\boldsymbol{r})\boldsymbol{n}$; the quantity $\boldsymbol{n}:\mathrm{d}\boldsymbol{r}$ is the magnitude of the radial component. The loading direction associated with $\mathrm{d}\boldsymbol{r}'$, denoted as $\boldsymbol{l}$, is considered as a linear combination of $\boldsymbol{l}'$, a unit tensor along $\mathrm{d}\boldsymbol{r}'(\boldsymbol{l}' = \mathrm{d}\boldsymbol{r}'/\sqrt{\mathrm{d}\boldsymbol{r}':\mathrm{d}\boldsymbol{r}'})$ and $\boldsymbol{n}$; specifically, the definition of $\boldsymbol{l}$ is given in Equation 3.23 (Equation 19 of Li and Dafalias, 2004).

$$\boldsymbol{l} = \frac{\gamma}{\sqrt{1-2\gamma(1-\gamma)}}\boldsymbol{l}' + \frac{1-\gamma}{\sqrt{1-2\gamma(1-\gamma)}}\boldsymbol{n} \qquad \textbf{(3.23)}$$

where γ is a positive scalar; it can be verified that $\boldsymbol{l}:\boldsymbol{l} = 1$ since $\boldsymbol{l}':\boldsymbol{n} = 0$ by the definition of $\boldsymbol{l}'$; $\gamma = \langle 1 - \eta/M_c \rangle$, where η is the stress ratio; M_c is the stress ratio of the critical state surface at the same Lode angle as the stress ratio; $\langle . \rangle$ is Macaulay's bracket. It may be noted that when critical state is attained, $\gamma = 0$; and hence, $\boldsymbol{l} = \boldsymbol{n}$, a purely coaxial flow. This is supported by experimental evidences, such as Gutierrez et al. (1991); Cai et al. (2013). Therefore, the plastic strain increment associated with $\boldsymbol{l}$ can be simply written as $\mathrm{d}L_3 = \boldsymbol{l}\mathrm{d}\boldsymbol{r}'/K_{p3}$ (the number 3 in the suffix indicates the quantities of the third mechanism; K_{p3} is the plastic modulus). Associated flow rule is followed; so the direction of the plastic strain

increment for the third mechanism is $\boldsymbol{l}$. It can be noted that the third mechanism is hypoplastic because the direction of plastic strain increment depends on the direction of stress increment via $\boldsymbol{l}'$. Separate definitions are proposed for the dilatancy and the plastic modulus for the third mechanism.

The novelty in this model is that the expression for K_{p3} is formulated in such a way that $K_{p3} \to \infty$ for $A = 0$ (an isotropic fabric). Therefore, the authors assumed that accumulation of plastic strain along rotational stress path is attributable to the inherent anisotropy. However, the definition of A for the non-rotational deviatoric mechanism is slightly different from that of Li and Dafalias (2002). The new definition of A (designated as $\bar{A}$) is based on the same method as Li and Dafalias (2002) , but $\hat{r_{ij}}$ is Equation 3.22 is defined as $M_c g(\theta)\, \bar{\boldsymbol{r}}/\sqrt{\bar{\boldsymbol{r}}:\bar{\boldsymbol{r}}}$ ($\bar{\boldsymbol{r}}$ is on the bounding surface and $\hat{r_{ij}}$ is on the critical state surface along the same direction). Model requires calibration of additional 5 parameters for the third mechanism (giving a total of 23 parameters). However, there is limited discussion in Li and Dafalias (2004) on the calibration method, which seems to be trial and error.

The model of Li and Dafalias (2002) was already complex because of the two plastic mechanisms and additional modifications on the account of fabric anisotropy. Now the introduction of the third mechanism renders the model almost intractable not only by further raising the analytical complexity, but also due to the complex calibration procedure of the parameters of the third mechanism. Validation of the third mechanism is rendered even more difficult by the limited availability of experimental data on rotational stress path. In contrast to the multi-mechanism approach, a single hypoplastic deviatoric mechanism, such as the flow rule postulated by Gutierrez et al. (1991) and used in Cubrinovski and Ishihara (1998b) seems to be more pragmatic for rotational stress paths. In this respect, the model formulated by Lashkari and Latifi (2007) requires mentioning because it combines the hypoplastic flow rule of Gutierrez et al. (1991) and the fabric anisotropic effect of Dafalias et al. (2004), although in plane-strain format, which appears to be the simplest approach to consider rotational stress path along with the fabric anisotropy. However, it has certain similarities with the model of Li and Dafalias (2004) of having separate definitions of the plastic modulus and the stress-dilatancy relation for rotational stress paths.

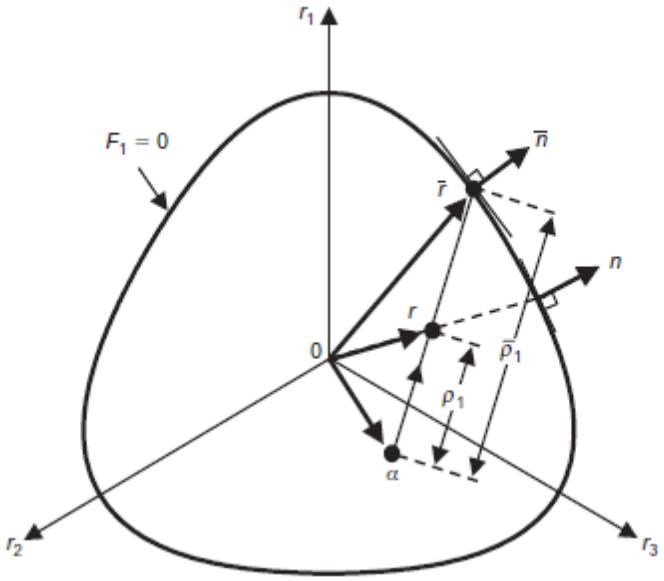

Figure 3.20 The projection rule for the rotational deviatoric mechanism, after Li and Dafalias (2004)

3.5 Discussion

The constitutive modelling of sand is complex and there is no unified approach or theory. The state-of-the-art plasticity-based models vary widely in concepts. Each model is based on certain assumptions, idealisations and simplifications. There is no single model that can necessarily capture all aspects of sand behaviour in a strict sense. A comparative summary of the mathematical features of the models reviewed herein is given in Table 3.1. These models collectively focus on the following features of sand behaviour: development of excess pore pressure during cyclic loading; influence of state parameter and critical state framework; accumulation of plastic strain along rotational stress path; effect of stress path relative to the orientation of initial fabric; and development of plastic strain during cyclic mobility. Depending upon the specific mathematical features of the models, they can be grouped as follows.

1. State concept based models. The models based on the state concept are theoretically more accomplished. The state concept allows continuous change in constitutive behaviour with the relative state during course of an analysis. The usefulness of the state concept is that it combines the effect of the void ratio (or relative density) and the confining stresses on the critical constitutive behaviour, such as the stress-strain response and the stress dilatrancy relation. Therefore, the state concept enables

capturing very subtle features of sand behaviour such as strain softening and hardening of dense and loose sands, respectively, in proximity to critical state. In state concept based approach critical state is considered as the reference state. Calibration of models without state concept is based on the initial void ratio and the confining pressure, or the initial relative state. The change in the relative state depends upon the geometry of the critical state line in the void ratio and effective pressure space which in turn depends on specific stress path. The state concept based models are those of Cubrinovski and Ishihara (1998b); Li (2002); and, Dafalias and Manzari (2004).

2. Hypoplastic models. To capture the effect of rotational stress paths, the models should be hypoplastic. The hypoplastic models are Wang et al. (1990); Cubrinovski and Ishihara (1998b); and, Li and Dafalias (2004). The accumulation of strain along rotational stress path can be attributed to induced anisotropy (Wong and Arthur, 1986).

3. Models considering the effect of fabric. In seismic response analysis, it can be assumed that the deviatoric stresses primarily comprise tangential shear stresses along two mutually orthogonal directions on the isotropic horizontal bedding plane. For such cases, the angle between the major principal plane and the bedding plane (α) is constant at $45°$, and so is the b-value at 0.5. Therefore, the fabric anisotropy effect will be also constant during the response. Thus, if a model which is based on the concept of isotropic fabric could be calibrated for the condition of $\alpha = 45°$ and $b = 0.5$ then it would directly incorporate the fabric anisotropic effect. The models which consider fabric anisotropy are Dafalias et al. (2004); Li and Dafalias (2002, 2004). These models postulate that the fabric anisotropy is the main reason for non-uniqueness and stress-path dependence of critical state. However, detailed experimental investigation is needed to support their postulation. In this regard, the model of Cubrinovski (1993); Cubrinovski and Ishihara (1998a,b) has attempted to incorporate the effect of initial fabric by defining state index using the quasi-steady state line for medium to loose sand, which appears to depend upon the sample preparation method, and thus, the initial fabric. However, as the model of Cubrinovski (1993); Cubrinovski and Ishihara (1998b) assumes uniqueness of quasi-steady state line for a given sample preparation method, the inherent assumption is isotropic fabric.

4. Models with novel stress-dilatancy relation to capture development of shear strain during cyclic mobility. The models proposed by Yang et al. (2003); Yang and Elgamal (2008); Zhang and Wang (2012) have specific formulations embedded in stress-dilatancy relations to directly control the spread of plastic strain during cyclic mobility. There is a possibility of strain saturation with the other models which do not have any explicit control over the post-liquefaction behaviour, although a double amplitude strain of 5-6% is often considered as sufficient for engineering purpose.

One important criterion for the model selection is the calibration requirement of the model constants because the performance of models can be quite sensitive to its parameters. Ideally, one should adopt a model with the least number of constants and those constants should lend themselves for simple calibration procedures based on physically measured quantities rather than the trial and error approach of data-fitting. Given that the models are intended for cyclic loading of saturated soils then such constants should be calibrated with cyclic drained and undrained tests. The models should be capable of accurately modelling liquefaction resistance curves for any relevant density or stress state, and produce typical strain development for loose and dense sands.

3.6 Summary

The chapter reviews plasticity-based 11 models which are based on isotropic fabric and 3 models which are based on anisotropic fabric for shear deformation of sand under cyclic loading condition. These models, in contrast to the conventional 'cap' models, follow non-associated flow wherein the dilatancy is explicitly controlled by various forms of stress-dilatancy relations. Furthermore, plastic mechanism is notionally split in two independent superimposable mechanisms: deviatoric and volumetric, each separately producing both the deviatoric and the hydrostatic plastic strains. The plastic volumetric mechanism, which requires a 'cap' surface, is generally considered as dormant in applications concerning earthquake-induced liquefaction behaviour because it is the shear deformation in low to moderate confining pressure that dominates the response. Sand, in contrast to clay, exhibits a very high equivalent pre-consolidation pressure in the order of magnitude of mega-pascal when particles begin to crush. Liquefaction is usually not observed in the particle crushing region because of the presence of very high confining pressure in the order of mega-pascal. The applicability of the models reviewed herein is thus limited to the lower range of

confining pressure such that the isotropic compression of sand can be assumed to be elastic. Although there are few models that have considered active 'cap' surface, they are not validated in the particle crushing region. It has been observed during the review that the bounding surface plasticity and hypoplastic flow rule have gained more success than the conventional plasticity-based approach.

The constitutive behaviour of sand is greatly affected by density, confining effective pressure and microstructure which is often referred to as fabric: an arrangement of particles in a representative volume. Fabric carries the depositional history of sands. Sands even with the same inherent fabric exhibit widely varying behaviour under different stress paths. It is assumed that fabrics undergo continuous change under action of applied stresses even if the stress path is purely rotational. The rearrangement of particles, and hence, the stress-induced change in fabric composition is manifested macroscopically as permanent or plastic strains. In contrast to the concepts of critical state soil mechanics, there is no unique critical state line for sands, which depends upon the deformation history. Different load paths produce different critical state line in void ratio-effective pressure space, although the stress ratio at critical state may be invariant. Even for a given critical state line, there is uncertainty whether there is a unique fabric for every void ratio-pressure combination.

Table 3.1: A comparative review of the constitutive models for sand

Models	Category	Scope	Relative mathematical complexity	Plastic volumetric mechanism	Lode angle effect	Backbone curve	Fabric anisotropy	Plastic behaviour in rotational stress path	State concept	Specialised for post-liquefaction behaviour	Number of parameters	Calibration data[1]
Multiple surface based model by Prevost (1985)	Classical plasticity theory	Three dimension	Simple	No	No	Stain hardening	No	No	No	No	6 parameters and additional 4 parameters for each yield surface. In the paper, 10 yield surfaces were used.	MDTC and MDTE
Critical state and bounding surface based model by Bardet (1986)	Bounding surface plasticity theory	Three dimension	Medium	Yes	Yes	Stain hardening	No	No	No	No	9	MDTC, MDTE, IC

[1] Monotonic drained (p-constant) test is mainly required to calibrate stress-strain backbone curve; undrained monotonic test is mainly used to obtain stress ratio at phase transformation and at steady state; cyclic drained and undrained test is used to calibrate other parameters of stress-dilatancy relation for cyclic situation; quasi-steady state and steady state lines are obtained by undrained triaxial compression test; some models, as specified, additionally use consolidation test to calibrate bulk modulus. Following acronyms are used: MUTC: Monotonic Undrained Triaxial Compression; MUTE: Monotonic Undrained Triaxial Extension; MDTC: Monotonic Drained Triaxial Compression; MDTE: Monotonic Drained Triaxial Extension; MDTX: Monotonic Drained Torsional; CDT: Cyclic Drained Triaxial; CUT: Cyclic Undrained Triaxial; CDTX: Cyclic Drained Torsional; CUTX: Cyclic Undrained Torsional; IC: Isotropic Consolidation; AIC: Anisotropic Consolidation.

Models	Category	Scope	Relative mathematical complexity	Plastic volumetric mechanism	Lode angle effect	Backbone curve	Fabric anisotropy	Plastic behaviour in rotational stress path	State concept	Specialised for post-liquefaction behaviour	Number of parameters	Calibration data[1]
Hypoplasticity and bounding surface based model by Wang et al. (1990)	Based on bounding surface plasticity	Three dimension	High	Yes	Yes	Stain hardening	No	Yes	No	No	15	MDTC, MDTE, MUTC, MUTE, AIC
Hypoplastic and strain dependent stress-dilatancy model by Cubrinovski (1993); Cubrinovski and Ishihara (1998b)	Uses the methods of both classical and bounding surface plasticity.	Plane-strain	Simple	No	No	Simulates both strain hardening and strain softening behaviour via state-dependence	No	Yes	Yes	No	11	MDTX, CUTX, MUTC
Bounding surface based model with state concept by Manzari and Dafalias (1997)	Based on bounding surface plasticity	Three dimension	Medium	No	Yes	Simulates both strain hardening and strain softening behaviour via state-dependence	No	No	Yes	No	11	MUTC, MUTE, MDTC, MDTE
Bounding surface with state dependent based dilatancy	Based on bounding surface	Three dimension	High	Yes	Yes	Simulates both strain hardening and strain	No	No	Yes	No	15	MUTC, MUTE, MDTC,

Models	Category	Scope	Relative mathematical complexity	Plastic volumetric mechanism	Lode angle effect	Backbone curve	Fabric anisotropy	Plastic behaviour in rotational stress path	State concept	Specialised for post-liquefaction behaviour	Number of parameters	Calibration data[1]
model Li and Dafalias (2000) and Li (2002)	plasticity					softening behaviour via state-dependence						MDTE
Multiple surface based model without Lode angle effect by Yang et al. (2003) and with Lode angle effect by Yang and Elgamal (2008)	Based on classical plasticity theory	Three dimension	Simple	No	Yes	Strain hardening	No	No	No	Yes	15	IC, MDTC, CUT
Bounding surface based model with fabric effect on dilatancy by Dafalias and Manzari (2004)	Based on bounding surface plasticity	Three dimension	Medium	No	Yes	Simulates both strain hardening and strain softening behaviour via state-dependence	No	No	Yes	No	15	MUTC, MUTE, MDTC, MDTE
Bounding surface plasticity based on large	Based on bounding surface plasticity	Three dimension	Medium	No	Yes	Strain hardening	No	No	No	Yes	11	MUTC, MUTE, MDTC, MDTE, IC,

Models	Category	Scope	Relative mathematical complexity	Plastic volumetric mechanism	Lode angle effect	Backbone curve	Fabric anisotropy	Plastic behaviour in rotational stress path	State concept	Specialised for post-liquefaction behaviour	Number of parameters	Calibration data[1]
deformation mechanism by Zhang and Wang (2012)												CDT or CDTX, CUTX
Model of Dafalias et al. (2004) based on the platform model Dafalias and Manzari (2004)	Based on bounding surface plasticity	Three dimension	Medium	No	Yes	Simulates both strain hardening and strain softening behaviour via state-dependence	Yes	No	Yes	No	17	Additionally, steady state lines for triaxial compression and extension stress paths are required
Model by Li and Dafalias (2002) based on the platform model Li (2002)	Based on bounding surface plasticity	Three dimension	High	Yes	Yes	Simulates both strain hardening and strain softening behaviour via state-dependence	Yes	No	Yes	No	15	Additionally, steady state lines for triaxial compression, extension and torsional stress paths are required
Model for rotational shear loading with fabric anisotropy by	Based on bounding surface plasticity	Three dimension	Very high	Yes	Yes	Simulates both strain hardening and strain softening	Yes	Yes	Yes	No	23	Additionally, rotational tests are required (using

Models	Category	Scope	Relative mathematical complexity	Plastic volumetric mechanism	Lode angle effect	Backbone curve	Fabric anisotropy	Plastic behaviour in rotational stress path	State concept	Specialised for post-liquefaction behaviour	Number of parameters	Calibration data[1]
Li and Dafalias (2004)						behaviour via state-dependence						torsional apparatus) to calibrate the third – rotational mechanism

4.0 Development of three-dimensional stress-strain-dilatancy model for shear deformation of sand

4.1 Introduction

Experimental studies and constitutive modelling of soils are often based on restrictive stress paths enforced by conventional triaxial and torsional apparatuses which can only partially simulate earthquake induced stresses. The triaxial stress path and the effective seismic stress path comprising bidirectional transverse shear stress from the consideration of nonlinear soil response, are along mutually orthogonal planes in complex stress space. Moreover, the triaxial test cannot simulate the rotation of principal stresses which is known to be significant and often observed during earthquake induced ground motions. It can be shown that under bidirectional shear stress, the third stress invariant becomes zero, and hence, corresponds to a stress path of $b = 0.5$. The torsional apparatus can imitate such a stress path, but only under unidirectional shear stress, e.g. Gutierrez et al. (1991). However, the effect of bidirectional shear stress on nonlinear soil response is much more profound than the unidirectional. As shown in Figure 1.1 adopted from Ishihara and Yamazaki (1980), the cyclic resistance ratio under different paths of bidirectional transverse shear is significantly less than that of the unidirectional; strength reduces consistently as the bidirectional effect is increased, with the cyclic resistance ratio reduced to almost 60% of the unidirectional value under circular stress path. Experimental studies on the bidirectional response of soils are very few, and this has been a major hindrance for validation of advanced constitutive models for bidirectional stress paths. Kammerer (2002) notes that *'Unfortunately, the use of advanced constitutive soil models for liquefiable soils is being hampered by a lack of the high-quality laboratory testing for use in the validation of existing models and development of new ones. In particular, very little modeling-quality testing has been performed on: a) medium dense to dense sand that exhibits dilative behavior, b) sands under initial driving shear conditions as would be found in sloping ground or under a structure, and c) sands experiencing multidirectional stress (or strain) paths.'* Although the effect of bidirectional stress path on seismic response of soils is recognised, it is considered to be the least known facet of earthquake geotechnical engineering. The University of California Berkeley bidirectional simple shear apparatus developed by Boulanger et al. (1993) is the only presently available apparatus for producing bidirectional transverse shear. The complexity of experimental

observations made under various types of bidirectional transverse shear, such as elliptical, circular and of rose-petal (lemnsicate) shapes by Kammerer (2002), seems to have obscured new ideas for specialised plasticity-modelling features for bidirectional shear; as far as the author is aware, not a single case is noted where constitutive modelling is attempted to simulate the cases investigated by Kammerer (2002). Simulation of bidirectional effect on ground response was attempted by Cubrinovski et al. (1996) by performing separate plane-strain analysis along pre-selected major and minor principal directions in terms of peak ground acceleration. The ground motion considered had a pronounced directionality, which indicates minimal bidirectional effect along the principal directions, and consequently, the pore pressure generation was controlled exclusively by the major principal direction. It appears that although a specialised constitutive model is required, it would be still based on the constitutive relations that are observed for unidirectional simple shear or torsional stress paths. In this context, a three-dimensional model is developed based on the existing plane-strain model of Cubrinovski (1993); Cubrinovski and Ishihara (1998b), a succinct review of which is presented in chapter 3.

The new formulation preserves the constitutive relationships of the plane-strain model of Cubrinovski (1993); Cubrinovski and Ishihara (1998b) with a primary aim to simulate liquefaction behaviour under bidirectional transverse shear, or the so-called torsional shear. The model includes all the desirable features of sand behaviour in shear deformation. First, the model is hypoplastic which renders the capability to reproduce plastic shear strain and consequent volumetric strain from dilatancy during continuous rotation of principal stress, even with a constant shear stress ratio. The hypoplastic flow rule enables the consideration of non-coaxial direction of plastic strain increment with that of the principal stresses, and consequently, pronounced dilatancy behaviour during such non-coaxial flow. Second, the stress-dilatancy relationship is strain-dependent, which causes the stress-dilatancy relation to be state-dependent. Third, the model includes the critical state framework, where critical state is represented either by the steady state (Poulos, 1981) or by the quasi steady state (Alarcon-Guzman et al., 1988). Fourth, the constitutive parameters are state-dependent (Cubrinovski and Ishihara, 1998a). The state-dependence enables characterisation of sands, such as the elastic and plastic moduli, the peak strength and the dilatancy depending upon the density and effective confining pressure. Thus, the constitutive behaviour is referenced to and tuned by

the state parameter that continuously change along a stress path and not only by a fixed set of parameters.

4.2 Deviatoric plastic mechanism

The rate-independent, incremental plastic flow theory is adopted based on the general framework of the bounding surface plasticity (Dafalias, 1986). All stress and strain quantities are expressed in standard tensor (indicial) notation. The stress tensor is resolved in deviatoric and hydrostatic (spherical) components as shown in Equation 4.1

$$\sigma_{ij} = s_{ij} + p\delta_{ij} \tag{4.1}$$

where σ_{ij} is the total stress tensor; s_{ij} is the deviatoric stress tensor; p is the effective pressure; δ_{ij} is the Kronecker delta. The incremental form of Equation 4.1 is shown in Equation 4.2, as follows.

$$\mathrm{d}\sigma_{ij} = p\mathrm{d}r_{ij} + \frac{\sigma_{ij}}{p}\mathrm{d}p \tag{4.2}$$

where $r_{ij} = s_{ij}/p$ is the deviatoric stress ratio. As can be seen from Equation 4.2, the stress increment can be resolved in two parts, each representing an independent mechanism. The first part, $p\mathrm{d}r_{ij}$, is due to the shear deformation or the deviatoric mechanism at a constant effective pressure, p; while the second part, $(\sigma_{ij}/p)\mathrm{d}p$, is from the consolidation mechanism at a constant stress ratio, r_{ij}. It is assumed that the latter mechanism is elastic under low to moderate confining stresses for which the model is applicable (Pestana and Whittle, 1995). A geometrical interpretation of Equation 4.2 is shown in Figure 4.1, where the vectors $\overrightarrow{OA} = \sigma_{ij}$ and $\overrightarrow{AC} = \overrightarrow{AB} + \overrightarrow{BC} = \mathrm{d}\sigma_{ij}$; it can be seen that $\overrightarrow{BC} = \overrightarrow{AD} = \mathrm{d}r_{ij}p$ is the stress increment due to the deviatoric mechanism and $\overrightarrow{AB} = r_{ij}\mathrm{d}p + \delta_{ij}\mathrm{d}p$ is due to the consolidation mechanism.

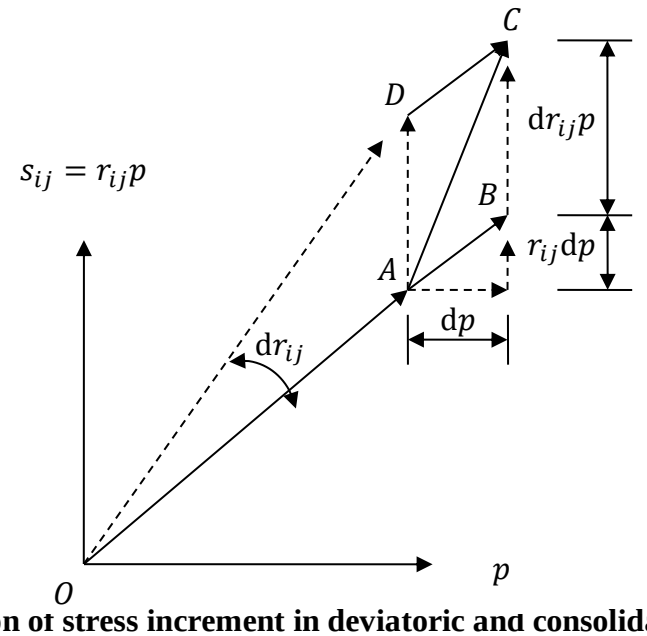

Figure 4.1 Resolution of stress increment in deviatoric and consolidation mechanisms

The total strain increment $\left(\mathrm{d}\epsilon_{ij}\right)$ is divided into elastic strain increment $\left(\mathrm{d}\epsilon_{ij}^{e}\right)$ and plastic strain increment $\left(\mathrm{d}\epsilon_{ij}^{p}\right)$ respectively, as shown in Equation 4.3.

$$\mathrm{d}\epsilon_{ij} = \mathrm{d}\epsilon_{ij}^{e} + \mathrm{d}\epsilon_{ij}^{p} \tag{4.3}$$

The total stress increment is determined from the elastic strain increment using the elastic and isotropic constitutive relation, as shown in Equation 4.4

$$\mathrm{d}\sigma_{ij} = 2G_e\mathrm{Dev}\left(\mathrm{d}\epsilon_{ij}^{e}\right) + K\mathrm{d}\epsilon_{kk}^{e} \tag{4.4}$$

where G_e is the elastic shear modulus; K is the bulk modulus; and $\mathrm{Dev}(.)$ is the deviatoric transform of a tensor.

4.3 Bounding surface

A circular bounding surface is assumed with an initial deviatoric back-stress tensor, as shown in Equation 4.5

$$F\left(\sigma_{ij}\right) = \sqrt{\frac{\left(s_{ij} - pa_{ij}\right)\left(s_{ij} - pa_{ij}\right)}{2}} - p\eta_{max} = 0 \tag{4.5}$$

where a_{ij} is the initial deviatoric back-stress tensor; η_{max} is the radius of the bounding surface projected on the reference deviatoric plane, $p = 1$. The bounding surface, $F = 0$, represents states of peak stress ratio, η_{max}, which depends on the current density (void ratio)

and the effective pressure; η_{max} was calibrated by Cubrinovski and Ishihara (1998a) for the plane-strain model at 10% strain in p-constant drained test in a torsional apparatus on various specimens with different initial states. Mathematically, the bounding surface, $F = 0$, can be also defined as a state of zero plastic modulus; alternatively, a bounding state of only positive plastic modulus. In the present formulation, no state of stress can lie outside the surface, $F = 0$; contrastingly, in the model of Manzari and Dafalias (1997), a state of stress can move outside the bounding surface, although temporarily, before collapsing again on the same, as the bounding surface continues to evolve with state parameters, namely, void ratio and effective pressure. This provides a definitive way of simulating strain-softening response via negative plastic modulus, which is not achieved in the similar manner in this model. Here η_{max}reduces, as the bounding surface shrinks with the state parameters. If a stress point has already reached the bounding surface, it also reduces in magnitude accordingly, while the plastic modulus remains constant at zero.

Equation 4.5 is anisotropic Drucker-Prager yield criterion which can be matched with Mohr-Coulomb for any given Lode angle (or b-value). For seismic stress path comprising bidirectional transverse shear, η_{max} has been adopted to correspond to the b-value of 0.5. The initial deviatoric back-stress tensor, a_{ij}, is constant and serves two purposes: first, to simply match Mohr-Coulomb yield criterion at triaxial compression and extension apices for triaxial stress path, if so desired, as followed by Prevost (1985); and second, to incorporate the effect of direction of stress path relative to the orientation of the initial fabric on the bounding surface. An isotropic bounding surface matched with Mohr-Coulomb for torsional stress path corresponding to Lode angle of 30°, or b-value of 0.5 is shown by solid line in Figure 4.2c. If the bounding surface is considered as isotropic $(a_{ij} = 0)$, then η_{max} is identical at points A and B. However, this is not observed in real sand behaviour because sand is inherently anisotropic along the direction of deposition, normal to the bedding plane. Therefore, sands are considered as transversely isotropic along the bedding plane. In Figure 4.2a, the bedding plane is denoted as the z-constant plane. The limits of the bounding surface for different stress paths depend on their directions relative to the bedding plane measured by the angle α between the major deviatoric principal stress plane and the bedding plane, as shown in Figure 4.2b. The angle $\alpha = 0, 90°$ correspond to points A and B in triaxial space, respectively, as shown in Figure 4.2c; while $\alpha = 45°$ at point C, which is along a plane normal to the

octahedral or the principal (triaxial) deviatoric plane. It was shown by Gao and Zhao (2012) via a cross-deviatoric invariant of a transversely isotropic fabric tensor and deviatoric stress tensor that the shear stress at failure would be maximum at A, minimum at B, and intermediate at C. Along with this requirement, and the need to preserve transverse isotropy, a_{ij} will be along that triaxial compression stress path for which the bedding plane is the major principal plane. Thus, if the reference system is chosen as per Figure 4.2a, then $a_{xx} = a_{yy} = -a_{zz}/2$; and point C is assumed to lie on the bounding surface shifted in the principal deviatoric space along the direction of s_{zz}. Despite the foregoing theoretical justification for a_{ij}, an isotropic bounding surface for predominantly bidirectional transverse shear (torsional) stress paths can be derived for simplification without compromising the theory, as presented subsequently.

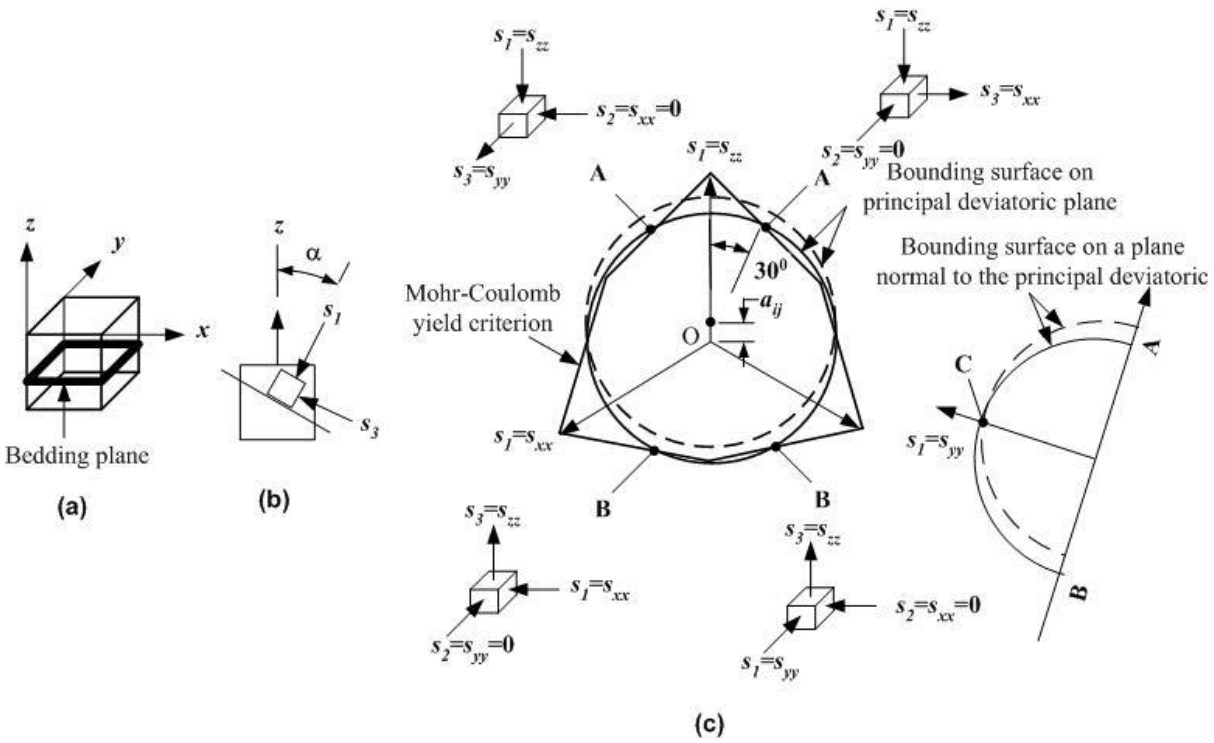

Figure 4.2 Geometrical interpretation of the bounding surface; (a) reference coordinate system; (b) non-coincidence of the major deviatoric principal plane with the bedding or *z* constant plane; (c) Drucker-Prager type bounding surface matched with Mohr-Coulomb for torsional stress path (shown by solid line) and then shifted towards the bedding plane to account for transverse isotropy (shown by dotted line)

4.3.1 Rationale for isotropic bounding surface for torsional stress path

While there have been some recent efforts to include the effects of inherent anisotropy by the aforementioned method of introducing an initial deviatoric back-stress tensor in the

equations of yield surfaces (Imam et al., 2002), there are several difficulties that preclude this methodology of anisotropic bounding surface. It can be seen from Figure 4.2 that the relative direction of the major deviatoric principal stress with the bedding plane measured by the angle α, will be 0, 45 and 90 degrees, respectively, at points A, B and C. Hence, it can be assumed that the same set of constitutive properties or relations will not be generally applicable for these stress paths in view of the anisotropic fabric. It can be inferred from the works of Vaid and Chern, 1985; Vaid et al., 1990; Vaid and Thomas, 1995; Reimer and Seed, 1997 that critical state line is responsive to stress path on the account of fabric anisotropy, which is also accepted by the state-of-the-art in constitutive modelling, e.g., Gutierrez (2003); Dafalias et al. (2004) amongst others, which explains the variations in the observed responses (such as in Yoshimine et al., 1998) for stress paths with different values of α and b; for example, Yoshimine et al. (1998) showed that response becomes more contractive with increase in α for a constant b-value and vice-versa.

The non-uniqueness of the critical state line means that evolution of the bounding surface with the state index, which represents the strength of a soil in terms of η_{max}at critical state on void ratio-effective pressure space, will be also anisotropic, i.e. a_{ij} will evolve with state index. However, such modelling effort is seriously impeded by unavailability of high quality experimental data, such as that of Verdugo and Ishihara (1996), on critical state behaviour under different stress paths characterised by α and b-value. Fortunately, this intractable problem can be circumvented for seismic stress paths of bidirectional transverse shear because both α and b-value are constant at $45°$ and 0.5, respectively, as in unidirectional torsional stress path. Since $a_{ij}s_{ij} = 0$ for bidirectional simple shear ($s_{ij} = 0$ for $i = j$ and $a_{ij} = 0$ for $i \neq j$) and a_{ij}, which depends on α and b-value, is also constant, Equation 4.5 can be modified to an isotropic form, as shown in Equation 4.6.

$$F(\sigma_{ij}) = \sqrt{\frac{s_{ij}s_{ij}}{2}} - p\eta_{max}\sqrt{1 - \frac{a_{kl}a_{kl}}{2{\eta_{max}}^2}} = 0 \qquad \textbf{(4.6)}$$

In the original plane-strain model of Cubrinovski (1993); Cubrinovski and Ishihara (1998b), η_{max} and the critical state line were established for torsional stress path with $\alpha = 45°$ and $b = 0.5$. Hence, η_{max} and its state dependent evolution corresponded to point C, and η_{max} implicitly included the effect of the term $\sqrt{1 - (a_{kl}a_{kl})/(2{\eta_{max}}^2)}$. This enables a

significant simplification of the model without introducing any error in the definition of the bounding surface for the assumed seismic stress path which essentially remains constant; moreover, as $0 \leq \sqrt{a_{kl}a_{kl}/2} \leq 0.15\eta_{max}$ (Imam et al., 2002), $1 \geq \sqrt{1-(a_{kl}a_{kl})/(2{\eta_{max}}^2)} \geq 0.9$. Therefore, the assumption of isotropic bounding surface also does not introduce any appreciable numerical error, provided the model parameters are calibrated for stress paths with $\alpha = 45°$ and $b = 0.5$.

4.4 Definitions of generalised shear stress and strain

The expressions for generalised shear stress (q), shear stress ratio (η) and plastic shear strain increment $(\mathrm{d}\lambda)$ are given by Equation 4.7.

$$\left.\begin{aligned} q &= \sqrt{\frac{(s_{ij}-pa_{ij})(s_{ij}-pa_{ij})}{2}} \\ \eta &= \frac{q}{p} = \sqrt{\frac{(r_{ij}-a_{ij})(r_{ij}-a_{ij})}{2}} \\ \mathrm{d}\lambda &= \sqrt{2\mathrm{Dev}(\mathrm{d}\epsilon_{ij}{}^{p})\mathrm{Dev}(\mathrm{d}\epsilon_{ij}{}^{p})} \end{aligned}\right\} \quad \textbf{(4.7)}$$

These quantities are thus invariants and are scaled to match with those of the plane-strain model of Cubrinovski and Ishihara (1998b), enabling use of the plastic modulus in the exact form as the plane-strain model.

4.5 Hypoplastic deviatoric flow rule

The model formulation is based on the projection of the bounding surface on the deviatoric reference plane of $p = 1$. Since the stress ratio, r_{ij}, is the same as s_{ij} on this reference plane, r_{ij} is used instead of s_{ij} in the model formulation (as shown by the second expression in Equation 4.7). In conventional plasticity theory, the plastic potential function, having the same parametric form as the yield surface, depends only on the stress invariants. Therefore, the principal direction of plastic strain increment becomes the same as that of the stresses. As opposed to the real sand behaviour, models based on such conventional flow rule cannot predict plastic strain during rotational stress paths where only directions of stresses are rotated keeping the magnitude constant. For materials with vanishingly small yield surface, direction of plastic strain increment depends additionally on the direction of stress increment,

and the aforementioned limitation of the conventional flow rule is overcome. Such a flow rule is known as hypoplastic flow rule, which was postulated by Dafalias (1986) in the formalism of bounding surface plasticity. Non-coaxiality is also common to those models which employ kinematically hardening finite yield surface within a bounding surface, which does not require dependence of direction of plastic strain increment on the direction of the stress increment; but the degree of non-coaxiality depends on the size of the yield surface. However, for soils having very small yield surface, non-coaxiality is only achieved via hypoplastic flow rule as observed by Gutierrez (1991) during a series of probe-tests on Toyoura sand specimens.

The deviatoric component of the plastic strain increment is given by the gradient of the bounding surface at an image point, X_{ij}. The image point is located by a special projection rule with the current stress ratio, r_{ij}, as the centre of projection and the direction along $\mathrm{d}r_{ij}$ as shown in Figure 4.3.

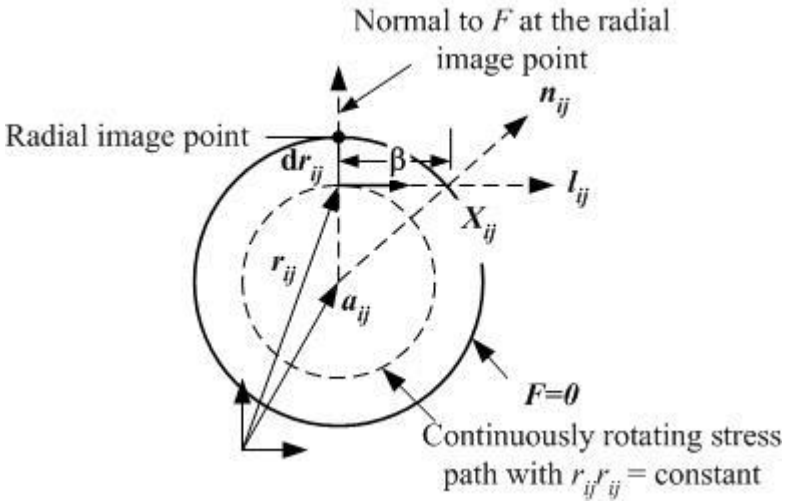

Figure 4.3 Hypoplastic flow rule after Gutierrez (1991) showing the direction of deviatoric plastic strain increment, n_{ij}; image point, X_{ij}; and, direction of stress increment, l_{ij}

The mathematical description of the hypoplastic flow rule is given by Equation 4.8.

$$\mathrm{Dev}\left(\frac{\partial g}{\partial \sigma_{ij}}\right) = \frac{n_{ij}}{\sqrt{2}} \tag{4.8}$$

where g symbolically represents a plastic potential surface so that $\mathrm{d}\epsilon_{ij}{}^{p} = \mathrm{d}\lambda\left(\partial g/\partial \sigma_{ij}\right)$; $\mathrm{d}\lambda$ is the plastic shear strain increment (the third expression of Equation 4.7); n_{ij} is the

normalised gradient of the bounding surface $F = 0$ at the image point, X_{ij} , such that $n_{ij}n_{ij} = 1$; Dev(.) is the deviatoric transform of a tensor. It follows from Equation 4.8 that $\mathrm{Dev}(\mathrm{d}\epsilon_{ij}{}^{p}) = \mathrm{d}\lambda\, n_{ij}/\sqrt{2}$, which satisfies the third expression of Equation 4.7. The previously discussed projection rule shown in Figure 4.3 is defined analytically by Equation 4.9.

$$F(X_{ij} \equiv r_{ij} + \beta l_{ij}) = 0 \tag{4.9}$$

where β is a scalar multiple; l_{ij} is the direction of $\mathrm{d}r_{ij}$ given as $l_{ij} = \mathrm{d}r_{ij}/\sqrt{\mathrm{d}r_{kl}\mathrm{d}r_{kl}}$. Thus, in the inverse formulation to determine $\mathrm{d}\sigma_{ij}$ from a given $\mathrm{d}\epsilon_{ij}$, an iterative approach is required to determine X_{ij}. The expressions for n_{ij} and β are given by Equations 4.10 and 4.11, respectively.

$$n_{ij} = \frac{X_{ij} - a_{ij}}{\eta_{max}\sqrt{2}} \tag{4.10}$$

$$\beta^2 + 2l_{ij}(r_{ij} - a_{ij})\beta + (r_{ij} - a_{ij})(r_{ij} - a_{ij}) - 2{\eta_{max}}^2 = 0 \tag{4.11}$$

Hence, $0 \leq \beta \leq \eta_{max}\sqrt{2}$ as $\eta_{max}\sqrt{2}$ is the radius of the bounding surface if the deviatoric stress space is not scaled by the factor $1/\sqrt{2}$ as has been done in Equations 4.2 and 4.3. It can be seen from Figure 4.3 that if the direction of the deviatoric plastic strain increment were merely a gradient of the bounding surface with a radial projection rule, then the stress increment $\mathrm{d}r_{ij}$ which is perpendicular to $r_{ij} - a_{ij}$ would cause no plastic strain. Such an increment of $\mathrm{d}r_{ij}$ implies that the stress path is neutral and represents a case of pure stress rotation.

4.6 Hydrostatic component of flow rule: stress-dilatancy relation

The hydrostatic component of the plastic strain increment is obtained from the stress-dilatancy relation. As dilatancy (D) is defined as the ratio of the plastic volumetric strain increment $(\mathrm{d}\epsilon_{ii}{}^{p})$ to the plastic shear strain $(\mathrm{d}\lambda)$, the hydrostatic component of the plastic strain increment can be written as $\mathrm{d}\epsilon_{ij}{}^{p} = (D\mathrm{d}\lambda/3)\delta_{ij}$. Therefore, the complete expression of the flow rule is given by Equation 4.12.

$$\frac{\partial g}{\partial \sigma_{ij}} = \frac{n_{ij}}{\sqrt{2}} + \frac{D}{3}\delta_{ij} \tag{4.12}$$

The dilatancy, D, is determined by equating dissipated energy $(\mathrm{d}\bar{W})$ normalised by the effective pressure p to the normalised internal work given by the scalar product $(\sigma_{ij}/p)\mathrm{d}\epsilon_{ij}{}^{p}$, where $\sigma_{ij}/p = r_{ij} + \delta_{ij}$ and $\mathrm{d}\epsilon_{ij}{}^{p} = \mathrm{d}\lambda(\partial g/\partial \sigma_{ij}) = \mathrm{d}\lambda(n_{ij}/\sqrt{2} + D/3\,\delta_{ij})$; subsequent simplification gives the multiaxial generation of the stress-dilatancy equation used in the original plane-strain model of Cubrinovski and Ishihara (1998b), as shown in Equation 4.13.

$$D = \frac{\mathrm{d}\bar{W}}{\mathrm{d}\lambda} - \frac{r_{ij}n_{ij}}{\sqrt{2}} \tag{4.13}$$

The rate of normalised dissipated energy $(\mu = \mathrm{d}\bar{W}/\mathrm{d}\lambda)$ was expressed as a unique function of the cumulative plastic strain $(\lambda = \sum \mathrm{d}\lambda)$ by Kablimany and Ishihara (1990) shown in Equation 4.14, and is found to depend only on the initial fabric, and independent of state parameters and stress paths.

$$\mu = \frac{\mathrm{d}\bar{W}}{\mathrm{d}\lambda} = \mu_0 + \frac{2}{\pi}(M - \mu_0)\tan^{-1}\left(\frac{\lambda}{S_c}\right) \tag{4.14}$$

where μ_0 is the slope of $\bar{W}$ versus λ plot at zero plastic strain; M is the slope at large strain approaching critical state; and S_c is a calibration constant, mathematically equal to the strain where the slope is $(\mu_0 + M)/2$. Since at large strain $\mu \to M$, a constant value, M can be approximated to the stress ratio at critical state. The dependence of dilatancy behaviour on density and confining pressure is enabled via evolution of μ with λ as given in Equation 4.14. At present, this model assumes an initial isotropic state. The strain-dependent function of the dilatancy coefficient, μ, is difficult to apply for samples with anisotropic initial configuration because the plastic strain, λ, is indeterminate from a current state; for samples with initial isotropic state, $\lambda = 0$, and it accumulates during loading in shear deformation mode. During cyclic loading, λ becomes zero at the instant of load reversal; μ_0 is also set to a constant value of zero for cyclic loading. This empirical approach has been adopted in the original model of Cubrinovski (1993); Cubrinovski and Ishihara (1998b). In order to extend the applicability of the model to anisotropic samples, a new empirical expression of μ has been tentatively proposed in Chapter 6 based on the initial state of stress, but further research is needed to comprehensively consider anisotropic initial states.

The term $r_{ij}n_{ij}/\sqrt{2}$ in Equation 4.13 can be simplified as $c\eta$, where c is the non-coaxiality factor used by Gutierrez (1991) for plane-strain problems with isotropic bounding surface; in complex stress state, $c = n_{ij}r_{ij}/\sqrt{r_{kl}r_{kl}}$ which is the cosine of the angle between the direction of the deviatoric plastic strain increment n_{ij} and that of the deviatoric stress ratio r_{ij}. Exactly the same expression for c was derived by Gutierrez and Ishihara (2000) for complex stress state, which is devoid of the factor a_{ij}. As the stress-dilatancy relation given by Equation 4.13 and 4.14 is independent of stress path, it is rational not to include a_{ij}, which is a signature of the stress path. Because the stress-dilatancy relation is independent of a_{ij}, the model is able to reproduce higher dilatancy for triaxial extension than triaxial compression, as commonly observed; this issue is further discussed in the next chapter where validation cases are presented. Although mathematically $-1 \leq c \leq 1$, negative value of c is physically inadmissible in models, like the present one, with vanishingly small yield surface. Equation 4.13 is therefore split in two expressions for the cases of negative and positive values of c, as shown in Equation 4.15; for complex stress state, $\mathrm{sgn}(\mathrm{d}\eta) = \mathrm{sgn}\left(r_{ij}\mathrm{d}r_{ij}\right)$, where $\mathrm{sgn}(.)$ is the sign function.

$$\left.\begin{array}{l} D = \mu + \eta; c < 0 \ \cap \mathrm{d}\eta < 0 \\ D = \mu - c\eta; c \geq 0 \cup \mathrm{d}\eta \geq 0 \end{array}\right\} \quad \textbf{(4.15)}$$

4.7 Determination of the plastic strain increment

A distinctive feature of bounding surface plasticity, on which the present model is based, is a vanishingly small yield surface degenerating to a point. Therefore, the consistency condition is trivially satisfied at all points lying within a bounding surface. In the formalism of bounding surface plasticity there is no requirement of consistency condition (Dafalias, 1986); the plastic modulus is determined by a model-specific distance-mapping rule along the direction of the plastic strain increment. The generic expression of the plastic strain increment which is typical of all bounding surface plasticity based models is given by Equation 4.16.

$$\mathrm{d}\lambda = \frac{1}{H_p}\frac{n_{ij}p\mathrm{d}r_{ij}}{\sqrt{2}} \quad \textbf{(4.16)}$$

where H_p is the plastic modulus; since the deviatoric mechanism is considered as plastic, the effective stress increment producing plastic strain is taken as $p\mathrm{d}r_{ij}$, the first expression on the right-hand-side of Equation 4.2. It can be noted that the direction of deviatoric plastic strain

increment is given as $n_{ij}/\sqrt{2}$ in view of Equation 4.8; the denominator $\sqrt{2}$ is only a scaling factor so that the same expression of H_p as that of the plane-strain model of Cubrinovski and Ishihara (1998b) can be used. Equation 4.16 is the mathematical expression of the 'single curve hypothesis' (Kachanov, 1971) which states that plastic modulus even for complex stress can be determined from uniaxial stress-strain curve provided stress and strain increments are coaxial. By combining Equations 4.2 to 4.4, the closed-form expression of $\mathrm{d}\lambda$ can be determined for inverse formulation, given by Equation 4.17.

$$\mathrm{d}\lambda = \frac{2G_e n_{ij}\mathrm{Dev}(\mathrm{d}\epsilon_{ij}) - K\mathrm{d}\epsilon_{kk} r_{ij} n_{ij}}{\sqrt{2}(H_p + G_e - KDc\eta)} \tag{4.17}$$

4.8 Elastic and plastic shear moduli

The expressions for both the elastic and plastic shear moduli are adopted from Cubrinovski and Ishihara (1998b). The expression for the elastic shear modulus, G_e, is given by Equation 4.18.

$$G_e = Ap_{atm}\frac{(2.17-e)^2}{1+e}\left(\frac{p}{p_{atm}}\right)^m \tag{4.18}$$

where A and m are calibration constants; m is usually assumed to be 0.5 for sandy soils; e is the void ratio; and p_{atm} is the atmospheric pressure.

The relation between the shear stress and the plastic shear strain, the so-called backbone curve, is given by Equation 4.19.

$$\eta = \frac{\eta_{max} G_N \lambda}{(\eta_{max} + G_N \lambda)} \tag{4.19}$$

where $G_N = (G_{N,max} - G_{N,min})\exp(-f_d\lambda) + G_{N,min}$ is the normalised plastic shear modulus with respect to the effective pressure p at $\lambda = 0$; and f_d is a calibration constant (is actually f_d/γ_0 in Cubrinovski and Ishihara, 1998b). G_N is inverse-exponentially varied with λ, within the bounds of $G_{N,min}$ and $G_{N,max}$, to obtain a close match with experimental results at low (~0.01%) and high (~2% or any other target value) strain levels, which is difficult with a constant G_N; and f_d is termed as the degradation constant that controls the rapidity in degradation of G_N from $G_{N,max}$ to $G_{N,min}$. Further discussion on Equation 4.19 is available in

Cubrinovski and Ishihara (1998b). The plastic modulus $H_p = \partial q / \partial \lambda$ given by Equation 4.20, is also obtained from Cubrinovski and Ishihara (1998b).

$$H_p = p\{G_N - (G_N - G_{N,min})(f_d \lambda)\}\left(1 - \frac{\eta}{\eta_{max}}\right)^2 \quad \textbf{(4.20)}$$

4.9 Specialisation for cyclic loading conditions

Since the adopted plasticity formulation is based on the concept of bounding surface plasticity, there should be a distance mapping rule, equivalent to the radial measure of η_L as shown in Figure 4.4. The distance-mapping rule can be described in several ways. The most straightforward way is to adopt the radial mapping rule along the direction of the plastic strain increment. However, in the present approach, the distance mapping rule is based on the concept of so-called loading surfaces, which are nested and homogeneous to the bounding surface. Each loading surface represents states of stress with equal plastic moduli. The distance mapping rule is defined as the ratio of the radius of the loading surface to the bounding surface. For monotonic loading, this is the same as the radial mapping rule as shown in Figure 4.4. However, during load reversals, new loading surfaces evolve from stress reversal points. Therefore, the centre of the loading surface is equivalent to the projection centre of the bounding surface plasticity. The mathematical description is presented as follows.

The methodology used is very similar to the anisotropic hardening rule of Mroz (1967), with the only difference that in the present method an infinite number of surfaces are used, while in Mroz's method, loading surfaces are finite in number.

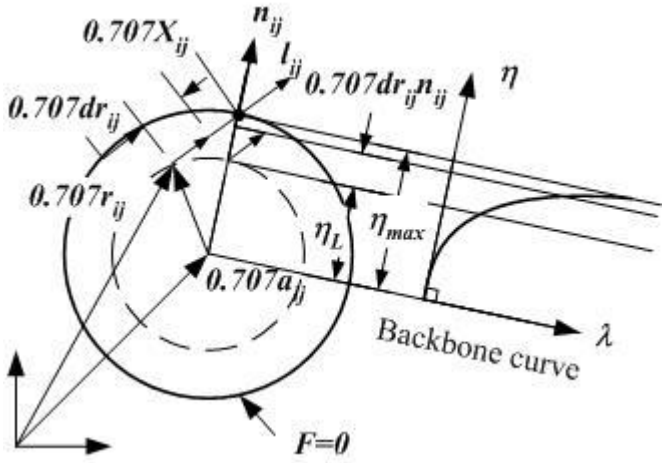

Figure 4.4 Interpretation of the distance mapping rule for the plastic modulus with η_L as the equivalent distance; the stress space is scaled by the factor $1/\sqrt{2}$ so that the radius of the bounding surface is η_{max}

The equation of the loading surface is given by Equation 4.21.

$$L^n = \sqrt{\frac{(r_{ij} - {c_{ij}}^n)(r_{ij} - {c_{ij}}^n)}{2}} - {\eta_L}^n = 0 \tag{4.21}$$

where the superscript n is the index of a loading surface; ${c_{ij}}^n$ is the deviatoric back-stress tensor of n^{th} loading surface; and ${\eta_L}^n$ is the radius. Each loading surface is a locus of equal plastic modulus, H_p, and equal dilatancy coefficient, μ. The largest loading surface $L^{n=1} = 0$ represents the backbone curve that caps hysteresis loops during a cyclic response. It should be noted that the loading surfaces are simply artefacts of distance mapping rule for complex stress conditions and are not yield surfaces, although they do represent strain hardening. For each loading surface two independent equations are required to solve c_{ij} and η_L. The first equation is obtained from the consistency condition of loading surfaces, i.e. $\mathrm{d}L^n = 0$; and the second equation from the condition that the loading surfaces are tangential at stress reversal point. The second condition implies uniqueness of the flow in conventional plasticity theory, where the loading surfaces are actually yield surfaces, the gradient of which gives the direction of plastic increment. Here, the condition of tangency does not imply uniqueness of the flow because the direction of plastic strain increment depends uniquely on the direction of stress increment rather than the stress point; if the direction of stress increment is not specified, then there could be infinite number of directions of the plastic strain increment at a given point. Therefore, instead of uniqueness of flow, the condition of tangency only ensures

that a reloading branch never overshoots the backbone curve. The anisotropic hardening rule for the so-called virgin loading surface, $L^{n=1} = 0$, and general loading surfaces, $L^{n>1} = 0$, are shown in Figure 4.5a and 4.5b, respectively. The analytical description is presented subsequently.

The solution of the parameters $c_{ij}$and η_L of the virgin loading surface $L^{n=1} = 0$ is given by Equation 4.22.

$$\left.\begin{aligned} {c_{ij}}^{n=1} &= \frac{{\eta_L}^{n=1}}{\eta_{max}} a_{ij} \\ \frac{{\eta_L}^{n=1}}{\eta_{max}} &= \kappa = \sqrt{\frac{r_{ij} r_{ij}}{Y_{kl} Y_{kl}}} \\ F\left(Y_{ij} \equiv \kappa r_{ij}\right) &= 0 \end{aligned}\right\} \quad \textbf{(4.22)}$$

where Y_{ij} is a collinear conjugate point of r_{ij} on the bounding surface, as shown in Figure 4.5. The first expression follows from the homogeneity of the loading and bounding surfaces, respectively. If Equation 4.22 is applied to two simple cases of monotonic triaxial compression and extension separately, then it can be shown that κ is nothing but the ratio η/η_{max} of Equation 4.20 where η_{max} is not the radius of the bounding surface, but the actual stress ratio (at critical state) at triaxial compression or extension, as the case may be. This verifies the anisotropic hardening rule.

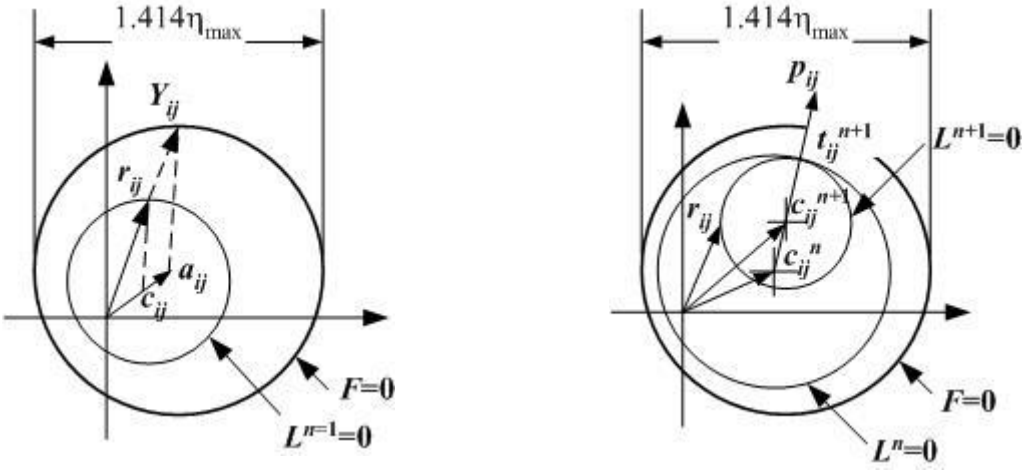

(a) **(b)**

Figure 4.5 Geometrical interpretation of the evolution rules of the loading surfaces; (a) for the virgin loading surface nested within the bounding surface; and (b) general loading surface nested within the virgin loading surface

For loading surfaces $n > 1$, the parameter ${c_{ij}}^{n+1}$ can be obtained from the geometry of the surface $L^n = 0$ by a set of recurrence relations shown in Equation 4.23.

$$\left.\begin{aligned} c_{ij}^{n+1} &= c_{ij}^{n} + \beta^{n+1} p_{ij}^{n} \\ p_{ij}^{n} &= \frac{t_{ij}^{n+1} - c_{ij}^{n}}{\sqrt{(t_{kl}^{n+1} - c_{kl}^{n})(t_{kl}^{n+1} - c_{kl}^{n})}} \\ \beta^{n+1} &= \frac{\{t_{ij}^{n+1}(t_{ij}^{n+1} - c_{ij}^{n}) + r_{ij}(c_{ij}^{n} - r_{ij}) + c_{ij}^{n}(r_{ij} - t_{ij}^{n+1})\}}{\{2 p_{kl}^{n}(t_{kl}^{n+1} - r_{kl})\}} \end{aligned}\right\} \quad \textbf{(4.23)}$$

where β^{n+1} is a scalar multiple; and t_{ij}^{n+1} is the stress reversal point where surfaces $L^n = 0$ and $L^{n+1} = 0$ are tangential. Hence, all the three points ${t_{ij}}^{n+1}$, ${c_{ij}}^{n}$ and ${c_{ij}}^{n+1}$ are collinear, the direction of which is given by the unit tensor ${p_{ij}}^{n}$, as shown in Figure 4.5b. The solution of β^{n+1} is obtained from the consistency condition of the surface $L^{n+1} = 0$, written as $\left(r_{ij} - {c_{ij}}^{n+1}\right)\left(r_{ij} - {c_{ij}}^{n+1}\right) = \left({t_{ij}}^{n+1} - {c_{ij}}^{n+1}\right)\left({t_{ij}}^{n+1} - {c_{ij}}^{n+1}\right)$; since ${p_{ij}}^{n}$ is already known, substituting ${c_{ij}}^{n+1}$ in terms of ${c_{ij}}^{n}$ yields the solution of β^{n+1}. Once ${c_{ij}}^{n+1}$ is solved, ${\eta_L}^{n+1}$ can be readily determined by substituting ${c_{ij}}^{n+1}$ in Equation 4.21. Therefore, a new surface evolves whenever there is a stress reversal. When $L^{n+1} = 0$ coincides with $L^n = 0$, the former surface is deleted from the memory and the latter becomes the current surface, i.e. $n \to n + 1$, in a recursive fashion. Each loading surface has a plastic shear strain associated with it (λ^n) accumulating as the surface grows in size. The recursive algorithm is shown in Figure 4.6 where the superscript t is the pseudo time, representing a step during stress integration.

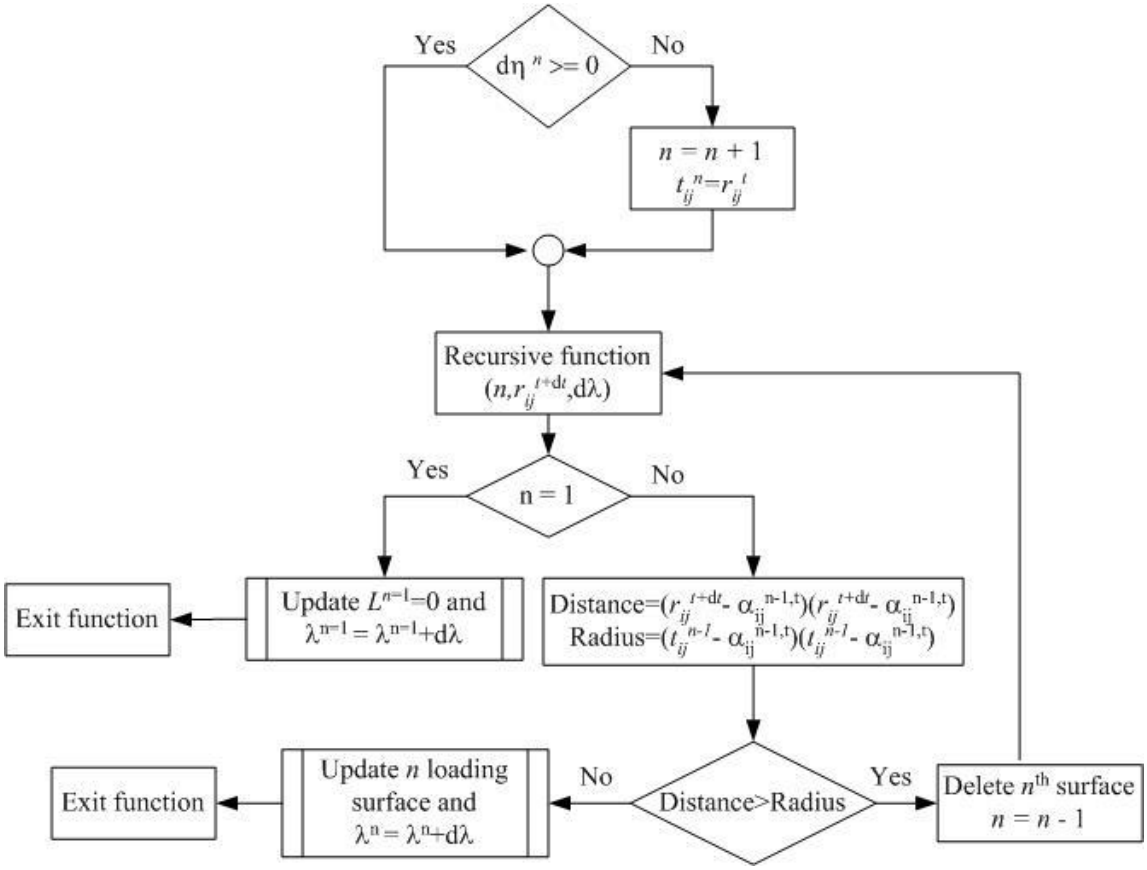

Figure 4.6 Recursive algorithm for evolution of loading surfaces under general loading conditions

The dilatancy coefficient, μ, and the plastic modulus, H_p, associated with current loading surface are obtained by substituting $\lambda = \lambda^n/2$ in Equations 4.14 and 4.20 respectively for $n > 1$ following Masing's rule. The parameter μ_0 is set to zero for all surfaces except for $n = 1$. Loading and reloading conditions are given as $\mathrm{d}\eta_L{}^n \geq 0$ and $\mathrm{d}\eta_L{}^n < 0$, respectively. The expressions for $\mathrm{d}\eta_L{}^{n=1}$ and $\mathrm{d}\eta_L{}^{n>1}$ are shown in Equations 4.24 and 4.25, respectively.

$$\left.\begin{aligned} \mathrm{d}\eta_L{}^{n=1} &= n_{ij}{}^{n=1}\mathrm{d}r_{ij} + \frac{\kappa n_{kl}{}^{b}\mathrm{d}r_{kl} - \mathrm{d}\eta_{max}}{n_{mn}{}^{b}r_{mn}} n_{ij}{}^{n=1}a_{ij} \\ n_{ij}{}^{n=1} &= \frac{r_{ij} - c_{ij}{}^{n=1}}{\sqrt{2\left(r_{ij} - c_{ij}{}^{n=1}\right)\left(r_{ij} - c_{ij}{}^{n=1}\right)}} \\ n_{ij}{}^{b} &= \frac{Y_{ij} - a_{ij}}{\sqrt{2\left(Y_{ij} - a_{ij}\right)\left(Y_{ij} - a_{ij}\right)}} \end{aligned}\right\} \quad \textbf{(4.24)}$$

The term $\mathrm{d}\eta_{max}$ is retained because η_{max} will modify at each step with state parameters. Equation 4.24 is derived from three sets of equations, namely, $\mathrm{d}L^{n=1} = 0$; $\mathrm{d}c_{ij}{}^{n=1} =$

$a_{ij}\mathrm{d}\kappa$; $\mathrm{d}F(Y_{ij}) = 0$; and Equation 4.25 by $\mathrm{d}L^{n>1} = 0$ and using properties of homogeneous surfaces.

$$\left.\begin{aligned} \mathrm{d}{\eta_L}^{n>1} &= \frac{{n_{ij}}^{n>1}\mathrm{d}r_{ij}}{(1-{n_{kl}}^{n>1}p_{kl})\sqrt{2}} \\ {n_{ij}}^{n>1} &= \frac{r_{ij}-{c_{ij}}^{n>1}}{\sqrt{2\left(r_{ij}-{c_{ij}}^{n>1}\right)\left(r_{ij}-{c_{ij}}^{n>1}\right)}} \end{aligned}\right\} \quad \textbf{(4.25)}$$

Although the closed-form expressions of $\mathrm{d}{\eta_L}^{n}$ have been derived for the sake of completeness, stress integration has been carried out using the explicit technique which requires only the term $\mathrm{d}{\eta_L}^{n} = {n_{ij}}^{n}\mathrm{d}r_{ij}$. It can be noted that for seismic stress paths orthogonal to triaxial, ${n_{ij}}^{n=1}a_{ij} = 0$ in Equation 4.24, and as also $-1 \leq n_{kl}^{L}\, p_{kl} < 1$ in Equation 4.25, the simplification in the expression of $\mathrm{d}{\eta_L}^{n}$ during stress integration is justified.

4.10 State dependence

Constitutive behaviour of sand depends profoundly on the current state characterised by the coexisting void ratio (e) and effective confining pressure (p). In constitutive modelling critical state is invariably considered as a reference state because conceptually critical state represents a unique fabric for a given combination of α and b-value that evolves at a large strain corresponding to the steady state of deformation (Poulos, 1981), which is independent of the initial or current e-p state. It has been observed that various specimens of a given sand with different initial states converge to a unique line in $e-p$ space at a large strain, for example, in the range of 20-30 percent axial strain in triaxial compression (Verdugo and Ishihara, 1996). This unique line, known as the critical state line, is the macroscopic expression of critical state. In order to model the dependence of sand behaviour on the current state, model components, such as the bounding surface, and internal variables are typically expressed as functions of the current state relative to the critical state line; such a relative measure of the current state is known as the state index (I_s), the early concept of which is due to Verdugo (1992); Ishihara (1993). In the present model, the definition of I_s is adopted from Cubrinovski and Ishihara (1998a), given by Equation 4.26.

$$I_s = \frac{(e_u - e)}{(e_u - e_c)} \quad \textbf{(4.26)}$$

where e_u is either the void ratio corresponding to the isotropic consolidation line in the loosest state, or the horizontal line in e-p space through the intercept of the quasi steady-state line with the void ratio axis; e_c corresponds to the quasi steady state (Alarcon-Guzman et al., 1998) or the true steady state (Poulos, 1981). The quasi-steady state was adopted by Cubrinovski (1993); Cubrinovski and Ishihara (1998b) instead of the ultimate steady state because the former characterises the initial fabric, as different sample preparation methods yield different quasi-steady state lines (Zlatovic and Ishihara, 1997). Moreover, achieving true steady state in laboratory for 'contractive-dilative' soils is often difficult leading to the alternate definition of the quasi steady state (Ishihara, 1993; Gutierrez, 2003). However, both the quasi-steady state line and the true steady state line are theoretically admissible for defining the state index. These reference lines are further assumed to be independent of α and b-value, and hence the model assumes an isotropic fabric.

The state dependence of the model is incorporated through the fact that the initial small and large strain plastic moduli, $G_{N,max}$ and $G_{N,min}$, respectively, and the radius of the bounding surface, η_{max} are expressed as linear functions of I_s (Cubrinovski and Ishihara, 1998a), as shown in Equation 4.27. This enabled stress-strain relation to be an attribute to I_s.

$$\chi = a_n + b_n I_s \tag{4.27}$$

where χ is a generic symbol for $G_{N,max}$, $G_{N,min}$ and η_{max}, respectively. The parameters a_n and b_n can be considered to depend on the initial fabric, varying with the type of sand. The two effects of such formulation for state dependence are: first, for denser specimens with $I_s > 0$, strain-softening behaviour during drained p-constant test can be simulated because as critical state is approached η_{max} reduces with I_s; a conceptually similar method for simulating strain-softening behaviour of dense sands is adopted by Manzari and Dafalias (1997) where the bounding surface shrinks with $I_s = e - e_c$; Wan and Guo (1999) where the state index is defined as $I_s = e/e_c$; amongst others. The second consequence is the dependence of the stress-dilatancy relation on the current state via the dependence of the dilatancy coefficient, μ on the accumulated plastic strain, λ as λ depends on I_s through the plastic modulus, H_p.

4.11 Model parameters

Finally, a complete definition of the model requires the following parameters defined in Table 4.1: elastic parameters, A, m and Poisson's ratio, ν; initial plastic moduli, $G_{N,max}$ and $G_{N,min}$; radius of the bounding surface, η_{max}; three pairs of constant, $a_n$and b_n to correlate $G_{N,max}$, $G_{N,max}$, η_{max} with I_s; calibration constant for the backbone curve, f_d; dilatancy parameters, μ_0, M, S_c; critical state line and isotropic consolidation line in $e-p$ space; and the initial deviatoric back-stress tensor, a_{ij}.

Table 4.1 Model parameters

Scope	Material parameters
Elastic moduli, G_e, K	A, m and Poisson's ratio, ν
Plastic modulus, $G_{N,max}$, $G_{N,min}, \eta_{max}$	a_{ij}, a_n, b_n, f_d
State index, I_s	e_u, e_c corresponding to effective pressures p_u, p_c on a steady state or quasi-steady state line and the upper reference line, respectively
Stress-dilatancy, D	μ_0, M, S_c

It should be noted that these parameters, excepting a_{ij}, are identical to those required in the plane-strain model of Cubrinovski and Ishihara (1998b). The experimental methods for obtaining the aforementioned parameters and the numerical procedures for calibration are given in Cubrinovski and Ishihara (1998a,b), and are not further elaborated herein.

As previously discussed the initial deviatoric back-stress tensor, a_{ij} is inherently present in η_{max} for torsional stress path and is not needed as the bounding surface will be isotropic. For triaxial stress path it can be readily determined by matching the circular bounding surface with Mohr-Coulomb yield criterion at triaxial compression and extension vertices, as shown in Figure 4.2 and given by Equation 4.28.

$$\eta_{TC} = \frac{2\sqrt{3}\,\eta_T}{3-\eta_T} \qquad \eta_{TE} = \frac{2\sqrt{3}\,\eta_T}{3+\eta_T} \qquad \textbf{(4.28)}$$

where η_{TC} and η_{TE} are stress ratios for triaxial compression and extension, respectively; and η_T is the stress ratio for torsional stress path. These expressions are obtained by expressing Mohr-Coulomb yield criterion as $\sqrt{J_2} - \eta p = 0$, where $J_2 = s_{ij}s_{ij}/2$. Because the model does not include fabric anisotropy, the critical state line, and consequently, the state dependent parameters of I_s ; a_n and b_n are invariant of stress paths leading to isotropic state-dependent evolution of the bounding surface; in contrast, the fabric-dependent models, such as those of Li and Dafalias (2002); Dafalias et al. (2004); Gao and Zhao (2012) amongst others, the state parameters depend on stress paths. Moreover, an isotropically hardening surface is also required for applicability of the hardening rule, which is conceptually based on Mroz's approach (Mroz, 1967). Hence, it is proposed to calibrate a_{ij} based on the initial state, which is a constant value (a similar approach was also adopted by Prevost, 1985), and the evolution rule of the bounding surface for all stress paths is considered as $\mathrm{d}\eta_{max} = \mathrm{d}\eta_T$.

4.12 Summary

A three-dimensional plasticity based model for shear deformation of sand based on the state concept is developed extending upon the plane-strain model of Cubrinovski and Ishihara (1998b). The plane-strain model provided the basic understanding of the key constitutive behaviour of sand under simple seismic stress paths, and the present effort lies in formalising a rigorous mathematical framework to apply the constitutive relations for complex stress state, which is strictly applicable for $\alpha = 45°$ and $b = 0.5$. The plane-strain model can be considered as a proper sub-set of the three-dimensional model because if the order of the tensor quantities is reduced to two in a two-dimensional space of a plane-strain state, then the formulas of the original plane-strain model can be retrieved.

The model is strictly valid for seismic stress paths comprising transverse shear stresses in two orthogonal directions along the bedding plane with b-value of 0.5 and the direction of the principal deviatoric plane with respect to the bedding plane as 45°. Therefore, the failure surface is circular (Drucker-Prager type); however, an initial deviatoric back-stress tensor is introduced to match the stress ratios at triaxial compression and extension in the same way as matching a Drucker-Prager yield surface with Mohr-Coulomb at triaxial compression and extension apices.

In bounding surface plasticity approach, a Drucker-Prager type bounding surface is assumed. The model adopts a hypoplastic flow rule where the direction of the deviatoric component of plastic strain increment is given by the gradient of the bounding surface at an image point located by a hypoplastic projection rule; the centre of projection is the current stress point and the direction is along the stress increment. This hypoplastic flow rule enables the model to predict accumulation of plastic strain along so-called 'neutral' or rotational stress paths. The hydrostatic or volumetric component of the plastic increment is determined from a multiaxial energy-based strain-dependent stress-dilatancy relation. The plastic modulus depends on a distance-mapping rule which is based on the concept of nested homogeneous loading surfaces, each of which is a locus of equal plastic modulus. The radius of the bounding surface and the initial plastic small strain and large strain plastic moduli are also state-dependent. The model does not incorporate the fabric anisotropic effect which would involve redefining the critical state line based on direction of stress path relative to the bedding plane, often characterised by the parameters, α and b-value. However, for predominantly seismic stress path with constant values of $\alpha = 45°$ and $b = 0.5$, the effect of fabric or inherent anisotropy will be tacitly included in the model if the parameters of the stress-strain relation and the bounding surface are calibrated for such a stress path.

5.0 Model validation and verification

5.1 Introduction

The three dimensional model developed in the previous chapter is the generalisation of the plane-strain model of Cubrinovski (1993); Cubrinovski and Ishihara (1998b) to complex stress space assuming an anisotropic Drucker-Prager type bounding surface using the techniques of bounding surface plasticity (Dafalias, 1986). The plane-strain model can be considered as a true subset of the three dimensional model, and the merits and demerits of the plane-strain model are also inherent in the three dimensional version. As the plane-strain model of Cubrinovski (1993); Cubrinovski and Ishihara (1998b) is already well-validated for undrained torsional stress path, validation cases are presented herein separately for torsional and triaxial stress paths, which are not covered in Cubrinovski and Ishihara (1998b).

Furthermore, as the model specialises on bidirectional shear stress with the concept of nested loading surface for cyclic behaviour, it is as important as the model validation to verify the algorithm under realistically complex bidirectional stress path. In this context, this chapter also presents the model verification by p-constant stress-controlled elemental simulation with bidirectional shear stress time series being generated from the horizontal components of two contrasting ground motions to retain actual complexity in applied bidirectional stress path.

5.2 Validation

Validation is carried out for undrained monotonic triaxial and simple shear stress path (Yoshimine et al., 1998); p-constant cyclic torsional stress path (Shahnazari and Towhata, 2002; Pradhan et al., 1989); p-constant cyclic triaxial stress path (Pradhan et al., 1989); and undrained cyclic triaxial stress path (Tatsuoka et al., 1986). Validation for undrained cyclic torsional stress path is not repeated herein because it is already available in Cubrinovski and Ishihara (1989b), although sample simulation results are included for the sake of completeness. However, the case of monotonic simple shear stress path (Yoshimine et al., 1998), which is also available in Cubrinovski and Ishihara (1989b), is presented herein to provide a discussion on the role of the initial deviatoric back-stress tensor, a_{ij} defined in Equation 4.5, as a fabric anisotropy parameter, which was not considered in the original

model of Cubrinovski and Ishihara (1989b), as well as on certain other aspects of the current three dimensional version. It is critically important to note that the above validation cases are performed using the same set of model parameters although the respective experimental data were produced by multiple authors under different experimental setups, which emphasises the versatility and theoretical robustness of the model.

The high quality experimental data in the corresponding literatures are available for dry-deposited Toyoura sand. Toyoura sand consists of 90% quartz and 4% chert with specific gravity of 2.65; diameter, D_{50}, of 0.16mm; uniformity coefficient, C_U, of 1.46; and void ratio between 0.977 and 0.605 (Pradhan et al., 1989). Although the experimental data have been collected from various sources, it circumvents two major difficulties often encountered in validation studies: first, limited availability of high quality experimental data; and second, the data required calibrating the model parameters which should be consistent with the model assumptions. This model requires 9 independent parameters in addition to the critical state and isotropic consolidation lines. These parameters were evaluated for torsional stress path with $\alpha = 45°$ and $b = 0.5$ by Cubrinovski and Ishihara (1998b) for dry-deposited Toyoura sand; where α is the angle between the bedding plane and the major principal deviatoric plane as illustrated in Figure 4.2; and b is the Lode's parameter. The same values as Cubrinovski and Ishihara (1998b) have been followed in the validation, except for μ_0 and M, defined in Equation 4.14, to illustrate the veracity of the model to simulate various stress paths. The parameters μ_0 and M are obtained from the stress-dilatancy plots available in Shahnazari and Towhata (2002) and Pradhan et al. (1989) by considering $\mu_0 = D$ at $\eta = 0$ and $M = \eta$ at $D = 0$ based on the assumption that the stress-dilatancy relation does not depend upon the stress path whether drained or undrained, torsional or triaxial; where η is the stress ratio defined in Equation 4.7; and D is the dilatancy defined in Equation 4.13. Due to inadequacy of data required for calibration of the model for triaxial stress path, the same parameters as the torsional stress path have been used for triaxial stress path. Equation 4.28 is applied to determine the radius of the bounding surface and the corresponding initial deviatoric back-stress tensor, while the state dependent evolution of the bounding surface is given by Equation 4.27. The elastic parameters, and the initial plastic moduli, $G_{N,max}$ and $G_{N,min}$ defined in Equation 4.19, theoretically correspond to plastic strain $\lambda = 0$ and hence are considered the same for both the torsional and triaxial stress paths. The model parameters

used in the validation study are given in Table 5.1; the parameters are defined in the respective equations as shown in Table 5.1.

Table 5.1 Parameters used for model validation

Scope	Model parameters	Values	Defining equations
Elastic moduli	A	250	Equation 4.18
	m	0.6	
	Poisson's ratio, ν	0.2	Equation 4.4
Plastic modulus	a_n, b_n for η_{max}	0.58, 0.023	Equation 4.19 and 4.27
	a_n, b_n for $G_{N,max}$	230,65	
	a_n, b_n for $G_{N,min}$	79,16	
	f_d	0.04	Equation 4.19
Stress-dilatancy	μ_0	0.375	Equation 4.14
	M	0.55	
	S_c	0.0055	
State index	Isotropic consolidation line	$e = 0.895$, a constant value for $p \leq 400$kPa	Equation 4.26
	Critical state line (quasi-steady state line) defined by the tabulated $e - p$ values where p is in kPa	$e = 0.873; p \leq 30$ $e = 0.870; p = 50$ $e = 0.860; p = 100$ $e = 0.850; p = 200$ $e = 0.833; p = 400$	

5.2.1 Validation under monotonic undrained stress path

The experimental data fromYoshimine et al. (1998) and simulated results for undrained monotonic simple shear stress path are shown in Figure 5.1 to 5.3. As can be seen from Figure 5.1 to 5.3, the shear stress and the shear strain are expressed using the principal components as $\sigma_{11} - \sigma_{33}$ and $\varepsilon_{11} - \varepsilon_{33}$, respectively; where σ_{11}: major principal stress; σ_{33}: minor principal stress; ε_{11}: major principal strain; and ε_{33}: minor principal strain. An anisotropic bounding surface has been assumed to allow variation in b-values during the simulation. In the experiments, b-values started from 0.5 and gradually decreased to 0.25, while in the simulation, b-values varied from 0.5 to 0.35; the sharp change in b-value occurs

when sufficient deviatoric stress is produced with respect to the initial deviatoric back-stress tensor a_{ij}. Moreover, the variation in b-value is also dependent on a_{ij}, which could have been adjusted by trial and error method so that a nearer lower range of b-value could be achieved. However, in order to maintain a theoretically consistence approach with the same values of parameters for all the validation cases, a_{ij} is determined by fitting a Mohr-Coulomb yield criterion via Equation 4.28.

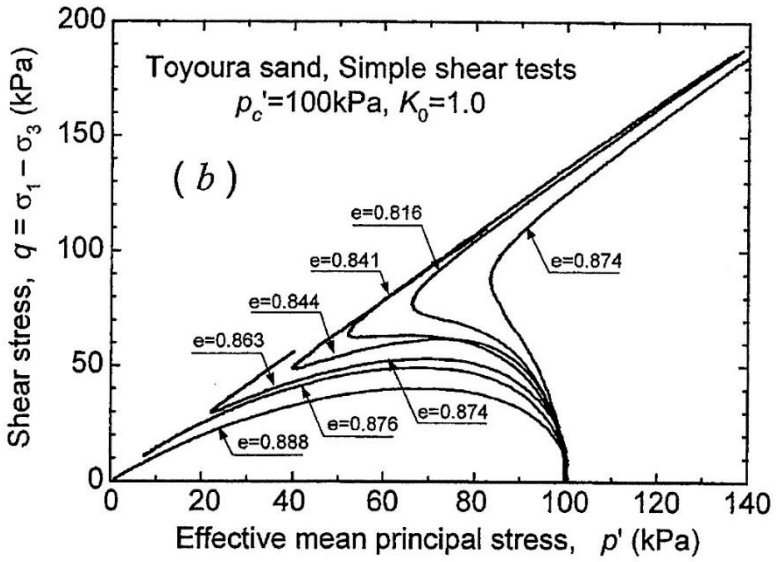

(a)

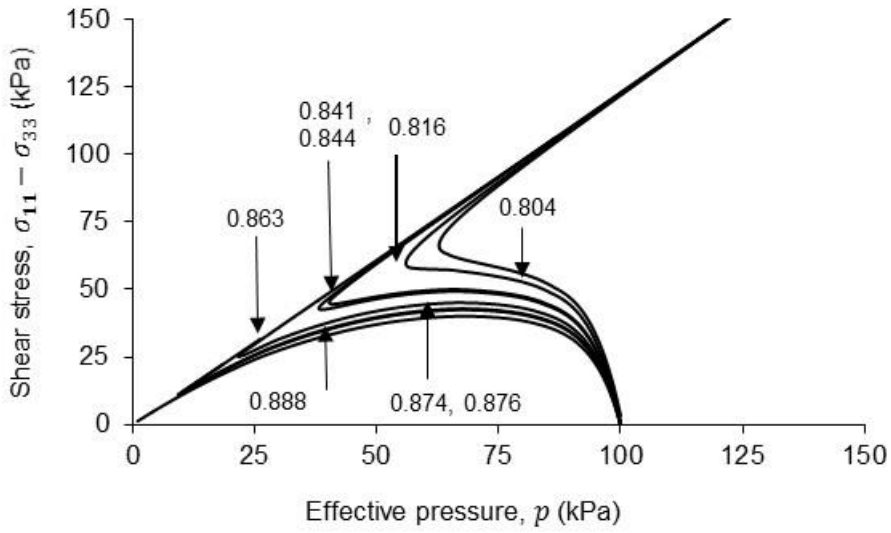

(b)

Figure 5.1 Comparison between experimental and simulated stress path for monotonic undrained simple shear stress path; (a) experimental results, from Yoshimine et al. (1998); and (b) simulated results

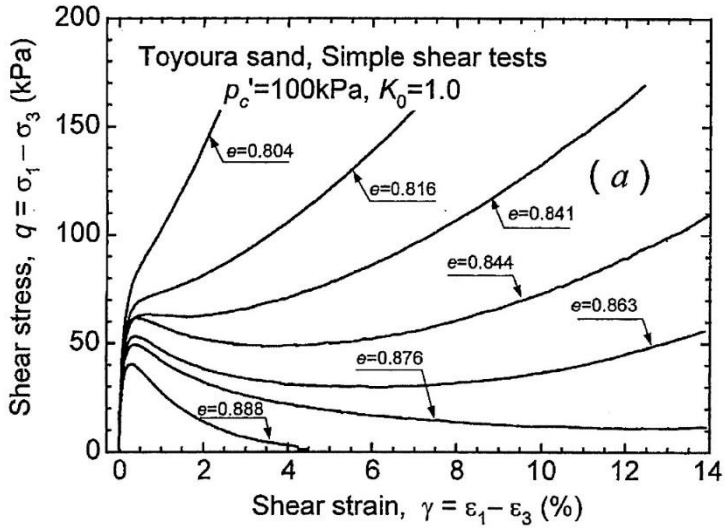

(a)

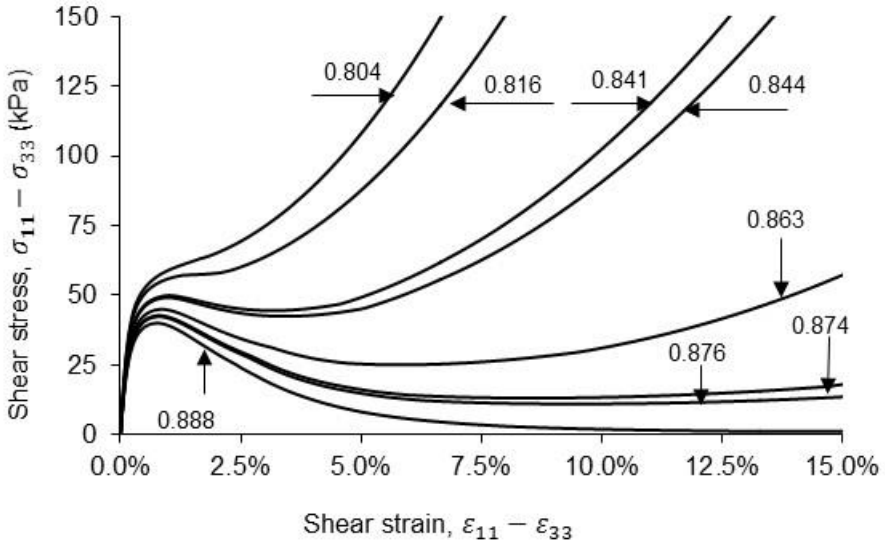

(b)

Figure 5.2 Comparison between experimental and simulated stress-strain response for monotonic undrained simple shear stress path; (a) experimental results, from Yoshimine et al. (1998); and (b) simulated results

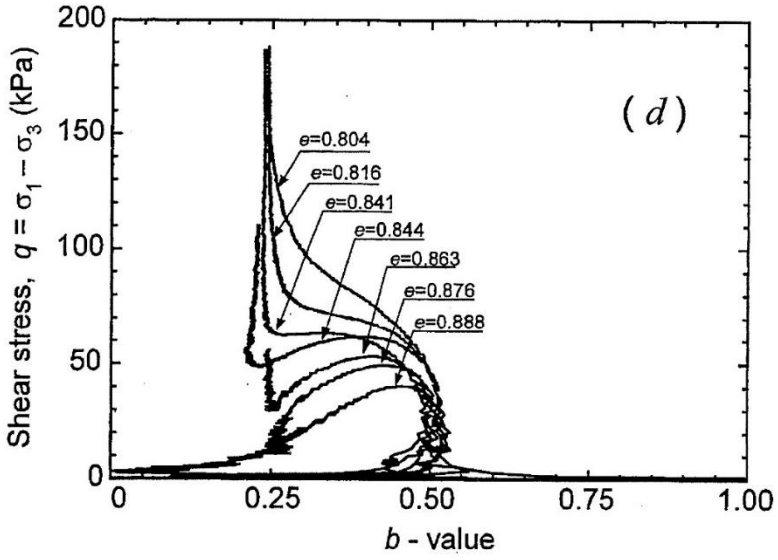

(a)

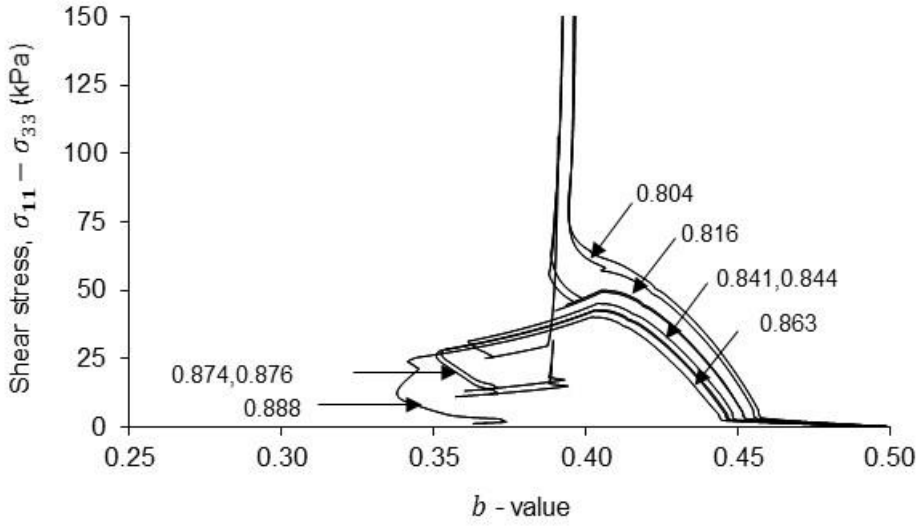

(b)

Figure 5.3 Comparison between experimental and simulated variation in *b*-values for monotonic undrained simple shear stress path; (a) experimental results, from Yoshimine et al. (1998); and (b) simulated results

For triaxial stress path the simulation results compared with the experimental are shown in Figure 5.4. The shear stress is defined as $\sigma_{11} - \sigma_{33}$ and the shear strain as $\varepsilon_{11} - \varepsilon_{33}$. Here, a_{ij} is the parameter which is playing the leading role in reproducing more dilatancy in triaxial extension than triaxial compression. As a_{ij} differentiates between the triaxial compression and extension stress paths, and the stress-dilatancy relation is considered to be path independent, Equation 4.13 should be independent of a_{ij}, as postulated earlier. If a dilatancy surface could be imagined with radius, μ, homogeneous to the bounding surface, then this surface is isotropic as the stress-dilatancy relation given by Equation 4.13 is independent of a_{ij}. Since the dilatancy and bounding surfaces are eccentric, a point near the bounding surface in triaxial compression will have a greater magnitude of negative dilatancy than the other in triaxial extension. It can be seen from Figure 5.4 that at strains greater than 5%, deviation between the simulated and the experimental results gradually increases in triaxial compression. At large strains, where this is observed, the stress points are almost on the bounding surface (which can be also seen from Figure 5.4a) and the stress-strain relation is almost singularly guided by the stress-dilatancy relation as the corresponding η versus λ plots will plateau off with negligible plastic modulus at strains in excess of 5%. Hence, the reason for such deviation is attributable to the approximation in determining the geometry of the bounding surface for triaxial stress path as well as the strain-dependent stress-dilatancy relationship.

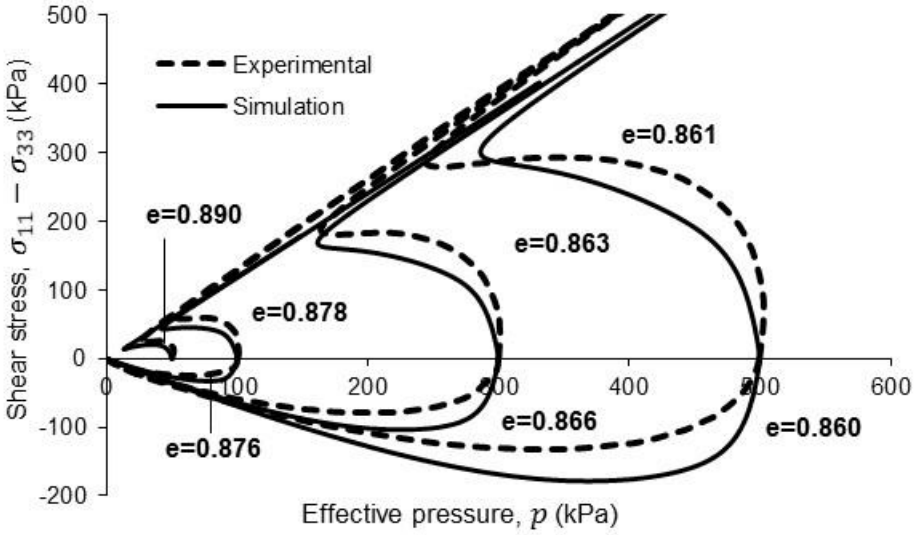

(a)

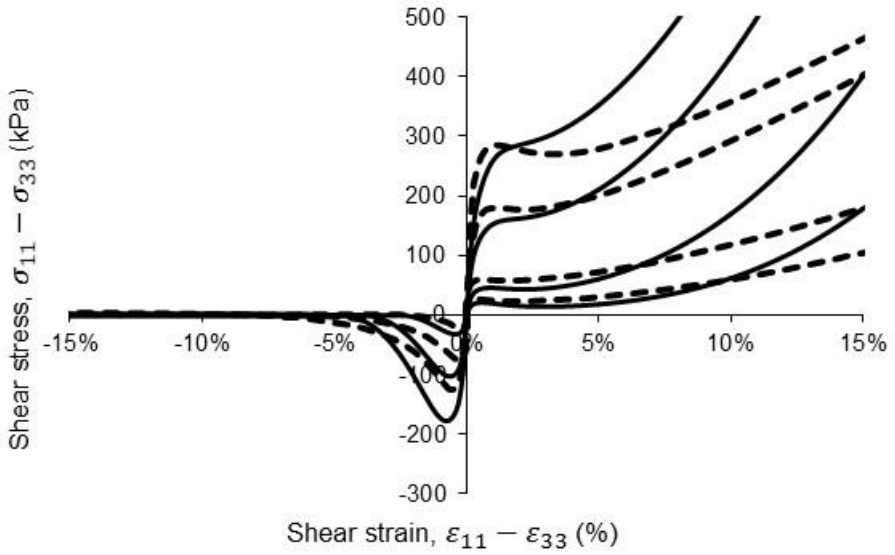

(b)

Figure 5.4 Comparison between experimental and simulated results for undrained monotonic triaxial stress path (a) effective stress path; and (b) stress-strain plots; experimental results are taken from Yoshimine et al. (1998)

5.2.2 Validation under cyclic p-constant stress path

A distinct advantage of drained tests over undrained is that both the backbone curve and the stress-dilatancy relation, which are the two pillars of constitutive models for sands, can be explicitly validated if p is held constant during drained tests. It should be noted that the plasticity models of sands are based on the concept of normalising the absolute stress

quantities by p that stems from the assumption of conical surfaces, which implies that the shear or deviatoric stress varies linearly with p permitting a linear scaling of deviatoric space. However, in reality, shear stress could vary non-linearly with p violating the modelling assumption. In this respect, drained p-constant test offers perfect match between the modelling assumption and the experimental protocol. Moreover, drained p-constant test also allows to rigorously test the state concept framework of the model.

In Figure 5.5 and 5.6, the experimental data from Shahnazari and Towhata (2002) and the simulated data are shown for stress-strain response and shear strain versus dilatancy induced volumetric strain (which is the plastic volumetric strain for p-constant stress path given as ε_{ii} following indicial notation), respectively, for a dry-deposited Toyoura specimen with relative density of 58% and $p = 98$kPa. In Figure 5.5, only the initial monotonic positive segment of experimentally obtained stress-strain curve is superimposed to show that the backbone curve matches perfectly with that of the model; thereafter, the cyclic response is exclusively controlled by the state concept framework. Some minor variation is noted in peak shear stress which is due to the values of a_n and b_n adopted to correlate η_{max} with I_s via Equation 4.27. After 40 cycles of single amplitude strain of 3%, the specimen accumulated approximately 5.5% dilatancy induced (plastic) volumetric strain, whereas in the simulation, it is slightly less than 6%. In Figure 5.7, torsional strain is plotted as a function of cyclic compaction occurring due to dilatancy induced volumetric strain for three specimens with $p = 98$kPa and relative densities of 22%, 38% and 58%, respectively. It can be seen from Figure 5.7b that for the latter two specimens, the final void ratio after 40 cycles is nearly 0.66, which matches almost exactly with the experimental values shown in Figure 5.7a. However, there are some moderate variations for the simulations with relative densities of 22% and 38% in the number of cycles required to achieve a given level of compaction in terms of reduction in void ratios as shown by the vertical lines in Figure 5.7.

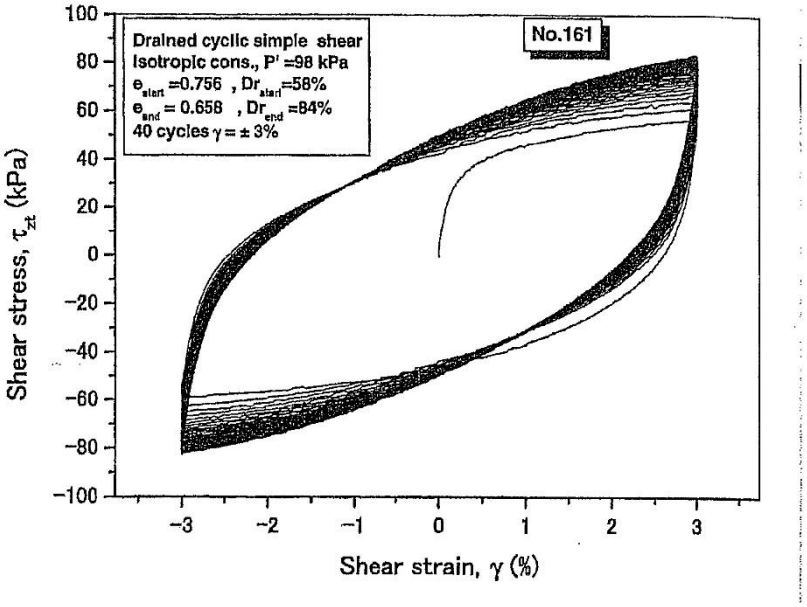

(a)

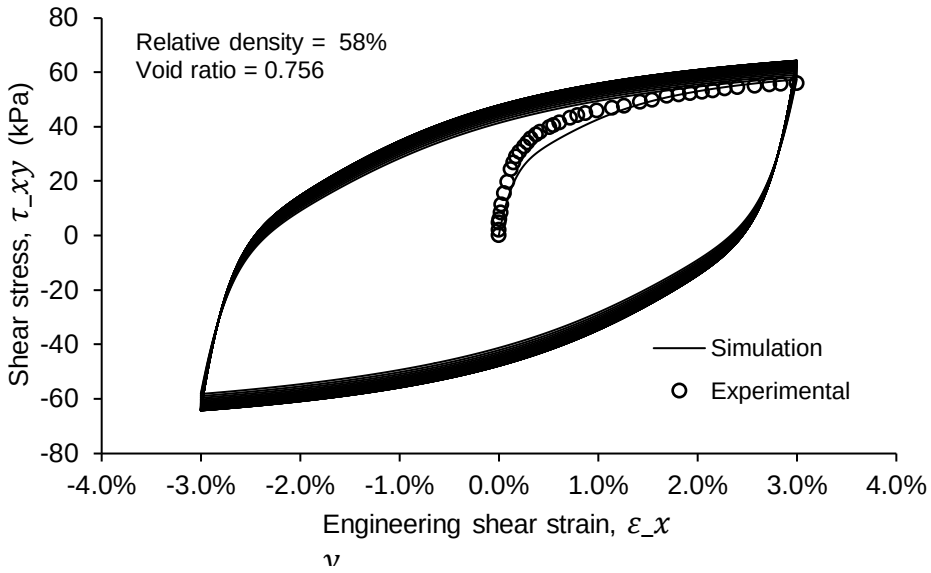

(b)

Figure 5.5 Comparison of experimental stress-strain plot with the simulation for torsional stress path in drained *p*-constant test; (a) experimental result, from Shahnazari and Towhata (2002); and (b) simulated result

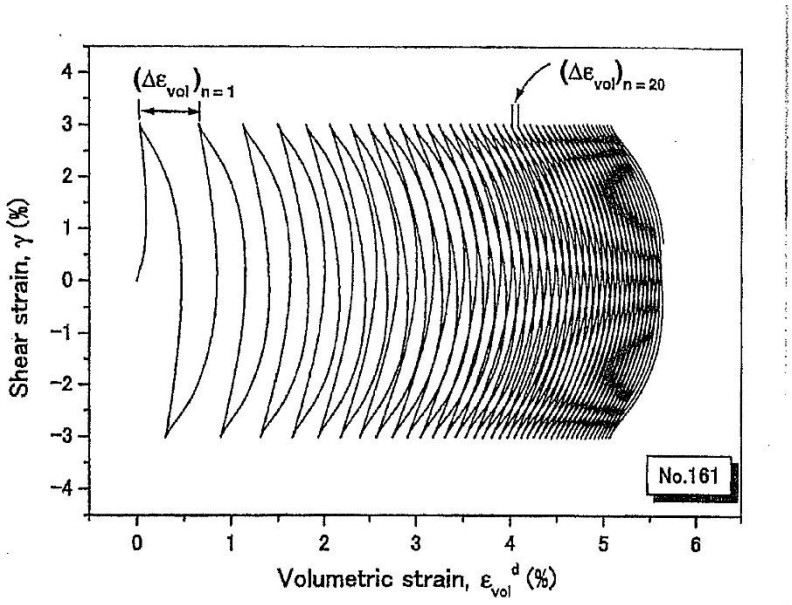

(a)

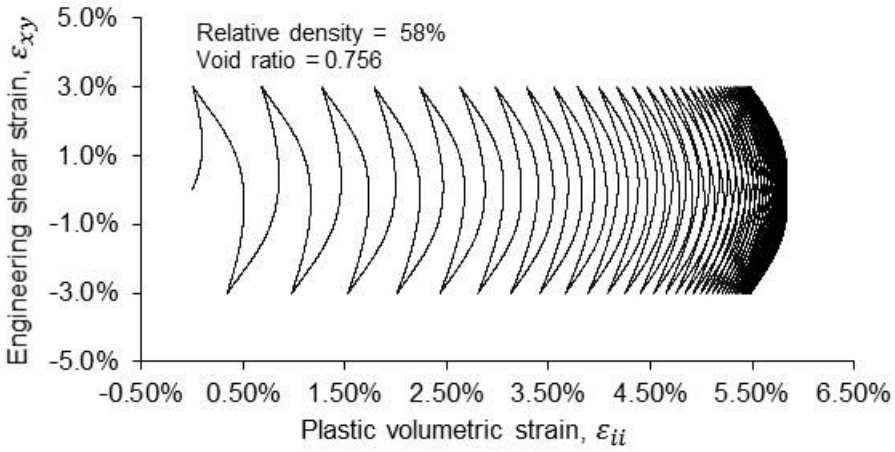

(b)

Figure 5.6 Comparison of experimentally obtained shear strain versus dilatancy induced volumetric strain with the simulation for torsional stress path in drained p-constant test; (a) experimental result, from Shahnazari and Towhata (2002); and (b) simulated result

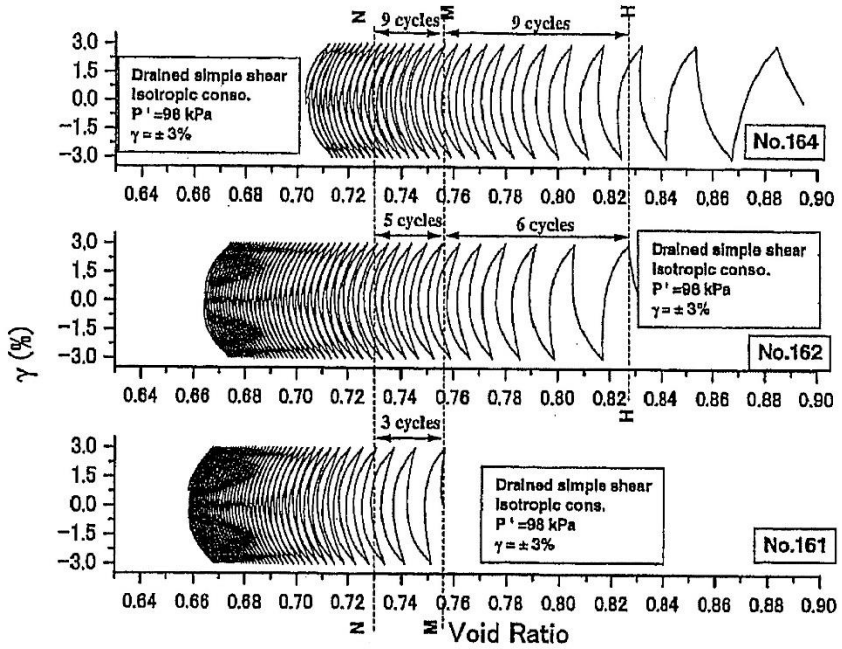

(a)

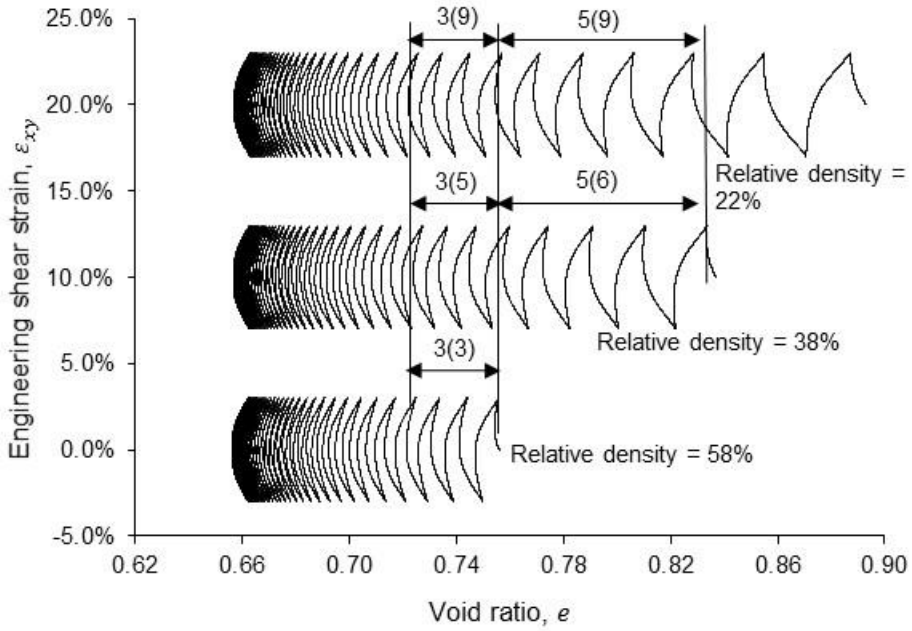

(b)

Figure 5.7 Comparison between experiment and simulation for dilatancy induced compaction of three specimens with different relative densities in drained *p*-constant torsional stress path; (a) experimental results, from Shahnazari and Towhata (2002); and (b) simulated results. The numbers in parentheses are the number of cycles actually required for the given compaction in terms of reduction in void ratio

Another set of validation for drained p-constant ($p = 98$kPa) torsional stress path is shown in Figure 5.8 for two different void ratios of 0.804 and 0. 677 with relative densities of 47% and 81%, respectively, where the experimental data is obtained from Pradhan et al. (1989). The only difference between this set and that of Shahnazari and Towhata (2002) is that in the former the strain is cyclically increased, while in the latter the strain is held constant for all the cycles. It can be seen from Figure 5.8, that η_{max} and the dilatancy parameters, μ_0 and M, adopted are slightly different from the actual ones. Again the use of trial and error is avoided in order to depict actual model validation using a set of constant parameters throughout. It is generally observed that soil properties do not assume any fixed set of value, rather fall within a certain range. Pending a probabilistic approach, a fixed set of values is required for implementation, and therefore, it is important to understand how much a model deviates from experiments under different conditions, such as stress paths, with the same set of data.

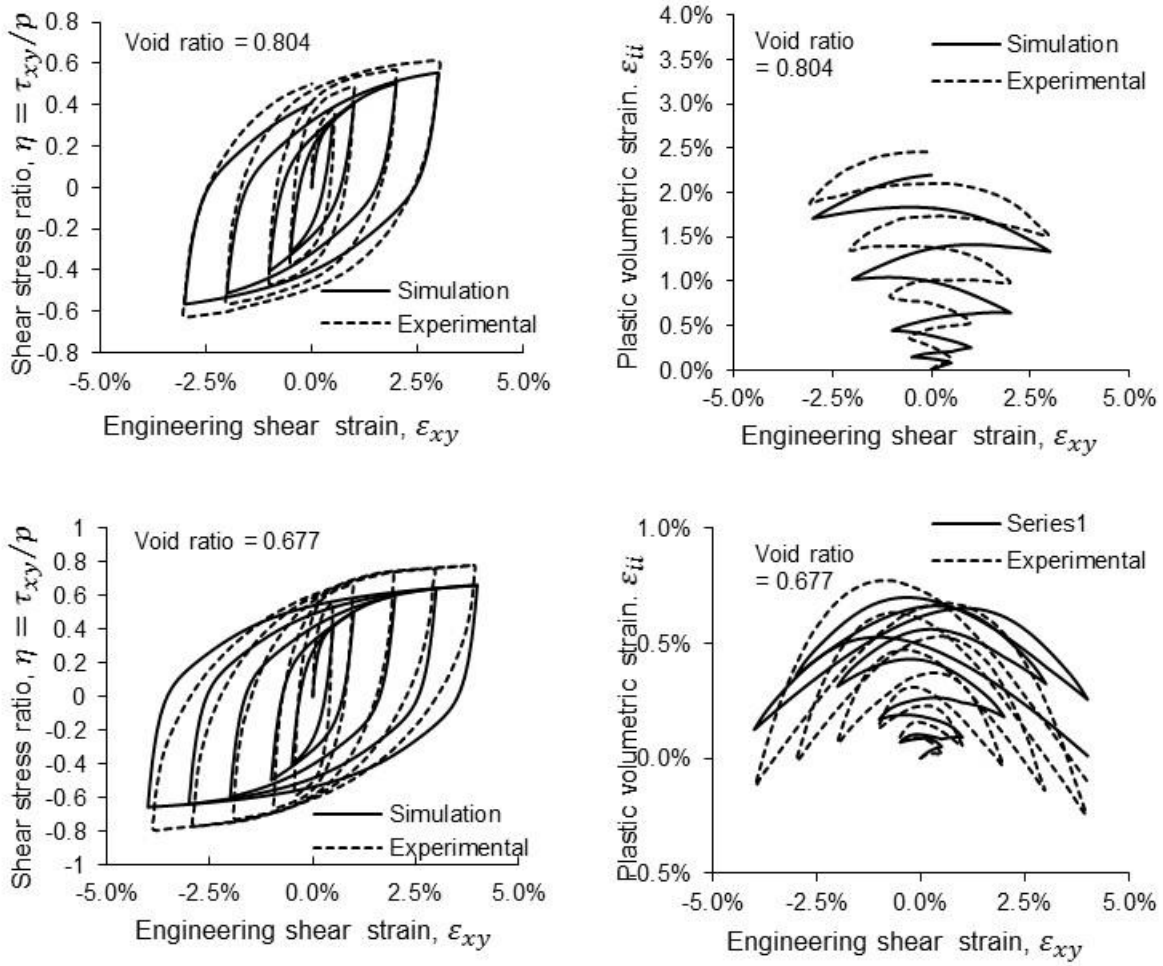

Figure 5.8 Comparison between experiment (Pradhan et al., 1989) and simulation for stress ratio and dilatancy induced volumetric strain plotted as functions of shear strain for drained p-constant torsional stress path for two void ratios

The validation for triaxial stress path is shown in Figure 5.9; the shear stress is defined as $\sigma_{11} - \sigma_{33}$ and the shear strain as $\varepsilon_{11} - \varepsilon_{33}$. As observed earlier with the results from Yoshimine et al. (1998) from Figure 5.4, there is some deviation from the experimental results. Since Mohr-Coulomb yield criterion is considered as a basis to evaluate η_{max} and a_{ij} from the correlation of η_{max} with I_s based upon the critical state line that was derived for torsional stress path, the calculated values appear to differ from the actual peak stress ratios for triaxial compression and extension; the difference is more in the triaxial compression than the extension. As the critical state lines for triaxial compression, triaxial extension and torsional stress path are different (Vaid and Chern, 1985; Vaid et al., 1990; Vaid and Thomas, 1995; Reimer and Seed, 1997), the state dependent parameters such as I_s; a_n and b_n will be also different for each of the above stress paths rather than assuming a unique value which

implies path independence. Unless a model incorporates fabric anisotropic effect such as Dafalias et al. (2004) to modify the state index and the critical state line for continuously varying stress path, achieving accurate model performance for both triaxial and torsional stress paths will be difficult. However, despite such limitations, the model is still nicely capturing the key trends observed in the experiment. Another interesting observation from simulated plots of stress ratio versus strain is that the anisotropic hardening rule of the first or the virgin loading surface is functioning as intended because the backbone is never crossed by reloading curves; in fact, the reloading curves are nicely asymptotic to the backbone curve although it is anisotropic.

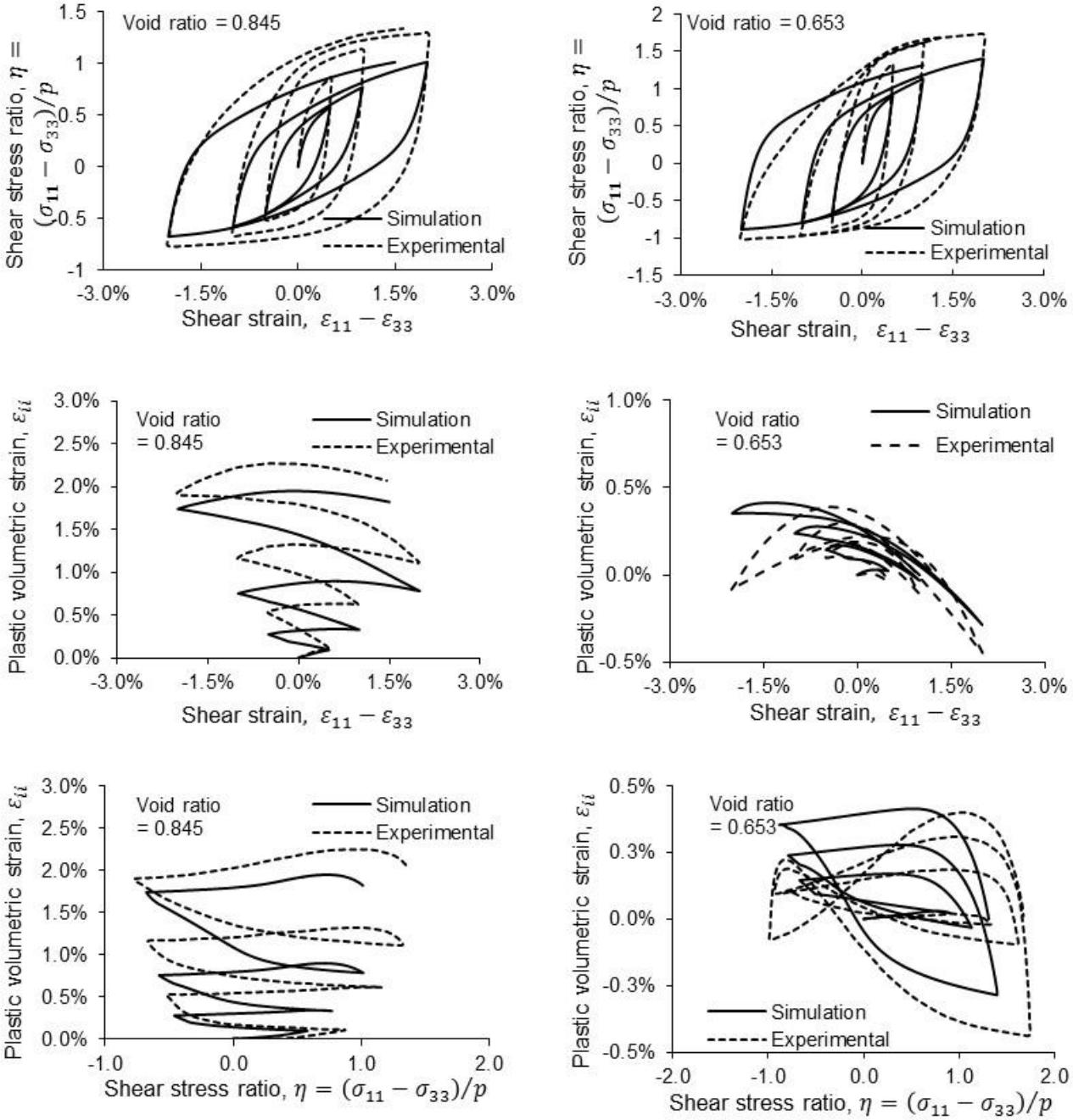

Figure 5.9 Comparison between cyclic triaxial experiment (Pradhan et al., 1989) and simulation for stress ratio plotted as a function of shear strain, and dilatancy induced volumetric strain plotted as functions of shear strain and stress ratio for drained p-constant triaxial stress path

5.2.3 Validation under cyclic undrained stress path

Figure 5.10 shows the comparison between the experimental results from Tatsuoka et al., (1986) and the simulation for cyclic stress ratio versus number of cycles to 3% double amplitude shear strain (the so-called liquefaction resistance curve) for triaxial stress path. The shear stress has been defined as $(\sigma_{11} - \sigma_{33})/2$ and the shear strain as $\varepsilon_{11} - \varepsilon_{33}$. The experimental curves shown in Figure 5.10 are not directly available in Tatsuoka et al. (1986), but are synthesised following a procedure described therein based on experimental results for four different methods of sample preparations, namely, dry-deposited, wet-tamped, wet-vibrated and water-vibrated. The individual results (not sufficient for model validation across the range of relative densities shown in Figure 5.10) show that the air-deposited samples, for which the model is being validated, are the weakest amongst the four. However, the procedure described in Tatsuoka et al. (1986) is the same for all four sample preparation methods which is based on some average measure. Hence, the experimental curves in Figure 5.10 are approximate to a certain extent, and actual curves for dry-deposited samples should be lower. It can be seen that the simulated liquefaction resistance curves closely follow those from experimental results, similar to those of Cubrinovski and Ishihara (1998b). Figure 5.11 shows sample simulated stress path and stress-strain response for two simulations with relative densities of 70% and 80%, respectively. It can be seen that the model is able to reproduce the 'butterfly curves' and also that there is an accumulation of permanent strain in the triaxial extension side. As discussed previously, the use of an isotropic dilatancy surface and an anisotropic bounding surface together result in reproducing higher dilatancy in triaxial extension. For the sake of completeness of the ongoing discussion on validation of the model, simulations of undrained cyclic torsional stress path are shown in Figure 5.12 for the same stress ratios and relative densities.

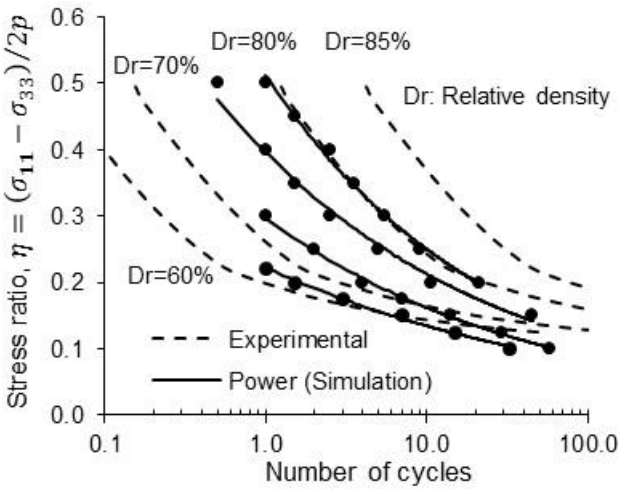

Figure 5.10 Comparison between experimental data of Tatsuoka et al. (1986) and simulations for stress ratio versus number of cycles to 3% double amplitude strain in triaxial stress path; simulation results are connected by best-fit power function for comparison with experimental observations

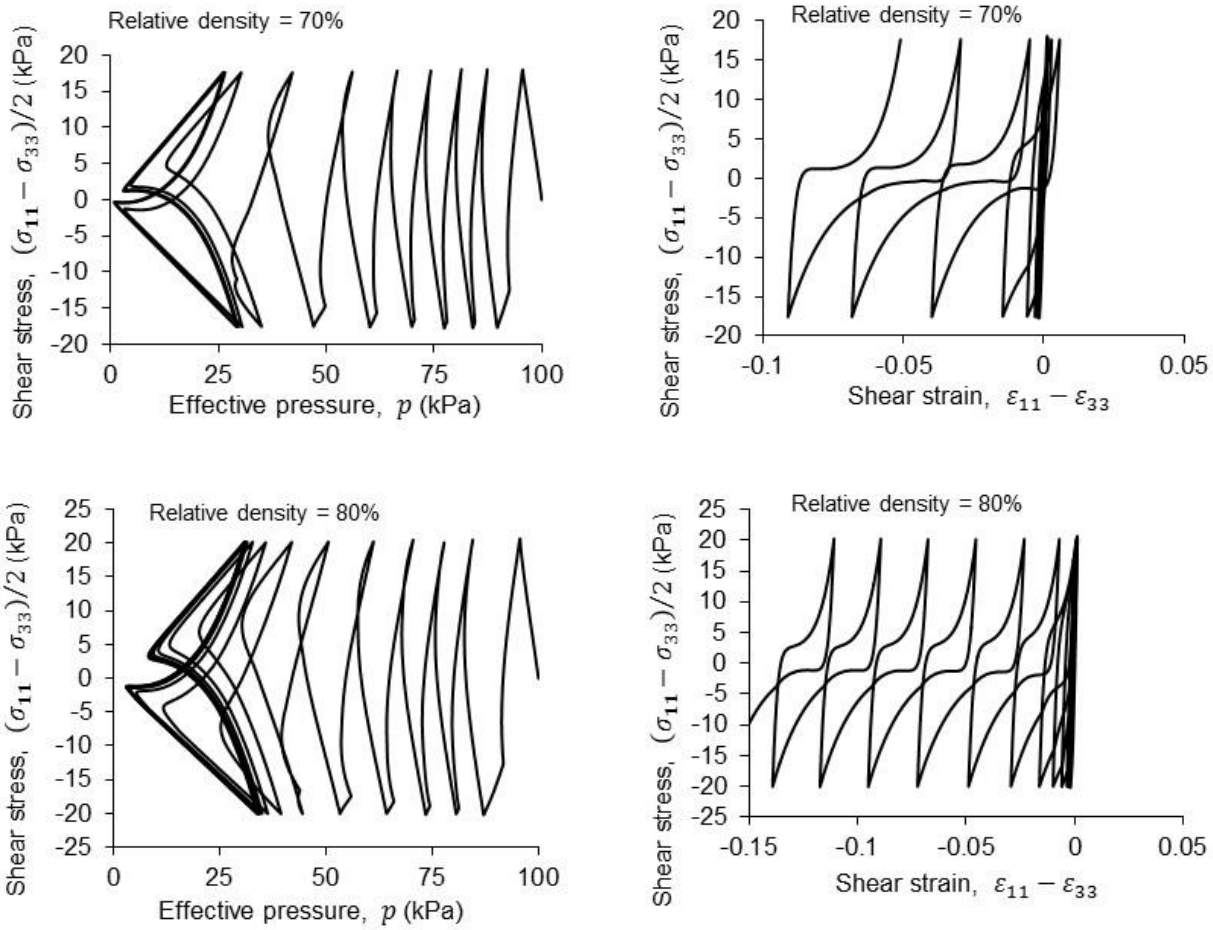

Figure 5.11 Examples of simulations for undrained cyclic triaxial stress path for two relative densities

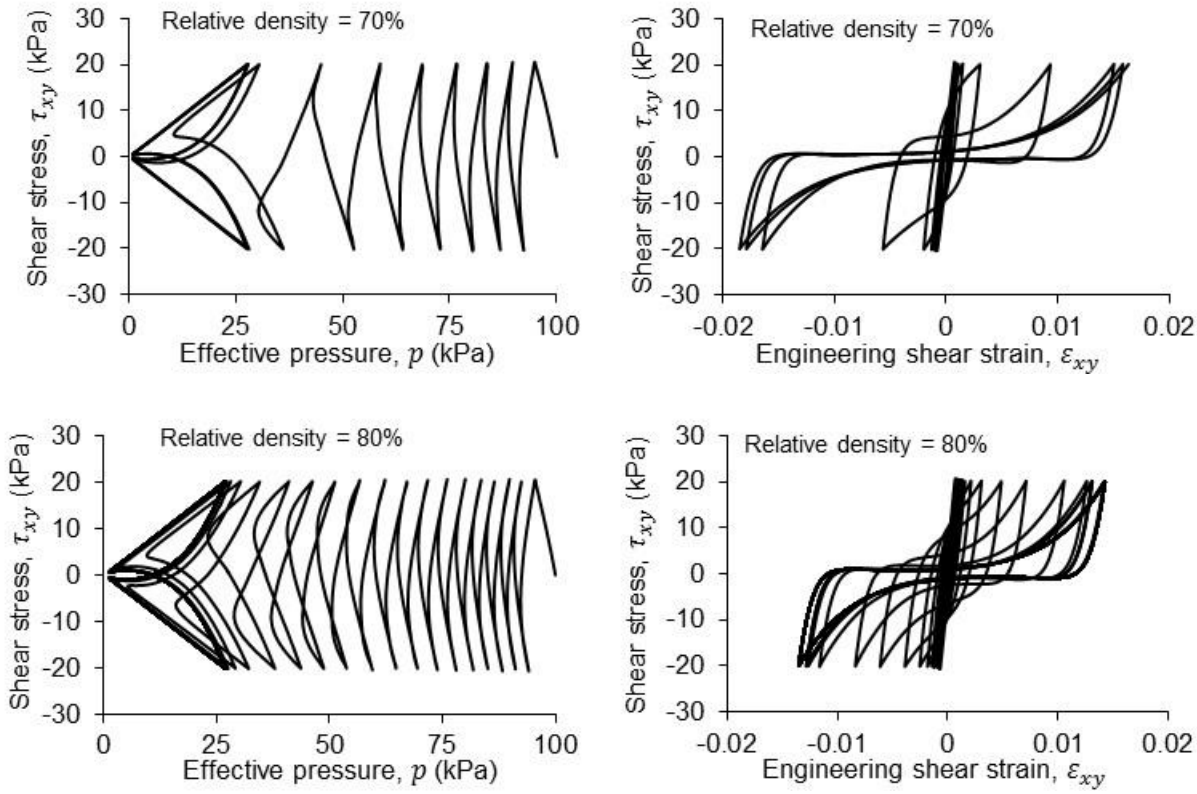

Figure 5.12 Examples of simulations for cyclic undrained unidirectional torsional stress path for two void ratios

5.3 Verification of the anisotropic hardening rule under complex bidirectional stress path

In addition to validation of the constitutive model against experimental data for simple stress paths it is also important to verify the computational algorithm of the model under highly irregular and complicated stress paths which are encountered in seismic response analysis, but for which no element experimental data is available. In order to verify the anisotropic hardening rule based on the concept of nested homogeneous surfaces for realistically complex bidirectional stress paths, *p*-constant stress controlled simulations are carried out by synthesising stress histories from actual ground motions.

Two ground motions are considered: the first was recorded in Urayasu during the M_w9 11 March 2011 Tohoku earthquake at station CHB008 of the K-NET (Kyoshin network) database (http://www.kyoshin.bosai.go.jp); and the second was recorded during the M_w6.3 22 February 2011 Christchurch earthquake at Christchurch Botanical Garden (CBGS) of GeoNet database (http://geonet.org.nz). Extensive liquefaction occurred during at these two stations and hence it is considered that the ground motions will preserve the effectual stress paths.

Also, the two ground motions are contrasting in nature: the first is a vibratory type with long duration (significant duration, $D_{s595} = 125s$), whereas the second is an impulsive type with relatively short duration ($D_{s595} = 10s$) (Bradley, 2012a). This will result in two opposing cyclic stress conditions: the stress history synthesized from Urayasu will have many cycles of almost similar but relatively small amplitudes, while that of the GBGS will have fewer cycles with relatively large amplitudes. In order to apply the ground motion to a single soil element, the bidirectional ground acceleration is converted to bidirectional shear stress by first normalising the ground acceleration time series with the maximum value obtained by vector summation of the directional components, and then multiplying by a peak shear stress value. Three peak shear stress values are chosen: 20kPa, 40kPa and 60kPa that correspond to the stress ratios η of 0.2, 0.4 and 0.6 respectively, for an effective pressure of 100kPa; where η is defined in Equation 4.7. These three levels of shear stresses are representing low, medium and high levels of inelastic seismic actions. Accordingly, the radius of the virgin loading surface can be matched with the target shear stress ratio.

The stress controlled simulations have been carried out on a Toyoura sand specimen with relative density of 50% (void ratio of 0.8 approximately) with the same model parameters as given in Table 5.1. The time series plots of the bidirectional shear stress generated from the Urayasu and the CBGS ground motions are shown in Figure 5.13 and 5.14, respectively, along with their bidirectional stress orbits. It can be seen that the actual bidirectional shear stress orbits are complex which can seriously challenge the algorithm for cyclic behaviour. The shear stress is applied in a stress controlled routine along the bedding plane, denoted as the y-constant plane in the following nomenclature for stresses and strains, which corresponds to $\alpha = 45°$ and $b = 0.5$, and therefore, conforms strictly to torsional stress path.

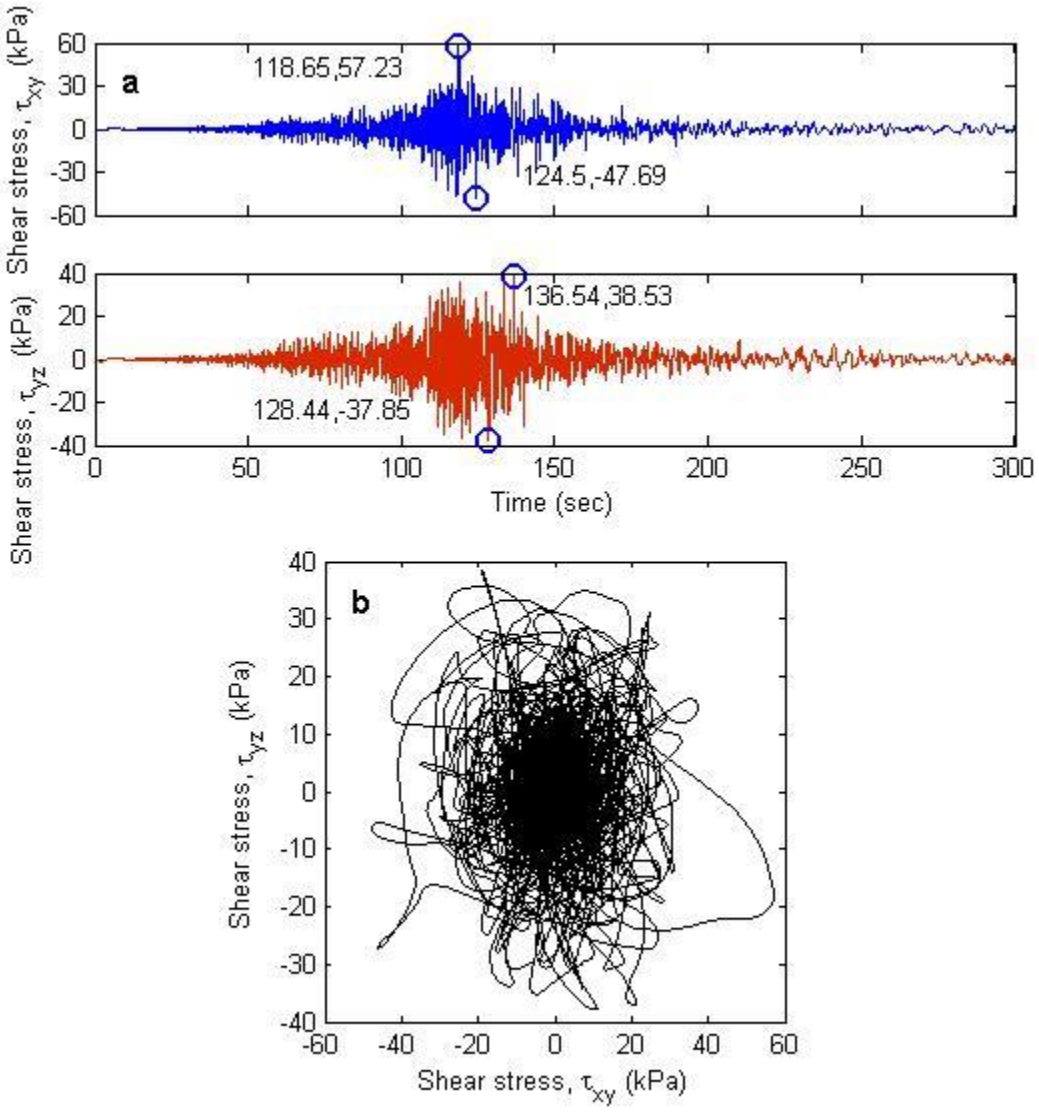

Figure 5.13 (a) Time series plot and (b) stress orbit of bidirectional shear stress generated to peak stress ratio of 0.6 and effective pressure of 100kPa from the ground motion recorded at Urayasu during the M_w9 11 March 2011 Tohoku earthquake

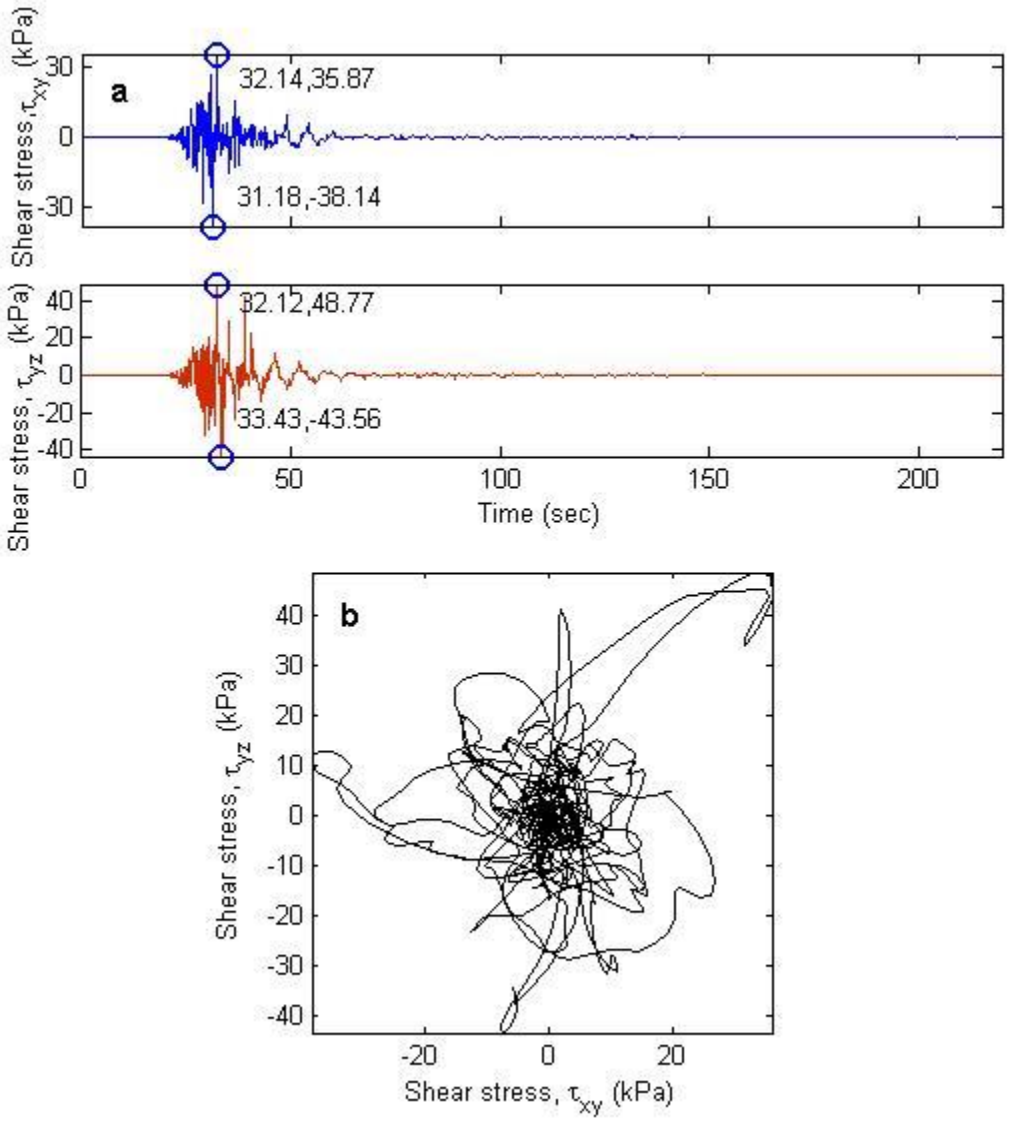

Figure 5.14 (a) Time series plot and (b) stress orbit of bidirectional shear stress generated to peak stress ratio of 0.6 and effective pressure of 100kPa from the ground motion recorded at CBGS during the M_w6.2 22 February 2011 Christchurch earthquake

Bidirectional hysteresis responses are shown in Figure 5.15 and 5.16 for Urayasu and GBGS ground motions, respectively. In each of these figures, three pairs of hysteresis plots are shown corresponding to the three different peak shear stress levels along two orthogonal directions. The response for the peak shear stress of 20kPa has the least nonlinearity effect, which gradually exaggerates with increase in the maximum shear stress to 40kPa and 60kPa reflected by attendant rise in maximum strain levels. In each of the simulations, hysteresis loops are found to be stable in the sense that the incremental slopes are positive throughout the response history; the area enclosed by the hysteresis loops is positive; and there is no

overshooting of the backbone curve. The maximum number of loading surfaces generated during the simulation is 35.

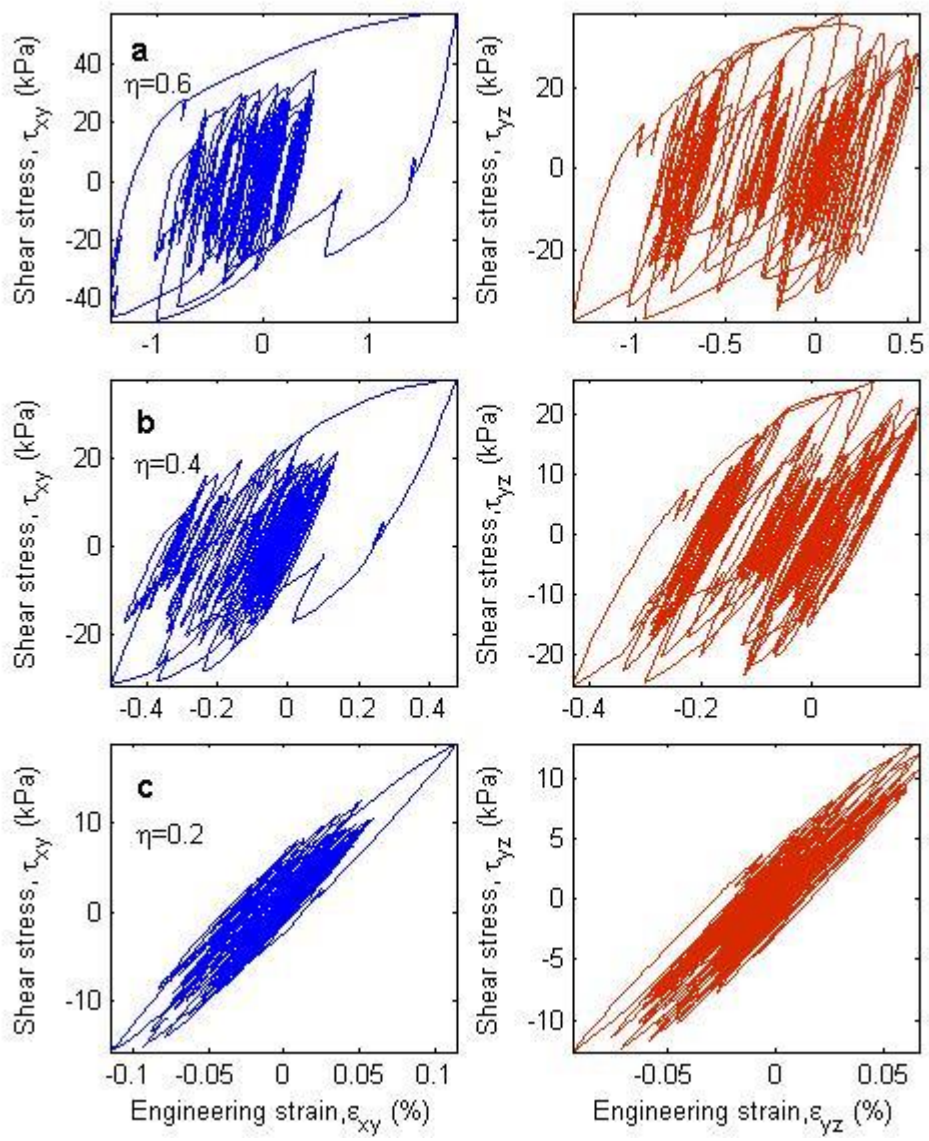

Figure 5.15 Hysteresis plots obtained from bidirectional stress controlled simulations corresponding to the Urayasu ground motion during the Mw9 11 March 2011 Tohoku earthquake for peaks stress ratios of (a) 0.6 (b) 0.4 and (c) 0.2 with a constant confining pressure of 100kPa

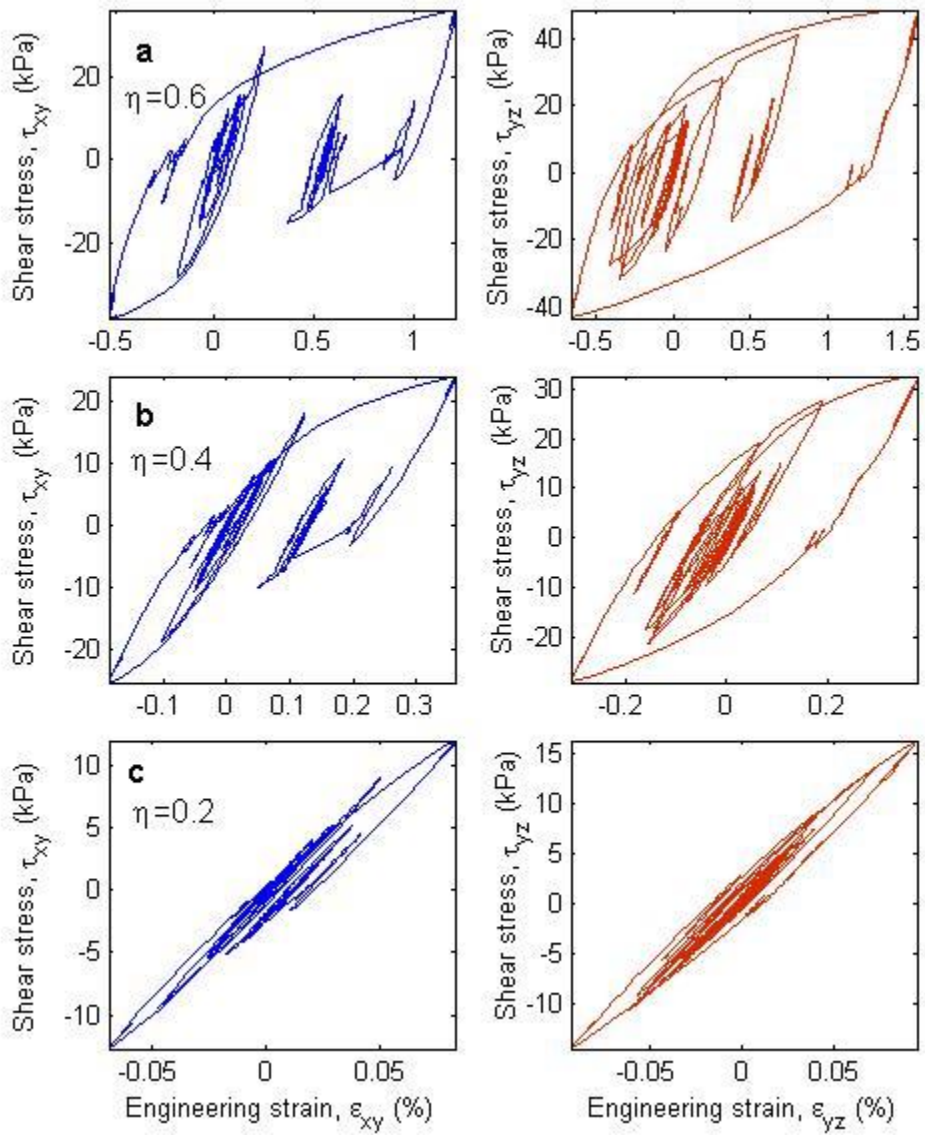

Figure 5.16 Hysteresis plots obtained from bidirectional stress controlled simulations corresponding to the CBGS ground motion during the Mw6.2 22 February 2011 Christchurch earthquake for peaks stress ratios of (a) 0.6 (b) 0.4 and (c) 0.2 with a constant confining pressure of 100kPa

The time series plot of the shear stress on deviatoric plane ($\sqrt{J_2}$, $J_2 = s_{ij}s_{ij}/2$, the second deviatoric stress invariant), response histories of shear strain (ε_{xy} and ε_{yz}), and dilatancy induced (plastic) volumetric strain (ε_{ii}) are shown in Figure 5.17 and 5.18 corresponding to three peak shear stress levels for Urayasu and CBGS ground motions, respectively. For both the ground motions permanent strains can be observed for the peak shear stress of 60kPa, which is due to more profound inelastic behaviour than the other two lower levels of peak shear stress. As previously noted, the Urayasu ground motion is vibratory, while the CBGS ground motion is impulsive. Such dissimilarity between the

ground motions is well reflected in volumetric strain response, which is a cumulative measure. Both the ground motions are scaled to the same levels of peak shear stress and are reproducing comparable values of peak shear strain and residual shear strain, but the accumulated volumetric strain for Urayasu ground motion is nearly four times that of CBGS. Clearly, the peak shear strain or the residual shear strain are instantaneous values and do not adequately represent the entire history of the shear stress to which the model has been subjected to. Since inelastic behaviour is path dependent, the cumulative effect of Urayasu ground motion is more severe as it contains many more cycles than CBGS. One measure of the cumulative effect, as can be seen from Figure 5.17 and 5.18, is the plastic volumetric strain, and the other is the dissipated energy through accumulation of plastic shear strain. The second measure can be obtained from the area enclosed by the hysteresis loops shown in Figures 5.15 and 5.16, normalised by the product of the peak shear stress and the peak shear strain for each direction separately, to compare the energy dissipation demand between the two directions as well as between the responses caused by the stress histories generated from the two ground motions. For the peak shear stress of 60kPa, the normalised area along the directions xy and yz are 1.18 and 2.04, respectively, for CBGS ground motion; the corresponding values for Urayasu ground motion are 4.02 and 2.53. It is evident from the values of the normalised energy dissipation that the principal component is yz for CBGS and xz for Urayasu ground motion. It can be also observed from Figure 5.17c and 5.18c, that most of the volumetric strain is attained within the significant duration $D_{s595}$of the individual ground motions. Summarily, it can be inferred from the results of the above simulation that the algorithm developed for cyclic behaviour is robust and can handle complex bidirectional stress paths.

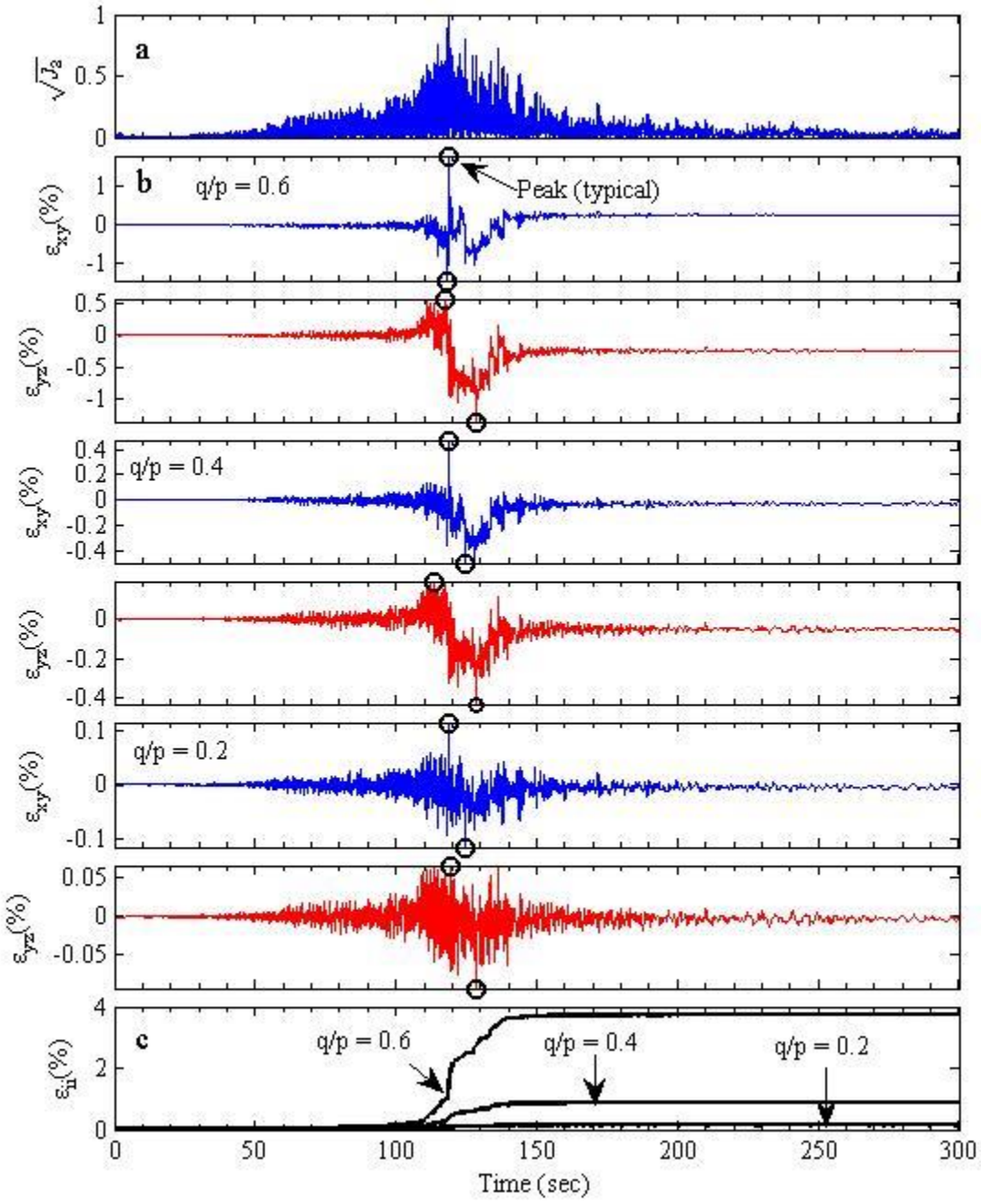

Figure 5.17 Time series plots of (a) shear stress on deviatoric plane (J_2: second deviatoric stress invariant); (b) shear strain; and (c) dilatancy induced volumetric strains obtained from stress controlled simulation corresponding to the Urayasu ground motion during the M_w9 11 March 2011 Tohoku earthquake

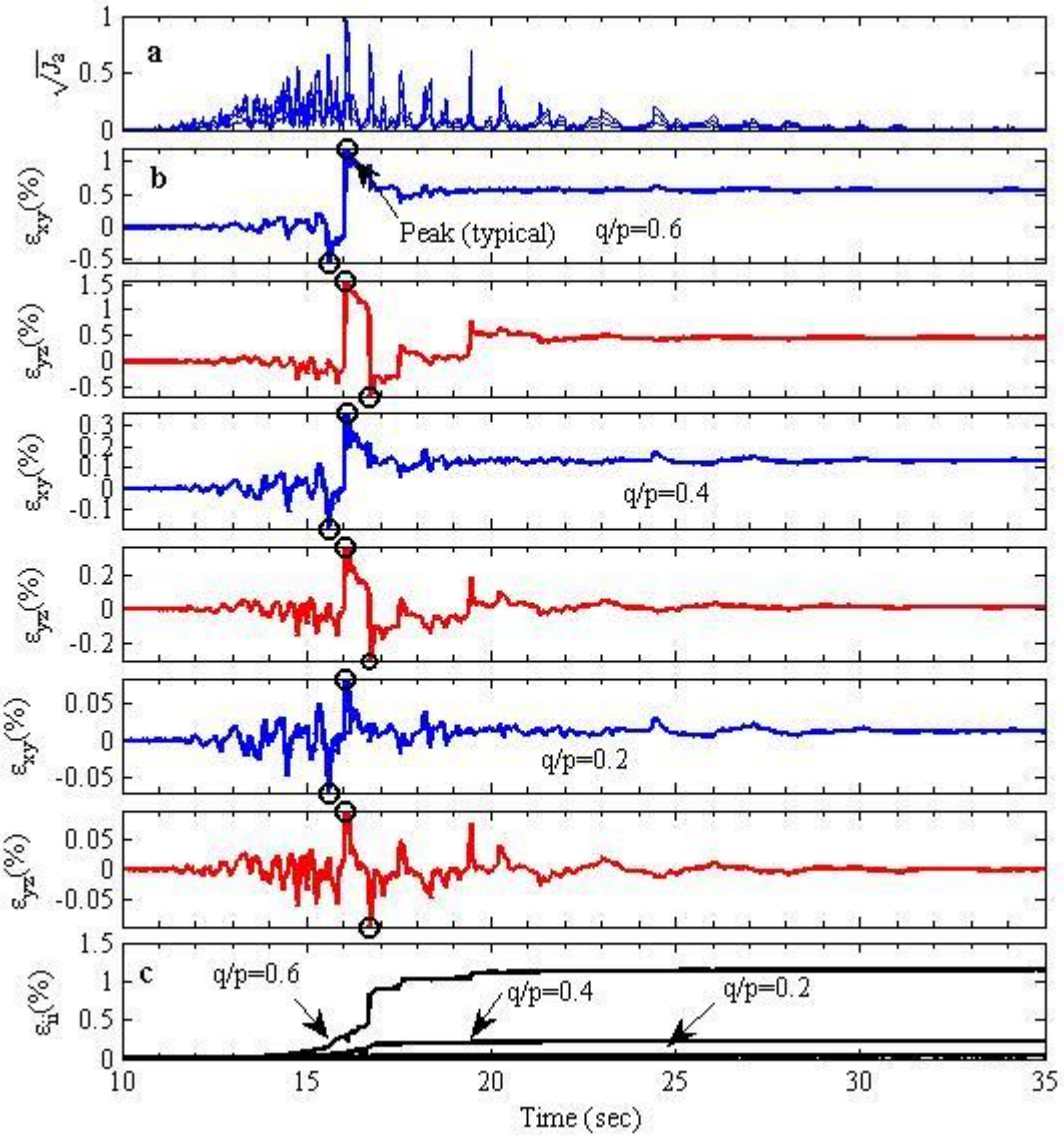

Figure 5.18 Time series plots of (a) shear stress on deviatoric plane (J_2: second deviatoric stress invariant); (b) shear strain; and (c) dilatancy induced volumetric strains obtained from stress controlled simulation corresponding to CBGS ground motion during the M_w6.2 22 February 2011 Christchurch earthquake

5.4 Effect of bidirectional shear stress path on liquefaction resistance

To understand the effect of bidirectional shear stress path on liquefaction resistance, undrained stress controlled elemental simulations have been carried out under bidirectional shear stress histories synthesised from Urayasu and CBGS ground motions. The experimental evidence on how the liquefaction resistance degrades with bidirectional interaction is very lucidly presented in Ishihara and Yamazaki (1980), shown in Figure 1.1, repeated in Figure 5.19 for convenience of readers.

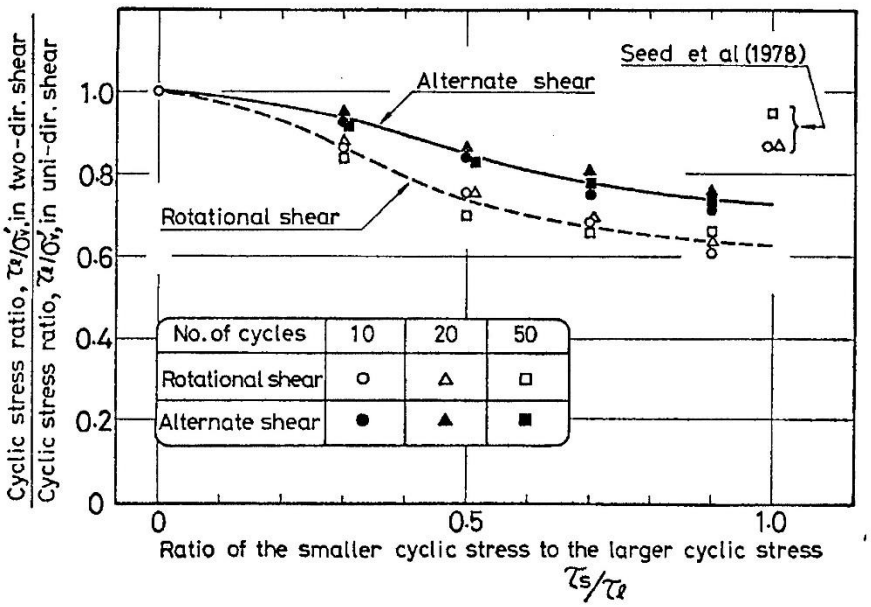

Figure 5.19 Cyclic strength under bidirectional shear loading normalised to the unidirectional shear loading (Ishihara and Yamazaki, 1980) (also shown in Figure 1.1)

Figure 5.19 shows that in general the liquefaction resistance under bidirectional shear is always less than that of the unidirectional, and the degradation depends mainly on the stress orbits, particularly the ratio of the minor (τ_s) to the principal component (τ_l). However, actual bidirectional stress orbits (Figure 5.13b and 5.14b) are complex and are difficult to decompose into 'rotational' or 'alternate' stress orbits. Hence, in order to understand the bidirectional effect on liquefaction resistance under realistically complex stress paths, undrained stress controlled simulations are carried out assuming a specimen of Toyoura sand with relative density of 50% (void ratio of 0.8) with the same model parameters as listed in Table 5.1.

Pending implementation of the model in a finite element solution, a simple analysis methodology is attempted for stress controlled undrained analysis: a constant effective

pressure is assumed in each step and dilatancy induced volumetric strain is obtained by a direct analysis. The effective pressure for the next step is reduced via the expression: $\mathrm{d}p = -K_f/n(\mathrm{d}\varepsilon_{ii}{}^p)$; K_f is the bulk modulus of pore fluid assumed as 2x10^{6}kPa; n is the porosity; $\mathrm{d}\varepsilon_{ii}{}^p$ is the plastic volumetric strain. However, undrained analysis becomes numerically unstable when the bulk modulus of the porous media becomes very large in comparison to that of the effective stress elasto-plastic parameters, as the situation becomes equivalent to undrained total stress Poisson's ratio approaching 0.5 (Potts and Zdravkovic, 1999). Moreover, stress controlled simulation will also fail when the plastic modulus, H_p, approaches a very low value as the plastic strain increment, $\mathrm{d}\lambda = 1/H_p\left(n_{ij}\mathrm{d}\sigma_{ij}\right)$ (n_{ij}: loading direction; $\mathrm{d}\sigma_{ij}$: stress increment) will become undetermined; the same will also occur with the elastic strain increment for sandy soils at low to negligible effective pressure as elastic modulus will also approach zero. When initial liquefaction occurs, which is set as effective pressure equals to 10kPa or less for an initial effective pressure of 100kPa, the effective stress elasto-plastic parameters become very negligible in comparison to K_f including the elastic and plastic moduli; consequently, numerical instability is encountered with large infeasible change in effective pressure in a single step, depending upon the stress increment in that step, rendering subsequent steps practically unusable. Hence, the peak shear stress to the initial liquefaction is considered here as a measure of liquefaction resistance. Furthermore as the purpose is to compare such liquefaction resistance between bidirectional and unidirectional stress paths, any inherent approximation in the methodology is equally applicable to both the cases of bidirectional and unidirectional analyses.

The comparison of the liquefaction resistance as described above between the bidirectional and unidirectional shear stress is quantified via Equation 5.1

$$q_r = \frac{q_{max,bi}}{q_{max,uni}} \tag{5.1}$$

where $q_{max,bi}$ is the peak shear stress to the initial liquefaction under bidirectional shear stress; $q_{max,uni}$ is the same, but under unidirectional shear stress; and, q_r is the liquefaction resistance ratio; when $q_r \leq 1$ then bidirectional shear stress is critical producing a lower liquefaction resistance. The liquefaction resistance ratio, q_r, is plotted against various peak shear stress values in Figure 5.20a and 5.20b for CBGS and Urayasu ground motions, respectively. The peak shear stress values drawn along abscissa are simply the peak ground

acceleration, obtained by vector summation of the bidirectional components, scaled to the stress ratio, $\eta_0 = q_0/p_0$ varying from 0.1 to 0.35 at an interval of 0.05; where q_0 : shear stress defined in Equation 4.7; and p_0: initial effective pressure assumed as 100kPa. When effective pressure becomes less than $0.1p_0$ (10kPa), it is assumed as the initial liquefaction, as per the earlier assertion. The principal component is the one which has higher peak ground acceleration. In addition, q_r is also plotted for unidirectional analysis along the principal direction, which is selected based on the directional variation of the peak ground acceleration (or the peak shear stress in this case).

The directional variation of the peak ground acceleration is shown in Figure 5.21a and 5.21b for CBGS and Urayasu ground motions, respectively. In Figure 5.21, the bidirectional components are normalised such that after vector summation the peak value is unity. Hence, there should be a direction along which the peak value must be unity, which is the principal direction. Therefore, the peak shear stress value, q_0, of the unidirectional time series data along the principal direction is the same as that of the bidirectional time series data.

It can be seen from Figure 5.20a, that in case of CBGS ground motion, the liquefaction resistance under bidirectional shear stress, $q_{max,bi}$, is consistently well below that of the unidirectional shear, $q_{max,uni}$, considering both the principal component and the principal direction; therefore, q_r plots well below the line drawn at unity. Moreover, as the stresses increase, which also increases inelastic action, bidirectional degradation becomes more pronounced further lowering the value of q_r. However, the observation for Urayasu ground motion, as shown in Figure 5.20b, is just the opposite. The liquefaction resistance is almost the same for both the bidirectional and unidirectional shear stress with q_r as almost unity. Apart from the obvious differences between the ground motions, such as CBGS is of impulsive type and Urayasu is of vibratory type, as well as their stress orbits, another important difference between them is the ratio of the peak ground acceleration (or the peak shear stress in this case) of the minor to the major or principal component. In CBGS ground motion the components have almost equal peak values in both the directions with principal direction between 30° and 45° (Figure 5.21a), while in case of Urayasu, the minor component is almost half of the principal component with principal direction along 115° (Figure 5.21b). It has been already shown in Figure 5.19 that resistance under bidirectional shear reduces as the ratio τ_s/τ_l increases. Corroborating observations are made in Figure

5.20, wherein CBGS ground motion has a higher ratio of τ_s/τ_l than Urayasu and consequently exhibiting more pronounced bidirectional effect.

Comparison with the respective principal directions also show that by mere artificially augmenting the peak shear stress or the peak ground acceleration by changing direction cannot replicate the effect of inelastic behaviour under bidirectional shear stress. It can be seen from both Figure 5.20a and 5.20b, that there is no significant difference between the principal component and the principal direction, although the peak shear stress of the principal direction is the same as that of the bidirectional shear stress. Besides, original signals are lost when two independent signals are merely superposed, and therefore ground motion along principal direction is an artificial one.

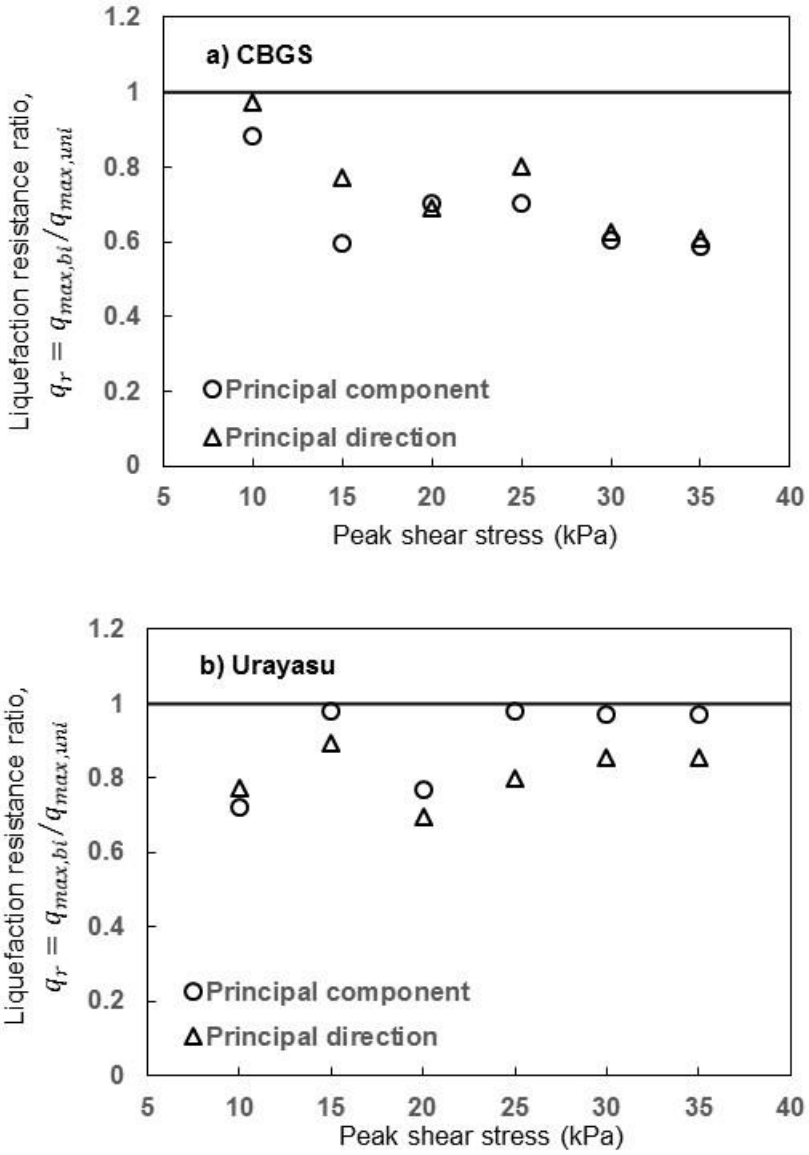

Figure 5.20 Ratio of the peak shear stress to the initial liquefaction from bidirectional analysis $(q_{max,bi})$ to that of unidirectional analysis $(q_{max,uni})$ for both the principal component and along the principal direction; peak shear stresses are generated from the ground motions (a) recorded at CBGS during the M_w6.2 22 February 2011 Christchurch earthquake; and (b) Urayasu during the M_w9 11 March 2011 Tohoku earthquake

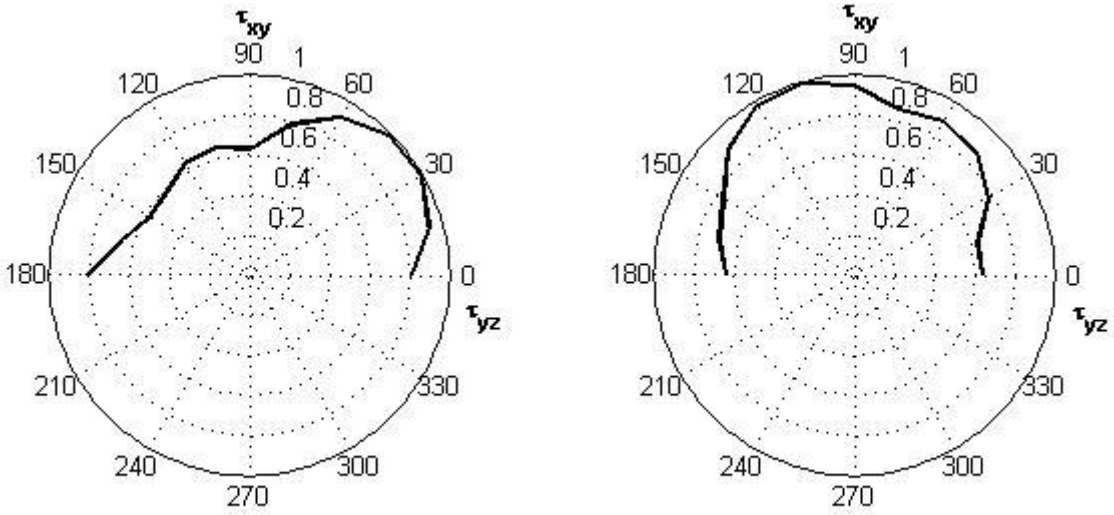

(a) CBGS **(b) Urayasu**

Figure 5.21 Directional variation of the peak ground acceleration (the peak shear stress) for the ground motions recorded at (a) recorded at CBGS during the M_w6.2 22 February 2011 Christchurch earthquake, with the principal direction along 30 degrees; and (b) Urayasu during the M_w9 11 March 2011 Tohoku earthquake, with the principal direction along 115 degrees

5.5 Summary and conclusion

Using a single set of parameters, the model is extensively validated for undrained monotonic simple shear and triaxial stress paths; drained cyclic torsional and triaxial stress paths; and undrained triaxial stress path for different relative densities. Detailed validation of the model under cyclic undrained torsional stress path is already available in Cubrinovski and Ishihara (1998b), and hence, not included herein, although sample simulation results are shown. The model performance is excellent for torsional stress paths; however, moderate, but acceptable, levels of deviation were occasionally observed for triaxial stress path because the parameters for triaxial stress path are obtained indirectly from the torsional stress path by assuming Mohr-Coulomb criterion. Furthermore, the critical state line and the correlation between the model parameters and the state index, which are obtained for torsional stress path, are assumed applicable for triaxial stress path as well. As the model does not incorporate the fabric anisotropic effect, framing a novel state concept responsive to stress path, such as Dafalias et al. (2004), is beyond the scope of the current version of the model. Hence, there will be always some approximation in triaxial stress path when the state concept

is based on torsional stress path. Despite such inherent approximation, the model performance is well within the acceptable limits for engineering analysis.

The algorithm for the anisotropic hardening rule consisting of an infinite number of homogeneous surfaces is rigorously verified by stress-controlled simulation under bidirectional components of real ground motions with varying levels of stress ratios. The algorithm is found to be stable as the resulting hysteresis plots of shear stress versus shear strain have positive incremental slopes throughout the response history; the area enclosed by the hysteresis loops is positive; and there is no overshooting of the backbone curve. Cyclic undrained stress controlled simulation are carried out to understand the effect of bidirectional shear stress imposed by the stress orbits of actual ground motions on liquefaction resistance. The results corroborated the experimental observations that liquefaction resistance degrades in bidirectional shear, and such degradation is the greatest if the minor and major components become equal. The study also revealed that principal direction in terms of the intensity measure of peak ground acceleration fails to replicate the effect of bidirectional shear stress on liquefaction resistance of medium dense sands.

Summarily, the three-dimensional model incorporates all the essential features of sand behaviour such as accumulation of plastic strain during rotation of principal stresses (rotational stress path); strain-dependent stress-dilatancy relation; and the state concept. These constitutive relations are already well-established through rigorous verification studies with the original plane-strain model of Cubrinovski and Ishihara (1998b), for example in Cubrinovski (2008). Thus the extension of the model for complex stress paths in three dimension widens the applicability of the model of Cubrinovski and Ishihara (1998b) for seismic response analysis with multidirectional components of ground motions.

6.0 Scope for Future Research

6.1 Incorporating anisotropic consolidation

The three dimensional model as well as the plane-strain model of Cubrinovski and Ishihara (1998b) consider initial isotropic state of stress. However, soils in in-situ condition are in triaxial compression state in level ground, while in sloping ground and below the foundations, transverse shears also exist. Therefore, the initial state of stress is complex and needs to be incorporated in the model. The consolidation process is therefore anisotropic, where slope of the stress path shown by vector $\overrightarrow{OA}$ in Figure 4.1, can be expressed as $\eta_0 = q_0/p_0 = \sqrt{3}\,(1-k)/(1+2k)$ in view of Equation 4.7; where $k = \sigma_3/\sigma_1$; σ_1 is the major principal stress; and σ_3 is the minor principal stress; the value of $\eta_0 = 0.43$ for $k = 0.5$. As the model is developed on the concept of strain-dependent stress-dilatancy relation, the dilatancy coefficient, μ in Equation 4.14, needs to be updated based on the shear strain, λ, accumulated at end of the consolidation process. Otherwise, depending upon the value of the non-coaxiality factor, c, the model sometimes predicts negative dilatancy when the value of μ is less than $c\eta_0$ via Equation 4.15, although η_0 could be less than that of the phase-transformation. In the majority of the sand models, including those reviewed herein, the equivalent dilatancy coefficient μ has been considered as the stress ratio at phase-transformation, which is generally greater than the range of η_0 encountered in practice. So this problem of negative dilatancy is due to the strain-dependent definition of the stress-dilatancy relation.

Two methods for incorporating the initial anisotropic stress are contemplated: first, the deviatoric strain associated with the stress path $\overrightarrow{OA}$ of Figure 4.1 will be determined and then this strain will be used in Equation 4.14 in place of λ to increase μ. As sand is relatively incompressible along $\overrightarrow{OA}$ (Pestana and Whittle, 1995), elastic mechanism can be assumed. However, initial trials have shown that the elastic deviatoric strain is inadequate and the problem persists. If a plastic mechanism is assumed then a curved 'cap' surface is required with a multi-mechanism approach, which does not fit within the existing framework. Alternatively, for the sake of simplicity, deviatoric p_0-constant stress path is assumed and stress controlled simulation has been carried out until η_0 to determine the deviatoric strain. The deviatoric strain approximated by this procedure is greater than the previously attempted

elastic analysis, but it is still not enough to increase μ to the desired level. In the second method, which is empirically motivated from Kato et al. (2001), modifies Equation 4.14 as Equation 6.1.

$$\mu = \mu_0 + \frac{2}{\pi}(M - \mu_0)\tan^{-1}\left(\frac{\lambda}{S_c}\right) + c_1\eta_0\exp(-c_2\lambda) \quad \textbf{(6.1)}$$

where c_1 and c_2 are additional positive model constants; the remaining parameters are defined previously in Equation 4.14. It can be seen that $\mu = \mu_0 + c_1\eta_0$ at λ =0 and as λ becomes large approaching the critical state, $\mu \to M$. Therefore, one of the scope of future research is calibration of constants c_1 and c_2 for validation of Equation 6.1. The plastic modulus in view of η_0 can be simply modified by assuming a deviatoric p_0-constant stress path; the resulting λ calculated by stress controlled simulation can be substituted in Equation 4.20.

6.2 Incorporation of Lode angle effect

6.2.1 Bounding surface

The second significant improvement which can attempted is incorporation of Lode angle effect, or the b-value via the third deviatoric stress invariant in the equation of the bounding surface. For this purpose, Lade and Duncan (1975) yield criterion as modified by Yang and Elgamal (2008) can be used. The equation of the bounding surface is given by Equation 6.2.

$$F(\sigma_{ij}) = pJ_2 - J_3 - \rho^3 p^3 = 0 \quad \textbf{(6.2)}$$

where $J_2 = s_{ij}s_{ij}/2$ is the second deviatoric stress invariant; $J_3 = s_{ij}s_{jk}s_{ki}/3$ is the third deviatoric stress invariant; s_{ij} is the deviatoric stress; p is the effective pressure; and ρ is a material constant. The constant, ρ can be easily calculated from the stress ratio given either for triaxial compression (η_{TC}), or torsional (η_T) or triaxial extension (η_{TE}). Equation 6.2 can be expressed as: $\sqrt{J_2} - \eta p = 0$ by replacing J_3 as $J_3 = 2\cos 3\theta (J_2/3)^{3/2}$, where $\theta = 0$ for triaxial compression ($\eta = \eta_{TC}$); $\theta = \pi/6$ for torsional ($\eta = \eta_T$); and $\theta = \pi/3$ for triaxial extension ($\eta = \eta_{TE}$). Hence, ρ can be related to η for the various stress paths as given by Equation 6.3

$$\rho^3 = \eta^2 - 2\left(\frac{\eta}{\sqrt{3}}\right)^3 \cos 3\theta \quad \textbf{(6.3)}$$

The bounding surface given by Equation 6.2 can evolve with the state-dependent function of ρ via the stress ratio, η, using Equation 6.3.

6.2.2 Loading surface and anisotropic hardening rule

The main challenge in this formulation is to obtain a method of solution for anisotropic hardening rule, which is developed as follows. The equation of n^{th} loading surface is given by Equation 6.4 and is formulated in such a way that each surface is homogeneous to the bounding surface.

$$L^n\left(r_{ij} - {c_{ij}}^n, \kappa^n\right) = \kappa^n \overline{J_2} - \overline{J_3} - (\kappa^n p)^3 = 0 \quad \textbf{(6.4)}$$

where κ is a scaling constant rendering Equation 6.4 homogeneous to Equation 6.3; κ varies between 0 and 1; when $\kappa = 1$, the loading surface becomes the bounding surface; c_{ij} is the deviatoric back-stress tensor; $r_{ij} = s_{ij}/p$ is the deviatoric stress ratio. Therefore $\overline{J_2} = \left(r_{ij} - {c_{ij}}^n\right)\left(r_{ij} - {c_{ij}}^n\right)/2$ and $\overline{J_3} = \left(r_{ij} - {c_{ij}}^n\right)\left(r_{jk} - {c_{jk}}^n\right)(r_{ki} - {c_{kl}}^n)/3$ are the second and third stress invariants of $r_{ij} - {c_{ij}}^n$, respectively. By applying Equation 3.3 of Mroz (1967) and subsequent simplification yields Equation 6.5, which also indicates that r_{ij}^{n+1} and r_{ij}^n have the same directions of tangent as $\text{Dev}\left(\partial L^n\left(r_{ij} - {c_{ij}}^n, \kappa^n\right)/\partial r_{ij}\right)$ is also a homogeneous function to second order; where Dev(.) is the deviatoric transform of a tensor.

$$r_{ij}^{n+1} - c_{ij}^{n+1} = \frac{\kappa^{n+1}}{\kappa^n}\left(r_{ij}^n - c_{ij}^n\right) \quad \textbf{(6.5)}$$

As per the hardening rule of the three dimensional model, smaller surface is tangential to the larger surface at the point of stress reversal. Let the stress reversal point between n and $n+1$ surfaces be denoted as ${t_{ij}}^{n+1}$. Because the direction of the tangent of the larger surface at ${t_{ij}}^{n+1}$ must be equal to that of the new surface that is going to evolve, and as ${t_{ij}}^{n+1}$ must also lie on the new surface, Equation 6.5 can be applied to derive a recurrence relation between c_{ij}^{n+1} and c_{ij}^n, as shown in Equation 6.6

$$c_{ij}^{n+1} = \beta c_{ij}^n + (1-\beta){t_{ij}}^{n+1};\ \beta = \frac{\kappa^{n+1}}{\kappa^n} \quad \textbf{(6.6)}$$

The scalar variable β can be solved by substituting Equation 6.6 in Equation 6.4 for $n+1$ loading surface which results in a quadratic of β.

6.2.3 Interpretation of plastic modulus

The plastic modulus of the three dimensional model given by equation 4.20 depends on the relative size of a current loading surface to the bounding surface via the term η/η_{max}, where η is the radius of the current surface and η_{max} is the radius of the bounding surface. In this Lode angle dependent version, this ratio can be defined as follows: consider r_{ij}^{CP} as the conjugate point lying on the bounding surface and homologous to r_{ij} that lies on a loading surface with the parameters c_{ij}^{n} and κ^{n}; the basis of the homology is that r_{ij} and r_{ij}^{CP} are related by linear scaling law given by Equation 6.5. Therefore, r_{ij} and r_{ij}^{CP} have the equal directions of tangent at the loading surface, L^{n} and at the bounding surface, F, respectively. From Equation 6.5 an equivalent expression for the term η/η_{max} can be derived as shown below in Equation 6.7 which tacitly incorporates the Lode angle effect via the parameter κ. Furthermore, each loading surface also becomes a locus of equal plastic modulus.

$$\left.\begin{aligned} r_{ij}-{c_{ij}}^{n} &= \kappa^{n}{r_{ij}}^{CP} \\ \left(r_{ij}-{c_{ij}}^{n}\right)\left(r_{ij}-{c_{ij}}^{n}\right) &= (\kappa^{n})^{2}{r_{ij}}^{CP}{r_{ij}}^{CP} \\ \frac{\eta}{\eta_{max}} &= \frac{\sqrt{\left(r_{ij}-{c_{ij}}^{n}\right)\left(r_{ij}-{c_{ij}}^{n}\right)}}{\sqrt{{r_{ij}}^{CP}{r_{ij}}^{CP}}} = \kappa^{n} \end{aligned}\right\} \quad \textbf{(6.7)}$$

As the stress-dilatancy relation is assumed to be path independent, it is not presently contemplated to modify it on the basis of Lode angle. However, in the majority of the Lode angle dependent models, the equivalent term for μ in Equation 4.15, which is the stress ratio at phase transformation, is also Lode angle dependent via a homogeneous surface.

6.3 Stress-dilatancy relation

The present stress-dilatancy relation leads to strain saturation during cyclic mobility, which has been a major drawback in many of the constitutive models which do not have any specific formulation to address this issue. The models which have specific formulations, albeit empirically derived, to facilitate spreading of plastic strain are those of Yang et al. (2003); Zhang and Wang (2012). The current model requires improvement of the stress-dilatancy relation in similar direction. However, every model functions within the constraint

of its constitutive relations; for example, in the present model, the hardening function and the stress-dilatancy, which are mutually connected via several internal variables, work together well; even if the stress-dilatancy relation is moderately altered, then the model performance could well become different. Hence, whatever improvement is attempted, it should not compromise with the existing formulation. Ideally, the improvement in the stress dilatancy relation should become active once the model enters into a dilation phase. If the attainment of a dilation phase can be progressively delayed with every cycle in terms of plastic shear strain accumulation, then the problem of strain saturation can be alleviated; the same philosophy is implemented in different ways in the aforementioned models of Yang et al. (2003); Zhang and Wang (2012). Still another mathematically possible way is to reduce the elastic modulus with some strain-dependent definition of the parameter m in Equation 4.18.

6.4 Closure

The improvements proposed herein are aimed to overcome the following three limitations of the current model: (1) assumption of initial isotropic stress; (2) independence of Lode angle; and, (3) saturation of strain during cyclic mobility. The formulas presented herein addressing the first two improvements fit well within the existing framework, which will not compromise with the rest of the formulation. It can be noted from Equation 6.2 and 6.4 that for seismic stress paths with $b = 0.5$ and $J_3 = 0$, the proposed formulas will be the same as the current ones. However, for triaxial stress path, the proposal for Lode angle dependent bounding surface via the third stress invariant will be a significant improvement, as the initial deviatoric back-stress tensor a_{ij} will no longer be required. The validation of the aforementioned two proposals and the improvement of the stress-dilatancy relation to promote the spread of plastic strain during cyclic mobility are identified as scope for future research.

7.0 Summary and Conclusions

7.1 Summary

A comprehensive seismic response analysis requires an integrated approach of Soil Structure Foundation Interaction (SFSI), particularly when structures are founded on soft liquefiable saturated sand. During both the M_w7.1 4 September 2010 Darfield and the M_w6.3 22 February 2011 Christchurch earthquakes, widespread liquefaction had been observed in Christchurch and its suburbs. There has been many studies, both experimental and case history based, devoted to the understanding of constitutive behaviour of sandy soils. Such studies are mostly restricted to plane-strain configuration, which is very common in soil mechanics, as many geo-technical structures conform to plane-strain configuration. However, SFSI is a three dimensional stress analysis problem because of two reasons: first, geometry of foundation systems is three dimensional; and second, the horizontal shear wave, which is generally considered as the primary excitation source in seismic analysis, is bidirectional. There are experimental evidences, although rare, that the cyclic resistance ratio under bidirectional shear stress can be as low as 60% of that of the unidirectional shear stress. Hence, there is a need to develop a computationally efficient and implementable three dimensional constitutive model for shear deformation of sandy soils which will specialise on liquefaction behaviour as three-dimensional stress analysis is always computationally demanding. For this purpose, it is considered sufficient to incorporate only those constitutive relations that are crucial for seismic stress paths. To achieve this objective, the plane-strain model by Cubrinovski (1993); Cubrinovski and Ishihara (1998b) is selected as the base model upon which the three dimensional model presented herein is developed. The plane-strain model as well as its three dimensional development is based on the theory of plasticity. To develop an understanding of the constitutive behaviour of sand, which is always interpreted using the concepts of the theory of plasticity, and the state-of-the-art in constitutive modelling for sand behaviour, a succinct review of the theory of plasticity and its applicability to soil mechanics, and a comprehensive review of 14 state-of-the-art sand models have been also presented herein.

The three dimensional model is developed within the framework of bounding surface plasticity comprising Drucker-Prager type bounding surface. It considers plastic deviatoric

mechanism and follows hypoplastic flow rule; energy-based strain-dependent stress-dilatancy relation; state concept; and anisotropic hardening rule. The model is validated for monotonic undrained simple shear and triaxial stress paths; cyclic p-constant torsional and triaxial stress paths; and cyclic undrained triaxial stress path. The original model of Cubrinovski and Ishihara (1998b) was validated for cyclic undrained torsional stress path, and hence the same validation results are not included herein, although sample simulation results have been presented. If the order of the tensor quantities is reduced to two for a two-dimensional stress space, then the original model can be retrieved. Therefore, the plane-strain model of Cubrinovski and Ishihara (1998b) is a true subset of the three dimensional model. The anisotropic hardening rule is verified under stress controlled bidirectional shear stress histories generated from actual ground motions to retain realistic complexity in bidirectional stress orbits during the verification. A simple undrained stress controlled simulation has been also carried to highlight the effect of bidirectional shear stress on liquefaction resistance of medium dense sand.

The model has the following limitations: consideration of initial isotropic stress prior to the deviatoric action; not explicitly incorporating Lode angle effect via the third stress invariant; and saturation of strain during cyclic mobility. In order to overcome the first two limitations, new formulation have been proposed; their validation along with the need to improve the stress-dilatancy relation to allow for spread of plastic strain during cyclic mobility are identified as scope for future research. Finally, the stress integration FORTRAN subroutine and the OPENSEES (Open System for Earthquake Simulation, downloadable from http://opensees.berkeley.edu/) C++ interface for implementation in OPENSEES are given in the appendix.

7.2 Conclusion

Based on the review of the theory of plasticity, the recent mathematical advances in the state-of-the-art in plasticity-based modelling of sand behaviour and the development of the three dimensional model, following conclusions can be drawn.

1. The model developed herein is intended for seismic response analysis with bidirectional tranverse shear stress applied along the bedding plane. For the sake of simiplicity, it has been considered that for this particular stress path, b-value is constant at 0.5 and α at 45°. The model uses the quasi-steady state line to define the

state index to incorporate the characteristics of initial fabric in an isotropic form as it does not include the mathematical framework to consider the fabric anisotropy. In view of such limitation, the assumption of the constant values of α and b-value can be considered as a theoretical compliance. Despite the aforementioned limitation for non-torsional stress paths, the model has shown reasonably acceptable results, with moderate deviations, for the triaxial stress path, which is achieved by simply matching the circular bounding surface through the triaxial compression and extension apices of Mohr-Coulomb criterion. In addition to the model validation, the verification of the anisotropic hardening rule in complex stress space, comprising bidirectional transverse shear stresses generated from bidirectional horizontal components of actual ground motions, is also successful. Hence, the objective of the thesis to not only develop a three-dimensional model for shear deformation of sand under bidirectional cyclic loading, but also to provide a holistic view of the state-of-the-art in constitutive modelling is successfully achieved.

2. A current trend is observed in the evolving models to consider fabric anisotropy by expressing the steady state line as a function of stress path characterised by the Lode's parameter, b-value, and the direction of the principal deviatoric plane with respect to the bedding plane, α. This novel modelling approach is in contrast to the models which have been developed based on the concept of uniqueness of the critical state, and hence on the notion of isotropic fabric. Although the fabric anisotropic models are successful in reproducing some of the interesting features of sand behaviour, such as progressively contracting and softening behaviour for increasing values of α for a given b-value and vice-versa, their basic postulation may require further experimental validation. Furthermore, based on the above trend, it can be inferred that the models which do consider such fabric anisotropic effect, may have theoretical limitation on reproducing constitutive behaviour for all stress paths.

8.0 References

Alarcon-Guzman, A., Leonards, G. A., and Chameau, J. L. (1988). "Undrained monotonic and cyclic strength of sands." *Journal of Geotechnical and Geoenvironmental Engineering, ASCE*, **114**(10), 1089-1109.

Arthur, J. R. F., and Menzies, B. K. (1972). "Inherent anisotropy in a sand." *Geotechnique*, **22**(1), 115-128.

Bardet, J. P. (1986). "Bounding surface plasticity model for sands." *Journal of Engineering Mechanics, ASCE*, **112**(11), 1198-1217.

Been, K., and Jefferies, M. G. (1985). "A state parameter for sands." *Geotechnique*, **35**(2), 99-112.

Beresnev, I. A., Nightengale, A. M., and Silva, W. J. (2002). "Properties of vertical ground motions." *Bulletin of the Seimological Society of America*, **92**(8), 3152-3164.

Boulanger, R. W., Chan, C. K., Seed, H. B., and Seed, R. B. (1993). "A low-compliance bi-directional cyclic simple shear apparatus." *Geotechnical Testing Journal*, **16**(1), 36-45.

Boulanger, R. W., Kutter, B. L., Brandenberg, S. J., Singh, P., and Chang, D. (2003). "Pile foundations in liquefied and laterally spreading ground during earthquakes: centrifuge experiments & analyses." *Report No. UCD/CGM-03/01*, University of California Davis.

Boulanger, R. W., and Ziotopoulou, K. (2012). "PM4SAND (Version 2): A sand plasticity model for earthquake engineering applications." *Department of Civil and Environmental Engineering, University of California at Davis*, **UCD/CGM-12/01**.

Bowen, H. J., and Cubrinovski, M. (2008). "Effective stress analysis of piles in liquefiable soil: a case study of a bridge foundation." *Bulletin of the New Zealand Society for Earthquake Engineering*, **41**(4).

Bradley, B. A. (2012a). "Ground motion comparison of the 2011 Tohoku, Japan and 2010-2011 Canterbury earthquakes: Implications for large events in New Zealand." *Proc. New Zealand Society of Earthquake Engineering Annual Conference, Christchurch*.

Bradley, B. A. (2012b). "Strong ground motion characteristics observed in the 4 September 2010 Darfield, New Zealand earthquake." *Soil Dynamics and Earthquake Engineering*, **42**, 32-26.

Bradley, B. A., and Cubrinovski, M. (2011). "Near-source strong ground motions observed in the 22 February 2011 Christchurch earthquake." *Seismological Research Letters*, **82**(6), 853-865.

Bradley, B. A., Cubrinovski, M., Dhakal, R. P., and MacRae, G. (2010). "Probabilistic seismic performance and loss assessment of a bridge-foundation-soil system." *Soil Dynamics and Earthquake Engineering, Elsevier*, **30**, 395-411.

Butt, F., and Omenzetter, P. (2012). "Pre and post-earthquake dynamic analysis of an RC building including soil-structure interaction." *Proc. New Zealand Society of Earthquake Engineering (NZSEE) Conference, Christchurch, New Zealand*.

References

Cai, Y., Yu, H. S., Wanatowski, D., and Li, X. (2013). "Noncoaxial behaviour of sand under various stress paths." *ASCE, Journal of Geotechnical and Geoenviromental Engineering*, **139**(8), 1381-1395.

Chakrabarty, J. (2006). *Theory of plasticity*, Elsevier Butterworth-Heinemann.

Chen, W. F., and Baladi, G. Y. (1985). *Soil plasticity Theory and Implementation*. Netherlands, Elsevier.

Clough, R. W., and Penzien, J. (1993). *Dynamics of structures*. New York, McGraw-Hill.

Cubrinovski, M. (1993). "A constitutive model for sandy soils based on a stress-dependent density parameter." Doctor of Engineering, University of Tokyo.

Cubrinovski, M., Bradley, B., Wotherspoon, L., Russell, G., Bray, J., Wood, C., Pender, M., Allen, J., Bradshaw, A., Rix, G., Taylor, M., Robinson, K., Henderson, D., Giorgini, S., Winkley, A., Zupan, J., Rourke, T. O., DePascale, G., and Wells, D. (2011a). "Geotechnical aspects of the 22 February 2011 Christchurch earthquake." *Bulletin of the New Zealand Society for Earthquake Engineering*, **44**(4), 205-226.

Cubrinovski, M., Bray, D. J., Taylor, M., Giorgini, S., Bradley, B., Wotherspoon, L., and Zupan, J. (2011b). "Soil liquefaction effects in the Central Business District during the February 2011 Christchurch earthquake." *Seismological Research Letters*, **82**(6), 893-904.

Cubrinovski, M., Green, R. A., John, A., Ashford, S., Bowman, E., Bradley, B., Cox, B., Hutchinson, T., Kavazanjian, E., Orense., R., Pender, M., Quigely, M., and Wotherspoon, L. (2010). "Geotechnical reconnaissance of the 2010 Darfield (Canterbury) earthquake." *Bulletin of the New Zealand Society for Earthquake Engineering*, **43**(4), 243-320.

Cubrinovski, M., Henderson, D., and Bradley, B. A. (2012). "Liquefaction impacts in residential areas in the 2010-2011 Christchurch earthquakes." *Proc. International Symposium on Engineering Lessons Learned from the Giant Earthquake, March, Tokyo, Japan*.

Cubrinovski, M., and Ishihara, K. (1998a). "Modelling of sand behaviour based on state concept." *Soils and Foundations, Japanese Geotechnical Society*, **38**(3), 115-127.

Cubrinovski, M., and Ishihara, K. (1998b). "State concept and elastoplasticity for sand modelling." *Soils and Foundations, Japanese Geotechnical Society*, **38**(4), 213-225.

Cubrinovski, M., Ishihara, K., and Tanizawa, K. (1996). "Numerical simulation of the Kobe Port Island liquefaction." *Proc. Eleventh World Conference on Earthquake Engineering, Elsevier*, **Paper No. 330**.

Cubrinovski, M., Taylor, M., Robinson, K., Winkley, M. H., Haskell, J., and Bradley, B. (2014). "Key factors in the liquefaction-induced damage to buildings and infrastructure in Christchurch: preliminary findings." *Proc., New Zealand Society for Earthquake Engineers Conference, Auckland*, 1-9.

Cubrinovski, M., Uzuoka, R., Sugita, H., Tokimatsu, K., Sato, M., Ishihara, K., Tsukamoto, Y., and Kamata, T. (2008). "Prediction of pile response to lateral spreading by 3-D soil-water coupled dynamic analysis: shaking in the direction of ground flow." *Soil Dynamics and Earthquake Engineering*, **28**, 421-435.

References

Dafalias, Y. F. (1986). "Bounding surface plasticity. I: Mathematical foundation and hypoplasticity." *Journal of Engineering Mechanics, ASCE*, **112**(9), 966-987.

Dafalias, Y. F., and Manzari, M. T. (2004). "Simple plasticity sand model accounting for fabric change effects." *Journal of Engineering Mechanics, ASCE*, **130**(6), 622-634.

Dafalias, Y. F., Papadimitriou, A. G., and Li, X. S. (2004). "Sand plasticity model accounting for inherent fabric anisotropy." *Journal of Engineering Mechanics, ASCE*, **130**(11), 1319-1333.

Dafalias, Y. F., and Popov, E. P. (1977). "Cyclic loading for materials with a vanishing elastic region." *Nuclear Engineering and Design*, **41**, 293-302.

Drucker, D. C., and Seereeram, D. (1987). "Remaining at yield during unloading and other unconventional elastic-plastic response." *ASME, Journal of Applied Mechanics*, **54**, 22-26.

Eleni, S., Tasiopoulou, P., Bal, I. E., and Gazetas, G. (2011). "Ground motions versus geotechnical and structural damage in the February 2011 Christchurch earhquake." *Seismological Research Letters*, **82**(6).

Elgamal, A., and He, L. (2004). "Vertical earthquake ground motion records: An overview." *Journal of Earthquake Engineering, Imperial College Press*, **8**(5), 663-697.

Gao, Z., and Zhao, J. (2012). "Efficient approach to characterize strength anisotropy in soils." *Journal of Engineering Mechanics, ASCE*, **138**(12), 1447-1456.

Goel, R. K., and Chopra, A. K. (1997). "Period formulas for moment-resisting frame buildings." *Journal of Structural Engineering, ASCE*, **123**(11), 1454-1461.

Gutierrez, M. (2003). "Modelling of the steady-state response of granular soils." *Soils and Foundations, Japanese Geotechnical Society*, **43**(5), 93-105.

Gutierrez, M., and Ishihara, K. (2000). "Non-coaxiality and energy dissipation in granular materials." *Soils and Foundations, Japanese Geotechnical Society*, **40**(2), 49-59.

Gutierrez, M., Ishihara, K., and Towhata, I. (1991). "Flow theory for sand during rotation of principal stress direction." *Soils and Foundations, Japanese Geotechnical Society*, **31**(4), 121-132.

Gutierrez, M., Ishihara, K., and Towhata, I. (1993). "Model for the deformation of sand during rotation of principal stress directions." *Soils and Foundations, Japanese Geotechnical Society*, **33**(3), 105-117.

Imam, S. M. R., Chan, D. H., Robertson, P. K., and Morgenstern, N. R. (2002). "Effect of anisotropic yielding on the flow liquefaction of loose sand." *Soils and Foundations, Japanese Geotechnical Society*, **42**(3), 33-44.

Ishihara, K. (1993). "Liquefaction and flow failure during earthquakes." *Proc. 33rd Rankine Lecture, Geotechnique*, **43**(3), 351-415.

Ishihara, K., Tatsuoka, F., and Yasuda, S. (1975). "Undrained deformation and liquefaction of sand under cyclic stresses." *Soils and Foundations, Japanese Geotechnical Society*, **15**(1), 29-44.

Ishihara, K., and Towhata, I. (1983). "Sand response to cyclic rotation of principal stress direction as induced by wave loads." *Soils and Foundations, Japanese Geotechnical Society*, **23**(4), 11-26.

References

Ishihara, K., and Yamazaki, F. (1980). "Cyclic simple shear tests on saturated sand in multi-directional loading." *Soils and Foundations, Japanese Geotechnical Society*, **20**(1), 45-59.

Kabilamany, K., and Ishihara, K. (1990). "Stress dilatancy and hardening laws for rigid granular model of sand." *Soil Dynamics and Earthquake Engineering*, **9**(2), 66-77.

Kachanov, L. M. (1971). *Foundations of the theory of plasticity, Lauwerier, H. A., and Koiter W. T. (eds.)*, North-Holland Publishing Company - Amsterdam, London.

Kam, Y. W., Pampanin, S., Dhakal, R., and Elwood, K. (2011). "Seismic performance of reinforced concrete buildings in the 22 February Christchurch (Lyttelton) earthquake." *Bulletin of the New Zealand Society for Earthquake Engineering*, **44**(4), 239-278.

Kam, Y. W., Pampanin, S., Dhakal, R., Gavin, P. H., and Roeder, C. (2010). "Seismic performance of reinforced concrete buildings in the September 2010 Darfield earthquake." *Bulletin of the New Zealand Society for Earthquake Engineering*, **43**(4), 340-350.

Kammerer, A. M. (2002). "Undrained response of Monterey 0/30 sand under multidirectional cyclic simple shear loading conditions." PhD dissertation, University of California Berkeley.

Kato, S., Ishihara, K., and Towhata, I. (2001). "Undrained shear characteristics of saturated sand under anisotropic consolidation." *Soils and Foundations, Japanese Geotechnical Society*, **41**(1), 1-11.

Lade, P. V., and Bopp, P. A. (2005). "Relative density effects on drained sand behaviour at high pressures." *Soils and Foundations, Japanese Geotechnical Society*, **45**(1), 1-13.

Lade, P. V., and Duncan, J. M. (1975). "Elastoplastic stress-strain theory for cohesionless soil." *Journal of Geotechnical and Geoenvironmental Engineering, ASCE*, **101**(GT10), 1037-1053.

Lashkari, A., and Latifi, M. (2007). "A non-coaxial constitutive model for sand deformation under rotation of prinicpal stress axes." *International Journal for Numerical and Analytical Methods in Geomechanics*, **32**, 1051-1086.

Li, X. S. (2002). "A sand model with state-dependent dilatancy." *Geotechnique*, **52**(3), 173-186.

Li, X. S., and Dafalias, Y. F. (2000). "Dilatancy for cohesionless soils." *Geotechnique*, **50**(4), 449-460.

Li, X. S., and Dafalias, Y. F. (2002). "Constitutive modeling of inherently anisotropic sand behaviour." *Journal of Geotechnical and Geoenvironmental Engineering, ASCE*, **128**(10), 868-880.

Li, X. S., and Dafalias, Y. F. (2004). "A constitutive framework for anisotropic sand including non-proportional loading." *Geotechnique*, **54**(1), 41-55.

Lubliner, J. (1990). *Plasticity theory*. New York, Pearson Education Inc.

Manzari, M. T., and Dafalias, Y. F. (1997). "A critical state two-surface plasticity model for sands." *Geotechnique*, **47**(2), 255-272.

References

Miura, K., Miura, S., and Toki, S. (1986). "Deformation behavior of anisotropic dense sand under prinicpal stress axes rotation." *Soils and Foundations, Japanese Geotechnical Society*, **26**(1), 36-52.

Miura, N., Murata, H., and Yasufuku, N. (1984). "Stress-strain characteristics of sand in a particle-crushing region." *Soils and Foundations, Japanese Geotechnical Society*, **24**(1), 77-89.

Mroz, Z. (1967). "On the description of anisotropic workhardening." *J. Mech. Phys. Solids*, **15**, 163-175.

New Zealand Parliament (2011). "Economic effects of the Canterbury earthquakes." Parliamentary Library Research Paper

Pestana, J. M., and Whittle, A. J. (1995). "Compression model for cohesionless soils." *Geotechnique*, **45**(4), 611-631.

Potts, D. M., and Zdravkovic, L. (1999). *Finite element analysis in geotechnical engineering, Theory*, Thomas Telford Publishing, London.

Poulos, S. J. (1981). "The steady state of deformation." *Journal of the Geotechnical Engineering Division, ASCE*, **107**(5), 553-562.

Poulos, S. J., Castro, G., and France, J. W. (1985). "Liquefaction evaluation procedure." *Journal of Geotechnical and Geoenvironmental Engineering, ASCE*, **111**(6), 772-792.

Pradhan, T. B. S., and Tatsuoka, F. (1989). "On stress-dilatancy equations of sand subjected to cyclic loading." *Soils and Foundations, Japanese Geotechnical Society*, **29**(1), 65-81.

Pradhan, T. B. S., Tatsuoka, F., and Sato, Y. (1989). "Experimental stress-dilatancy relations of sand subjected to cyclic loading." *Soils and Foundations, Japanese Geotechnical Society*, **29**(1), 45-64.

Prevost, J. H. (1985). "A simple plasticity theory for frictional cohesionless soils." *Soil Dynamics and Earthquake Engineering*, **4**(1), 9-17.

Reimer, M. F., and Seed, R. B. (1997). "Factors affecting apparent position of steady-state line." *Journal of Geotechnical and Geoenvironmental Engineering, ASCE*, **123**(3), 281-288.

Roscoe, K. H., and Poorooshasb, H. B. (1963). "A fundamental principle of similarity in model tests for earth pressure problems." *Proc. of 2nd Asian Conference Soil Mechanics*, **1**, 134-140.

Schofield, A. N., and Wroth, C. P. (1968). *Critical State Soil Mechanics*, McGraw-Hill.

Shahnazari, H., and Towhata, I. (2002). "Torsional shear tests on cyclic stress-dilatancy relationship of sand." *Soils and Foundations, Japanese Geotechnical Society*, **42**(1), 105-119.

Standards, N. Z. (2004). Structural Design Actions. Part 5- Earthquake actions - New Zealand. Wellington, New Zealand Standards

Tatsuoka, F., Ochi, K., Fujii, S., and Okamoto, M. (1986). "Cyclic undrained triaxial and torsional shear strength of sands for different sample preparation methods." *Soils and Foundations, Japanese Geotechnical Society*, **26**(3), 23-41.

References

Timoshenko, S. (1940). "Mechanical properties of materials." *Strength of Materials, Part I Elementary Theory and Problems, 2nd ed.*, 396-498.

Vaid, Y. P., and Chern, J. C. (1985). "Cyclic and monotonic undrained response of saturated sands." *Proc. Advances in the Art of Testing Soils Under Cyclic Loading, ASCE, New York*, 120-147.

Vaid, Y. P., Chung, E. K. F., and Kuerbis, R. H. (1990). "Stress path and steady state." *Can. Geotech. J.*, **27**, 1-7.

Vaid, Y. P., and Thomas, J. (1995). "Liquefaction and postliquefaction behaviour of sand." *Journal of Geotechnical and Geoenvironmental Engineering, ASCE*, **121**(2), 163-173.

Verdugo, R. (1992). "Characterization of sandy soil behaviour under large deformation." PhD dissertation, University of Tokyo.

Verdugo, R., and Ishihara, K. (1996). "The steady state of sandy soils." *Soils and Foundations, Japanese Geotechnical Society*, **36**(2), 81-91.

Wan, R. G., and Guo, P. J. (1999). "A pressure and density dependent dilatancy model for granular materials." *Soils and Foundations, Japanese Geotechnical Society*, **39**(6), 1-11.

Wan, R. G., and Guo, P. J. (2001). "Effect of microstructure on undrained behaviour of sands." *Can. Geotech. J.*, **38**, 16-28.

Wang, Z., Dafalias, Y., Li, X., and Makdisi, F. (2002). "State pressure index for modeling sand behaviour." *Journal of Geotechnical and Geoenvironmental Engineering, ASCE*, **128**(6), 511-519.

Wang, Z. L., Dafalias, Y. F., and Shen, C. K. (1990). "Bounding surface hypoplasticity model for sand." *ASCE, Journal of Engineering Mechanics*, **116**(5), 983-1001.

Wong, R. K. S., and Arthur, J. R. F. (1985). "Induced and inherent anisotropy in sand." *Geotechnique*, **35**(4), 471-481.

Wong, R. K. S., and Arthur, J. R. F. (1986). "Sand sheared by stresses with cylic variations in direction." *Geotechnique*, **36**(2), 215-226.

Wotherspoon, L., Bradshaw, A., Green, R., Wood, C., Palermo, A., Cubrinovski, M., and Bradley, B. (2011). "Performance of bridges during the 2010 Darfield and 2011 Christchurch earthquakes." *Seismological Research Letters*, **82**(6).

Yang, Z., and Elgamal, A. (2008). "Multi-surface cyclic plasticity sand model with Lode angle effect." *Geotech Geol Eng*, **26**, 335-348.

Yang, Z., Elgamal, A., and Parra, E. (2003). "Computational model for cyclic mobility and associated shear deformation." *Journal of Geotechnical and Geoenvironmental Engineering, ASCE*, **129**(12), 1119-1127.

Yao, Y. P., Sun, D. A., and Luo, T. (2004). "A critical state model for sands dependent on stress and density." *International Journal for Numerical and Analytical Methods in Geomechanics*, **28**, 323-337.

Yoshimine, M., Ishihara, K., and Williams, V. (1998). "Effects of prinicpal stress direction and intermediate principal stress on undrained shear behaviour of sand." *Soils and Foundations, Japanese Geotechnical Society*, **38**(3), 179-188.

References

Zhang, J. M., and Wang, G. (2012). "Large post-liquefaction deformation of sand, part I: physical mechanism, constitutive description and numerical algorithm." *Acta Geotechnica*, **7**, 69-113.

Zlatovic, S., and Kenji, I. (1997). "Normalized behavior of very loose non-plastic soils: effects of fabric." *Japanese Geotechnical Society, Soils and Foundations*, **37**(4), 47-56.

9.0 Appendix

9.1 FORTRAN listing

The appendix contains listing of a FORTRAN program of the three dimensional model developed for strain controlled stress integration using the explicit technique. The FORTRAN program contains seven modules. These are as follows.

- Module 1: contains the interface of the subroutine SDM3D which can be invoked from host program such as C++ in case of OPENSEES;
- Module 2 'MODULE KIND_DBL_3D': contains the definitions of double precision for machine portability, global constants and error tolerances;
- Module 3 'MODULE TENSOR_HANDLE_3D': contains library functions, including definitions for overloaded operators for tensor operation;
- Module 4 'MODULE GLOBAL_DATA_3D_E': contains definitions of global variables, several subroutines and functions to communicate with the global variables and the local variables passed on as the arguments of the SDM3D subroutine;
- Module 5 'MODULE ALL_INTERFACES_3D_E': contains the main stress integration block;
- Module 6 'MODULE PLASTIC_FLOW_3D_E': contains the subroutine to calculate the plastic strain increment using the conventional inverse incremental form;
- Module 7 'MODULE_HARDENING_RULE_3D_E': contains the subroutine to implement the anisotropic hardening rule.

9.2 OPENSEES Classes

The class structure is shown in Figure 8.1. The C++ listing for the concrete derived class: 'StressDilatancyModel' and its three dimensional subclass 'StressDilatancyModel3D' are also given in the Appendix. The full TCL command with the optional arguments is available in 'StressDilatancyModel'.

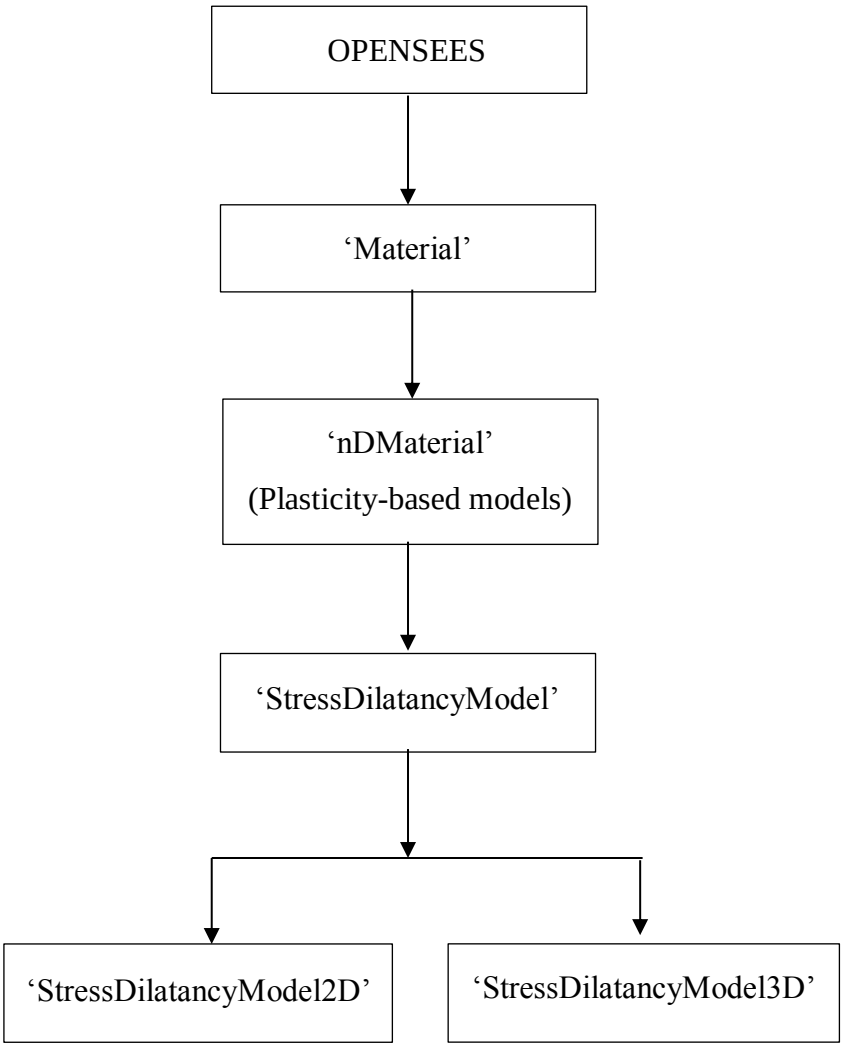

Figure 9.1 Class structure for implementation of the stress-strain-dilatancy model in OPENSEES

9.2.1 TCL command

The TCL commands are given as follows, where the keywords or the commands are italicised.

- To instantiate the class 'StressDilatancyModel' (this command should be read in conjunction with Table 4.1):

  'nDMaterial StressDilatancyModel $matTag $density $elasticShearModulus $voidRatio $constA $exponentM $poissonRatio $b1 $a1 $b2 $a2 $b3 $a3 $muMono $muCyclic $scStrain $muMax $sslP1 … $sslP10 $hslP1 …

$hslP10 $refP1 … $refP10 <$aniStress1 … $aniStress6>'; where $constA is A; $exponentM is m; $a1, $b1 are a_n, b_n for η_{max}; $a2, $b2 are a_n, b_n for $G_{N,max}$; $a3, $b3 are a_n, b_n for $G_{N,min}$; $muMono is μ_0; $muCyclic is the same as μ_0 for cyclic behaviour, usually zero; $scStrain is S_c; $muMax is M; $sslP1 … $sslP10 are the void ratios for the steady state line corresponding to the reference pressures, $refP1 … $refP10; $hslP1 … $hslP10 are the void ratio of the isotropic consolidation line for the same set of reference pressures; $aniStress1 … $aniStress6 are the optional arguments for the initial deviatoric back-stress tensor a_{ij}.

- To invoke the FORTRAN subroutine:

'*updateMaterialStage -material* $matTag *-stage 1*'

Appendix

FORTRAN LISTING OF THE THREE DIMENIONAL MODEL FOR STRESS INTEGRATION

```
!  -------------------------------------------------
!  THIS SUBROUTINE IS CALLED FROM C++
!  -------------------------------------------------

SUBROUTINE SDM3D (STRESS_CURRENT, &
                  STRAIN_CURRENT, &
                  STRAIN_NEXT,    &
                  MODEL_PARAMETER,&
                  SSL_VOID_RATIO, &
                  SSL_PRESSURE,   &
                  HSL_VOID_RATIO, &
                  HSL_PRESSURE,   &
                  HARDENING_PARAMETER_REAL, &
                  HARDENING_PARAMETER_INT, &
                  ANISOTROPY, &
                  TANGENT)

    USE KIND_DBL_3D_E
    USE ALL_INTERFACES_3D_E
    IMPLICIT NONE

   !DEC$ ATTRIBUTES DLLEXPORT::SDM3D

    REAL(KIND=DBL),DIMENSION(6),INTENT(INOUT)::STRESS_CURRENT
    REAL(KIND=DBL),DIMENSION(6),INTENT(IN)::STRAIN_NEXT
    REAL(KIND=DBL),DIMENSION(6),INTENT(INOUT)::STRAIN_CURRENT
    REAL(KIND=DBL),DIMENSION(15),INTENT(INOUT)::MODEL_PARAMETER
    REAL(KIND=DBL),DIMENSION(10),INTENT(IN)::SSL_VOID_RATIO
    REAL(KIND=DBL),DIMENSION(10),INTENT(IN)::SSL_PRESSURE
    REAL(KIND=DBL),DIMENSION(10),INTENT(IN)::HSL_VOID_RATIO
    REAL(KIND=DBL),DIMENSION(10),INTENT(IN)::HSL_PRESSURE
    REAL(KIND=DBL),DIMENSION(13*NSURFACE+3),INTENT(INOUT)::HARDENING_PARAMETER_REAL
    INTEGER,DIMENSION(2),INTENT(INOUT)::HARDENING_PARAMETER_INT
    REAL(KIND=DBL),DIMENSION(6),INTENT(IN)::ANISOTROPY
    REAL(KIND=DBL),DIMENSION(6,6),INTENT(INOUT)::TANGENT

    CALL MODEL_3D(STRESS_CURRENT, &
                  STRAIN_CURRENT, &
                  STRAIN_NEXT,    &
                  MODEL_PARAMETER,&
                  SSL_VOID_RATIO, &
                  SSL_PRESSURE,   &
                  HSL_VOID_RATIO, &
                  HSL_PRESSURE,   &
                  HARDENING_PARAMETER_REAL, &
                  HARDENING_PARAMETER_INT, &
                  ANISOTROPY,   &
                  TANGENT)

END SUBROUTINE SDM3D
```

```
!----------------------------
! EXPLANATION OF THE MODULE
!----------------------------

! THIS MODULE CONTAINS DEFINITION OF DOUBLE PRECISION FOR REALS
! AND INITIALISATION OF CONSTANTS

MODULE KIND_DBL_3D_E

INTEGER,PARAMETER::DBL=SELECTED_REAL_KIND(15,307)
INTEGER,PARAMETER::SIZE_PROB=3                                    ! SIZE OF PROBLEM:
2D OR 3D
INTEGER,PARAMETER::NSURFACE=35                                    ! NUMBER OF SURFACES
INTEGER,PARAMETER::NDIVISION=100                                  ! NUMBER OF
DIVISIONS FOR OPTIMISATION
REAL(KIND=DBL),PARAMETER::PREF=1.0D0,PMIN=1D0,PATM=98.1D0       ! IN KPA
REAL(KIND=DBL),PARAMETER::TOLERANCE=TINY(1D0)                     ! IN DLL VERSION

END MODULE KIND_DBL_3D_E
```

```
!----------------------------
! EXPLANATION OF THE MODULE
!----------------------------
! IT IS THE MODULE FOR TENSOR MANIPULATION
! IT IS APPLICABLE FOR TENSORS OF MAXIMUM SIZE 3 AND OF RANK 2 (STRESS/STRAIN)
! THE DERIVED TYPE TENSOR OF RANK 2 IS ASSIGNED FROM THE CALLING PROCEDURE
! BY MATRIX OF DIMENSION (2,2) OR (3,3) AS APPROPRIATE
! IT IS ALSO APPLICABLE FOR TENSORS OF MAXIMUM SIZE 3 AND OF RANK 3 (CONSTITUTIVE)
! THE DERIVED TYPE TENSOR OF RANK 4 IS CREATED BY THE RESPECTIVE FUNCTION FROM
! THE CALLING PROCEDURE BY SHEAR MODULUS AND POISSON'S RATIO
! IT ONLY HAS A FUNCTION FOR MULTIPLYING A RANK 4 TENSOR WITH RANK 2 RESULTING IN
! RANK 2 TENSOR. ANY OTHER PROCEDURE IS NOT REQD.
!-------------------
! MODULE PROCEDURES
!-------------------
! OPERATION(+)       - ELEMENT BY ELEMENT SIMPLE SUM
! OPERATION(-)       - IS ELEMENT BY ELEMENT SIMPLE MINUS
! OPERATION(*)       - IS MULTIPLICATION BY A SCALAR
! OPERATION(.DDOT.) - TENSOR CONTRACTION (DDOT MEANS DOUBLE DOT PRODUCT)
! TENSORMULTIPLY     - GENERIC NAME FOR TWO TYPES OF MULTIPLICATION RULES
! CREATETENSOR       - CREATES A TENSOR FROM A MATRIX (FUNCTION)
! GETTENSOR          - RETRIEVES COMPONENTS OF A GIVEN TENSOR (SUBROUTINE)
! NORMALISE          - NORMALISES A TENSOR SO THAT AFTER NORMALISATION IT BECOMES
EQUIVALENT TO A UNIT VECTOR (FUNCTION)
! FIRSTINVARIANT     - COMPUTES I1 (FUNCTION)
! HYDROSTATIC        - COMPUTES HYDROSTATIC COMPONENT (FUNCTION)
! DEVIATORIC         - COMPUTES DEVIATORIC COMPONENT (FUNCTION)
! SECINVDEV          - COMPUTES DIRECTLY THE J2 (FUNCTION)
! TENSORMULTIPLY222 - MULTIPLICATION OF TWO TENSORS OF RANK 2 RESULTING IN A TENSOR
OF RANK 2 (FUNCTION)
! CONSTITUTIVETENSOR- CREATE A RANK 4 CONSTITUTIVE TENSOR FOR GIVEN SHEAR MODULUS
AND POISSON'S RATIO
! TENSORMULTIPLY422 - MULTIPLICATION OF TWO TENSORS OF RANK 4 AND 2 RESULTING IN A
TENSOR OF RANK 2 (FUNCTION)
! NORM               - DOUBLE NORM OF A TENSOR, GIVES THE LENGTH (FUNCTION)


MODULE TENSOR_HANDLE_3D_E

    USE KIND_DBL_3D_E

    IMPLICIT NONE

    INTEGER,PARAMETER::MAXSIZE=3

    TYPE,PUBLIC::TENSOR_2R
        PRIVATE
        INTEGER::TSIZE
        REAL(KIND=DBL),DIMENSION(MAXSIZE,MAXSIZE)::COMPONENT
    END TYPE TENSOR_2R

    TYPE,PUBLIC::TENSOR_4R
        INTEGER::TSIZE
        REAL(KIND=DBL),DIMENSION(MAXSIZE,MAXSIZE,MAXSIZE,MAXSIZE)::COMPONENT
    END TYPE TENSOR_4R

    INTERFACE OPERATOR (+)
```

```
    MODULE PROCEDURE TSUM
END INTERFACE

INTERFACE OPERATOR (-)
    MODULE PROCEDURE SUBTRACT
END INTERFACE

INTERFACE OPERATOR (.DDOT.)
    MODULE PROCEDURE CONTRACT
END INTERFACE

INTERFACE OPERATOR (*)
    MODULE PROCEDURE MULTIPLY_DOUBLE_REAL, MULTIPLY_SINGLE_REAL

END INTERFACE

INTERFACE TENSORMULTIPLY
    MODULE PROCEDURE TENSORMULTIPLY222, TENSORMULTIPLY422
END INTERFACE

CONTAINS

TYPE(TENSOR_2R) FUNCTION TSUM (DATA1, DATA2)
    TYPE(TENSOR_2R),INTENT(IN)::DATA1,DATA2
    IF (DATA1%TSIZE.NE.DATA2%TSIZE)THEN
        WRITE(*,*)'STRESS DILATANCY MODEL::TENSOR_HANDLE::SUM, TENSORS ARE OF
        DIFFERENT SIZES'
        STOP
    ELSE
        TSUM%TSIZE=DATA1%TSIZE
        TSUM%COMPONENT = DATA1%COMPONENT+DATA2%COMPONENT
    END IF
END FUNCTION TSUM

TYPE (TENSOR_2R) FUNCTION SUBTRACT (DATA1, DATA2)
    TYPE(TENSOR_2R),INTENT(IN)::DATA1,DATA2
    IF (DATA1%TSIZE.NE.DATA2%TSIZE) THEN
        WRITE(*,*)'STRESS DILATANCY MODEL::TENSOR_HANDLE::SUBTRACT, TENSORS ARE
        OF DIFFERENT SIZES'
        STOP
    ELSE
        SUBTRACT%TSIZE=DATA1%TSIZE
        SUBTRACT%COMPONENT=DATA1%COMPONENT-DATA2%COMPONENT
    END IF
END FUNCTION SUBTRACT

REAL (KIND=DBL) FUNCTION CONTRACT(DATA1,DATA2)
    TYPE(TENSOR_2R),INTENT(IN)::DATA1,DATA2
    IF (DATA1%TSIZE.NE.DATA2%TSIZE)THEN
        WRITE(*,*)'STRESS DILATANCY MODEL::TENSOR_HANDLE::CONTRACT, TENSORS ARE
        OF DIFFERENT SIZE'
        STOP
    ELSE
        CONTRACT = SUM(DATA1%COMPONENT*DATA2%COMPONENT)
    END  IF
END FUNCTION CONTRACT
```

```
    TYPE (TENSOR_2R) FUNCTION MULTIPLY_DOUBLE_REAL (DATA1, DATA2)
        REAL(KIND=DBL),INTENT(IN)::DATA1
        TYPE(TENSOR_2R),INTENT(IN)::DATA2
        MULTIPLY_DOUBLE_REAL%TSIZE=DATA2%TSIZE
        MULTIPLY_DOUBLE_REAL%COMPONENT=DATA1*DATA2%COMPONENT
    END FUNCTION MULTIPLY_DOUBLE_REAL

    TYPE (TENSOR_2R) FUNCTION MULTIPLY_SINGLE_REAL (DATA1, DATA2)
        REAL,INTENT(IN)::DATA1
        TYPE(TENSOR_2R),INTENT(IN)::DATA2
        MULTIPLY_SINGLE_REAL%TSIZE=DATA2%TSIZE
        MULTIPLY_SINGLE_REAL%COMPONENT=DATA1*DATA2%COMPONENT
    END FUNCTION MULTIPLY_SINGLE_REAL

    TYPE (TENSOR_2R) FUNCTION CREATETENSOR (TENSORDATA,DSIZE)
        INTEGER,INTENT(IN)::DSIZE
        REAL(KIND=DBL),DIMENSION(DSIZE,DSIZE),INTENT(IN)::TENSORDATA
        IF (DSIZE.GT.MAXSIZE) THEN
            WRITE(*,*)'STRESS DILATANCY MODEL::TENSOR_HANDLE::CREATETENSOR, EXCEEDS
            MAXIMUM DIMENSIONS OF 3'
            STOP
        ELSE
            CREATETENSOR%TSIZE=DSIZE
            CREATETENSOR%COMPONENT=TENSORDATA
        END IF
    END FUNCTION CREATETENSOR

    SUBROUTINE GETTENSOR (TENSORDATA,ARRAYDATA,DSIZE)
        TYPE (TENSOR_2R),INTENT(IN)::TENSORDATA
        INTEGER,INTENT(IN)::DSIZE
        REAL(KIND=DBL),DIMENSION(DSIZE,DSIZE),INTENT(OUT)::ARRAYDATA
        ARRAYDATA=TENSORDATA%COMPONENT
    END SUBROUTINE GETTENSOR

    TYPE (TENSOR_2R) FUNCTION NORMALISE(TENSORDATA)
        TYPE(TENSOR_2R),INTENT(IN)::TENSORDATA
        REAL(KIND=DBL)::NORM
        NORM=CONTRACT(TENSORDATA,TENSORDATA)**0.5D0
        NORMALISE=1D0/NORM*TENSORDATA
    END FUNCTION NORMALISE

    REAL(KIND=DBL) FUNCTION FIRSTINVARIANT (TENSORDATA)
        TYPE(TENSOR_2R),INTENT(IN)::TENSORDATA
        INTEGER::I
        FIRSTINVARIANT=0D0
        DO I=1,TENSORDATA%TSIZE
          FIRSTINVARIANT=TENSORDATA%COMPONENT(I,I)+FIRSTINVARIANT
        END DO
    END FUNCTION FIRSTINVARIANT

    TYPE (TENSOR_2R) FUNCTION HYDROSTATIC (TENSORDATA)
        TYPE(TENSOR_2R),INTENT(IN):: TENSORDATA
        INTEGER::I
        REAL(KIND=DBL)::INV1
        INV1=FIRSTINVARIANT(TENSORDATA)/REAL(TENSORDATA%TSIZE)
        HYDROSTATIC%TSIZE=TENSORDATA%TSIZE
        HYDROSTATIC%COMPONENT=0D0
```

```
      DO I=1,HYDROSTATIC%TSIZE
          HYDROSTATIC%COMPONENT(I,I)= INV1
      END DO
  END FUNCTION HYDROSTATIC

  TYPE (TENSOR_2R) FUNCTION DEVIATORIC (TENSORDATA)
      TYPE(TENSOR_2R),INTENT(IN):: TENSORDATA
      INTEGER::I
      REAL(KIND=DBL)::INV1
      INV1=FIRSTINVARIANT(TENSORDATA)/REAL(TENSORDATA%TSIZE,KIND=DBL)
      DEVIATORIC%TSIZE=TENSORDATA%TSIZE
      DEVIATORIC%COMPONENT=TENSORDATA%COMPONENT
      DO I=1,DEVIATORIC%TSIZE
        DEVIATORIC%COMPONENT(I,I)=DEVIATORIC%COMPONENT(I,I)-INV1
      END DO
  END FUNCTION DEVIATORIC

  REAL(KIND=DBL) FUNCTION SECINVDEV (TENSORDATA)
      TYPE (TENSOR_2R), INTENT(IN):: TENSORDATA
      SECINVDEV=((DEVIATORIC(TENSORDATA).DDOT.DEVIATORIC (TENSORDATA))/2D0)**0.5D0
  END FUNCTION SECINVDEV

  TYPE (TENSOR_2R) FUNCTION TENSORMULTIPLY222 (DATA1,DATA2,DUMMY1,DUMMY2)
      TYPE (TENSOR_2R),INTENT(IN)::DATA1,DATA2
      ! DUMMY1 IS DUMMY INDEX OF THE TENSOR DATA1
      ! DUMMY2 IS DUMMY INDEX OF THE TENSOR DATA2
      INTEGER,INTENT(IN)::DUMMY1,DUMMY2
      INTEGER::I,J,K
      IF (DATA1%TSIZE.NE.DATA2%TSIZE) THEN
          WRITE(*,*)'STRESS DILATANCY MODEL::TENSOR_HANDLE::TENSORMULTIPLY222,
          TENSORS ARE OF DIFFERENT SIZES'
          STOP
      END IF
      TENSORMULTIPLY222%TSIZE=DATA1%TSIZE
      !FORALL(I=1:DATA1%TSIZE,J=1:DATA1%TSIZE) TENSORMULTIPLY222%COMPONENT(I,J)=0D0
      TENSORMULTIPLY222%COMPONENT=0D0
      SELECT CASE (DUMMY1)
        CASE(1)
          IF (DUMMY2.EQ.1) THEN
                DO I=1,DATA1%TSIZE
                DO J=1,DATA1%TSIZE
                DO K=1,DATA1%TSIZE
                !FORALL(I=1:DATA1%TSIZE,J=1:DATA1%TSIZE,K=1:DATA1%TSIZE) &
                TENSORMULTIPLY222%COMPONENT(I,J)=DATA1%COMPONENT(K,I)*DATA2%COMPON
                ENT(K,J) + &
                & TENSORMULTIPLY222%COMPONENT(I,J)
                END DO
                END DO
                END DO
          ELSE
                DO I=1,DATA1%TSIZE
                DO J=1,DATA1%TSIZE
                DO K=1,DATA1%TSIZE
                !FORALL(I=1:DATA1%TSIZE,J=1:DATA1%TSIZE,K=1:DATA1%TSIZE) &
                TENSORMULTIPLY222%COMPONENT(I,J)=DATA1%COMPONENT(K,I)*DATA2%COMPON
                ENT(J,K) + &
                & TENSORMULTIPLY222%COMPONENT(I,J)
```

```
                END DO
                END DO
                END DO
            END IF
          CASE(2)
            IF (DUMMY2.EQ.1) THEN
                DO I=1,DATA1%TSIZE
                DO J=1,DATA1%TSIZE
                DO K=1,DATA1%TSIZE
                !FORALL(I=1:DATA1%TSIZE,J=1:DATA1%TSIZE,K=1:DATA1%TSIZE) &
                TENSORMULTIPLY222%COMPONENT(I,J)=DATA1%COMPONENT(I,K)*DATA2%COMPON
                ENT(K,J) + &
                & TENSORMULTIPLY222%COMPONENT(I,J)
                END DO
                END DO
                END DO
            ELSE
                DO I=1,DATA1%TSIZE
                DO J=1,DATA1%TSIZE
                DO K=1,DATA1%TSIZE
                !FORALL(I=1:DATA1%TSIZE,J=1:DATA1%TSIZE,K=1:DATA1%TSIZE) &
                TENSORMULTIPLY222%COMPONENT(I,J)=DATA1%COMPONENT(I,K)*DATA2%COMPON
                ENT(J,K) + &
                & TENSORMULTIPLY222%COMPONENT(I,J)
                END DO
                END DO
                END DO
            END IF
        END SELECT
    END FUNCTION TENSORMULTIPLY222

    TYPE(TENSOR_4R) FUNCTION CONSTITUTIVETENSOR (SHEAR_MODULUS, MU, DSIZE)
        REAL(KIND=DBL),INTENT(IN)::SHEAR_MODULUS, MU
        INTEGER,INTENT(IN):: DSIZE
        REAL(KIND=DBL),DIMENSION(DSIZE,DSIZE)::KDELTA !KRONECKER'S DELTA
        INTEGER::I,J,K,L
        KDELTA=0D0
        FORALL(I=1:DSIZE,J=1:DSIZE,I==J) KDELTA(I,J)=1D0
        CONSTITUTIVETENSOR%TSIZE=DSIZE
        CONSTITUTIVETENSOR%COMPONENT=0D0
        DO I=1,DSIZE
        DO J=1,DSIZE
        DO K=1,DSIZE
        DO L=1,DSIZE
        !FORALL(I=1:DSIZE,J=1:DSIZE,K=1:DSIZE,L=1:DSIZE) &
        CONSTITUTIVETENSOR%COMPONENT(I,J,K,L)=2D0*SHEAR_MODULUS*MU/(1-2D0*MU)
        *KDELTA(I,J)*KDELTA(K,L)+&
        & SHEAR_MODULUS*(KDELTA(I,K)*KDELTA(J,L)+KDELTA(I,L)*KDELTA(J,K))
        END DO
        END DO
        END DO
        END DO
    END FUNCTION CONSTITUTIVETENSOR

    TYPE(TENSOR_2R) FUNCTION TENSORMULTIPLY422(DATA1,DATA2)
        TYPE(TENSOR_4R),INTENT(IN)::DATA1
        TYPE(TENSOR_2R),INTENT(IN)::DATA2
```

```
      INTEGER::I,J,K,L
      IF(DATA1%TSIZE.NE.DATA2%TSIZE) THEN
        WRITE(*,*)'STRESS DILATANCY MODEL::TENSOR_HANDLE::TENSORMULTIPLY422,
        TENSORS ARE OF DIFFERENT SIZE'
        STOP
      END IF
      TENSORMULTIPLY422%TSIZE=DATA1%TSIZE
      TENSORMULTIPLY422%COMPONENT=0D0
      DO I=1,DATA1%TSIZE
      DO J=1,DATA1%TSIZE
      DO K=1,DATA1%TSIZE
      DO L=1,DATA1%TSIZE
      !FORALL(I=1:DATA1%TSIZE,J=1:DATA1%TSIZE,K=1:DATA1%TSIZE,L=1:DATA1%TSIZE) &
      TENSORMULTIPLY422%COMPONENT(I,J)=TENSORMULTIPLY422%COMPONENT(I,J)+DAT
      A1%COMPONENT(I,J,K,L)*DATA2%COMPONENT(K,L)
      END DO
      END DO
      END DO
      END DO
    END FUNCTION TENSORMULTIPLY422

    REAL(KIND=DBL) FUNCTION NORM (TENSORDATA)
      TYPE (TENSOR_2R),INTENT(IN)::TENSORDATA
      NORM = (TENSORDATA.DDOT.TENSORDATA)**0.5D0
    END FUNCTION NORM

END MODULE TENSOR_HANDLE_3D_E
```

```
!---------------------------
! EXPLANATION OF THE MODULE
!---------------------------
! THIS MODULE CONTAINS INTERFACES FOR ALL EXTERNAL SUBROUTINES AND FUNCTIONS
! THIS MODULE IS MEANT FOR FUTURE EXPANSION AS AN EMPTY SLOT. ANY NEW SUBROUTINES
! OR FUNCTIONS OF GENERAL PURPOSE SHOULD BE WRITTEN HERE

MODULE ALL_INTERFACES_3D_E

    USE KIND_DBL_3D_E
    USE TENSOR_HANDLE_3D_E
    USE GLOBAL_DATA_3D_E
    USE PLASTIC_FLOW_3D_E
    USE HARDENING_RULE_3D_E

    IMPLICIT NONE


        ! EXPLANATION OF THE VARIABLES:

        ! STRESS_CURRENT        :   ARRAY OF 6/3 DIMENSIONS TO STORE CURRENT VALUES
        OF CURRENT STRESS
        ! STRAIN_CURRENT        :   ARRAY OF 6/3 DIMENSIONS TO STORE CURRENT VALUES
        OF CURRENT STRAIN
        ! STRAIN_NEXT           :   ARRAY OF 6/3 DIMENSIONS TO STORE CURRENT VALUES
        OF NEXT STRAIN

        ! MODEL_PARAMETERS AS PER: CUBRINOVSKI AND ISHIHARA (1998)

        ! MODEL_PARAMETER(1)    :   VOID_RATIO
        ! MODEL_PARAMETER(2)    :   SHEAR_CONST_A
        ! MODEL_PARAMETER(3)    :   SHEAR_CONST_N
        ! MODEL_PARAMETER(4)    :   POISSON
        ! MODEL_PARAMETER(5)    :   ETAMAX_CONST_A1
        ! MODEL_PARAMETER(6)    :   ETAMAX_CONST_B1
        ! MODEL_PARAMETER(7)    :   GNMAX_CONST_A2
        ! MODEL_PARAMETER(8)    :   GNMAX_CONST_B2
        ! MODEL_PARAMETER(9)    :   GNMIN_CONST_A3
        ! MODEL_PARAMETER(10)   :   GNMIN_CONST_B3
        ! MODEL_PARAMETER(11)   :   DEGRADATION
        ! MODEL_PARAMETER(12)   :   DILATANCY_COEFF_MU_MONO
        ! MODEL_PARAMETER(13)   :   DILATANCY_COEFF_MU_CYCLIC
        ! MODEL_PARAMETER(14)   :   DILATANCY_STRAIN_SC
        ! MODEL_PARAMETER(15)   :   CRITICAL_STRESS_RATIO_M

        ! SSL_VOID_RATIO(10)    :   STEADY STATE LINE DATA - VOID RATIO VERSUS
        EFFECTIVE PRESSURE
        ! SSL_PRESSURE(10)

        ! HSL_VOID_RATIO(10)    :   HYDROSTATIC LINE DATA - VOID RATIO VERSUS
        EFFECTIVE PRESSURE
        ! HSL_PRESSURE(10)

        ! HARDENING_PARAMETER_INT(1): SURFACE
        ! HARDENING_PARAMETER_INT(2): KEY

        ! HARDENING_PARAMETER_REAL(1:6*NSURFACE)                    : CENTRE
```

```
        ! HARDENING_PARAMETER_REAL(6*NSURFACE+1:12*NSURFACE)         :
        REVERSAL_ORDINATE
        ! HARDENING_PARAMETER_REAL(12*NSURFACE+1:13*NSURFACE)        : PLASTIC_STRAIN
        ! HARDENING_PARAMETER_REAL(13*NSURFACE+1)                    : MAX_STRAIN
        ! HARDENING_PARAMETER_REAL(13*NSURFACE+2)                    : GEFFECTIVE
        ! HARDENING_PARAMETER_REAL(13*NSURFACE+3)                    : INITIAL_STRAIN

    CONTAINS

    SUBROUTINE MODEL_3D (STRESS_CURRENT, STRAIN_CURRENT, STRAIN_NEXT, MODE
    L_PARAMETER, SSL_VOID_RATIO, &
    & SSL_PRESSURE, HSL_VOID_RATIO, HSL_PRESSURE, HARDENING_PARAMETER_REAL,
    HARDENING_PARAMETER_INT, ANISOTROPY,TANGENT)

    REAL(KIND=DBL),DIMENSION(6),INTENT(IN)::STRAIN_NEXT
    REAL(KIND=DBL),DIMENSION(10),INTENT(IN)::SSL_VOID_RATIO, SSL_PRESSURE
    REAL(KIND=DBL),DIMENSION(10),INTENT(IN)::HSL_VOID_RATIO, HSL_PRESSURE
    REAL(KIND=DBL),DIMENSION(6),INTENT(INOUT)::STRAIN_CURRENT
    REAL(KIND=DBL),DIMENSION(6),INTENT(INOUT)::STRESS_CURRENT
    REAL(KIND=DBL),DIMENSION(15),INTENT(INOUT)::MODEL_PARAMETER
    REAL(KIND=DBL),DIMENSION(13*NSURFACE+3),INTENT(INOUT)::HARDENING_PARAMETER_REAL
    INTEGER,DIMENSION(2),INTENT(INOUT)::HARDENING_PARAMETER_INT
    REAL(KIND=DBL),DIMENSION(6),INTENT(IN)::ANISOTROPY
    REAL(KIND=DBL),DIMENSION(6,6),INTENT(INOUT)::TANGENT
    REAL(KIND=DBL)::PRESSURE,CURRENT_STRAIN,CURRENT_RADIUS,CURRENT_MU0,GN,
    K1_HP,K2_MU,TEMP(3,3)
    TYPE(TENSOR_2R)::SIJ, SIJ_NEXT, DEPSILON, FIJ, NIJ, XIJ_CP
    LOGICAL::ERROR

    !OPEN(UNIT=100,FILE='DEBUG.TXT',STATUS='REPLACE',ACTION='WRITE',POSITION='APPEND')


    !*********************************************************************
    **********
    ! ASSIGN TO GLOBAL VARIABLES

    !*********************************************************************
    **********

    CALL RECEIVEDATA(DATAIN=STRESS_CURRENT,DSIZE=6,CHOICE=1)
    CALL RECEIVEDATA(DATAIN=STRAIN_CURRENT,DSIZE=6,CHOICE=2)
    CALL RECEIVEDATA(DATAIN=STRAIN_NEXT,DSIZE=6,CHOICE=3)
    CALL RECEIVEDATA(DATAIN=MODEL_PARAMETER,DSIZE=15,CHOICE=4)
    CALL RECEIVEDATA(DATAIN=SSL_VOID_RATIO,DSIZE=10,CHOICE=5)
    CALL RECEIVEDATA(DATAIN=SSL_PRESSURE,DSIZE=10,CHOICE=6)
    CALL RECEIVEDATA(DATAIN=HSL_VOID_RATIO,DSIZE=10,CHOICE=7)
    CALL RECEIVEDATA(DATAIN=HSL_PRESSURE,DSIZE=10,CHOICE=8)
    CALL RECEIVEDATA(DATAIN=HARDENING_PARAMETER_REAL,DSIZE=13*NSURFACE+3,CHOICE=9)
    CALL RECEIVEDATA(DATAIN=ANISOTROPY,DSIZE=6,CHOICE=10)
    CALL RECEIVEDATA(DATAIN=HARDENING_PARAMETER_INT,DSIZE=2)
    CALL RECEIVEDATA(DATAIN=TANGENT,DSIZE=6)


    !*********************************************************************
    ***********
    ! NEGATIVE EFFECTIVE PRESSURE - ABORT
```

```
!*******************************************************************************
************

PRESSURE=FIRSTINVARIANT(STRESS_TENSOR_CURRENT)
IF(PRESSURE.LE.TOLERANCE) THEN
    ! DLL VERSION
    TEMP=0D0
    STRESS_TENSOR_NEXT = CREATETENSOR(TEMP,SIZE_PROB)
    ELPL_TANGENT_NEXT = 0D0
    WRITE(*,*)'STRESS DILATANCY MODEL::ALL INTERFACES, NEGATIVE HYDROSTATIC
    PRESSURE'
    CALL UPDATE_PARAMETERS()
    RETURN
END IF


!*******************************************************************************
************
! NO CHANGE IN STRAIN - RETURN

!*******************************************************************************
************

DEPSILON=STRAIN_TENSOR_NEXT-STRAIN_TENSOR_CURRENT
IF (NORM(DEPSILON).LE.TOLERANCE) RETURN


!*******************************************************************************
**************
! CALCULATE GE, GNMAX, GNMIN, ETAMAX AND RANK 4 CONSTITUTIVE TENSOR

!*******************************************************************************
**************

CALL CALCULATE_ELASTIC_SHEAR_MODULUS()
CALL CALCULATE_GNMAX()
CALL CALCULATE_GNMIN()
CALL CALCULATE_ETAMAX()
CALL CALCULATE_RADIUS()
CALL SETINITIALTANGENT()
CONSTITUTIVE_TENSOR=CONSTITUTIVETENSOR(ELASTIC_SHEAR_MODULUS,POISSON,SIZE_PROB)


!*******************************************************************************
**************
! CHECK IF THE STRAIN INCREMENT IS HYDROSTATIC IN NATURE

!*******************************************************************************
**************

DEPSILON = STRAIN_TENSOR_NEXT-STRAIN_TENSOR_CURRENT
IF(NORM(DEVIATORIC(DEPSILON)).LE.TOLERANCE) THEN
    STRESS_TENSOR_NEXT=STRAIN_TENSOR_CURRENT+TENSORMULTIPLY(CONSTITUTIVE_TENSOR,
    DEPSILON)
    CALL UPDATE_PARAMETERS()
    RETURN
END IF
```

```
!*******************************************************************************
**************
! PROJECT EXISTING STRESS TO A REFERENCE PLANE

!*******************************************************************************
**************

SIJ=DEVIATORIC(STRESS_TENSOR_CURRENT)
SIJ=PREF/HYDROSTATIC_PRESSURE*SIJ


!*******************************************************************************
*************
! INITIALISE PLASTIC MODULUS, DILATANCY & YIELD SURFACE AT THE START OF LOADING
WHEN KEY = 0

!*******************************************************************************
*************

IF (KEY.EQ.0) THEN

    SURFACE           = 1

    REVERSAL(SURFACE) = SIJ

    ! GET ANISOTROPIC STRAIN FROM THE BACKBONE CURVE

    INITIAL_STRAIN = CALCULATE_EQV_STRAIN(SECINVDEV(SIJ))

    ! NOW ASSIGN THIS TO ALL LOADING SURFACES AS THE INITIAL STRAIN

    GAMMA(1:NSURFACE)=INITIAL_STRAIN

    ! LOCATE CENTRE OF LOADING SURFACE 1

    NIJ = NORMALISE(SIJ)
    XIJ_CP=SOLVECONJUGATE(SIJ,NIJ)
    CENTRE(SURFACE)=SIJ-(NORM(SIJ)/NORM(XIJ_CP))*(XIJ_CP-ORIGIN)

    ! CALCULATE TANGENT

    ELPL_TANGENT_CURRENT    = EL_TANGENT

END IF

 CURRENT_RADIUS = NORM(REVERSAL(SURFACE)-CENTRE(SURFACE))

 CURRENT_STRAIN = GAMMA(SURFACE)

 IF(SURFACE.EQ.1) THEN

    K1_HP = 1D0
    K2_MU = 1D0
    CURRENT_MU0 = DILATANCY_COEFF_MU_MONO
```

```
 ELSE

     K1_HP = 2D0

     IF (CURRENT_STRAIN.LE.0.001D0) THEN
         K2_MU = 2D0
     ELSEIF (CURRENT_STRAIN.GE.0.003D0) THEN
         K2_MU = 1D0
     ELSE
         K2_MU = 2D0-(CURRENT_STRAIN-0.001D0)/(0.003D0-0.001D0)*(2D0-1D0)
     END IF

     CURRENT_MU0 = DILATANCY_COEFF_MU_CYCLIC

 END IF


PRESSURE = FIRSTINVARIANT(STRESS_TENSOR_CURRENT)/REAL(SIZE_PROB,KIND=DBL)

GN=(GNMAX-GNMIN)*DEXP(-DEGRADATION*CURRENT_STRAIN/0.01D0/K1_HP)+GNMIN

PLASTIC_SHEAR_MODULUS = (GN-(GN-GNMIN)*(DEGRADATION*CURRENT_STRAIN/0
.01D0/K1_HP))* &
& (1D0-CURRENT_RADIUS/RADIUS)**2*PRESSURE

GN=(GNMAX-GNMIN)*DEXP(-DEGRADATION*INITIAL_STRAIN/0.01D0/K1_HP)+GNMIN

PLASTIC_MODULUS_REVERSAL = (GN-(GN-GNMIN)*(DEGRADATION*INITIAL_STRAI
N/0.01D0/K1_HP))*PRESSURE

DILATANCY=CURRENT_MU0+(CRITICAL_STRESS_RATIO_M-CURRENT_MU0)* &
& REAL(ATAN(CURRENT_STRAIN/DILATANCY_STRAIN_SC/K2_MU),KIND=DBL)/REAL
(ASIN(1D0),KIND=DBL)

DILATANCY_AT_REVERSAL = DILATANCY_COEFF_MU_CYCLIC+(CRITICAL_STRESS_R
ATIO_M-DILATANCY_COEFF_MU_CYCLIC)* &
& REAL(ATAN(INITIAL_STRAIN/DILATANCY_STRAIN_SC/K2_MU),KIND=DBL)/REAL
(ASIN(1D0),KIND=DBL)

CALL OPTIMISE()

 ! IN DLL VERSION

 IF(ERROR) THEN
     CALL UPDATE_PARAMETERS()
     RETURN
 ELSE
     CALL HARDENING (FIJ, SIJ, SIJ_NEXT)
     GEFFECTIVE = SECINVDEV(STRESS_TENSOR_NEXT-STRESS_TENSOR_CURRENT)/SECI
     NVDEV(DEPSILON)
     CALL UPDATE_PARAMETERS()
 END IF

 CONTAINS

 SUBROUTINE OPTIMISE ()
```

```
!DSIJ               : INCREMENTAL STRESS RATIO
!XIJE               : CONJUGATE POINT BASED ON ELASTIC RESPONSE
!XIJP               : CONJUGATE POINT BASED ON PLASTIC RESPONSE
!XIJA               : CONJUGATE POINT BASED ON ASSUMPTION
!XIJC               : SOLVED STRESS TENSOR NEXT
!SOLN_STRESS_NEXT   : CONTAINS SOLVED STRESS TENSOR NEXT
!SOLN_SIJ_NEXT      : CONTAINS SOLVED SIJ_NEXT

TYPE(TENSOR_2R)::DSIJ, XIJE, XIJP, XIJA, XIJC, SOLN_STRESS_NEXT, SOLN_SIJ_NEXT
INTEGER::I
REAL(KIND=DBL)::THETA_MIN, THETA_CURRENT, TEMP(3,3),SOLN_TANGENT(6,6)
LOGICAL::FLAG

FLAG = .FALSE.

ERROR =.FALSE.

DSIJ = NORMALISE(DEVIATORIC(DEPSILON))
XIJE = SOLVECONJUGATE(SIJ,DSIJ)-ORIGIN
XIJP = RADIUS * NORMALISE(DEVIATORIC(DEPSILON))

THETA_MIN = 2D0

DO I = 1, NDIVISION

  XIJA = REAL(I,KIND=DBL)/REAL(NDIVISION,KIND=DBL) * (XIJE-XIJP) + XIJP
  XIJA = RADIUS * NORMALISE(XIJA)
  DSIJ = NORMALISE(XIJA-SIJ)

  IF (NORM(SIJ).LE.TOLERANCE.AND.KEY.EQ.0) THEN     ! LOADING POTENTIAL:
  DEVIATORIC COMPONENT
    FIJ = NORMALISE(DEPSILON)
  ELSE
    FIJ = NORMALISE(SIJ-CENTRE(SURFACE))
  END IF

  IF ((FIJ.DDOT.DSIJ).LE.0D0) THEN
    SIJ_NEXT = CALCULATE_STRESS(GIJ=NORMALISE(XIJA), FIJ=NORMALISE(XIJA),
    SIJ=SIJ, ERROR=ERROR, OPTION =
    1)

  ELSE
    SIJ_NEXT = CALCULATE_STRESS(GIJ=NORMALISE(XIJA), FIJ=NORMALISE(XIJA),
    SIJ=SIJ, ERROR=ERROR)
  END IF

  IF(ERROR) EXIT

  DSIJ = SIJ_NEXT-SIJ

  IF(NORM(DSIJ).LE. TOLERANCE) THEN
    SOLN_SIJ_NEXT = SIJ_NEXT
    SOLN_STRESS_NEXT = STRESS_TENSOR_NEXT
    SOLN_TANGENT = ELPL_TANGENT_NEXT
    FLAG = .TRUE.
    EXIT
  END IF
```

```
            DSIJ = NORMALISE(DSIJ)
            XIJC = SOLVECONJUGATE(SIJ,DSIJ)-ORIGIN

          THETA_CURRENT = 1D0-(NORMALISE(XIJC).DDOT.NORMALISE(XIJA))

          IF(THETA_CURRENT.LT.THETA_MIN.OR.DABS(THETA_MIN).LE.TOLERANCE) THEN
            THETA_MIN = THETA_CURRENT
            SOLN_STRESS_NEXT = STRESS_TENSOR_NEXT
            SOLN_SIJ_NEXT = SIJ_NEXT
            SOLN_TANGENT = ELPL_TANGENT_NEXT
            FLAG = .TRUE.
          END IF

        END DO

        IF(FLAG) THEN
         STRESS_TENSOR_NEXT = SOLN_STRESS_NEXT
         SIJ_NEXT = SOLN_SIJ_NEXT
         ELPL_TANGENT_NEXT = SOLN_TANGENT
        ELSE
          STRESS_TENSOR_NEXT = STRESS_TENSOR_CURRENT
          ELPL_TANGENT_NEXT = ELPL_TANGENT_CURRENT
          ERROR=.TRUE.
          RETURN
        END IF

    END SUBROUTINE OPTIMISE

    SUBROUTINE UPDATE_PARAMETERS()
        CALL UPDATE_VOID_RATIO()
        STRAIN_CURRENT=STRAIN_NEXT
        CALL SENDDATA(DATAOUT=STRESS_CURRENT,DSIZE=6,CHOICE=1)
        CALL SENDDATA(DATAOUT=MODEL_PARAMETER,DSIZE=15,CHOICE=2)
        CALL SENDDATA(DATAOUT=HARDENING_PARAMETER_REAL,DSIZE=13*NSURFACE+3,CHOICE=7)
        CALL SENDDATA(DATAOUT=HARDENING_PARAMETER_INT,DSIZE=2)
        CALL SENDDATA(DATAOUT=TANGENT,DSIZE=6)
    END SUBROUTINE UPDATE_PARAMETERS

    END SUBROUTINE MODEL_3D

END MODULE ALL_INTERFACES_3D_E
```

```
!--------------------------
! EXPLANATION OF THE MODULE
!--------------------------
! THIS MODULE CONTAINS ALL THE DATA REQUIRED FOR THE MODEL DEFINITION.
! IT ASSIGNS THE DATA SEND BY THE HOSTING PROCEDURE TO THE DESIGN FORMAT,
! E.G. THE DERIVED TYPES FOR TENSORS. THE DATA SENT BY THE HOSTING PROCEDURE
! IS ASSUMED TO BE OF ARRAY FORM WITH SINGLE SUBSCRIPT. IT ALSO SENDS THE
! UPDATED DATA AFTER INVOKING THE MODEL TO THE HOSTING PROCEDURE IN THE SAME FORMAT.
!-------------------
! MODULE DATA
!-------------------
! PUBLIC    :   ALL GLOBAL DATA
! PRIVATE   :   STATE DATA
!-------------------
! MODULE PROCEDURES
!-------------------
! RECEIVEDATA                       :   ASSIGNS DATA FROM THE HOST PROCEDURE TO
MODULE PUBLIC DATA
! SENDDATA                          :   ASSIGNS DATA FROM THE MODULE PUBLIC DATA TO
THE HOST PROCEDURE
! CALCULATE_HYDROSTATIC_PRESSURE    :   CALCULATES THE HYDROSTATIC PRESSURE
! CALCULATE_ELASTIC_SHEAR_MODULUS   :   CALCULATES THE ELASTIC MODULUS
! CALCULATE_STEADY_STATE_VOID_RATIO :   CALCULATES THE STEADY STATE VOID RATIO
CORRESPONDING TO CURRENT PRESSURE
! CALCULATE_HYDROSTATIC_VOID_RATIO  :   CALCULATES THE HYDROSTATIC LINE
CORRESPONDING TO CURRENT PRESSURE
! CALCULATE_STATE_INDEX             :   CALCULATES THE STATE_INDEX
! CALCULATE_GNMAX                   :   CALCULATES THE GNMAX
! CALCULATE_GNMIN                   :   CALCULATE THE GNMIN
! CALCULATE_ETAMAX                  :   CALCULATE THE ETAMAX
! UPDATE_VOID_RATIO                 :   UPDATES THE VOID_RATIO (AT THE END OF THE
PROGRAM)
! CALCULATE_RADIUS                  :   CALCULATES RADIUS OF UNSCALED DEVIATORIC
CIRCLE
! GET_STATE_DATA                    :   RETREIVES THE PRIVATE STATE DATA

MODULE GLOBAL_DATA_3D_E

    USE KIND_DBL_3D_E

    USE TENSOR_HANDLE_3D_E

    IMPLICIT NONE

    ! STRESS AND STRAIN
    TYPE(TENSOR_2R)::STRESS_TENSOR_CURRENT, STRESS_TENSOR_NEXT, STRAIN_TEN
    SOR_CURRENT, STRAIN_TENSOR_NEXT, &
    & PLASTIC_STRAIN_INCREMENT,ORIGIN

    TYPE(TENSOR_4R)::CONSTITUTIVE_TENSOR
    REAL(KIND=DBL)::EL_TANGENT(6,6),ELPL_TANGENT_CURRENT(6,6),ELPL_TANGENT_NEXT(6,6)

    ! MODEL PARAMETERS
    REAL(KIND=DBL)::VOID_RATIO
    REAL(KIND=DBL)::SHEAR_CONST_A, SHEAR_CONST_N, POISSON
    REAL(KIND=DBL)::ETAMAX_CONST_A1, ETAMAX_CONST_B1
    REAL(KIND=DBL)::GNMAX_CONST_A2, GNMAX_CONST_B2
```

```
      REAL(KIND=DBL)::GNMIN_CONST_A3, GNMIN_CONST_B3,DEGRADATION
      REAL(KIND=DBL)::DILATANCY_COEFF_MU_MONO, DILATANCY_COEFF_MU_CYCLIC, DI
      LATANCY_STRAIN_SC, CRITICAL_STRESS_RATIO_M
      REAL(KIND=DBL)::INITIAL_STRAIN

      ! COORDINATES OF THE STEADY STATE LINE IN VOID RATIO - HYDROSTATIC PRESSURE SPACE
      REAL(KIND=DBL)::STEADY_STATE_DATA(10,2)

      ! COORDINATES OF THE HYDROSTATIC COMPRESSION LINE IN VOID RATIO-HYDROSTATIC
      PRESSURE SPACE
      REAL(KIND=DBL)::HYDROSTATIC_DATA(10,2)

      ! PARAMETERS OF THE HARDENING SURFACES
      TYPE(TENSOR_2R),DIMENSION(NSURFACE)::CENTRE,REVERSAL
      REAL(KIND=DBL)::GAMMA(NSURFACE),MAX_STRAIN,GEFFECTIVE
      INTEGER::SURFACE,KEY

      ! PLASTICITY PARAMETERS
      REAL(KIND=DBL)::HYDROSTATIC_PRESSURE, ELASTIC_SHEAR_MODULUS, GNMAX, GNMIN,
      ETAMAX, LAMDA, RADIUS, &
      & PLASTIC_SHEAR_MODULUS, PLASTIC_MODULUS_REVERSAL, DILATANCY, DILATANC
      Y_AT_REVERSAL

      ! STATE PARAMETERS
      REAL(KIND=DBL),PRIVATE::STATE_INDEX, STEADY_STATE_VOID_RATIO, HYDROSTA
      TIC_VOID_RATIO, DELTA_VOLUMETRIC_STRAIN

      INTERFACE RECEIVEDATA
          MODULE PROCEDURE RECEIVEDATA_REAL,RECEIVEDATA_INT,RECEIVEDATA_REAL_A
      END INTERFACE

      INTERFACE SENDDATA
          MODULE PROCEDURE SENDDATA_REAL,SENDDATA_INT,SENDDATA_REAL_A
      END INTERFACE

      INTERFACE SOLVECONJUGATE
          MODULE PROCEDURE SOLVECONJUGATE_TYPE1, SOLVECONJUGATE_TYPE2
      END INTERFACE

    CONTAINS

      SUBROUTINE RECEIVEDATA_REAL(DATAIN, DSIZE, CHOICE)
          INTEGER,INTENT(IN)::DSIZE,CHOICE
          REAL(KIND=DBL),DIMENSION(DSIZE),INTENT(IN)::DATAIN
          REAL(KIND=DBL),DIMENSION(MAXSIZE,MAXSIZE)::TEMP !MAXSIZE IS 2, DEFINED IN
          THE MODULE TENSOR_HANDLE
          INTEGER::I
          SELECT CASE (CHOICE)
            CASE(1)
              TEMP=0D0
              TEMP(1,1)=DATAIN(1) ! XX
              TEMP(2,2)=DATAIN(2) ! YY
              TEMP(3,3)=DATAIN(3) ! ZZ
              TEMP(1,2)=DATAIN(4) ! XY
              TEMP(2,3)=DATAIN(5) ! YZ
              TEMP(3,1)=DATAIN(6) ! ZX
              TEMP(2,1)=TEMP(1,2) ! YX=XY
```

```
      TEMP(3,2)=TEMP(2,3) ! ZY=YZ
      TEMP(1,3)=TEMP(3,1) ! XZ=ZX
      STRESS_TENSOR_CURRENT=CREATETENSOR(TEMP,SIZE_PROB) ! SIZE_PROB IS
      DEFINED IN THE MODULE KIND_DBL
    CASE(2)
      TEMP=0D0
      TEMP(1,1)=DATAIN(1)      ! XX
      TEMP(2,2)=DATAIN(2)      ! YY
      TEMP(3,3)=DATAIN(3)      ! ZZ
      TEMP(1,2)=DATAIN(4)      ! XY
      TEMP(2,3)=DATAIN(5)      ! YZ
      TEMP(3,1)=DATAIN(6)      ! ZX
      TEMP(2,1)=TEMP(1,2)      ! YX=XY
      TEMP(3,2)=TEMP(2,3)      ! ZY=YZ
      TEMP(1,3)=TEMP(3,1)      ! XZ=ZX
      STRAIN_TENSOR_CURRENT=CREATETENSOR(TEMP,SIZE_PROB) ! SIZE_PROB IS
      DEFINED IN THE MODULE KIND_DBL
    CASE(3)
      TEMP=0D0
      TEMP(1,1)=DATAIN(1)      ! XX
      TEMP(2,2)=DATAIN(2)      ! YY
      TEMP(3,3)=DATAIN(3)      ! ZZ
      TEMP(1,2)=DATAIN(4)      ! XY
      TEMP(2,3)=DATAIN(5)      ! YZ
      TEMP(3,1)=DATAIN(6)      ! ZX
      TEMP(2,1)=TEMP(1,2)      ! YX=XY
      TEMP(3,2)=TEMP(2,3)      ! ZY=YZ
      TEMP(1,3)=TEMP(3,1)      ! XZ=ZX
      STRAIN_TENSOR_NEXT=CREATETENSOR(TEMP,SIZE_PROB) ! SIZE_PROB IS DEFINED
      IN THE MODULE KIND_DBL
    CASE(4)
      VOID_RATIO               =DATAIN(1)
      SHEAR_CONST_A            =DATAIN(2)
      SHEAR_CONST_N            =DATAIN(3)
      POISSON                  =DATAIN(4)
      ETAMAX_CONST_A1          =DATAIN(5)
      ETAMAX_CONST_B1          =DATAIN(6)
      GNMAX_CONST_A2           =DATAIN(7)
      GNMAX_CONST_B2           =DATAIN(8)
      GNMIN_CONST_A3           =DATAIN(9)
      GNMIN_CONST_B3           =DATAIN(10)
      DEGRADATION              =DATAIN(11)
      DILATANCY_COEFF_MU_MONO  =DATAIN(12)
      DILATANCY_COEFF_MU_CYCLIC=DATAIN(13)
      DILATANCY_STRAIN_SC      =DATAIN(14)
      CRITICAL_STRESS_RATIO_M  =DATAIN(15)
    CASE(5)
      STEADY_STATE_DATA=0D0
      STEADY_STATE_DATA(:,2)=DATAIN    ! ASSIGNS VOID_RATIOS
    CASE(6)
      STEADY_STATE_DATA(:,1)=DATAIN    ! ASSIGNS PRESSURE
    CASE (7)
      HYDROSTATIC_DATA=0D0
      HYDROSTATIC_DATA(:,2)=DATAIN     ! ASSIGNS VOID_RATIOS
    CASE (8)
      HYDROSTATIC_DATA(:,1)=DATAIN     ! ASSIGNS PRESSURE
    CASE(9)
```

```
            DO I=1,NSURFACE
                TEMP=0D0
                TEMP(1,1)=DATAIN((I-1)*6+1)
                TEMP(2,2)=DATAIN((I-1)*6+2)
                TEMP(3,3)=DATAIN((I-1)*6+3)
                TEMP(1,2)=DATAIN((I-1)*6+4)
                TEMP(2,3)=DATAIN((I-1)*6+5)
                TEMP(3,1)=DATAIN((I-1)*6+6)
                TEMP(2,1)=TEMP(1,2)
                TEMP(3,2)=TEMP(2,3)
                TEMP(1,3)=TEMP(3,1)
                CENTRE(I)= CREATETENSOR(TEMP, SIZE_PROB)
            END DO
            DO I=1,NSURFACE
                TEMP=0D0
                TEMP(1,1)=DATAIN(6*NSURFACE+(I-1)*6+1)
                TEMP(2,2)=DATAIN(6*NSURFACE+(I-1)*6+2)
                TEMP(3,3)=DATAIN(6*NSURFACE+(I-1)*6+3)
                TEMP(1,2)=DATAIN(6*NSURFACE+(I-1)*6+4)
                TEMP(2,3)=DATAIN(6*NSURFACE+(I-1)*6+5)
                TEMP(3,1)=DATAIN(6*NSURFACE+(I-1)*6+6)
                TEMP(2,1)=TEMP(1,2)
                TEMP(2,1)=TEMP(1,2)
                TEMP(3,2)=TEMP(2,3)
                TEMP(1,3)=TEMP(3,1)
                REVERSAL(I) = CREATETENSOR(TEMP, SIZE_PROB)
            END DO
            DO I=1,NSURFACE
                GAMMA(I) = DATAIN(12*NSURFACE+I)
            END DO
            MAX_STRAIN  = DATAIN(13*NSURFACE+1)
            GEFFECTIVE  = DATAIN(13*NSURFACE+2)
            INITIAL_STRAIN = DATAIN(13*NSURFACE+3)
          CASE(10)
            TEMP=0D0
            TEMP(1,1)=DATAIN(1) ! XX
            TEMP(2,2)=DATAIN(2) ! YY
            TEMP(3,3)=DATAIN(3) ! ZZ
            TEMP(1,2)=DATAIN(4) ! XY
            TEMP(2,3)=DATAIN(5) ! YZ
            TEMP(3,1)=DATAIN(6) ! ZX
            TEMP(2,1)=TEMP(1,2) ! YX=XY
            TEMP(3,2)=TEMP(2,3) ! ZY=YZ
            TEMP(1,3)=TEMP(3,1) ! XZ=ZX
            ORIGIN=CREATETENSOR(TEMP,SIZE_PROB) ! SIZE_PROB IS DEFINED IN THE MODULE
            KIND_DBL
          END SELECT
      END SUBROUTINE RECEIVEDATA_REAL

      SUBROUTINE RECEIVEDATA_INT(DATAIN,DSIZE)
          INTEGER,INTENT(IN)::DSIZE
          INTEGER,DIMENSION(DSIZE),INTENT(IN)::DATAIN
          SURFACE = DATAIN(1)
          KEY     = DATAIN(2)
      END SUBROUTINE RECEIVEDATA_INT

     SUBROUTINE RECEIVEDATA_REAL_A(DATAIN,DSIZE)
```

```
      INTEGER,INTENT(IN)::DSIZE
      REAL(KIND=DBL),DIMENSION(DSIZE,DSIZE),INTENT(IN)::DATAIN
      ELPL_TANGENT_CURRENT=DATAIN
    END SUBROUTINE RECEIVEDATA_REAL_A

    SUBROUTINE SENDDATA_REAL (DATAOUT,DSIZE,CHOICE)
      INTEGER,INTENT(IN)::DSIZE,CHOICE
      REAL(KIND=DBL),DIMENSION(DSIZE),INTENT(OUT)::DATAOUT
      REAL(KIND=DBL),DIMENSION(MAXSIZE,MAXSIZE)::TEMP !MAXSIZE IS 3, DEFINED IN
      THE MODULE TENSOR_HANDLE
      INTEGER::I
      SELECT CASE (CHOICE)
        CASE(1)
          TEMP=0D0
          CALL GETTENSOR(STRESS_TENSOR_NEXT,TEMP,SIZE_PROB) ! SIZE_PROB IS DEFINED
          IN THE MODULE KIND_DBL
          DATAOUT(1)=TEMP(1,1) ! XX
          DATAOUT(2)=TEMP(2,2) ! YY
          DATAOUT(3)=TEMP(3,3) ! ZZ
          DATAOUT(4)=TEMP(1,2) ! XY
          DATAOUT(5)=TEMP(2,3) ! YZ
          DATAOUT(6)=TEMP(3,1) ! ZX
        CASE(2)
          DATAOUT(1)=VOID_RATIO
          DATAOUT(2)=SHEAR_CONST_A
          DATAOUT(3)=SHEAR_CONST_N
          DATAOUT(4)=POISSON
          DATAOUT(5)=ETAMAX_CONST_A1
          DATAOUT(6)=ETAMAX_CONST_B1
          DATAOUT(7)=GNMAX_CONST_A2
          DATAOUT(8)=GNMAX_CONST_B2
          DATAOUT(9)=GNMIN_CONST_A3
          DATAOUT(10)=GNMIN_CONST_B3
          DATAOUT(11)=DEGRADATION
          DATAOUT(12)=DILATANCY_COEFF_MU_MONO
          DATAOUT(13)=DILATANCY_COEFF_MU_CYCLIC
          DATAOUT(14)=DILATANCY_STRAIN_SC
          DATAOUT(15)=CRITICAL_STRESS_RATIO_M
        CASE(3)
          DATAOUT=STEADY_STATE_DATA(:,2)! ASSIGNS VOID_RATIOS
        CASE(4)
          DATAOUT=STEADY_STATE_DATA(:,1)! ASSIGNS PRESSURE
        CASE(5)
          DATAOUT=HYDROSTATIC_DATA(:,2) ! ASSIGNS VOID_RATIOS
        CASE(6)
          DATAOUT=HYDROSTATIC_DATA(:,1)! ASSIGNS PRESSURE
        CASE(7)
          DO I=1,NSURFACE
            TEMP=0D0
            CALL GETTENSOR(CENTRE(I),TEMP,SIZE_PROB)
            DATAOUT((I-1)*6+1)=TEMP(1,1)
            DATAOUT((I-1)*6+2)=TEMP(2,2)
            DATAOUT((I-1)*6+3)=TEMP(3,3)
            DATAOUT((I-1)*6+4)=TEMP(1,2)
            DATAOUT((I-1)*6+5)=TEMP(2,3)
            DATAOUT((I-1)*6+6)=TEMP(3,1)
          END DO
```

```
            DO I=1,NSURFACE
              TEMP=0D0
              CALL GETTENSOR(REVERSAL(I),TEMP,SIZE_PROB)
              DATAOUT(6*NSURFACE+(I-1)*6+1)=TEMP(1,1)
              DATAOUT(6*NSURFACE+(I-1)*6+2)=TEMP(2,2)
              DATAOUT(6*NSURFACE+(I-1)*6+3)=TEMP(3,3)
              DATAOUT(6*NSURFACE+(I-1)*6+4)=TEMP(1,2)
              DATAOUT(6*NSURFACE+(I-1)*6+5)=TEMP(2,3)
              DATAOUT(6*NSURFACE+(I-1)*6+6)=TEMP(3,1)
            END DO
            DO I=1,NSURFACE
              DATAOUT(12*NSURFACE+I)=GAMMA(I)
            END DO
            DATAOUT(13*NSURFACE+1)=MAX_STRAIN
            DATAOUT(13*NSURFACE+2)=GEFFECTIVE
            DATAOUT(13*NSURFACE+3)=INITIAL_STRAIN
        END SELECT
    END SUBROUTINE SENDDATA_REAL

    SUBROUTINE SENDDATA_INT(DATAOUT,DSIZE)
        INTEGER,INTENT(IN)::DSIZE
        INTEGER,DIMENSION(DSIZE),INTENT(OUT)::DATAOUT
        DATAOUT(1)=SURFACE
        DATAOUT(2)=KEY
    END SUBROUTINE SENDDATA_INT

   SUBROUTINE SENDDATA_REAL_A(DATAOUT,DSIZE)
        INTEGER,INTENT(IN)::DSIZE
        REAL(KIND=DBL),DIMENSION(DSIZE,DSIZE),INTENT(OUT)::DATAOUT
        DATAOUT=ELPL_TANGENT_NEXT
    END SUBROUTINE SENDDATA_REAL_A

    SUBROUTINE CALCULATE_HYDROSTATIC_PRESSURE ()
        HYDROSTATIC_PRESSURE=FIRSTINVARIANT(STRESS_TENSOR_CURRENT)/REAL(SIZE_
        PROB,KIND=DBL)
    END SUBROUTINE CALCULATE_HYDROSTATIC_PRESSURE

    SUBROUTINE CALCULATE_ELASTIC_SHEAR_MODULUS ()
        REAL(KIND=DBL)::N, FACTOR
        CALL CALCULATE_HYDROSTATIC_PRESSURE()
        N = SHEAR_CONST_N
        IF(MAX_STRAIN.GE.0.02D0)THEN
          FACTOR=MIN(MAX_STRAIN/0.05D0,1.0D0)
          N = N+(0.85D0-N)*FACTOR
        END IF
        ELASTIC_SHEAR_MODULUS=SHEAR_CONST_A*PATM*(2.17D0-VOID_RATIO)**2/(1+VO
        ID_RATIO)* &
        & (HYDROSTATIC_PRESSURE/PATM)**N
    END SUBROUTINE CALCULATE_ELASTIC_SHEAR_MODULUS

    SUBROUTINE CALCULATE_STEADY_STATE_VOID_RATIO ()
        INTEGER::I
        CALL CALCULATE_HYDROSTATIC_PRESSURE()
        IF(HYDROSTATIC_PRESSURE.LT.STEADY_STATE_DATA(1,1)) THEN
            STEADY_STATE_VOID_RATIO = STEADY_STATE_DATA(1,2)
        ELSEIF (HYDROSTATIC_PRESSURE.GT.STEADY_STATE_DATA(10,1)) THEN
            STEADY_STATE_VOID_RATIO = STEADY_STATE_DATA(10,2)
```

```
    ELSE
      DO I=1,9
        IF(HYDROSTATIC_PRESSURE.GE.STEADY_STATE_DATA(I,1).AND.HYDROSTATIC_PR
        ESSURE.LE.STEADY_STATE_DATA(I+1,1)) THEN
          STEADY_STATE_VOID_RATIO = STEADY_STATE_DATA(I,2)+ &
          (HYDROSTATIC_PRESSURE - STEADY_STATE_DATA(I,1))/(STEADY_STATE_DATA
          (I+1,1)-STEADY_STATE_DATA(I,1))* &
          (STEADY_STATE_DATA(I+1,2)-STEADY_STATE_DATA(I,2))
          EXIT
        END IF
      END DO
    END IF
END SUBROUTINE CALCULATE_STEADY_STATE_VOID_RATIO

SUBROUTINE CALCULATE_HYDROSTATIC_VOID_RATIO ()
    INTEGER::I
    CALL CALCULATE_HYDROSTATIC_PRESSURE()
    IF(HYDROSTATIC_PRESSURE.LT.HYDROSTATIC_DATA(1,1)) THEN
        HYDROSTATIC_VOID_RATIO = HYDROSTATIC_DATA(1,2)
    ELSEIF (HYDROSTATIC_PRESSURE.GT.HYDROSTATIC_DATA(10,1)) THEN
        HYDROSTATIC_VOID_RATIO = HYDROSTATIC_DATA(10,2)
    ELSE
      DO I=1,9
        IF(HYDROSTATIC_PRESSURE.GE.HYDROSTATIC_DATA(I,1).AND.HYDROSTATIC_PRE
        SSURE.LE.HYDROSTATIC_DATA(I+1,1)) THEN
          HYDROSTATIC_VOID_RATIO = HYDROSTATIC_DATA(I,2)+ &
          (HYDROSTATIC_PRESSURE - HYDROSTATIC_DATA(I,1))/(HYDROSTATIC_DATA(I
          +1,1)-HYDROSTATIC_DATA(I,1))* &
          (HYDROSTATIC_DATA(I+1,2)-HYDROSTATIC_DATA(I,2))
          EXIT
        END IF
      END DO
    END IF
END SUBROUTINE CALCULATE_HYDROSTATIC_VOID_RATIO

SUBROUTINE CALCULATE_STATE_INDEX ()
    CALL CALCULATE_STEADY_STATE_VOID_RATIO()
    CALL CALCULATE_HYDROSTATIC_VOID_RATIO()
    STATE_INDEX=(HYDROSTATIC_VOID_RATIO-VOID_RATIO)/(HYDROSTATIC_VOID_RAT
    IO-STEADY_STATE_VOID_RATIO)
END SUBROUTINE CALCULATE_STATE_INDEX

 SUBROUTINE CALCULATE_ETAMAX ()
    CALL CALCULATE_STATE_INDEX()
    ETAMAX=ETAMAX_CONST_A1+ETAMAX_CONST_B1*STATE_INDEX
END SUBROUTINE CALCULATE_ETAMAX

SUBROUTINE CALCULATE_GNMAX ()
    CALL CALCULATE_STATE_INDEX()
    GNMAX=GNMAX_CONST_A2+GNMAX_CONST_B2*STATE_INDEX
END SUBROUTINE CALCULATE_GNMAX

SUBROUTINE CALCULATE_GNMIN ()
    CALL CALCULATE_STATE_INDEX()
    GNMIN=GNMIN_CONST_A3+GNMIN_CONST_B3*STATE_INDEX
END SUBROUTINE CALCULATE_GNMIN
```

```
SUBROUTINE CALCULATE_DELTA_VOLUMETRIC_STRAIN ()
    DELTA_VOLUMETRIC_STRAIN=FIRSTINVARIANT(STRAIN_TENSOR_NEXT)-FIRSTINVAR
    IANT(STRAIN_TENSOR_CURRENT)
END SUBROUTINE CALCULATE_DELTA_VOLUMETRIC_STRAIN

SUBROUTINE UPDATE_VOID_RATIO ()
    CALL CALCULATE_DELTA_VOLUMETRIC_STRAIN
    VOID_RATIO=VOID_RATIO*(1D0-DELTA_VOLUMETRIC_STRAIN)
END SUBROUTINE UPDATE_VOID_RATIO

SUBROUTINE CALCULATE_RADIUS ()
    CALL CALCULATE_ETAMAX
    RADIUS=2D0**0.5D0*ETAMAX*PREF
END SUBROUTINE CALCULATE_RADIUS

SUBROUTINE GET_STATE_DATA(DATASTORE, SIZE)
    INTEGER,INTENT(IN)::SIZE
    REAL(KIND=DBL),DIMENSION(SIZE),INTENT(OUT)::DATASTORE
    DATASTORE(1)=STEADY_STATE_VOID_RATIO
    DATASTORE(2)=HYDROSTATIC_VOID_RATIO
    DATASTORE(3)=STATE_INDEX
END SUBROUTINE GET_STATE_DATA

TYPE(TENSOR_2R) FUNCTION SOLVECONJUGATE_TYPE1 (SIJ, NIJ)
    TYPE(TENSOR_2R),INTENT(IN)::SIJ,NIJ
    REAL(KIND=DBL)::A, B, C, DETERMINANT, ROOT
    CALL CALCULATE_RADIUS
    ! PARAMETERS OF THE QUADRATIC
    A = 1.D0
    B = 2.D0*(SIJ-ORIGIN).DDOT.NIJ
    C = ((SIJ-ORIGIN).DDOT.(SIJ-ORIGIN))-RADIUS**2
    DETERMINANT=B*B-4.D0*A*C
    IF (DETERMINANT .LT. 0D0) THEN
        ROOT=0D0
        STOP
    ELSE
        ROOT=(-B+DETERMINANT**0.5D0)/(2.D0*A)
    END IF
    SOLVECONJUGATE_TYPE1=ROOT*NIJ+SIJ
END FUNCTION SOLVECONJUGATE_TYPE1

 TYPE(TENSOR_2R) FUNCTION SOLVECONJUGATE_TYPE2 (NIJ)
    TYPE(TENSOR_2R),INTENT(IN)::NIJ
    REAL(KIND=DBL)::A, B, C, DETERMINANT, ROOT
    CALL CALCULATE_RADIUS
    ! PARAMETERS OF THE QUADRATIC
    A = 1.D0
    B = -2.D0*(ORIGIN.DDOT.NIJ)
    C = (ORIGIN.DDOT.ORIGIN)-RADIUS**2
    DETERMINANT=B*B-4.D0*A*C
    IF (DETERMINANT .LT. 0D0) THEN
        ROOT=0D0
        STOP
    ELSE
        ROOT=(-B+DETERMINANT**0.5D0)/(2.D0*A)
    END IF
    SOLVECONJUGATE_TYPE2=ROOT*NIJ
```

```
END FUNCTION SOLVECONJUGATE_TYPE2

SUBROUTINE SETINITIALTANGENT()

    REAL(KIND=DBL)::MU,G

    EL_TANGENT = 0D0
    MU = POISSON
    G  = ELASTIC_SHEAR_MODULUS

    !-------------------------------------------------------------
    ! THE MATRIX IS IN TERMS OF ENGINEERING STRAIN
    !-------------------------------------------------------------

    EL_TANGENT(1,1)=2D0*G/(1D0-2D0*MU)*(1D0-MU)
    EL_TANGENT(1,2)=2D0*G/(1D0-2D0*MU)*MU
    EL_TANGENT(1,3)=2D0*G/(1D0-2D0*MU)*MU

    EL_TANGENT(2,1)=2D0*G/(1D0-2D0*MU)*MU
    EL_TANGENT(2,2)=2D0*G/(1D0-2D0*MU)*(1D0-MU)
    EL_TANGENT(2,3)=2D0*G/(1D0-2D0*MU)*MU

    EL_TANGENT(3,1)=2D0*G/(1D0-2D0*MU)*MU
    EL_TANGENT(3,2)=2D0*G/(1D0-2D0*MU)*MU
    EL_TANGENT(3,3)=2D0*G/(1D0-2D0*MU)*(1D0-MU)

    EL_TANGENT(4,4)=G
    EL_TANGENT(5,5)=G
    EL_TANGENT(6,6)=G

END SUBROUTINE SETINITIALTANGENT

REAL(KIND=DBL) FUNCTION CALCULATE_EQV_STRAIN(ETA)

    REAL(KIND=DBL),INTENT(IN)::ETA
    REAL(KIND=DBL)::STRAIN_INITIAL, STRAIN_FINAL,GN
    INTEGER::COUNTER

    IF(ETA.LE.TOLERANCE) THEN
        CALCULATE_EQV_STRAIN = 0D0
        RETURN
    END IF

    STRAIN_INITIAL = 0D0
    STRAIN_FINAL   = 0D0
    COUNTER        = 0

    DO

        GN=(GNMAX-GNMIN)*DEXP(-DEGRADATION*STRAIN_INITIAL/0.01D0)+GNMIN
        STRAIN_FINAL = ETA/(1D0-ETA/ETAMAX)/GN
        COUNTER = COUNTER+1

        IF(DABS(STRAIN_FINAL-STRAIN_INITIAL).LE.1D-6) EXIT

        IF(COUNTER.GT.100) EXIT
```

```
                STRAIN_INITIAL = STRAIN_FINAL

            END DO

            CALCULATE_EQV_STRAIN = 0.5D0*(STRAIN_INITIAL+STRAIN_FINAL)

        END FUNCTION CALCULATE_EQV_STRAIN

    END MODULE GLOBAL_DATA_3D_E
```

```
!---------------------------
! EXPLANATION OF THE MODULE
!---------------------------
! THIS MODULE CONTAINS THE PROCEDURE FOR CALCULATING PLASTIC STRAIN INCREMENT.

MODULE PLASTIC_FLOW_3D_E

    USE KIND_DBL_3D_E
    USE TENSOR_HANDLE_3D_E
    USE GLOBAL_DATA_3D_E

    IMPLICIT NONE

    CONTAINS

    TYPE(TENSOR_2R) FUNCTION CALCULATE_STRESS(GIJ, FIJ, SIJ, ERROR, OPTION)

        TYPE(TENSOR_2R),INTENT(IN)::GIJ,FIJ,SIJ
        INTEGER, INTENT(IN), OPTIONAL::OPTION
        LOGICAL,INTENT(INOUT)::ERROR

        REAL(KIND=DBL)::C,Q,P,TEMP(MAXSIZE,MAXSIZE)

        TYPE(TENSOR_2R)::LOADING_POTENTIAL,LOADING_POTENTIAL_DEVIATORIC, LOAD
        ING_POTENTIAL_HYDROSTATIC, &
        & PLASTIC_POTENTIAL,PLASTIC_POTENTIAL_DEVIATORIC,PLASTIC_POTENTIAL_HY
        DROSTATIC, &
        & NXIJ, SIJ_SHIFTED, NSIJ, DEPSILON

        INTEGER::I,J


        !*************************************************************************
        ******************
        ! CALCULATE COAXIALITY AND THE Q/P TERM FOR DILATANCY

        !*************************************************************************
        ******************

        IF (NORM(SIJ).LE. TOLERANCE) THEN    ! ASSUME SIJ AND GIJ ARE PARALLEL
            C = 1
        ELSE
            C = NORMALISE(SIJ).DDOT.GIJ      ! NOTE: GIJ IS ALREADY NORMALISED
        END IF

        Q=SECINVDEV(STRESS_TENSOR_CURRENT)   ! NOTE: Q = (J2)^0.5
        P=HYDROSTATIC_PRESSURE

        IF(P.LE.PMIN) THEN
          Q = ETAMAX*P
          C = 1D0
        END IF


        !*************************************************************************
        ******************
        ! CALCULATE PLASTIC AND LOADING POTENTIALS
```

```
!***********************************************************************
******************

PLASTIC_POTENTIAL_DEVIATORIC = REAL((1D0/2D0)**0.5D0,KIND=DBL)* GIJ
TEMP = 0D0

IF(PRESENT(OPTION)) THEN

    ! THIS MODIFICATION IS TO ACCOUNT FOR INITIAL ANISOTROPIC STRAIN

    DO I=1,SIZE_PROB
        DO J=1,SIZE_PROB
            IF(I.EQ.J) TEMP(I,J) = (DILATANCY_AT_REVERSAL-C*Q/P)/REAL(
            SIZE_PROB,KIND=DBL)
        END DO
    END DO

    PLASTIC_SHEAR_MODULUS = PLASTIC_MODULUS_REVERSAL

ELSE

    DO I=1,SIZE_PROB
        DO J=1,SIZE_PROB
            IF(I.EQ.J) TEMP(I,J) = (DILATANCY-C*Q/P)/REAL(SIZE_PROB,KIND=DBL)

        END DO
    END DO

END IF

PLASTIC_POTENTIAL_HYDROSTATIC = CREATETENSOR(TEMP,SIZE_PROB)

PLASTIC_POTENTIAL = PLASTIC_POTENTIAL_DEVIATORIC+PLASTIC_POTENTIAL_HYDROSTATIC

LOADING_POTENTIAL_DEVIATORIC = REAL((1D0/2D0)**0.5D0,KIND=DBL)* FIJ

DO I=1,SIZE_PROB
    DO J=1,SIZE_PROB
        IF(I.EQ.J) TEMP(I,J) = -C*Q/P/REAL(SIZE_PROB,KIND=DBL)
    END DO
END DO

LOADING_POTENTIAL_HYDROSTATIC=CREATETENSOR(TEMP,SIZE_PROB)

LOADING_POTENTIAL=LOADING_POTENTIAL_DEVIATORIC+LOADING_POTENTIAL_HYDROSTATIC


!***********************************************************************
******************
! CALCULATE LAMDA

!***********************************************************************
******************

DEPSILON=STRAIN_TENSOR_NEXT-STRAIN_TENSOR_CURRENT
```

```
        LAMDA=(LOADING_POTENTIAL.DDOT.TENSORMULTIPLY(CONSTITUTIVE_TENSOR,DEPSILON))/ &
        & (PLASTIC_SHEAR_MODULUS+(LOADING_POTENTIAL.DDOT.TENSORMULTIPLY(CONST
        ITUTIVE_TENSOR,PLASTIC_POTENTIAL)))

        IF (LAMDA.LT. 0D0) LAMDA = 0.0D0

        PLASTIC_STRAIN_INCREMENT=LAMDA*PLASTIC_POTENTIAL


        !**********************************************************************
        ******************
        ! CALCULATE NEW STRESS STATE

        !**********************************************************************
        ******************

        STRESS_TENSOR_NEXT=STRESS_TENSOR_CURRENT+ &
        & TENSORMULTIPLY(CONSTITUTIVE_TENSOR,(DEPSILON-PLASTIC_STRAIN_INCREMENT))



        !**********************************************************************
        ******************
        ! PROJECT DEVIATORIC COMPONENTS ON TO THE STANDARD PLANE

        !**********************************************************************
        ******************

        P=FIRSTINVARIANT(STRESS_TENSOR_NEXT)/REAL(SIZE_PROB,KIND=DBL)

        IF(P.LT.TOLERANCE) THEN
            STRESS_TENSOR_NEXT = STRESS_TENSOR_CURRENT
            ERROR=.TRUE.
            RETURN
        END IF

        Q = SECINVDEV(STRESS_TENSOR_NEXT)

        IF(Q.GT.P*ETAMAX) THEN
            CALL STRESSCORRECTION(DEPSILON)
        ELSE
            CALL SETELASTOPLASTICTANGENT(PLASTIC_POTENTIAL,LOADING_POTENTIAL)
        END IF

        P=FIRSTINVARIANT(STRESS_TENSOR_NEXT)/REAL(SIZE_PROB,KIND=DBL)

        CALCULATE_STRESS=PREF/P*DEVIATORIC(STRESS_TENSOR_NEXT)

    END FUNCTION CALCULATE_STRESS

    SUBROUTINE STRESSCORRECTION(DEPS)
        TYPE(TENSOR_2R),INTENT(IN)::DEPS
        TYPE(TENSOR_2R)::NIJ
        REAL(KIND=DBL)::TEMP(3,3),Q,DELQ,P,DELP,ETA
        DELQ = GEFFECTIVE*SECINVDEV(DEPS)
        ETA  = SECINVDEV(STRESS_TENSOR_CURRENT)/HYDROSTATIC_PRESSURE
        DELP = DELQ/MAX(ETA,ETAMAX)
```

```
            Q     = SECINVDEV(STRESS_TENSOR_CURRENT)+DELQ
            P     = HYDROSTATIC_PRESSURE+DELP
            NIJ   = NORMALISE(DEVIATORIC(STRESS_TENSOR_NEXT))
            TEMP=0D0
            TEMP(1,1)=P
            TEMP(2,2)=P
            TEMP(3,3)=P
            STRESS_TENSOR_NEXT = (2D0**0.5D0)*Q*NIJ + CREATETENSOR(TEMP,SIZE_PROB)
        END SUBROUTINE STRESSCORRECTION

        SUBROUTINE SETELASTOPLASTICTANGENT(PLASTIC_POTENTIAL,LOADING_POTENTIAL)
            TYPE(TENSOR_2R),INTENT(IN)::PLASTIC_POTENTIAL,LOADING_POTENTIAL
            REAL(KIND=DBL)::TEMP(SIZE_PROB,SIZE_PROB),DELG(6,1),DELF(6,1),DENOMIN
            ATOR,CORRECTOR(6,6)
            DELG = 0D0 ! VECTOR FORM OF PLASTIC_POTENTIAL
            DELF = 0D0 ! VECTOR FORM OF LOADING_POTENTIAL
            CALL GETTENSOR(PLASTIC_POTENTIAL,TEMP,SIZE_PROB)
            DELG(1,1)=TEMP(1,1)
            DELG(2,1)=TEMP(2,2)
            DELG(3,1)=TEMP(3,3)
            DELG(4,1)=2D0*TEMP(1,2)
            DELG(5,1)=2D0*TEMP(2,3)
            DELG(6,1)=2D0*TEMP(3,1)
            CALL GETTENSOR(LOADING_POTENTIAL,TEMP,SIZE_PROB)
            DELF(1,1)=TEMP(1,1)
            DELF(2,1)=TEMP(2,2)
            DELF(3,1)=TEMP(3,3)
            DELF(4,1)=2D0*TEMP(1,2)
            DELF(5,1)=2D0*TEMP(2,3)
            DELF(6,1)=2D0*TEMP(3,1)
            DENOMINATOR = PLASTIC_SHEAR_MODULUS+(LOADING_POTENTIAL.DDOT.TENSORMUL
            TIPLY(CONSTITUTIVE_TENSOR,PLASTIC_POTENTIAL))
            CORRECTOR = MATMUL(EL_TANGENT,MATMUL(MATMUL(DELG,TRANSPOSE(DELF)),EL_TANGENT))
            CORRECTOR = CORRECTOR/DENOMINATOR
            ELPL_TANGENT_NEXT = EL_TANGENT - CORRECTOR
        END SUBROUTINE SETELASTOPLASTICTANGENT

    END MODULE PLASTIC_FLOW_3D_E
```

```
!---------------------------
! EXPLANATION OF THE MODULE
!---------------------------
! THIS MODULE CALCULATES PLASTIC MODULUS AND DILATANCY COEFFICIENT BASED ON NESTED
SURFACE APPROACH
! THE TAU EFFECTIVE IS TAKEN AS CUMULATIVE STRESS ALONG THE DIRECTION AT CONJUGATE
POINT

MODULE HARDENING_RULE_3D_E

    USE KIND_DBL_3D_E
    USE TENSOR_HANDLE_3D_E
    USE GLOBAL_DATA_3D_E

    IMPLICIT NONE

    CONTAINS

    SUBROUTINE HARDENING(FIJ,SIJ,SIJ_TRIAL)
        TYPE(TENSOR_2R),INTENT(IN)::FIJ, SIJ, SIJ_TRIAL
        TYPE(TENSOR_2R):: DSIJ
        REAL(KIND=DBL):: DGAMMA

        DSIJ    = SIJ_TRIAL-SIJ


        !*************************************************************************
        **************
        ! SWITCH ON KEY

        !*************************************************************************
        **************

        IF (KEY.EQ.0) KEY = 1


        !*************************************************************************
        **************
        ! PLASTIC STRAIN INCREMENT

        !*************************************************************************
        **************

         DGAMMA =  2D0*SECINVDEV(STRAIN_TENSOR_NEXT-STRAIN_TENSOR_CURRENT)


        !*************************************************************************
        **************
        ! CASE OF PLASTIC FLOW: SIJ = SIJ_NEXT

        !*************************************************************************
        **************

        IF(NORM(DSIJ).LT.TOLERANCE) THEN
            GAMMA(SURFACE)=GAMMA(SURFACE)+DGAMMA
            RETURN
        END IF
```

```
      !*****************************************************************************
      **************
      ! CASE OF LOADING   : DELETE SMALLER SURFACES AND ACTIVATE THE NEXT LARGER
      SURFACE
      ! CASE OF UNLOADING : CREATE NEW SURFACE

      !*****************************************************************************
      **************

      IF((DSIJ.DDOT.FIJ).GE.0D0) THEN
                                                              ! LOADING
          CALL ACTIVATE_SURFACE(SURFACE,SIJ_TRIAL,DGAMMA)
                                                              ! POPULATE / UPDATE
                                                              CURRENT SURFACE
      ELSE
                                                              ! UNLOADING
          MAX_STRAIN=MAX(MAX_STRAIN,GAMMA(SURFACE))

          SURFACE = SURFACE+1
                                                              ! CREATES ONE
                                                              ADDITIONAL SURFACE
                                                              UPTO NSURFACE+1
          IF (SURFACE.LE.NSURFACE) THEN
            REVERSAL(SURFACE) = SIJ
          ELSE
            REVERSAL(SURFACE-1) = SIJ
          END IF
                                                              ! ASSIGNS THE
                                                              REVERSAL STRESS
          CALL ACTIVATE_SURFACE(SURFACE,SIJ_TRIAL,DGAMMA)
                                                              ! GENERATE NEW
                                                              SURFACE LIMITED TO
                                                              NSURFACE
      END IF

  END SUBROUTINE HARDENING

  RECURSIVE SUBROUTINE ACTIVATE_SURFACE(N,SIGMA,DGAMMA)
      INTEGER,INTENT(IN)::N
      TYPE(TENSOR_2R),INTENT(IN)::SIGMA
      REAL(KIND=DBL),INTENT(IN)::DGAMMA
      TYPE(TENSOR_2R)::XIJ_CP,NIJ
      REAL(KIND=DBL)::DIST,RADIUS
      REAL(KIND=DBL)::TEMP(MAXSIZE,MAXSIZE)
      INTEGER::I,J

      IF(N.EQ.1)THEN
                                          ! TERMINATE THE RECURSION
          SURFACE = N
          REVERSAL(SURFACE) = SIGMA
          GAMMA(SURFACE) = GAMMA(SURFACE)+DGAMMA
          NIJ=NORMALISE(SIGMA)
          XIJ_CP=SOLVECONJUGATE(SIGMA,NIJ)
          CENTRE(SURFACE)=SIGMA-(NORM(SIGMA)/NORM(XIJ_CP))*(XIJ_CP-ORIGIN)
```

```
        ELSE

            DIST =  NORM(SIGMA - CENTRE(N-1))
            RADIUS = NORM(REVERSAL (N-1)- CENTRE(N-1))

            IF (DIST.GT.RADIUS) THEN
                                                ! DELETE THE CURRENT SURFACE IF N <=
                                                NSURFACE
                                                ! FOR N = NSURFACE+1 THERE IS NO
                                                MEMORY
                                                ! MAKE CURRENT SURFACE = N-1
                IF(N.LE.NSURFACE) THEN

                    FORALL(I=1:MAXSIZE,J=1:MAXSIZE) TEMP(I,J)=0D0
                    REVERSAL(N) = CREATETENSOR(TEMP, SIZE_PROB)
                    CENTRE(N)   = CREATETENSOR(TEMP, SIZE_PROB)
                    GAMMA(N)    = INITIAL_STRAIN

                END IF

                CALL ACTIVATE_SURFACE(N-1,SIGMA,0D0)

            ELSE                                ! POPULATE THE CURRENT SURFACE

                IF(N.LE.NSURFACE) THEN

                    SURFACE = N
                    CENTRE(SURFACE) = LOCATE_CENTRE(REVERSAL(SURFACE),CENTRE(SURFACE-
                    1),SIGMA)
                    GAMMA(SURFACE)= GAMMA(SURFACE)+DGAMMA

                ELSE
                                                ! DUMMY SURFACE =  NSURFACE + 1 IS
                                                RE-ASSIGNED AS
                                                ! SURFACE = NSURFACE; SIJ IS THE
                                                STRESS REVERSAL OF
                                                ! THE DUMMY SURFACE
                    SURFACE = N-1
                    CENTRE(SURFACE) = LOCATE_CENTRE(REVERSAL(SURFACE), CENTRE(SURFACE
                    ), SIGMA)
                    GAMMA(SURFACE) = GAMMA(SURFACE)+DGAMMA

                END IF

            END IF

        END IF

    END SUBROUTINE ACTIVATE_SURFACE

    TYPE(TENSOR_2R) FUNCTION LOCATE_CENTRE(SIGMA_R, SIGMA_C, SIGMA) RESULT(Z)
        TYPE(TENSOR_2R),INTENT(IN)::SIGMA_R, SIGMA_C, SIGMA
        TYPE(TENSOR_2R)::NIJ
        REAL(KIND=DBL)::BETA,NUMERATOR,DENOMINATOR

        NIJ = NORMALISE(SIGMA_R-SIGMA_C)
```

```
            NUMERATOR = (SIGMA_R.DDOT.(SIGMA_R-SIGMA_C))+(SIGMA.DDOT.(SIGMA_C-SIG
            MA))+(SIGMA_C.DDOT.(SIGMA-SIGMA_R))

            DENOMINATOR = NIJ.DDOT.(SIGMA_R-SIGMA)

            IF(DABS(DENOMINATOR).LE.TINY(1D0)) THEN
                Z = SIGMA_C
                RETURN
            ELSE
                BETA = 0.5D0*NUMERATOR/((NIJ.DDOT.(SIGMA_R-SIGMA)))
                Z = BETA*(NIJ)+SIGMA_C
            END IF

        END FUNCTION LOCATE_CENTRE


    END MODULE HARDENING_RULE_3D_E
```

Appendix

C++ LISTING OF THE CONCRETE DERIVED CLASSES FOR OPENSEES IMPLEMENTATION

```
/* University of Canterbury
   Written by: Saumyasuchi Das, May 2013 */

#ifndef StressDilatancyModel_h
#define StressDilatancyModel_h

# include <ElementAPI.h>
# include <ID.h>
# include <Vector.h>
# include <Matrix.h>
# include <NDMaterial.h>
# include <Channel.h>
# include <Response.h>
# include <MaterialResponse.h>
# include <Parameter.h>

#define ND_TAG_STRESSDILATANCYMODEL 1

class StressDilatancyModel : public NDMaterial {

public:

    //default constructor - does nothing, never called

    StressDilatancyModel() {};

    //initialisation constructor

    StressDilatancyModel(int tag,
                         double constDensity,
                         double constG,
                         // SD model  parameters
                         double initialVoidRatio,
                         double constA,
                         double exponentN,
                         double poissonRatio,
                         double constBeta1,
                         double constAlpha1,
                         double constBeta2,
                         double constAlpha2,
                         double constBeta3,
                         double constAlpha3,
                         double constDegradation,
                         double constMumin,
                         double constMucyclic,
                         double constDilatancyStrain,
                         double constMumax,
                         // steady state line void ratio
                         double constsslvoidatP1,
                         double constsslvoidatP2,
                         double constsslvoidatP3,
                         double constsslvoidatP4,
                         double constsslvoidatP5,
                         double constsslvoidatP6,
                         double constsslvoidatP7,
                         double constsslvoidatP8,
                         double constsslvoidatP9,
```

```
                        double constsslvoidatP10,
                        // hydrostatic state line void ratio
                        double consthslvoidatP1,
                        double consthslvoidatP2,
                        double consthslvoidatP3,
                        double consthslvoidatP4,
                        double consthslvoidatP5,
                        double consthslvoidatP6,
                        double consthslvoidatP7,
                        double consthslvoidatP8,
                        double consthslvoidatP9,
                        double consthslvoidatP10,
                        // reference pressures
                        double constP1,
                        double constP2,
                        double constP3,
                        double constP4,
                        double constP5,
                        double constP6,
                        double constP7,
                        double constP8,
                        double constP9,
                        double constP10,
                        //offset of the failure surface
                        double constRxx=0,
                        double constRyy=0,
                        double constRzz=0,
                        double constRxy=0,
                        double constRyz=0,
                        double constRzx=0);

    virtual ~StressDilatancyModel();

    double getRho(void);

    int setParameter(const char **argv, int argc, Parameter &param);

    int updateParameter(int parameterID, Information &info);

    void Print(OPS_Stream &s, int flag =0);

    // Virtual functions of the base class:
    // Virtual construct added in case the following functions are used in subclasses

    virtual int commitState(void);

    virtual int revertToLastCommit(void);

    virtual int revertToStart(void);

    virtual NDMaterial *getCopy(void);

    virtual NDMaterial *getCopy(const char *code);

    virtual const char *getType(void) const;

    virtual int sendSelf(int commitTag, Channel &theChannel);
```

```
    virtual int recvSelf(int commitTag, Channel &theChannel,FEM_ObjectBroker &
    theBroker);

protected:

    double  theG,
            theDensity,
            *modelParameter,
            *sslVoidratio,
            *hslVoidratio,
            *refPressure,
            *refOrigin;

    int theTag;

    int theStage;

    const static int Nsurface = 35;

private:

};

#endif
```

```
/* University of Canterbury
   Written by: Saumyasuchi Das, May 2013 */

# include <StressDilatancyModel.h>
# include <StressDilatancyModel2D.h>
# include <StressDilatancyModel3D.h>

//int StressDilatancyModel::theStage=0;

#define OPS_Export

OPS_Export void *
OPS_NewStressDilatancyMaterial(void)
{
    static int numStressDilatancyModel = 0;

    if(numStressDilatancyModel == 0) {

        OPS_Error("\nStress Dilatancy nDmaterial - Written: Saumyasuchi Das
        U.Canterbury\n", 1);

        numStressDilatancyModel++;

    }


  // Pointer to an NDmaterial that will be returned
    NDMaterial *theMaterial = 0;
    int numArgs;
    const int numDbl=47;
    const char *variable[]={
        "Density",
        "Shear Modulus",
        "Void Ratio",
        "Const A",
        "Exponent n",
        "Poisson's ratio",
        "Beta1",
        "Alpha1",
        "Beta2",
        "Alpha2",
        "Beta3",
        "Alpha3",
        "Degradation",
        "Mumin",
        "Mucyclic",
        "Dilatancy Strain",
        "Mumax",
        "SSL void ratio at P1",
        "SSL void ratio at P2",
        "SSL void ratio at P3",
        "SSL void ratio at P4",
        "SSL void ratio at P5",
        "SSL void ratio at P6",
        "SSL void ratio at P7",
        "SSL void ratio at P8",
        "SSL void ratio at P9",
```

```
        "SSL void ratio at P10",
        "HSL void ratio at P1",
        "HSL void ratio at P2",
        "HSL void ratio at P3",
        "HSL void ratio at P4",
        "HSL void ratio at P5",
        "HSL void ratio at P6",
        "HSL void ratio at P7",
        "HSL void ratio at P8",
        "HSL void ratio at P9",
        "HSL void ratio at P10",
        "Reference pressure P1",
        "Reference pressure P2",
        "Reference pressure P3",
        "Reference pressure P4",
        "Reference pressure P5",
        "Reference pressure P6",
        "Reference pressure P7",
        "Reference pressure P8",
        "Reference pressure P9",
        "Reference pressure P10"
  };

  numArgs = OPS_GetNumRemainingInputArgs()-1; //numArgs = 47

  if (numArgs < numDbl) {

     opserr << "WARNING: Insufficient number of arguments" << endln;

     for(int i=numArgs+1; i < numDbl; i++)
         opserr << "Want: nDMaterial StressDilatancyModel::"<<variable[i]<<" ?"<<
         endln;

     return 0;
  }

//tag = variable to contain tag of the material
//numData =  number of arguments, same as argc

  int tag, numData;
  double dData[numDbl+6];

  numData = 1;
  if (OPS_GetInt(&numData, &tag) != 0) {

      opserr << "WARNING invalid nDMaterial StressDilatancy material  tag" << endln;
      return 0;
  }

  numData = numArgs;
  if (OPS_GetDouble(&numData, dData) != 0) {

      opserr << "WARNING invalid material data for nDMaterial StressDilatancy
      material  with tag: " << tag << endln;
      return 0;
  }
```

```
    if (numArgs == 47) {

        theMaterial = new StressDilatancyModel(tag, dData[0], dData[1], dData[2],
        dData[3], dData[4], dData[5],
        dData[6], dData[7], dData[8], dData[9], dData[10], dData[11], dData[12],
        dData[13], dData[14],
        dData[15],dData[16],dData[17],dData[18],dData[19],dData[20],dData[21],dData[
        22],dData[23],dData[24],
        dData[25],dData[26],dData[27],dData[28],dData[29],dData[30],dData[31],dData[
        32],dData[33],dData[34],
        dData[35],dData[36],dData[37],dData[38],dData[39],dData[40],dData[41],dData[
        42],dData[43],dData[44],
        dData[45],dData[46]);}

    if (numArgs == 48)
        theMaterial = new StressDilatancyModel(tag, dData[0], dData[1], dData[2],
        dData[3], dData[4], dData[5],
        dData[6], dData[7], dData[8], dData[9], dData[10], dData[11], dData[12],
        dData[13], dData[14],
        dData[15],dData[16],dData[17],dData[18],dData[19],dData[20],dData[21],dData[
        22],dData[23],dData[24],
        dData[25],dData[26],dData[27],dData[28],dData[29],dData[30],dData[31],dData[
        32],dData[33],dData[34],
        dData[35],dData[36],dData[37],dData[38],dData[39],dData[40],dData[41],dData[
        42],dData[43],dData[44],
        dData[45],dData[46],dData[47]);

    if (numArgs == 49)
        theMaterial = new StressDilatancyModel(tag, dData[0], dData[1], dData[2],
        dData[3], dData[4], dData[5],
        dData[6], dData[7], dData[8], dData[9], dData[10], dData[11], dData[12],
        dData[13], dData[14],
        dData[15],dData[16],dData[17],dData[18],dData[19],dData[20],dData[21],dData[
        22],dData[23],dData[24],
        dData[25],dData[26],dData[27],dData[28],dData[29],dData[30],dData[31],dData[
        32],dData[33],dData[34],
        dData[35],dData[36],dData[37],dData[38],dData[39],dData[40],dData[41],dData[
        42],dData[43],dData[44],
        dData[45],dData[46],dData[47],dData[48]);

    if (numArgs == 50)
        theMaterial = new StressDilatancyModel(tag, dData[0], dData[1], dData[2],
        dData[3], dData[4], dData[5],
        dData[6], dData[7], dData[8], dData[9], dData[10], dData[11], dData[12],
        dData[13], dData[14],
        dData[15],dData[16],dData[17],dData[18],dData[19],dData[20],dData[21],dData[
        22],dData[23],dData[24],
        dData[25],dData[26],dData[27],dData[28],dData[29],dData[30],dData[31],dData[
        32],dData[33],dData[34],
        dData[35],dData[36],dData[37],dData[38],dData[39],dData[40],dData[41],dData[
        42],dData[43],dData[44],
        dData[45],dData[46],dData[47],dData[48],dData[49]);

    if (numArgs == 51)
        theMaterial = new StressDilatancyModel(tag, dData[0], dData[1], dData[2],
        dData[3], dData[4], dData[5],
        dData[6], dData[7], dData[8], dData[9], dData[10], dData[11], dData[12],
```

```
            dData[13], dData[14],
            dData[15],dData[16],dData[17],dData[18],dData[19],dData[20],dData[21],dData[
            22],dData[23],dData[24],
            dData[25],dData[26],dData[27],dData[28],dData[29],dData[30],dData[31],dData[
            32],dData[33],dData[34],
            dData[35],dData[36],dData[37],dData[38],dData[39],dData[40],dData[41],dData[
            42],dData[43],dData[44],
            dData[45],dData[46],dData[47],dData[48],dData[49],dData[50]);

        if (numArgs == 52)
            theMaterial = new StressDilatancyModel(tag, dData[0], dData[1], dData[2],
            dData[3], dData[4], dData[5],
            dData[6], dData[7], dData[8], dData[9], dData[10], dData[11], dData[12],
            dData[13], dData[14],
            dData[15],dData[16],dData[17],dData[18],dData[19],dData[20],dData[21],dData[
            22],dData[23],dData[24],
            dData[25],dData[26],dData[27],dData[28],dData[29],dData[30],dData[31],dData[
            32],dData[33],dData[34],
            dData[35],dData[36],dData[37],dData[38],dData[39],dData[40],dData[41],dData[
            42],dData[43],dData[44],
            dData[45],dData[46],dData[47],dData[48],dData[49],dData[50],dData[51]);

        if (numArgs == 53)
            theMaterial = new StressDilatancyModel(tag, dData[0], dData[1], dData[2],
            dData[3], dData[4], dData[5],
            dData[6], dData[7], dData[8], dData[9], dData[10], dData[11], dData[12],
            dData[13], dData[14],
            dData[15],dData[16],dData[17],dData[18],dData[19],dData[20],dData[21],dData[
            22],dData[23],dData[24],
            dData[25],dData[26],dData[27],dData[28],dData[29],dData[30],dData[31],dData[
            32],dData[33],dData[34],
            dData[35],dData[36],dData[37],dData[38],dData[39],dData[40],dData[41],dData[
            42],dData[43],dData[44],
            dData[45],dData[46],dData[47],dData[48],dData[49],dData[50],dData[51],dData[
            52]);


        if (theMaterial == 0){

         opserr << "WARNING ran out of memory for nDMaterial StressDilatancy material
         with tag: " << tag << endln;
      }

       return theMaterial;
    }

    StressDilatancyModel::StressDilatancyModel (
                            int tag,
                            double constDensity,
                            double constG,
                            // SD model  parameters
                            double initialVoidRatio,
                            double constA,
                            double exponentN,
                            double poissonRatio,
                            double constBeta1,
                            double constAlpha1,
```

```
                                double constBeta2,
                                double constAlpha2,
                                double constBeta3,
                                double constAlpha3,
                                double constDegradation,
                                double constMumin,
                                double constMucyclic,
                                double constDilatancyStrain,
                                double constMumax,
                                // steady state line void ratio
                                double constsslvoidatP1,
                                double constsslvoidatP2,
                                double constsslvoidatP3,
                                double constsslvoidatP4,
                                double constsslvoidatP5,
                                double constsslvoidatP6,
                                double constsslvoidatP7,
                                double constsslvoidatP8,
                                double constsslvoidatP9,
                                double constsslvoidatP10,
                                // hydrostatic state line void ratio
                                double consthslvoidatP1,
                                double consthslvoidatP2,
                                double consthslvoidatP3,
                                double consthslvoidatP4,
                                double consthslvoidatP5,
                                double consthslvoidatP6,
                                double consthslvoidatP7,
                                double consthslvoidatP8,
                                double consthslvoidatP9,
                                double consthslvoidatP10,
                                // reference pressures
                                double constP1,
                                double constP2,
                                double constP3,
                                double constP4,
                                double constP5,
                                double constP6,
                                double constP7,
                                double constP8,
                                double constP9,
                                double constP10,
                                //offset of the failure surface
                                double constRxx,
                                double constRyy,
                                double constRzz,
                                double constRxy,
                                double constRyz,
                                double constRzx):
    NDMaterial(tag,ND_TAG_STRESSDILATANCYMODEL),
    theTag(tag),
    theG(constG),
    theDensity(constDensity),
    theStage(2)
    {
        modelParameter  = new double [15];
        sslVoidratio    = new double [10];
```

```
    hslVoidratio     = new double [10];
    refPressure      = new double [10];
    refOrigin        = new double [6];

    if(modelParameter==0) {
        opserr<<"Fail to allocate modelParameter[]"<<endln;
        exit(1);
    }

    if(sslVoidratio==0) {
        opserr<<"Fail to allocate sslVoidratio[]"<<endln;
        exit(1);
    }

    if(hslVoidratio==0) {
        opserr<<"Fail to allocate sslVoidratio[]"<<endln;
        exit(1);
    }

    if(refPressure==0) {
        opserr<<"Fail to allocate refPressure[]"<<endln;
        exit(1);
    }

    if(refOrigin==0) {
        opserr<<"Fail to allocate refOrigin[]"<<endln;
        exit(1);
    }

    for(int i=0;i<15;i++) modelParameter[i]=0.;
    for(int i=0;i<10;i++) sslVoidratio[i]=0.;
    for(int i=0;i<10;i++) hslVoidratio[i]=0.;
    for(int i=0;i<10;i++) refPressure[i]=0.;
    for(int i=0;i<6;i++)  refOrigin[i]=0.;

    modelParameter[0] = initialVoidRatio;
    modelParameter[1] = constA;
    modelParameter[2] = exponentN;
    modelParameter[3] = poissonRatio;
    modelParameter[4] = constBeta1;
    modelParameter[5] = constAlpha1;
    modelParameter[6] = constBeta2;
    modelParameter[7] = constAlpha2;
    modelParameter[8] = constBeta3;
    modelParameter[9] = constAlpha3;
    modelParameter[10] = constDegradation;
    modelParameter[11] = constMumin;
    modelParameter[12] = constMucyclic;
    modelParameter[13] = constDilatancyStrain;
    modelParameter[14] = constMumax;

    sslVoidratio[0] = constsslvoidatP1;
    sslVoidratio[1] = constsslvoidatP2;
    sslVoidratio[2] = constsslvoidatP3;
    sslVoidratio[3] = constsslvoidatP4;
    sslVoidratio[4] = constsslvoidatP5;
    sslVoidratio[5] = constsslvoidatP6;
```

```
    sslVoidratio[6] = constsslvoidatP7;
    sslVoidratio[7] = constsslvoidatP8;
    sslVoidratio[8] = constsslvoidatP9;
    sslVoidratio[9] = constsslvoidatP10;

    hslVoidratio[0] = consthslvoidatP1;
    hslVoidratio[1] = consthslvoidatP2;
    hslVoidratio[2] = consthslvoidatP3;
    hslVoidratio[3] = consthslvoidatP4;
    hslVoidratio[4] = consthslvoidatP5;
    hslVoidratio[5] = consthslvoidatP6;
    hslVoidratio[6] = consthslvoidatP7;
    hslVoidratio[7] = consthslvoidatP8;
    hslVoidratio[8] = consthslvoidatP9;
    hslVoidratio[9] = consthslvoidatP10;

    refPressure[0] = constP1;
    refPressure[1] = constP2;
    refPressure[2] = constP3;
    refPressure[3] = constP4;
    refPressure[4] = constP5;
    refPressure[5] = constP6;
    refPressure[6] = constP7;
    refPressure[7] = constP8;
    refPressure[8] = constP9;
    refPressure[9] = constP10;

    refOrigin[0] = constRxx;
    refOrigin[1] = constRyy;
    refOrigin[2] = constRzz;
    refOrigin[3] = constRxy;
    refOrigin[4] = constRyz;
    refOrigin[5] = constRzx;

}

StressDilatancyModel::~StressDilatancyModel()
{
    delete [] modelParameter;
    delete [] sslVoidratio;
    delete [] hslVoidratio;
    delete [] refPressure;
    delete [] refOrigin;
}

double
StressDilatancyModel::getRho(void)
{
    return theDensity;
}

int
StressDilatancyModel::setParameter(const char **argv, int argc, Parameter &param)
{

    if (argc < 2) return -1;
```

```
    int matTag;
    matTag = atoi(argv[1]);

    if (this->getTag() == matTag){
        if (strcmp(argv[0],"updateMaterialStage") == 0)
            return param.addObject(1, this);
        else
            return -1;
    }
    else
        return -1;

}

int
StressDilatancyModel::updateParameter(int parameterID, Information &info)
{
    if(parameterID==1){
        theStage=info.theInt;
        return 0;
    }
    else
        return -1;
}

void
StressDilatancyModel::Print(OPS_Stream &s, int flag)
{
    s<<"StressDilatancyModel::Tag "<<this->getTag()<<endln;
    s<<"Material Stage: "<<theStage;
}

int
StressDilatancyModel::commitState(void) {

    return 0;
}

int
StressDilatancyModel::revertToLastCommit(void){

    return 0;

}

int
StressDilatancyModel::revertToStart(void)
{
    return 0;
}

NDMaterial *
StressDilatancyModel::getCopy(void){

    return 0; //Subclass responsibility
}
```

```
const char *
StressDilatancyModel::getType(void) const{

    return 0; //Subclass responsibility

}

NDMaterial *
StressDilatancyModel::getCopy(const char *code)
{

    if (strcmp(code, "PlaneStrain")==0||strcmp(code,"2D")==0) {
        StressDilatancyModel2D *theCopy = 0;

        theCopy = new StressDilatancyModel2D (
                                              this->getTag(),
                                              this->theDensity,
                                              this->theG,
                                              //SD model parameters
                                              this->modelParameter[0],
                                              this->modelParameter[1],
                                              this->modelParameter[2],
                                              this->modelParameter[3],
                                              this->modelParameter[4],
                                              this->modelParameter[5],
                                              this->modelParameter[6],
                                              this->modelParameter[7],
                                              this->modelParameter[8],
                                              this->modelParameter[9],
                                              this->modelParameter[10],
                                              this->modelParameter[11],
                                              this->modelParameter[12],
                                              this->modelParameter[13],
                                              this->modelParameter[14],
                                              // steady state line void ratio
                                              this->sslVoidratio[0],
                                              this->sslVoidratio[1],
                                              this->sslVoidratio[2],
                                              this->sslVoidratio[3],
                                              this->sslVoidratio[4],
                                              this->sslVoidratio[5],
                                              this->sslVoidratio[6],
                                              this->sslVoidratio[7],
                                              this->sslVoidratio[8],
                                              this->sslVoidratio[9],
                                              // hydrostatic state line void ratio
                                              this->hslVoidratio[0],
                                              this->hslVoidratio[1],
                                              this->hslVoidratio[2],
                                              this->hslVoidratio[3],
                                              this->hslVoidratio[4],
                                              this->hslVoidratio[5],
                                              this->hslVoidratio[6],
                                              this->hslVoidratio[7],
                                              this->hslVoidratio[8],
                                              this->hslVoidratio[9],
                                              //ref pressures
```

```
                                        this->refPressure[0],
                                        this->refPressure[1],
                                        this->refPressure[2],
                                        this->refPressure[3],
                                        this->refPressure[4],
                                        this->refPressure[5],
                                        this->refPressure[6],
                                        this->refPressure[7],
                                        this->refPressure[8],
                                        this->refPressure[9],
                                        //offset of the failure surface
                                        this->refOrigin[0],
                                        this->refOrigin[1],
                                        this->refOrigin[2]);

    return theCopy;

} else if  (strcmp(code, "ThreeDimensional")==0||strcmp(code,"3D")==0) {

    StressDilatancyModel3D *theCopy=0;

    theCopy = new StressDilatancyModel3D(
                                        this->getTag(),
                                        this->theDensity,
                                        this->theG,
                                        //SD model parameters
                                        this->modelParameter[0],
                                        this->modelParameter[1],
                                        this->modelParameter[2],
                                        this->modelParameter[3],
                                        this->modelParameter[4],
                                        this->modelParameter[5],
                                        this->modelParameter[6],
                                        this->modelParameter[7],
                                        this->modelParameter[8],
                                        this->modelParameter[9],
                                        this->modelParameter[10],
                                        this->modelParameter[11],
                                        this->modelParameter[12],
                                        this->modelParameter[13],
                                        this->modelParameter[14],
                                        // steady state line void ratio
                                        this->sslVoidratio[0],
                                        this->sslVoidratio[1],
                                        this->sslVoidratio[2],
                                        this->sslVoidratio[3],
                                        this->sslVoidratio[4],
                                        this->sslVoidratio[5],
                                        this->sslVoidratio[6],
                                        this->sslVoidratio[7],
                                        this->sslVoidratio[8],
                                        this->sslVoidratio[9],
                                        // hydrostatic state line void ratio
                                        this->hslVoidratio[0],
                                        this->hslVoidratio[1],
                                        this->hslVoidratio[2],
                                        this->hslVoidratio[3],
```

```
                                                this->hslVoidratio[4],
                                                this->hslVoidratio[5],
                                                this->hslVoidratio[6],
                                                this->hslVoidratio[7],
                                                this->hslVoidratio[8],
                                                this->hslVoidratio[9],
                                                //ref pressures
                                                this->refPressure[0],
                                                this->refPressure[1],
                                                this->refPressure[2],
                                                this->refPressure[3],
                                                this->refPressure[4],
                                                this->refPressure[5],
                                                this->refPressure[6],
                                                this->refPressure[7],
                                                this->refPressure[8],
                                                this->refPressure[9],
                                                //offset of the failure surface
                                                this->refOrigin[0],
                                                this->refOrigin[1],
                                                this->refOrigin[2],
                                                this->refOrigin[3],
                                                this->refOrigin[4],
                                                this->refOrigin[5]);

        return theCopy;
    }
    else {
        opserr<<"StressDilatancyModel::getCopy failed to get copy: " << code << endln;
        return 0;
    }
}

int
StressDilatancyModel::sendSelf(int commitTag, Channel &theChannel){

    return 0; //subclass responsibility
}

int
StressDilatancyModel::recvSelf(int commitTag, Channel &theChannel,FEM_ObjectBroker &
theBroker){

    return 0; //subclass responsibility
}
```

```
/* Saumyasuchi Das, May 2013 */

# include <StressDilatancyModel3D.h>

double StressDilatancyModel3D :: _stress_current[6];
double StressDilatancyModel3D :: _strain_current[6];
double StressDilatancyModel3D :: _strain_next[6];
double StressDilatancyModel3D :: _model_parameter[15];
double StressDilatancyModel3D :: _ssl_void_ratio[10];
double StressDilatancyModel3D :: _ssl_pressure[10];
double StressDilatancyModel3D :: _hsl_void_ratio[10];
double StressDilatancyModel3D :: _hsl_pressure[10];
double StressDilatancyModel3D :: _hard_para_real[13*Nsurface+3];
double StressDilatancyModel3D :: _tangent[6][6];
double StressDilatancyModel3D :: _anisotropy[6];
int    StressDilatancyModel3D :: _hard_para_int[2];

StressDilatancyModel3D :: StressDilatancyModel3D (int tag,
                          double constDensity,
                          double constG,
                          // SD model  parameters
                          double initialVoidRatio,
                          double constA,
                          double exponentN,
                          double poissonRatio,
                          double constBeta1,
                          double constAlpha1,
                          double constBeta2,
                          double constAlpha2,
                          double constBeta3,
                          double constAlpha3,
                          double constDegradation,
                          double constMumin,
                          double constMucyclic,
                          double constDilatancyStrain,
                          double constMumax,
                          // steady state line void ratio
                          double constsslvoidatP1,
                          double constsslvoidatP2,
                          double constsslvoidatP3,
                          double constsslvoidatP4,
                          double constsslvoidatP5,
                          double constsslvoidatP6,
                          double constsslvoidatP7,
                          double constsslvoidatP8,
                          double constsslvoidatP9,
                          double constsslvoidatP10,
                          // hydrostatic state line void ratio
                          double consthslvoidatP1,
                          double consthslvoidatP2,
                          double consthslvoidatP3,
                          double consthslvoidatP4,
                          double consthslvoidatP5,
                          double consthslvoidatP6,
                          double consthslvoidatP7,
                          double consthslvoidatP8,
                          double consthslvoidatP9,
```

```
                                    double consthslvoidatP10,
                                    // reference pressures
                                    double constP1,
                                    double constP2,
                                    double constP3,
                                    double constP4,
                                    double constP5,
                                    double constP6,
                                    double constP7,
                                    double constP8,
                                    double constP9,
                                    double constP10,
                                    //offset of the failure surface
                                    double constRxx,
                                    double constRyy,
                                    double constRzz,
                                    double constRxy,
                                    double constRyz,
                                    double constRzx):

                                    StressDilatancyModel(tag,
                                                         constDensity,
                                                         constG,
                                                        // SD model  parameters
                                                        initialVoidRatio,
                                                        constA,
                                                        exponentN,
                                                        poissonRatio,
                                                        constBeta1,
                                                        constAlpha1,
                                                        constBeta2,
                                                        constAlpha2,
                                                        constBeta3,
                                                        constAlpha3,
                                                        constDegradation,
                                                        constMumin,
                                                        constMucyclic,
                                                        constDilatancyStrain,
                                                        constMumax,
                                                        // steady state line void ratio
                                                        constsslvoidatP1,
                                                        constsslvoidatP2,
                                                        constsslvoidatP3,
                                                        constsslvoidatP4,
                                                        constsslvoidatP5,
                                                        constsslvoidatP6,
                                                        constsslvoidatP7,
                                                        constsslvoidatP8,
                                                        constsslvoidatP9,
                                                        constsslvoidatP10,
                                                        // hydrostatic state line void ratio
                                                        consthslvoidatP1,
                                                        consthslvoidatP2,
                                                        consthslvoidatP3,
                                                        consthslvoidatP4,
                                                        consthslvoidatP5,
                                                        consthslvoidatP6,
```

```
                                                    consthslvoidatP7,
                                                    consthslvoidatP8,
                                                    consthslvoidatP9,
                                                    consthslvoidatP10,
                                                    // reference pressures
                                                    constP1,
                                                    constP2,
                                                    constP3,
                                                    constP4,
                                                    constP5,
                                                    constP6,
                                                    constP7,
                                                    constP8,
                                                    constP9,
                                                    constP10,
                                                    //offset of the failure surface
                                                    constRxx,
                                                    constRyy,
                                                    constRzz,
                                                    constRxy,
                                                    constRyz,
                                                    constRzx),
                                                    stressCurrent(6),
                                                    stressNext(6),
                                                    strainCurrent(6),
                                                    strainNext(6),
                                                    initialTangent(6,6),
                                                    currentTangent(6,6)
{

    hard_para_real  = new double [13*Nsurface+3];
    hard_para_int   = new int [2];

    if(hard_para_real==0) {
        opserr<<"Fail to allocate hard_para_real"<<endln;
        exit(1);
    }

    if(hard_para_int==0) {
        opserr<<"Fail to allocate hard_para_int"<<endln;
        exit(1);
    }

    for(int i=0;i<13*Nsurface+3;i++) hard_para_real[i]=0.;

    for(int i=0;i<2;i++)hard_para_int[i]=0;

    CalInitialTangent();

    currentTangent = initialTangent;

}

StressDilatancyModel3D::~StressDilatancyModel3D() {

    delete [] hard_para_real;
    delete [] hard_para_int;
```

```
}

NDMaterial *
StressDilatancyModel3D::getCopy(void){

    StressDilatancyModel3D *theCopy = 0;
    if(theCopy){
        *theCopy=*this;
        return theCopy;
    } else {
        opserr<<"StressDilatancyModel3D::getCopy failed to get copy: " << endln;
        return 0;
    }
}

const char *
StressDilatancyModel3D::getType(void) const {

    return "ThreeDimensional";
}

int
StressDilatancyModel3D::getOrder( ) const {

    return 6;
}

int
StressDilatancyModel3D::setTrialStrain(const Vector &v) {

    strainNext=v;
    GetCurrentStress(); //calculates stresses as well as the current tangent
    return 0;

}

int
StressDilatancyModel3D::setTrialStrain(const Vector &v, const Vector &r) {

    strainNext=v;
    GetCurrentStress(); //calculates stresses as well as the current tangent
    return 0;

}

const Matrix &
StressDilatancyModel3D::getTangent(void) {

    return currentTangent;

}

const Matrix &
StressDilatancyModel3D::getInitialTangent(void){

    CalInitialTangent();
```

```
    return initialTangent;

}

const Vector &
StressDilatancyModel3D::getStress(void){

    return stressNext;
}

const Vector &
StressDilatancyModel3D::getStrain(void){

    return strainCurrent;

}

int
StressDilatancyModel3D::commitState(void){

    GetCommittedCurrentStress(); // commits stresses, strains, hardening parameters
    and current tangent
    return 0;
}

Response *
StressDilatancyModel3D::setResponse (const char **argv, int argc, OPS_Stream &s){

    s<<"StressDilatancyModel"<<endln<<"Material Tag "<<this->getTag()<<endln;

    if(strcmp(argv[0],"stress") == 0 || strcmp(argv[0],"stresses") == 0) {
        return new MaterialResponse (this, 1, stressCurrent);
    }

    else if(strcmp(argv[0],"strain") == 0 || strcmp(argv[0],"strains") == 0) {
        return new MaterialResponse(this, 2, strainCurrent);
    }

    else
        return 0;

}

int
StressDilatancyModel3D::getResponse (int responseID, Information &matInformation){

    switch (responseID) {
    case 1:
        if (matInformation.theVector != 0)
            *(matInformation.theVector) = stressCurrent;
        return 0;
    case 2:
        if (matInformation.theVector != 0)
            *(matInformation.theVector) = strainCurrent;
        return 0;
    default:
        return -1;
```

```
    }
}

int
StressDilatancyModel3D::sendSelf(int commitTag, Channel &theChannel){

    static ID iData(4);                    // Material tag, theStage,
    _hard_para_int(2)
    static Vector vData(65+Nsurface*13+3); // 53 model information, 12 stress &
    strain,and _hard_para_real(Nsurface*13+3)
    static Matrix mData(6,6);              // Current Tangent

    int res;

    iData(0)=this->getTag();
    iData(1)=theStage;
    iData(2)=hard_para_int[0];
    iData(3)=hard_para_int[1];

    res = theChannel.sendID(this->getDbTag(), commitTag, iData);

    if (res < 0) {
    opserr << "StressDilatancyModel::sendSelf() - failed to send iData\n";
    return res;
    }

    vData(0) = this->theDensity;
    vData(1) = this->theG;

    for(int i=0;i<15;i++) vData(i+2)=this->modelParameter[i];
    for(int i=0;i<10;i++) vData(i+17)=this->sslVoidratio[i];
    for(int i=0;i<10;i++) vData(i+27)=this->hslVoidratio[i];
    for(int i=0;i<10;i++) vData(i+37)=this->refPressure[i];
    for(int i=0;i<6;i++)  vData(i+47)=this->refOrigin[i];
    for(int i=0;i<6;i++)  vData(i+53)=this->stressCurrent(i);
    for(int i=0;i<6;i++)  vData(i+59)=this->strainCurrent(i);
    for(int i=0;i<Nsurface*13+3;i++) vData(i+65)=this->hard_para_real[i];

    res = theChannel.sendVector(this->getDbTag(), commitTag, vData);

    if (res < 0) {
    opserr << "StressDilatancyModel::sendSelf() - failed to send vData\n";
    return res;
    }

    mData=currentTangent;

    res = theChannel.sendMatrix(this->getDbTag(), commitTag, mData);

    if (res < 0) {
    opserr << "StressDilatancyModel::sendSelf() - failed to send vData\n";
    return res;
    }

    return res;

}
```

```
int
StressDilatancyModel3D::recvSelf(int commitTag, Channel &theChannel,FEM_ObjectBroker
&theBroker){

    static ID iData(4);                    //Material tag, theStage, _hard_para_int(2)
    static Vector vData(65+Nsurface*13+2); //53 model information, 12 stress &
    strain,and _hard_para_real(Nsurface*13+2)
    static Matrix mData(6,6);              //Current tangent
    int res;

    res = theChannel.recvID(this->getDbTag(), commitTag, iData);

    if (res < 0) {
        opserr << "StressDilatancyModel::recvSelf() - failed to recv iData\n";
        return res;
    } else {

        this->setTag(iData(0));
        this->theStage=iData(1);
        this->hard_para_int[0]=iData(2);
        this->hard_para_int[1]=iData(3);
    }

    res = theChannel.recvVector(this->getDbTag(), commitTag, vData);

    if (res < 0) {
        opserr << "StressDilatancyModel::recvSelf() - failed to recv vData\n";
        return res;
    } else {

    this->theDensity = vData(0);
    this->theG = vData(1);

    for(int i=0;i<15;i++) this->modelParameter[i]=vData(i+2);
    for(int i=0;i<10;i++) this->sslVoidratio[i]=vData(i+17);
    for(int i=0;i<10;i++) this->hslVoidratio[i]=vData(i+27);
    for(int i=0;i<10;i++) this->refPressure[i]=vData(i+37);
    for(int i=0;i<6;i++)  this->refOrigin[i]=vData(i+47);
    for(int i=0;i<6;i++)  this->stressCurrent(i)=vData(i+53);
    for(int i=0;i<6;i++)  this->strainCurrent(i)=vData(i+59);
    for(int i=0;i<Nsurface*13+3;i++) this->hard_para_real[i]=vData(i+65);

    }

    res = theChannel.recvMatrix(this->getDbTag(),commitTag,mData);

    if (res < 0) {
        opserr << "StressDilatancyModel::recvSelf() - failed to recv mData\n";
        return res;
    } else
        mData=currentTangent;

    return res;

}
```

```
// ****************************** PRIVATE METHODS *********************************
/*-----------------------------------------------------------------------------
This method calculates current stress from a given current strain but does not update
the model. The intial state remains the same during iteration. The intial state is
stored in class members.

The class members are nor directly passed to the FORTRAN subroutine. They are first
copied in temporary variables (of static construct and hence are the same for all
instances of this class) and then passed to FORTRAN subroutine.

If the state is committed, the class members are updated from these temporary
variables; else not.

The temporary variables have an underscore as the prefix.
-----------------------------------------------------------------------------*/

void
StressDilatancyModel3D::GetCurrentStress(void){

    double p;

    // Elastic
    // ---------

    if (theStage!=1){
        stressNext=stressCurrent+currentTangent*(strainNext-strainCurrent);
        return;
    }

    // Plastic
    // ---------

    // Copy the temporary variables

    // Change the sign of the input data from OPENSEES
    // Compressive (normal) stress and strain is +ve

    if (hard_para_int[1] == 0) {
        p = (stressCurrent(0)+stressCurrent(1)+stressCurrent(2))/3.;
        stressCurrent(0)=p;
        stressCurrent(1)=p;
        stressCurrent(2)=p;
    }

    for(int i=0;i<3;i++)_stress_current[i] = -stressCurrent(i);
    for(int i=3;i<6;i++)_stress_current[i] =  stressCurrent(i);

    for(int i=0;i<3;i++)_strain_current[i] = -strainCurrent(i);
    for(int i=3;i<6;i++)_strain_current[i] =  strainCurrent(i)/2.;  //convert to
    true strain

    for(int i=0;i<3;i++)_strain_next[i] = -strainNext(i);
    for(int i=2;i<6;i++)_strain_next[i] =  strainNext(i)/2.;        // convert to
    true strain

    for(int i=0;i<15;i++)_model_parameter[i] = modelParameter[i];
```

```
    for(int i=0;i<10;i++)_ssl_void_ratio[i] = sslVoidratio[i];

    for(int i=0;i<10;i++)_ssl_pressure[i] = refPressure[i];

    for(int i=0;i<10;i++)_hsl_void_ratio[i] = hslVoidratio[i];

    for(int i=0;i<10;i++)_hsl_pressure[i] = refPressure[i];

    for(int i=0;i<Nsurface*13+3;i++)_hard_para_real[i] = hard_para_real[i];

    for(int i=0;i<2;i++)_hard_para_int[i] = hard_para_int[i];

    for(int i=0;i<6;i++)_anisotropy[i] = refOrigin[i];

    // in Fortran the double-scripted arrays will be transposed

    for(int i=0;i<6;i++)
        for(int j=0;j<6;j++) _tangent[j][i]=currentTangent(i,j);

    //Fortran subroutine for stress integration...

    SDM3D(
    _stress_current,
    _strain_current,
    _strain_next,
    _model_parameter,
    _ssl_void_ratio,
    _ssl_pressure,
    _hsl_void_ratio,
    _hsl_pressure,
    _hard_para_real,
    _hard_para_int,
    _anisotropy,
    _tangent);

    //Update the stress variable only as the state is not committed

    for(int i=0;i<3;i++) stressNext(i) = -_stress_current[i];
    for(int i=3;i<6;i++) stressNext(i) =  _stress_current[i];

    // in Fortran the double-scripted arrays will be transposed
    // in this section tangent is calculated for the Full-Newton-Raphson scheme

    for(int i=0;i<6;i++)
        for(int j=0;j<6;j++) currentTangent(i,j) = _tangent[j][i];

}

void
StressDilatancyModel3D::GetCommittedCurrentStress(void){

    double p;

    // Elastic
    //----------

    if (theStage!=1){
```

```
    stressNext=stressCurrent+currentTangent*(strainNext-strainCurrent);
    stressCurrent=stressNext;
    strainCurrent=strainNext;
    return;
}

// Plastic
// ---------

// Copy the temporary variables

// Change the sign of the input data from OPENSEES
// Compressive (normal) stress and strain is +ve

if (hard_para_int[1] == 0) {
    p = (stressCurrent(0)+stressCurrent(1)+stressCurrent(2))/3.;
    stressCurrent(0)=p;
    stressCurrent(1)=p;
    stressCurrent(2)=p;
}

for(int i=0;i<3;i++)_stress_current[i] = -stressCurrent(i);
for(int i=3;i<6;i++)_stress_current[i] =  stressCurrent(i);

for(int i=0;i<3;i++)_strain_current[i] = -strainCurrent(i);
for(int i=3;i<6;i++)_strain_current[i] =  strainCurrent(i)/2.;  //convert to
true strain

for(int i=0;i<3;i++)_strain_next[i] = -strainNext(i);
for(int i=3;i<6;i++)_strain_next[i] =  strainNext(i)/2.;        // convert to
true strain

for(int i=0;i<15;i++)_model_parameter[i] = modelParameter[i];

for(int i=0;i<10;i++)_ssl_void_ratio[i] = sslVoidratio[i];

for(int i=0;i<10;i++)_ssl_pressure[i] = refPressure[i];

for(int i=0;i<10;i++)_hsl_void_ratio[i] = hslVoidratio[i];

for(int i=0;i<10;i++)_hsl_pressure[i] = refPressure[i];

for(int i=0;i<Nsurface*13+3;i++)_hard_para_real[i] = hard_para_real[i];

for(int i=0;i<2;i++)_hard_para_int[i] = hard_para_int[i];

for(int i=0;i<6;i++)_anisotropy[i] = refOrigin[i];

// in Fortran the double-scripted arrays will be transposed

for(int i=0;i<6;i++)
    for(int j=0;j<6;j++) _tangent[j][i]=currentTangent(i,j);

//Fortran subroutine for stress integration...

SDM3D(
```

```
        _stress_current,
        _strain_current,
        _strain_next,
        _model_parameter,
        _ssl_void_ratio,
        _ssl_pressure,
        _hsl_void_ratio,
        _hsl_pressure,
        _hard_para_real,
        _hard_para_int,
        _anisotropy,
        _tangent);

        //Update the stress variable

        for(int i=0;i<3;i++) stressNext(i) = -_stress_current[i];
        for(int i=3;i<6;i++) stressNext(i) =  _stress_current[i];

        //Commit stress and strain

        stressCurrent=stressNext;
        strainCurrent=strainNext;

        //Commit hardening parameters

        for(int i=0;i<Nsurface*13+3;i++)hard_para_real[i] = _hard_para_real[i];
        for(int i=0;i<2;i++)hard_para_int[i]= _hard_para_int[i];

        //Commit tangent

        for(int i=0;i<6;i++)
            for(int j=0;j<6;j++) currentTangent(i,j)=_tangent[j][i];

    }

    void
    StressDilatancyModel3D::CalInitialTangent(void){

        double nu;
        double G;

        G = theG;
        nu = modelParameter[3];

        initialTangent(0,0) = 2*G/(1-2*nu)*(1-nu);
        initialTangent(0,1) = 2*G/(1-2*nu)*nu;
        initialTangent(0,2) = 2*G/(1-2*nu)*nu;
        initialTangent(0,3) = 0.;
        initialTangent(0,4) = 0.;
        initialTangent(0,5) = 0.;

        initialTangent(1,0) = 2*G/(1-2*nu)*nu;
        initialTangent(1,1) = 2*G/(1-2*nu)*(1-nu);
        initialTangent(1,2) = 2*G/(1-2*nu)*nu;
        initialTangent(1,3) = 0.;
        initialTangent(1,4) = 0.;
        initialTangent(1,5) = 0.;
```

```
    initialTangent(2,0) = 2*G/(1-2*nu)*nu;
    initialTangent(2,1) = 2*G/(1-2*nu)*nu;
    initialTangent(2,2) = 2*G/(1-2*nu)*(1-nu);
    initialTangent(2,3) = 0.;
    initialTangent(2,4) = 0.;
    initialTangent(2,5) = 0.;

    initialTangent(3,0) = 0.;
    initialTangent(3,1) = 0.;
    initialTangent(3,2) = 0.;
    initialTangent(3,3) = G;
    initialTangent(3,4) = 0.;
    initialTangent(3,5) = 0.;

    initialTangent(4,0) = 0.;
    initialTangent(4,1) = 0.;
    initialTangent(4,2) = 0.;
    initialTangent(4,3) = 0.;
    initialTangent(4,4) = G;
    initialTangent(4,5) = 0.;

    initialTangent(5,0) = 0.;
    initialTangent(5,1) = 0.;
    initialTangent(5,2) = 0.;
    initialTangent(5,3) = 0.;
    initialTangent(5,4) = 0.;
    initialTangent(5,5) = G;

}
```

```
/* Saumyasuchi Das, May 2013 */

# include <StressDilatancyModel.h>

extern "C"  {
            void SDM3D(
            double _stress_current[],
            double _strain_current[],
            double _strain_next[],
            double _model_parameter[],
            double _ssl_void_ratio[],
            double _ssl_pressure[],
            double _hsl_void_ratio[],
            double _hsl_pressure[],
            double _hard_para_real[],
            int    _hard_para_int[],
            double _anisotropy[],
            double (*_tangent)[6]);
}


class StressDilatancyModel3D : public StressDilatancyModel {

public:

    //default constructor - does nothing, never called

    StressDilatancyModel3D() {};

    //initialisation constructor

    StressDilatancyModel3D(int tag,
                        double constDensity,
                        double constG,
                        // SD model  parameters
                        double initialVoidRatio,
                        double constA,
                        double exponentN,
                        double poissonRatio,
                        double constBeta1,
                        double constAlpha1,
                        double constBeta2,
                        double constAlpha2,
                        double constBeta3,
                        double constAlpha3,
                        double constDegradation,
                        double constMumin,
                        double constMucyclic,
                        double constDilatancyStrain,
                        double constMumax,
                        // steady state line void ratio
                        double constsslvoidatP1,
                        double constsslvoidatP2,
```

```
                        double constsslvoidatP3,
                        double constsslvoidatP4,
                        double constsslvoidatP5,
                        double constsslvoidatP6,
                        double constsslvoidatP7,
                        double constsslvoidatP8,
                        double constsslvoidatP9,
                        double constsslvoidatP10,
                        // hydrostatic state line void ratio
                        double consthslvoidatP1,
                        double consthslvoidatP2,
                        double consthslvoidatP3,
                        double consthslvoidatP4,
                        double consthslvoidatP5,
                        double consthslvoidatP6,
                        double consthslvoidatP7,
                        double consthslvoidatP8,
                        double consthslvoidatP9,
                        double consthslvoidatP10,
                        // reference pressures
                        double constP1,
                        double constP2,
                        double constP3,
                        double constP4,
                        double constP5,
                        double constP6,
                        double constP7,
                        double constP8,
                        double constP9,
                        double constP10,
                        //offset of the failure surface
                        double constRxx=0,
                        double constRyy=0,
                        double constRzz=0,
                        double constRxy=0,
                        double constRyz=0,
                        double constRzx=0);

    //destructor

    ~StressDilatancyModel3D();

    NDMaterial *getCopy(void);

    const char *getType(void) const;

    int getOrder( ) const ;

    int setTrialStrain(const Vector &v);

    int setTrialStrain(const Vector &v, const Vector &r);

    const Matrix &getTangent(void);
```

```
    const Matrix &getInitialTangent(void);

    const Vector &getStress(void);

    const Vector &getStrain(void);

    int commitState(void);

    Response *setResponse (const char **argv, int argc, OPS_Stream &s);

    int getResponse (int responseID, Information &matInformation);

    int sendSelf(int commitTag, Channel &theChannel);

    int recvSelf(int commitTag, Channel &theChannel,FEM_ObjectBroker &theBroker);

    protected:

    private:

        Vector stressCurrent,
               stressNext,
               strainCurrent,
               strainNext;

        Matrix initialTangent,
               currentTangent;

        void CalInitialTangent(void),
             GetCurrentStress(void),
             GetCommittedCurrentStress(void);

        static double _stress_current[6],
                      _strain_current[6],
                      _strain_next[6],
                      _model_parameter[15],
                      _ssl_void_ratio[10],
                      _ssl_pressure[10],
                      _hsl_void_ratio[10],
                      _hsl_pressure[10],
                      _hard_para_real[13*Nsurface+3],
                      _anisotropy[6],
                      _tangent [6][6];

        static int  _hard_para_int[2];

        double *hard_para_real;

        int *hard_para_int;
};
```